THE GEOCHEMISTRY OF THE KAROO IGNEOUS VOLCANIC AND INTRUSIVE ROCKS OF BOTSWANA

by
ROCHELLE WIGLEY

Department of Geological Sciences
University of Cape Town
February 1995

Thesis submitted in fulfilment of the requirements for the degree Master of Science in the Department of Geological Sciences at the University of Cape Town.

uT 550 WIGL

96/1001

ABSTRACT

The Mesozoic basalts and dolerites of Botswana underlie an estimated area of 150 000km^2 and form part of the Karoo Igneous Province of southern Africa. The distribution of Karoo basalts in Botswana is limited essentially to three main sub-basins, the Central Kalahari Sub-basin, northern Botswana and the Tuli Syncline and a major dyke swarm, with a WNW strike, extends across Botswana from the Namibian to Zimbabwean borders. This dissertation is a reconnaissance study which concentrates on the recognition and definition of distinct geochemical sub-groups within the Karoo volcanic and intrusive rocks of Botswana. 128 new whole rock samples were analyzed for major and trace element concentrations, in addition to the 70 whole rock analyses from Botswana which were available in the UCT database. Mineral analyses and rare earth element compositions for selected samples are also presented.

The basalts and dolerites of Botswana are assigned to one of the three geochemical lineages, *i.e.* the low-K_2O, the high-K_2O and the felsite lineages on the basis of SiO_2, MgO and K_2O concentrations. A number of distinct geochemical sub-groups are recognised within these lineages according to whole rock compositions, normative mineralogy, petrography and outcrop character.

The low-K_2O lineage is subdivided into two main sub-groups on the basis of the TiO_2 and Zr concentrations, *i.e.* the LTZ- and HTZ-type basalt and dolerite sub-groups. The LTZ-type basalt sub-group (with ≤2% TiO_2 and ≤250ppm Zr) represents the bulk of the Botswana dataset where the LTZ basalts of Botswana are shown to be lateral equivalents to the Lesotho Formation basalts of the Central Karoo area, considerably expanding the known outcrop area of this basalt type. Two dolerites are the only samples of intrusive equivalents of this voluminous LTZ basalt type in Botswana.

The HTZ-type basalt and dolerite sub-group includes both the HTLZ- (with ≥2% TiO_2 and ≤250ppm Zr) and the HTZ- (with ≥2% TiO_2 and ≥250ppm Zr) basalts and dolerites and is subdivided into two different sub-groups on the basis of TiO_2 and Fe_2O_3* concentrations, *i.e.* the HTLZ/HTZ basalt and dolerite and HTZ (low Fe) basalt and dolerite sub-groups. The HTLZ/HTZ basalts and dolerites of Botswana have been correlated with the HTZ.HF basalt type of the Central Lebombo and Tuli areas. The HTZ (low Fe) basalt and dolerite sub-group has an enriched whole rock geochemistry (*e.g.* Ce/Y > 2.1; high Ba and Zr concentrations) with respect to both the HTLZ/HTZ basalt and dolerite and LTZ-type basalt sub-groups of Botswana and the HTZ (low Fe) sub-group is proposed to be equivalent to the HTZ.LF basalts of the Central Lebombo and Tuli areas.

The high-K_2O lineage is subdivided into two sub-groups on the basis of the MgO concentration. The high-K_2O picritic basalts, which were collected along the southern margin of the basalt outcrop in the Botswana portion of the Tuli Syncline, are correlated with the Letaba Formation picritic basalts. The shoshonites sampled during this study have anomalously high Nb concentrations and low Zr/Nb ratios with respect to the high-K_2O (Letaba Formation) picritic basalts, however these shoshonites and the Mashikiri Formation nephelinites have similar Nb concentrations and similar values for their Zr/Nb ratios, suggesting a similar style of source area enrichment.

The two felsite samples are the only known unequivocal examples of Karoo felsic magmatism in either Botswana or the Tuli Syncline area. The felsites have been tentatively interpreted as lateral equivalents to the Nuanetsi rhyolites, although a single initial Sr-isotope composition suggests that contamination en route to the surface may have occurred.

Two of the sub-groups with an apparent LTZ-type geochemical signature cannot be easily differentiated from the remaining dolerite samples by their outcrop appearance in the field, although evidence suggests that the two sub-groups are not Karoo aged. The TYPE II LTZ dolerites are characterised by a low-grade greenschist metamorphic assemblage and have been tentatively correlated with the Proterozoic suite of intrusive dolerites of Botswana. The high-MgO LTZ picrites have a mesocumulus texture and have been tentatively correlated with the Archaean Olivine Norites, which are intruded into the basement gneisses of the Limpopo Mobile Belt.

The basalts from both the Central Kalahari Sub-basin and northeast Botswana are dominated by an LTZ-type basalt composition, although no LTZ-type basalts or dolerites were recognised from the Tuli Syncline area. The HTZ (low Fe) basalts are present in the Tuli Syncline area and overlie a considerable thickness of LTZ-type basalts in three separate stratigraphic sections in northeast Botswana, where it has been suggested that the basalts of northeast Botswana flowed in from the north. The dolerites sampled from the dyke swarm appear to have an exclusively HTLZ/HTZ geochemistry, and the presence and distribution of HTLZ/HTZ basalts appear to be closely related to the intrusion of the dyke swarm as HTLZ/HTZ basalts are found in the Tuli Syncline area, in the Central Kalahari Sub-basin and in western Botswana. The basalt stratigraphy observed in Botswana broadly corresponds with the overall basalt stratigraphy of the Karoo Igneous Province, although no Lebombo-type LTZ basalts were recognised. The distribution of basalts in Botswana is inconsistent with an apparently linear boundary separating dominantly "enriched" basalts to the north from basalts with a "normal" chemistry to the south in Botswana. The Botswana dyke swarm represents the failed arm of a rift-rift-rift triple junction centred in the Nuanetsi,

where the felsite and the shoshonite samples of Botswana are both found closely associated with the dyke swarm. The intrusion of the dyke swarm is proposed to post-date both the LTZ and HTZ (low Fe) basalt magmatic events and if this proposed age is correct, it suggests that the rifting and magmatism associated with the Nuanetsi area occurred after the eruption of the voluminous LTZ-type basalts of the Karoo Igneous Province.

TABLE OF CONTENTS

ACKNOWLEDGMENTS

I wish to extend my deepest sympathies to the family and friends of the late Prof. Tony Erlank. I was extremely fortunate to have had Tony as a supervisor in the initial stages of this study and I am greatly appreciative of all the help and encouragement he gave me.

I would like to express my gratitude to my supervisor, Prof. Andy Duncan, for the support, guidance and encouragement he gave me during the preparation and the writing of this dissertation. However, without the help and support of a number of people this dissertation would never have been completed and I thank them all. The assistance of Andy Moore in the organisation of the field trip to Botswana and in the collection of samples is greatly appreciated. Roy and Charlotte Young and Roger Petty are thanked for their hospitality. All the people at the Geological Survey of Botswana and at De Beers Prospecting Botswana (PTY) Limited in Lobatse are thanked for their assistance during the collection of the core and drill chip samples. Heidrun Hannig is thanked for her invaluable help in the preparation and analysis of a number of basalt core samples and I would also like to thank Ernest Stout for all his help in the "crushing room". Andy Duncan and Dave Hill are thanked for introducing me to the computer systems at UCT which were used extensively during the preparation of this thesis. David Wilson is thanked for producing an alarmingly large number of thin-sections and probe slides, often at very short notice. Dick Rickard is thanked for his all his help with the microprobe. Ron Watkins is thanked for introducing me (briefly) to the HPIC laboratory and his help in obtaining the REE analyses is appreciated. I would also like to thank my fellow students Isay, Steve, Ingrid, Gail, Andreas, Leon, Protea, Iuma, Karen and Paul, without whom the last few years would have been a lot less interesting.

Shirley Butcher and Dan Wilson from the GIS unit in the Department of Surveying and Geodetic Engineering are thanked introducing me to the ins and outs of PC ARC/INFO and all of their patience and assistance in the generation of the maps in chapter 1 and 5 is greatly appreciated.

The Foundation for Research and Development and Andy Duncan are thanked for their financial assistance in 1991/1992.

I am deeply grateful to my parents for all the encouragement, understanding and support that they have given me over the years and I thank them for their unending generosity and the much appreciated financial support. A special thanks to Helen, Greg and my house mates for everything, especially during the final stages of the "writing up" of this dissertation.

Finally I would like to thank all at Campus Security who so tirelessly walked me home after many late nights spent in the department.

1 INTRODUCTION AND GENERAL GEOLOGY

1.1 INTRODUCTION

The break-up of Gondwanaland during the late Triassic to early Cretaceous period was associated with the production of an exceptional volume of continental flood basalts in a broad band parallel to the southern margin of the Gondwana supercontinent (Cox, 1978). A major magmatic episode in the Jurassic, associated with the opening of the Indian ocean, produced a series of continental flood basalt provinces extending from southern Africa and Dronning Maud Land (Karoo) to Antarctica, Tasmania and southeast Australia (Ferrar). A second magmatic episode in the Cretaceous, associated with the opening of the Atlantic Ocean, produced the Etendeka and Paraná flood basalt provinces.

Following the prolonged sedimentation of the Karoo Supergroup in southern Africa, the Karoo Igneous Province magmatism was initiated as a number of isolated intrusions around 204±5Ma, where the magmatic activity reached a maximum at 180±2Ma (Marsh *et al.*, 1995). Only remnants of the once extensive Karoo Igneous Province, with a former extent of perhaps 3 000 000km^2 (Cox, 1988a), are preserved and outcrops are found across most of southern Africa from Malawi and Barotseland in Zambia in the north to the southern Cape Province and from Namibia to Mozambique. The distribution and characteristics of the different regions in which remnant Karoo igneous rocks are found are described in detail in Eales *et al.* (1984). The intrusive and extrusive Karoo rocks of southern Africa are dominated by low MgO tholeiitic compositions, although nephelinites, picritic basalts and rhyolites are locally abundant. As the Karoo Igneous Province has been the focus of an extensive ongoing investigation, a number of detailed reviews are available in the literature and a special volume published by the Geological Society of South Africa (edited by A.J. Erlank, 1984) presents the results of the Geodynamics Project on Karoo Volcanism.

Although the present outcrop area of the Karoo Igneous Province is estimated at 140 000km^2 (Eales *et al.*, 1984), the Karoo basalts of Botswana are estimated to underlie an area in excess of 150 000km^2 (Eales *et al.*, 1984) with a maximum thickness exceeding 800m in eastern Botswana (Key, *pers. comm.*, 1995). However, largely due to the poor outcrop exposure in Botswana the Karoo basalts and dolerites of Botswana have received little attention in the past, although a preliminary study (Eales *et al.*, 1984; Erlank *et al.*, 1990) suggested that some of the basalt and dolerite samples where enriched in incompatible

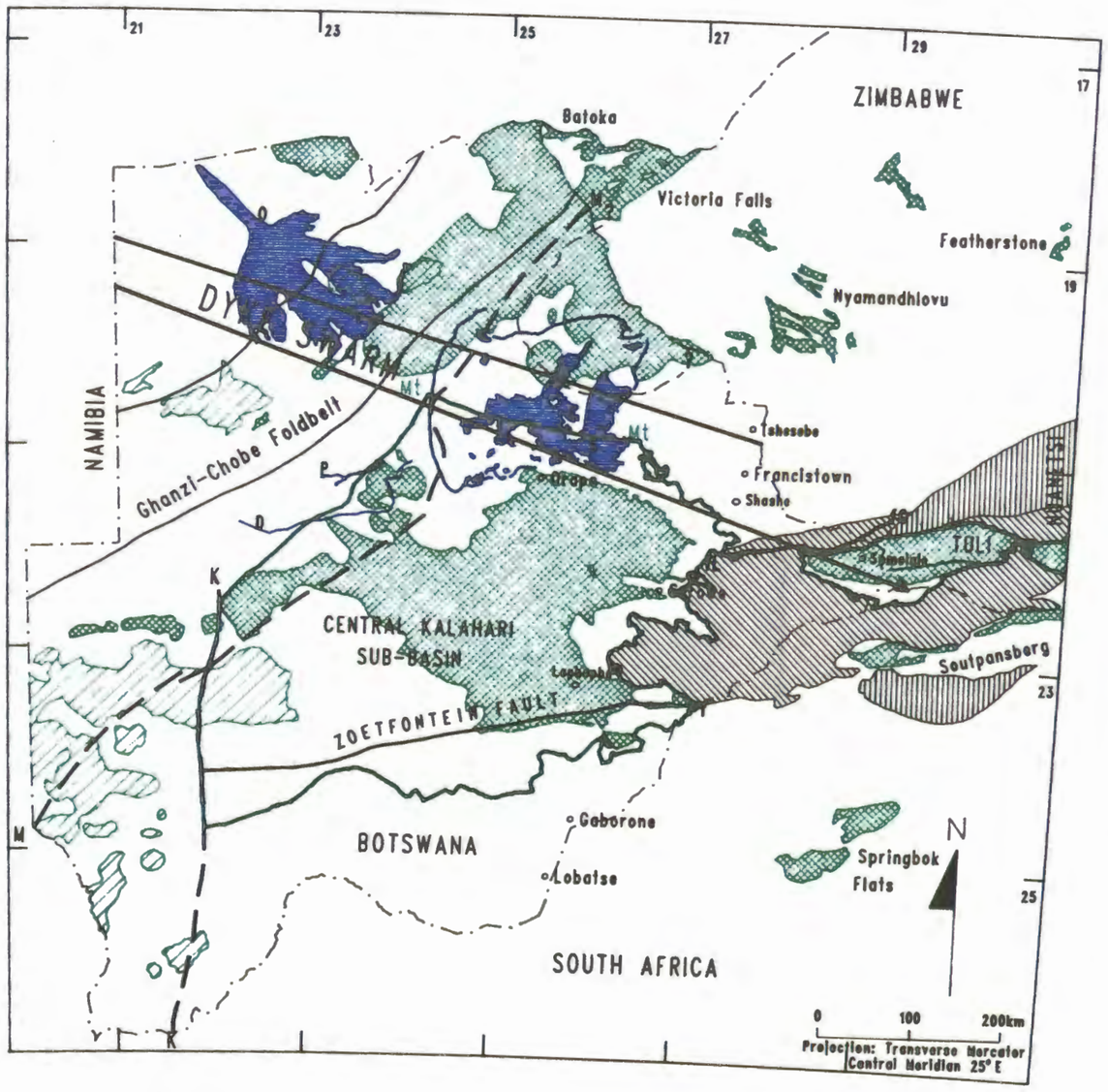

Fig. 1.1 Aspects of the general geology of Botswana

LEGEND

- Pans and swamps
- Basalts
- Sills
- KAROO
- Marginal Zones
- Central Zone
- LIMPOPO MOBILE BELT
- Shoreline of former Lake Makgadikgadi
  - O: Okavango delta
  - P: Passarge Mekgacha
  - D: Deception Mekgacha
  - S: Sua Pan
- Approximate northern limit of Letaba Picrites in the Tuli Syncline (Zimbabwe)
- Central Kalahari and Tuli Karoo Sedimentary Sub-basins
- ---? Postulated position of the Nata Sub-basin
- Faults
  - L: Letlakhane Fault
  - G: Gobojango Fault Zone
- Mt Trace of the Makgadikgadi high
- M Makgadikgadi line
- K Kalahari line
- International boundary

elements, characteristic of the basalts of the Nuanetsi and Lebombo areas, whereas others had a composition similar to that of the Lesotho Formation basalts of the Central Karoo area.

1.2 ASPECTS OF THE GENERAL GEOLOGY OF BOTSWANA

1.2.1 INTRODUCTION

Approximately 80 percent of Botswana is covered by superficial sediments which are known, collectively, as the "Kalahari Beds". Reasonable geological outcrop, or sub-outcrop, is therefore found only in eastern Botswana and along the Ghanzi-Chobe high ground in northwest Botswana.

Although this extensive superficial sediment cover has hindered the geological investigation of Botswana a combination of geophysical and geological projects, including the Reconnaissance Aeromagnetic Survey, have been undertaken by, and in affiliation with, the Geological Survey of Botswana. The results of this work have been published as a series of Bulletins by the Geological Survey.

The following section discusses specific aspects of the geology of Botswana which are pertinent to this study, including the basement geology, the pre-eruption sedimentary basins, the Karoo basalts and the associated intrusive rocks and the post-eruption superficial cover. The aspects of the geology of Botswana which are described in the following section are summarised in Fig. 1.1. The relevant information was captured from a number of sources which include the Distribution of Karoo in Botswana, 1:2 000 000 (Geological Survey of Botswana, 1981), the Geological Map of Botswana, 1:1 000 000 (Geological Survey and Mines Department, Botswana, 1973), the Geological Map of Southern Africa, 1:4 000 000 (Geological Society of South Africa, 1985), Aldiss (1983a), Coates *et al.* (1979), Eales *et al.* (1984), Meixner and Peart (1984), Reeves (1978), Smith (1984), Tankard *et al.* (1982) and Vail *et al.* (1969).

1.2.2 BASEMENT GEOLOGY

1.2.2.1 Archaean basement

The Kaapvaal and Zimbabwean Cratons together with the Limpopo Mobile Belt form the basement to the areas covered by the Karoo basalts in Botswana. The western margin of the Kaapvaal Craton is represented by a line of magnetic anomalies, referred to as the Kalahari line, and the Zoetfontein fault is taken to represent the northern boundary of the Kaapvaal

Craton. The Zoetfontein fault, an ancient tectonic feature which may extend approximately 1000km east to the present outline of the African coast, is an ancient fracture line of continental scale (Meixner and Peart, 1984). The western margin of the Zimbabwean craton, referred to as the Makgadikgadi line, represents the southern faulted boundary of a rift which separates the Ghanzi-Chobe Foldbelt and Damaran rocks of northwest Botswana from the Zimbabwean Craton (Meixner and Peart, 1984).

The predominant rock types in the Archaean basement are banded, granoblastic or porphyroblastic gneisses together with minor amphibolites and metasediments (quartzites and Mg-marbles). Pervasive granitic to pegmatitic veins intrude these basement rocks. The ENE-striking Limpopo Mobile Belt, which links the Kaapvaal and Zimbabwean Cratons, is characterised by a Central Zone of complex interference folding which is bound to the north and south by marginal zones of granulite-grade metamorphism (Key, 1977) which grade metamorphically and structurally into the adjacent cratons. The pervasive structural fabric of the Limpopo Mobile Belt strikes ENE.

Associated with the basement rocks, including both the Archaean cratons and the Limpopo Mobile Belt, are a number of ultramafic to mafic rock types of which amphibolites are the most abundant. These minor mafic rock types, in particular those types which have no structural fabric, can be confused in the field with Karoo intrusive rock types especially in areas where the outcrop exposure is poor. The amphibolite belts which are associated with metapyroxenites, serpentinites and ultramafic granulites, are usually elongated parallel to the strike of the Limpopo Mobile Belt and apart from a well developed fabric these amphibolitic rocks are usually very altered. The only other important group of Archaean mafic rock types in eastern Botswana, in relation to this study, are referred to as Norites or Olivine Norites (Aldiss, 1983a & b). The Olivine Norites typically have an irregularly curved shape outcrop and are sub-horizontal bodies of varying size, but rare dykes with a WNW trend, parallel to the Karoo dyke swarm, are observed (Aldiss, 1983a). The Olivine Norites, recrystallised at high metamorphic grades, show a variation from mild to extreme mylonization. The petrography of the least-deformed Olivine Norites is typically mesocumulate with euhedral olivine and orthopyroxene, which may be rimmed in clinopyroxene, in a matrix of plagioclase, granular clinopyroxene, biotite, spinel and an opaque phase. The olivine typically develops a reaction rim where it is in contact with plagioclase. Incipient mylonization is recognised by the deformation of twins and the cleavage and microfracturing of an otherwise primary igneous texture (Aldiss, 1983a). The exact age of the Olivine Norites is not known, but they are interpreted by Aldiss (1983a) as possibly being of a syntectonic intrusive origin.

1.2.2.2 Proterozoic dolerites

A group of mafic rocks in eastern Botswana, referred to as the Proterozoic dolerites, are characterised by the absence of any deformational fabric and they are present as both large sill-like bodies and as rare feeder dykes. In the Tshesebe - Shashe area the dolerite sills and their associated feeder dykes, which often have a WNW strike direction, have often been assumed to be of a Karoo age (Litherland, 1975) although these sills may be cut by dyke lineaments which are parallel to the dyke swarm (Crocket, 1967). Aldiss (1989) notes that the dolerite sills of the Shashe area closely resemble the Proterozoic quartz dolerites of Zimbabwe and, in particular, the Mashonaland dolerite sills. The characteristic texture of the Proterozoic dolerites in Botswana (and Zimbabwe - Wilson *et al.*, 1987) is ophitic to sub-ophitic with a mineral assemblage of plagioclase (sometimes as glomerophenocrysts), clinopyroxene and interstitial magnetite (Aldiss, 1989). A patchy style of alteration is characteristic of these dolerites with the increased sericitization of plagioclase and the replacement of clinopyroxene by amphibole associated with late stage interstitial domains of biotite, granophyre, anhedral quartz and occasionally apatite (Aldiss, 1989).

A variety of Proterozoic intrusive dolerites with similar field characteristics are recognised in Zimbabwe. The Sabanga dolerite dykes of Central Zimbabwe have a predominantly NNW strike direction and are closely associated with the ±1800 Ma Mashonaland dolerites (Compston and McElhinny, 1975; Wilson *et al.*, 1987 and Cahen *et al.*, 1984). The post-Waterberg Umkondo dolerites of Zimbabwe are most easily differentiated from the Mashonaland and Sabanga dolerites by their reversed magnetic pole position and equivalent dolerites are intruded into the Waterberg Group in the Transvaal and Botswana (Wilson *et al.*, 1987). In the Tshesebe - Francistown area a set of prominent dolerite dykes with an approximate NE strike direction have been assigned Karoo-ages (Litherland, 1975), however Wilson *et al.* (1987) suggest that these dolerite dykes may in fact belong to the Plumtree Dyke Swarm. The 450km long early Proterozoic arcuate Plumtree Dyke Swarm, with strike lengths of the individual dykes of approximately 60km, extends from the Botswana - Zimbabwe border in the Tshesebe area, where the strike direction is NE - SW, to west of Harare, where the predominant strike direction has changed to being N - S. The Plumtree Dyke Swarm has been related to the ±2150Ma Deweras basalts of northwest Zimbabwe (Wilson *et al.*, 1987). The Deweras basalts and the associated dolerite dykes are all very altered and have undergone low grades (greenschist) of regional metamorphism (*i.e.* extensive replacement by chlorite, epidote and amphibole (tremolite/actinolite)) and have a mineral assemblage of plagioclase, pyroxene (replaced by amphibole, chlorite ±biotite), leucoxene, quartz, chlorite, biotite, epidote and apatite (Tennick *et al.*, 1976; Bliss, 1971; Wilson *et al.*, 1987).

1.2.3 THE KAROO SUPERGROUP

1.2.3.1 Karoo sedimentary rocks

Karoo sediments are found in a number of sub-basins within Botswana (Smith, 1984) and the most important of these in relation to this study are the Central Kalahari Sub-basin, the Tuli Sub-basin or Syncline and the sediments of northeast Botswana. The Karoo sedimentary rocks of Botswana are broadly comparable with the lateral equivalents in Southern Africa and according to Smith (1984) the Karoo sedimentary succession in Botswana is sub-divided into the Dwyka Group, Ecca Group, Tlhabala (or Kwetla) Formations, Lebung Group and the Stormberg Group. The lower Mosoltsane Formation and upper Ntane Formation of the Lebung Group are lateral equivalents to the Elliot Formation and Clarens Sandstone Formation, respectively.

A complete succession of Karoo sediments from the Dwyka through to the Lebung Group are preserved in the Central Kalahari Sub-basin, a broad, slowly subsiding cratonic basin, and the sediments achieve a maximum thickness of approximately 500 metres (Reeves, 1978). In the southeast of the Sub-basin thicker sequences of sediments, and the overlying Stormberg basalts, are preserved in a series of troughs in the basement with a WNW trend. South of the Zoetfontein fault the Karoo Supergroup is preserved in a complex set of horsts and grabens which are commonly triangular in shape. The intersection of two sets of faults, normal NNW to WNW faults and ENE faults of the basement (*e.g.* ENE Zoetfontein fault), produce this characteristic pattern.

The Central Kalahari Sub-basin is separated from the sediments of northeast Botswana by a WNW striking ridge of Archaean basement which is known as the Makgadikgadi high (Smith, 1984). The sediments of the Central Kalahari Sub-basin thin up against this basement high and the Ntane Formation oversteps older Karoo Formations until it lies directly on the basement rocks of the Makgadikgadi high (Smith, 1984).

Swift (1961) noted the presence of a plateau in central Zimbabwe which separated the Zambezi basin and Makgadikgadi depression to the north and west from the Sabi-Limpopo basins to the southeast and the sediments and overlying basalts of northeast Botswana are therefore part of a larger basin which extends westwards into Zimbabwe. In contrast to the Central Kalahari Sub-basin the sedimentary sequence of northeast Botswana is condensed and Dwyka and Ecca Group sediments are often completely absent. Thicker and more complete sedimentary and thicker basalt sequences are, however, preserved in NE trending troughs, *e.g.* the Nata Sub-basin, in northeast Botswana and northern Zimbabwe where the troughs have been interpreted as the half-graben structures reactivating NE trending

basement shear zones as a result of compression associated with the Cape Fold Belt (Daly *et al.*, 1991; Cox, 1992). North of the Nata Sub-basin, basalts often lie directly on the Archaean basement.

The Tuli Sub-basin, a shallow synclinal structure, extends eastwards into Zimbabwe and has a total length of approximately 230km (Vail *et al.*, 1969) and a cross-basin width in Botswana of approximately 60km (Clark and Machacha, 1982). The northern margin of the Tuli Sub-basin is defined by a post-Karoo fault system, the Gobojango Fault Zone with an ENE trend (Aldiss, 1983a) parallel to the underlying Limpopo Mobile Belt. Although the Tuli Syncline is now isolated from the Central Kalahari Sub-basin, a number of Karoo outliers along the line of the Letlhakane Fault (after Key, 1976 in Smith, 1984) suggests that the Tuli and Central Kalahari Sub-basins may once have been connected. Dwyka Group sediments are absent in the Tuli Syncline in Botswana and the Tsheung Formation (lateral equivalent to the Ntane Formation) is less well sorted than the Ntane Formation and the presence of poorly to well developed cross bedding suggests a more fluvial origin (Aldiss, 1983a) for these sediments in the Tuli area.

1.2.3.2 Karoo basalts

Although little work has been undertaken on the Karoo basalts of Botswana the distribution of the basalts, referred to as the Stormberg lavas in the literature (Smith, 1984), is summarised in Fig. 1.1. Karoo basalts are found in three main areas in Botswana which are the Central Kalahari Sub-basin, northern Botswana and the Tuli Syncline, each of which is discussed below.

1.2.3.2.1 The Central Kalahari Sub-basin

In the Central Kalahari Sub-basin the basalts unconformably overlie the Ntane Formation and, in rare deflation hollows, the Mosoltsane Formation (Smith, 1984). The thickness of the lava pile, for the most part depends on the topography of the paleodunefield (preserved as the Ntane Formation) and on syn- to post-Karoo faulting. The greatest thickness of basalt is believed to be preserved north of the Zoetfontein fault, which has a post-Karoo downthrow of 300 metres to the north (Jones, 1968). The Shadishadi borehole, sited near Lephephe in the southeast corner of the Central Kalahari Sub-basin, intercepted almost exactly 800m of basalt where drilling was stopped before the base of the basalt interval was reached (Key, *pers. comm.*, 1995). Interbedded sandstone lenses found near the base of the lava pile south of the Zoetfontein fault and the ±6m of interbedded mudstone sampled in the borehole T529, north of Serowe, are the only sediments interbedded with the basalts that are recognised in the Central Kalahari Sub-basin.

The flat lying basalts of the Central Kalahari Sub-basin are typically green - black in colour when fresh and alter to a red - purple colour. Individual basalt flows, up to 80m thick, have well developed flow top and bottom features. The flow tops are highly amygdaloidal and typically altered and an increase in the degree of veining and the presence of pipe amygdales marks the base of an individual flow. The amygdales are filled with chlorite, zeolite, quartz and rare calcite and epidote (Smith, 1984). Rare thin tuffaceous layers, interbedded with the basalt, have been recognised by Smith (1984) in the borehole T529, drilled north of Serowe, and by Jennings (1965) southwest of Serowe.

1.2.3.2.2 Northern Botswana

The basalts of northwest Botswana are preserved in a number of grabens, which strike parallel to the Ghanzi-Chobe foldbelt. These basalts were erupted on an uneven surface and overly both the Bodibeng Sandstone Formation (Thomas, 1969) and the Ghanzi-Chobe basement. The Bodibeng Sandstone Formation is a lateral equivalent to the Ntane sandstone (Smith, 1984). The absence of basalt between Lebung Group sediments and the Kalahari Beds, in some stratigraphic successions, suggests that either erosion occurred prior to the deposition of the Kalahari Beds or that the distribution of the basalts in the northwest of Botswana is more localised and preserved mainly in grabens (Smith, 1984). Reeves (1978) suggests that the "sills" mapped beneath the Okavango delta may in fact be magnetically anomalous basalts. The basalts of northwest Botswana are interpreted as a westward extension of the basalts of northeast Botswana and the basalts of northern Botswana were erupted over Zimbabwean Craton, Ghanzi-Chobe basement and Ntane/Bodibeng sediments alike. The basalts of northeast Botswana are only a part of a large basalt field which includes the Batoka, Hwange (Wankie), Victoria Falls and Nyamandhlovu basalt outliers. The thickness of the lava pile in northern Botswana is very variable where the greatest volumes of basalts are preserved in the NE fault-controlled grabens in northeast Botswana and a minimum thickness of 370m of basalt was intercepted in the borehole P11 which was drilled by Shell Coal in the Nata Sub-basin.

The purplish-grey to brown basalts of northeast Botswana form well defined flows, of up to 50m thick, with amygdaloidal and altered flow tops. The base of flows may be amygdaloidal and fractured and the association between the base of a flow with thin tuffaceous bands was noted by Smith (1984). Ellis (1978) reports the presence of sandy siltstone lenses interbedded with the basalts of northeast Botswana and red siltstone layers were recognised near the top of the lava interval in the core P8 where the adjacent basalts were extremely altered. Rare rhyolites have been identified in the lava field (Smith, 1984). Interpretation of basalt thickness and elevation maps led Ellis (1978) to suggest that the basalts flowed from the north into northeast Botswana.

1.2.3.2.3 The Tuli Syncline

The basalts of the Tuli Syncline in eastern Botswana are referred to as the Bobonong Lava Formation in the literature (Smith, 1984; Aldiss, 1983a & b) and not as the Stormberg basalts as the Tuli lava pile contains distinctive picritic basalt types which are not recognised elsewhere in Botswana and the lower basalt units are interbedded with sedimentary lenses. Vail *et al.* (1969) has described, in detail, the Karoo basalts of the Zimbabwean side of the Tuli Syncline with the succession of picritic basalts overlain by tholeiitic basalts, which is similar to that of the Nuanetsi (Cox *et al.*, 1965). However the rhyolites which in turn overly the tholeiites of the Nuanetsi area have not been recognised in the Tuli Syncline. The lower picritic basalts in Botswana have been referred to as limburgites and olivine-phyric basalts in the literature. These lower picritic basalts are overlain by quartz-normative tholeiites which are grey-green in colour when fresh and alter to a lighter brown colour. Samples analyzed in the Baines Drift area (Coates, 1980) have high K_2O compositions similar to the K_2O-rich basalts in the Tuli Syncline in Zimbabwe (Vail *et al.*, 1969) and in the Nuanetsi area (Cox *et al.*, 1967).

No detailed mapping of the extent of individual lava flows nor detailed geochemical characterisation of the basalts has been undertaken. The thickness of the lava pile is unknown, however greater than 222.5m of basalt is intercepted in a borehole near Bobonong and 249.3m of basalt is intercepted 6km south of the Gobojango fault zone in the vicinity of the only outlier of Bobonong basalt and Tsheung Formation north of the fault zone (Gerrard, 1965). Individual flows are recognised in the field and flow tops are typically highly amygdaloidal. The amygdales are commonly rimmed by green chalcedony and filled with quartz, chlorite, calcite and zeolite. Gerrard (1965) recognised 15-30cm thick tuffaceous layers interbedded with the basalts of the western Tuli Syncline.

The Tuli picritic basalts were erupted over the uneven surface of Tsheung sandstone (the lateral equivalent to the Ntane sandstone) and the lower flows are interbedded with sandstone and limestone layers which are collectively referred to as the Madikama Beds (Smith, 1984). Intercalations of Karoo sediments (of aeolian and fluvial origins) near the base of the lava pile have been recognised in the Central Karoo area (Eales *et al.*, 1984), Etendeka (Erlank *et al.*, 1984) and in the Tuli Syncline of Zimbabwe (Vail *et al.*, 1969). The presence of sandstone lenses led Mason (1967) to suggest the presence of a transitional period between Tsheung deposition and Bobonong basalt eruption, however more detailed studies (Aldiss, 1983b) demonstrated that the Madikama intercalated lenses are often continuous with the Tsheung sandstone and that the basal basalt flows wedge out toward the east beneath discontinuous sandstone lenses. 25-140m above the Madikama Beds the younger Madikolola Member is interbedded with the Tuli basalts and this thin discontinuous

layer often has its upper surface disturbed by pillow lavas. Aldiss (1983b) identifies a sandstone lens in the Matloutse river bed which lies below pillow lava and which maybe a lateral equivalent to the Madikolola Member. No other pillow lavas are reported in Karoo basalts of Botswana.

1.2.3.3 Karoo intrusive rocks

1.2.3.3.1 The dyke swarm

Green (1966) noted that many of the Karoo dolerite dykes in a number of areas in eastern Botswana have a WNW strike, which is either parallel to, or complimentary to the dominant fault strike direction. As many of the dolerite dykes tend to form negative topographic features (Clark and Machacha, 1982) and due to the poor exposure of outcrop in Botswana most of the dolerite dykes are mapped from aerial photographs. The Reconnaissance Aeromagnetic Survey of Botswana (Reeves, 1978) revealed the presence of a well defined dyke swarm, with a strike of N110E, which cuts across northern Botswana from the Namibian to the Zimbabwean borders, a distance of some 800km. The width of the dyke swarm is 110km at 27°E and narrows to a width of 55km at 21°E. The presence of dolerite dykes in the Tuli Syncline of Zimbabwe with a strike of N100E (Vail *et al.*, 1969) suggests that the dyke swarm extends westwards into Zimbabwe. Many of the dolerite dykes of Botswana which are not part of the dyke swarm proper also have, on average, a strike of N110E.

The dolerite dykes tend to have an average strike length of 10 - 20km and Reeves (1978) suggests that individual dykes can be traced, with reasonable certainty, for greater than 100km. The width of these dykes varies from a few centimetres to greater than 500m, but average widths are between 10 - 30m (Aldiss, 1983a & b; Smith *et al.*, 1985). The forms of the dolerite dykes in Botswana range from straight to sinuous and the dolerite dykes are sometimes branched (Aldiss, 1983b). The relationship between dolerite dykes is often fairly complex and several generations of intrusion are observed. Well developed chill margins are commonly developed in the coarser dolerite dykes.. Smith *et al.* (1985) report the presence of partly digested granite xenoliths in dolerite dykes of the Foley area as well as evidence for partial melting of the wall rock adjacent to some of the larger dolerite dykes, which suggests that contamination of at least some of the dolerite dykes may have occurred, and Stansfield noted the presence of xenolithic inclusions of acidic gneisses in the dolerites near the eastern margin of the former Lake Makgadikgadi.

Two dolerite types can be distinguished in the field, a porphyritic and an aphyric type. The porphyritic dolerite tends to be coarser-grained with glomeroporphyritic aggregates of plagioclase (and pyroxene) and a glassy matrix. Porphyritic dolerites with up to 50% of the

rock represented by the phenocryst assemblage are recognised (Aldiss, 1983b). The aphyric dolerites tend to be very fine-grained, black in colour and have an even-grained (Green, 1966) or ophitic (Aldiss, 1983b) texture. The relationship between the two petrographic types is not known, but the porphyritic dolerites are frequently intruded and cut by aphyric dolerite dykes (Green, 1966; Clark and Machacha, 1982).

1.2.3.3.2 Other Karoo intrusive rocks

Although the dominant strike direction of the dolerite dykes in Botswana is WNW parallel to the dyke swarm, dolerite dykes with a range in strike directions are present in eastern Botswana. A number of dolerite dykes have an ENE trend, parallel to the structural trends of the Limpopo Mobile Belt, and others have an approximate E-W trend, parallel to the strike of the Tuli Syncline (Aldiss, 1983b).

Vail *et al.* (1969) reported the presence of rare shoshonite dykes in the Tuli syncline of Zimbabwe and a single shoshonite dyke had previously been recognised in Botswana along the Tuli back line at 29°E (Aldiss,1983a). Six more shoshonite dykes from the Tuli syncline of Zimbabwe and Botswana have been sampled in the present study. The shoshonite dykes of Botswana and Zimbabwe have a strike, where it is possible to measure, which is approximately parallel to the strike of the dyke swarm. The shoshonite KLB-099, sampled in the Semolale area, has a strike of N100E and the shoshonite dyke sampled in Zimbabwe (by courtesy of A.E. Moore) has a ±E-W strike direction.

Two felsite dykes were sampled in the Tuli area during this study. One of the felsite dykes, which is exposed in the Matloutse River bed, had a width of ± 10m and formed a prominent positive topographic feature with a strike of N65E. The second felsite dyke has an approximate N-S strike and is situated ± 1.5km to the SW of the Matloutse River dyke. The felsite dykes are very fine-grained to glassy and include glomeroporphyritic aggregates of feldspar and pyroxene. The felsites are a pale grey colour and difficult to differentiate from fine-grained dolerite dykes in the area. Crocket (1967) also noted the presence of two Karoo "felsic" dykes in the Shashe area. These dykes included blocks of granite and vein quartz and were described as having quartz and altered feldspar phenocrysts set in a devitrified glass matrix. A combination of the petrography and the presence of granite blocks suggests that these felsic dykes are pseudotachylytes and are not of primary igneous origin. Key (1976) also recognised the presence of pseudotachylyte at the contact of some of the dolerite dykes with the country rock.

1.2.3.4 Relative ages

The Stormberg basalts of the Central Kalahari Sub-basin of Botswana are reported as having K-Ar ages of 180±10Ma (after Rundle, 1983 in Smith, 1984), but unfortunately no details of sample location or description were available.

Aldiss *et al.* (1984) and Aldiss (1983a & b) assign the best estimate age 181±4Ma to the Bobonong basalts of the Tuli syncline, but a range in K-Ar ages from 182±6 to 158±4Ma were obtained from seven basalts from three separate localities in eastern Botswana. Rundle (1983) suggests that the younger ages may be due to Ar loss as the younger basalts are correlated with low K_2O concentrations in whole rock compositions. K-Ar ages of 169±4 to 71±2Ma have been obtained for other samples in the Tuli area (whether dolerites or basalts was not stipulated) and these younger ages were also assumed to be the result of Ar loss. Fossil evidence in the Madikolola member (*i.e.* the presence of the fossil pollen *C. intrareticulatis*) give an age of approximately 195 to 200Ma according to present knowledge (Aldiss *et al.*, 1984) and this suggests that the age of 181±4Ma for the Bobonong basalts of the Tuli Syncline may be an underestimate. However, the K-Ar ages of 181±4Ma compare favourably with recent $^{40}Ar/^{39}Ar$ ages of 180±2Ma (Marsh *et al.*, 1995) and 182±2Ma obtained by R.A. Duncan (unpubl. data) for the Lesotho basalts of the Central Karoo area.

As the dolerite dykes are compositionally similar to the surrounding Stormberg basalts they are often assumed to act as feeders to the lava field. However the dolerites are seen to intrude the basalts in a number of places (Green, 1966; Aldiss, 1983a & b) and these dolerite dykes have been interpreted as feeders to basalts lying higher up in the lava pile. The minimum K-Ar ages of two dolerites dykes in east Botswana are 162±3 and 143±3Ma (after Rundle, 1983) and Coates *et al.* (1979) report an age of 140Ma for dolerite dykes of the Swaneng Hill near Serowe (after Rundle, *pers. comm.*). If these younger ages are correct then the dolerites may post date the basalts and, if this is true, are unlikely to be feeders to the basalts of Botswana as has been previously assumed.

1.2.4 KALAHARI BEDS

The term "Kalahari Bed" was introduced by Boocock *et al.* (1962) as an informal lithostratigraphic term to encompass all Tertiary to Quaternary sediments in the Kalahari basin. Cahen *et al.* (1952) recognised that the Kalahari Syncline, an elongated basin with a long synclinal axis with a northerly strike, is made up of a number of smaller basins and it is not known if they all have a uniform history. The sediments of the Kalahari Sub-basin in Botswana reflect the changes in climate from the Tertiary to the present time and the

general chronological sequence of the dominant climate condition, in decreasing age, is accepted as arid, humid, semi-arid, humid and finally semi-arid (Coates *et al.*, 1979). Most of the Kalahari is now vegetated and aeolian sand is found only in local dune fields (Green, 1966).

Ancient shorelines are evidence for the presence of an extensive lake, the former Lake Makgadikgadi, in the north of Central Botswana. Numerous playa-type pans, particularly along the southern margin of Lake Makgadikgadi, are the remnants of the former lake. Furthermore, pans which occur as either small interdune pans or along fossil drainage lines, *e.g.* the Deception and Passarge Mekgachas, are also preserved in the Kalahari Beds (Coates *et al.*, 1979).

1.2.5 HYDROLOGY

The composition of the water in the Karoo basalts of Botswana is very variable and they are reported to range from being fresh to saline to rich in sulphates, however the water is typically fresher in compact and undisturbed basalts (Coates *et al.*, 1979). The basalts, however, tend to develop a secondary permeability along altered flow tops and along joints and fractures. Mazor *et al.* (1977) demonstrated a hydraulic continuity between saline aquifers, basalts and the Ntane Formation sandstones along these paths of secondary permeability.

1.3 AIMS AND OBJECTIVES OF THIS STUDY

As no previous detailed geochemical studies are available in the literature for the Karoo igneous rocks of Botswana, this thesis concentrates essentially on the recognition and definition of these rock types.

The principle aims of this study can therefore be summarised as follows:

(1) To describe the geochemistry of the various Karoo igneous rocks of Botswana
(2) To evaluate geochemical variations within and between the different Karoo igneous rock types of Botswana
(3) To compare the Botswana data with that for other Karoo igneous rocks
(4) To consider the distribution of the different geochemical rock types in Botswana and suggest correlations between the Botswana units and the stratigraphic relationships elsewhere in the Karoo Igneous Province
(5) To investgate the petrogenesis of the various geochemical rock types of Botswana in

the context of petrogenetic models for equivalent Karoo igneous rock types

(6) To assess the significance of the Botswana data in relation to the present views associated with the petrogenesis of the Karoo Igneous Province in general

As this thesis can be only a reconnaissance study, a further objective of the present investigation is to highlight areas which clearly require more detailed work in the future.

1.4 THE SAMPLE COLLECTION

The complete sample collection used during this study is assembled from four major sources, which include a pre-existing sample set, samples collected in the field area in eastern Botswana, basalt cores from the Geological Survey of Botswana and drill chips from De Beers Prospecting, Botswana (PTY) Limited.

The pre-existing sample set of 70 samples were collected in Botswana and the Tuli area of Zimbabwe for the Department of Geological Sciences at UCT between 1987 and 1991. The basalt interval within ten separate boreholes was logged and 100 basalt samples were collected at the core sheds of the Geological Survey of Botswana. Only four of the one hundred basalt samples collected from drill chips, of 24 separate boreholes, stored in the core sheds of De Beers Prospecting, Botswana, have been used during this study. A field trip to the Tuli Syncline and the eastern edge of the Dyke Swarm resulted in the addition of thirty-three intrusive and eight extrusive samples to the collection.

The full details of the sample type, character and location, together with the logs of the individual boreholes, are included in APPENDIX A and the distribution of rock types and their outcrop character are discussed in more detail in the appropriate chapters.

2 DEFINITION OF GEOCHEMICAL GROUPS

2.1 INTRODUCTION

The primary aim of this chapter is to define geochemical groups within the dataset now available for the lavas and dykes in Botswana which are of a presumed Karoo age. These geochemical groups are defined in order to facilitate the more detailed discussion that follows and they do not necessarily have any genetic implications. A number of different geochemical classification schemes have been adopted during this study and they follow, as closely as is appropriate, the schemes previously defined in the literature for the Karoo Igneous Province. A preliminary consideration of rock compositions, where the compositions are normalised to a 100% on a volatile-free basis, is required to define the geochemical groups, but a more detailed interpretation of the data will form part of subsequent chapters.

2.2 CLASSIFICATION INTO MAJOR GEOCHEMICAL TYPES

Bristow and Cox (1984) and Duncan *et al.* (1984a) in their classification of rocks comprising the Karoo Igneous Province use the SiO_2 and MgO concentrations and the degree of silica saturation to distinguish between mafic, felsic and nephelinitic rock types. Their classification scheme is here applied to both the extrusive and intrusive Karoo igneous rocks of Botswana. The SiO_2 concentration is used to make the first primary division and defines two major geochemical groups (see Fig. 2.1), a high SiO_2 felsic group (>60% SiO_2) and a low SiO_2 mafic group (<60% SiO_2). The two samples which contain >60 wt% (weight percent) SiO_2 are subsequently referred to as felsites.

The majority of the low SiO_2 mafic rocks (*i.e.* with <60 wt% SiO_2) are tholeiitic in character, with hypersthene in the norm (Yoder and Tilley, 1962), as seen in the basalt quadrilateral in Fig. 2.2 and have low total alkali (Na_2O + K_2O) concentrations (Kuno, 1968). The CIPW norms were calculated using an assumed Fe_2O_3/FeO ratio of .15 (Brooks, 1976 and Cox, Bell and Pankhurst, 1979) on data normalised to 100% on a volatile-free basis. The mafic rocks show a variation from being Si-oversaturated (hypersthene-quartz) to Si-undersaturated (nepheline-olivine), with the majority of the samples being quartz-hypersthene normative (see Fig. 2.2).

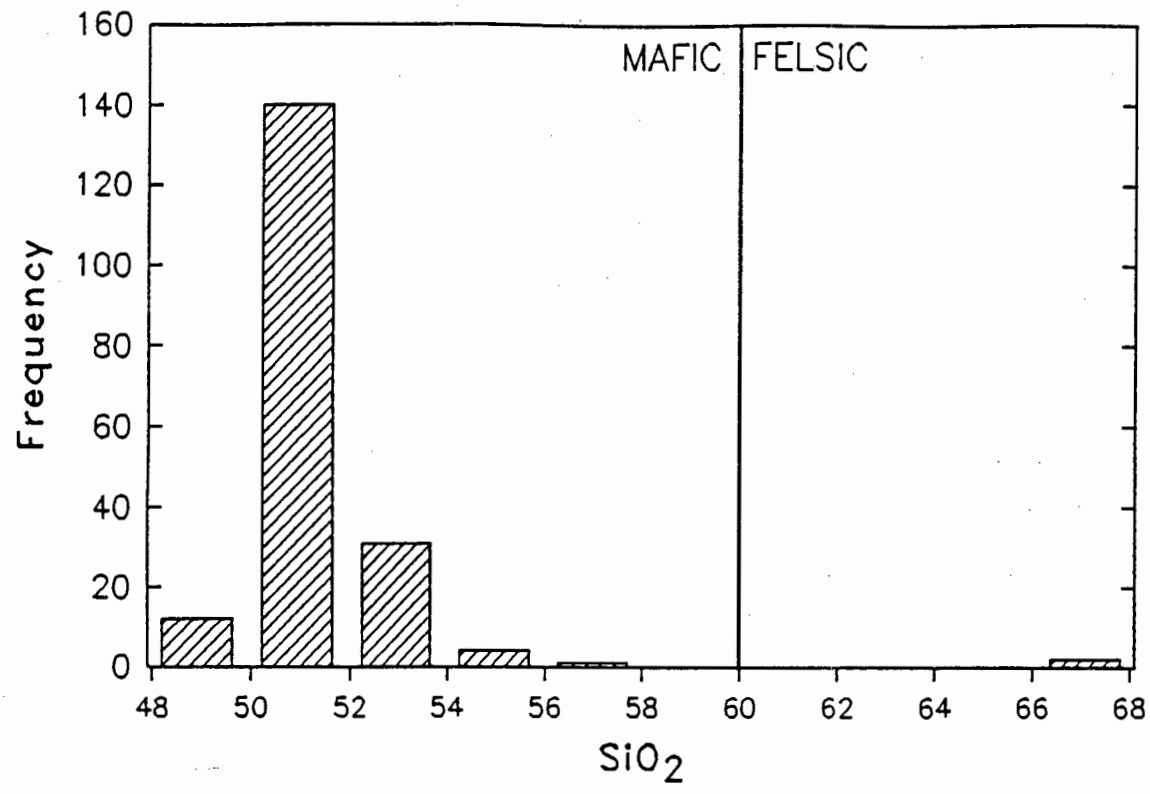

Fig. 2.1. The SiO_2 histogram demonstrating the bimodal distribution of the Botswana data with respect to the SiO_2 concentration.

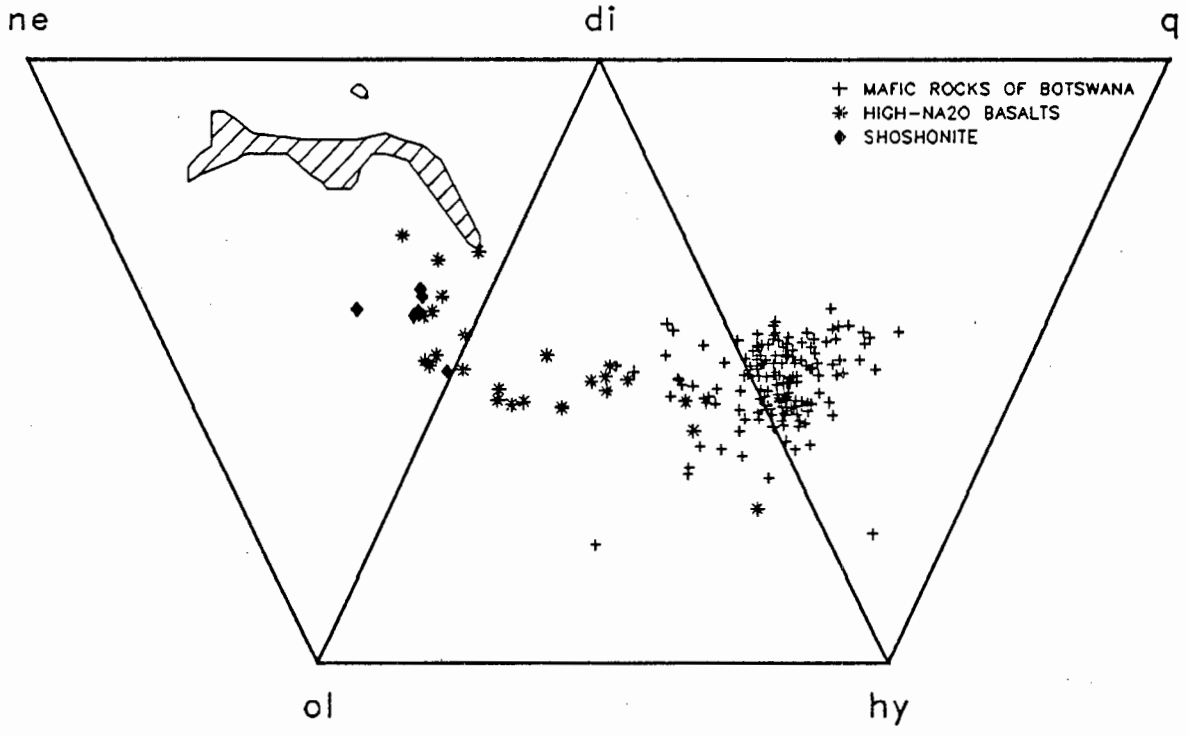

Fig. 2.2. The CIPW norm compositions of the Botswana mafic rocks, including both the high Na_2O basalts and shoshonites defined in later sections, plotted in the basalt quadrilateral. The shaded area represents the normative composition of the Northern Lebombo and Nuanetsi nephelinites (after Bristow, 1984a).

The samples with nepheline in the norm (see Fig. 2.2) are not, by definition, tholeiitic and according to the classification scheme of Bristow and Cox (1984) those samples with >5% normative nepheline would be classified as nephelinites although the Botswana samples with nepheline in the norm have a normative mineral composition which is distinctly different to that of the nephelinites of the Northern Lebombo and Nuanetsi areas (see the shaded field in Fig. 2.2). However the degree of Si-saturation in a norm calculation is strongly influenced by the amount of SiO_2, Na_2O and K_2O present in the whole rock analysis and as the amount of (Na_2O + K_2O) increases, so does the degree of Si-undersaturation (Cox, Bell and Pankhurst, 1979).

In Fig. 2.3 (MgO *vs.* Na_2O) a group of tholeiites (KLB-011, 017, 018, 048, 055, 117, 165, 170-175, 185-187, 195, 197-199, 206-209) are shown to contain anomalously high Na_2O concentrations in comparison to the remaining mafic rocks of similar MgO concentrations. This group of high-Na_2O basalts account for some of the nepheline-normative mineral compositions as well as for a large proportion of the range in normative mineralogy away from the quartz-normative triangle in Fig. 2.2.

Following the classification scheme of Bristow and Cox (1984) the Karoo mafic rocks of Botswana are further subdivided into geochemical types according to their MgO and K_2O concentrations (see the geochemical fields defined by the MgO and K_2O concentrations in Fig. 2.4). The whole rock compositions of the mafic rocks of Botswana define two distinct groups in Fig. 2.4 according to their K_2O concentrations, *i.e.* the high-K_2O and low-K_2O lineages.

The high-K_2O lineage includes both picritic basalts (with >9 wt% MgO) and evolved basalts (with between 2-5 wt% MgO). The high-K_2O, high-MgO samples are subsequently referred to as the high-K_2O picritic basalts, while the high-K_2O, low-MgO samples are defined as shoshonites according to the Bristow and Cox (1984) classification scheme (see Fig. 2.4). These high-K_2O shoshonites account for the remaining nepheline normative compositions of the Karoo mafic rocks of Botswana (in addition to the high-Na_2O LTZ basalts above).

The remaining Karoo mafic rocks of Botswana therefore belong, by definition, to the low-K_2O lineage, although the low-K_2O lineage exhibits a variation in the K_2O concentration from concentrations typical of the low-K to the intermediate-K fields defined by Bristow and Cox (1984) in Fig. 2.4. The low-K_2O lineage can be subdivided further according to their MgO concentrations into picritic basalts (with >9 wt% MgO), basalts (with between 5-9 wt% MgO) and evolved basalts (with between 2-5 wt% MgO). The division proposed by Bristow and Cox (1984) between basalts and evolved basalts at 5% MgO has been retained,

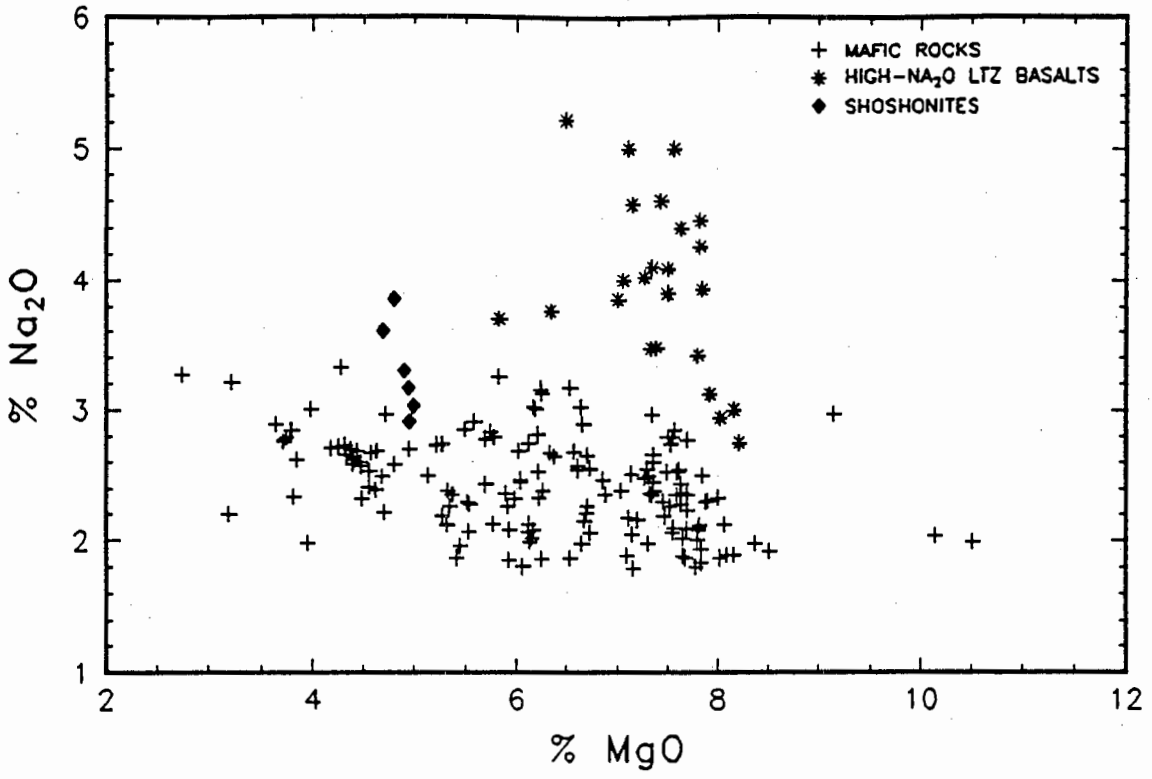

Fig. 2.3. MgO *vs.* Na_2O for the mafic rocks of Botswana which contain <12% MgO. The high-Na_2O basalts are defined in the text.

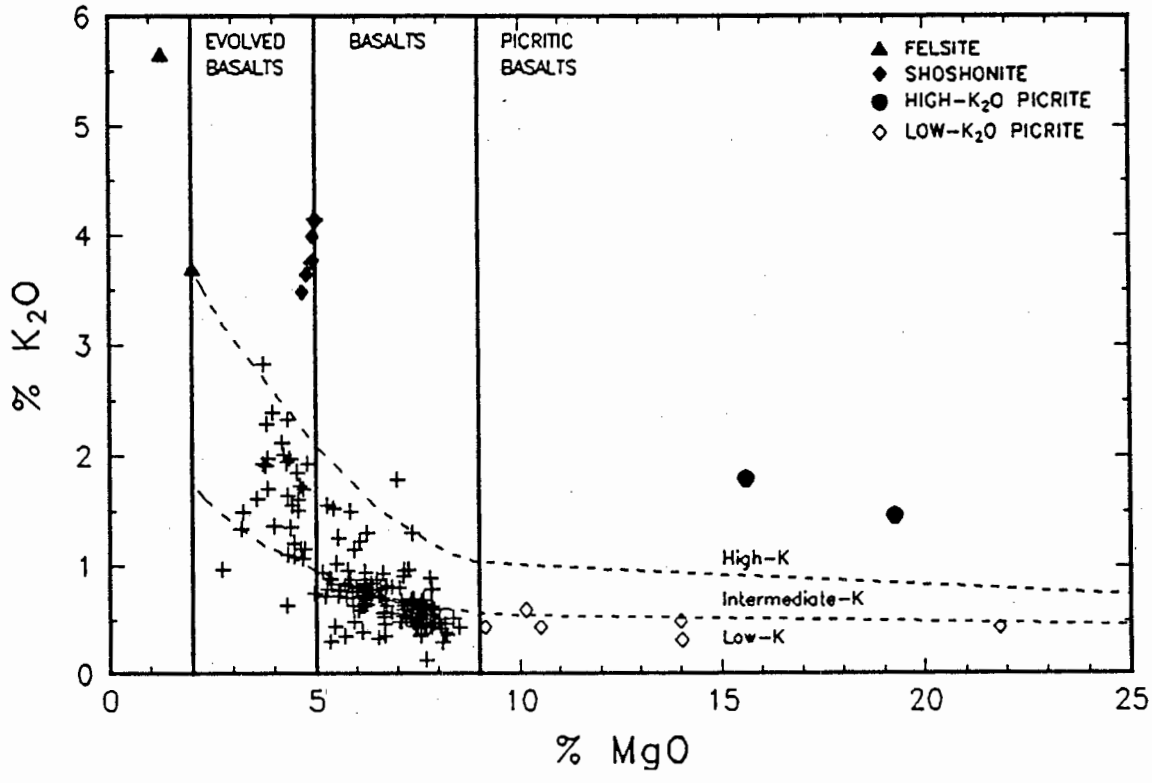

Fig. 2.4. The Botswana data plotted in the MgO-K_2O classification diagram after Bristow and Cox (1984).

initially, for the Botswana data as below 5% MgO the compositions of the mafic rocks of the low-K_2O lineage changes from a predominantly low-K to an intermediate-K type K_2O concentration according to the fields defined by Bristow and Cox (1984) in Fig. 2.4.

Three major geochemical sub-groups are therefore recognised in the Botswana data on the basis of their SiO_2, MgO and K_2O concentrations; *i.e.* the felsites, the high-K_2O lineage (which includes the shoshonites and the picritic basalts) and the low-K_2O lineage (which includes picrites, basalts and evolved basalts). At this point the low-K_2O lineage must be looked at in more detail as the mafic rocks which define this lineage are characterised by a considerable range in character and geochemistry.

2.3 LOW-K_2O LINEAGE

2.3.1 DEFINITION OF GROUPS WITHIN THE LOW-K_2O LINEAGE

This section will deal exclusively with the classification of all the Karoo mafic rocks from Botswana (*i.e.* picritic basalts, basalts and evolved basalts) which define the low-K_2O lineage in Fig. 2.4.

2.3.1.1 Background

Cox *et al.* (1967) first noted that two distinct geochemical varieties of basalt could be recognised within the Karoo Igneous Province. They defined a northern or "enriched" basalt type, which showed a relative enrichment in TiO_2, K_2O, P_2O_5, Ba, Sr, Zr, Nb, Y and LREE (Light Rare Earth Elements) when compared to the southern or "normal" basalt type at similar MgO concentrations. All of these elements are "incompatible" (*i.e.* have low bulk-D values) in basalt melting and fractionation processes. The "enriched" basalts also display a relative depletion in CaO and Al_2O_3 when compared to the "normal" basalts and this apparent depletion in CaO and Al_2O_3 has been used to explain the difference in the order of crystallization between the two basalt types. The order of crystallization in the "normal" basalts is typically spinel-olivine-plagioclase-augite (*e.g.* Walker and Poldervaart, 1949; for the Lesotho basalts), whereas for the "enriched" basalts the order of crystallization is typically olivine-augite-plagioclase ± apatite (*e.g.* Cox *et al.*, 1967; for the Nuanetsi area). This difference in order of crystallization has a marked effect on the overall texture which is predominantly an intergranular texture in the "enriched" basalts, while in the "normal" basalts the texture is predominantly sub-ophitic.

Subsequent studies (Erlank *et al.*, 1988; Sweeney, 1988) have used TiO_2, Zr and Y as the most suitable of the incompatible elements for distinguishing between the "enriched" and

"normal" basalt types as these elements are least affected by late stage processes such as alteration. The terms "enriched" and "normal" have genetic implications and so the terms HTZ (high TiO_2 and Zr) and LTZ (low TiO_2 and Zr) were defined using the TiO_2 - Zr bivariate plot and the expressions HTZ and LTZ replaced the terms "enriched" and "normal" respectively. The HTZ basalts are typically characterised as having >2.5% TiO_2, >250ppm Zr, a Zr/Y ratio of >6 and a Ti/Y ratio >400 and the LTZ basalts as having <2.5% TiO_2, <250ppm Zr, a Zr/Y ratio of <6 and a Ti/Y ratio <400 (Erlank *et al.*, 1990).

HTZ basalts have been recognised in the Northern Lebombo (Cox and Bristow, 1984 and Sweeney, 1988), Nuanetsi (Cox *et al.*, 1967) and Springbok Flats areas (Eales *et al.*, 1984). The LTZ basalts have been recognised in the Central Karoo area (Marsh and Eales, 1984), the Southern Lebombo (Sweeney, 1988), Springbok Flats (Eales *et al.*, 1984) and in the Mariental area of Namibia (Eales *et al.*, 1984). The recognition of LTZ basalts in northern Botswana, Zimbabwe, Zambia (Ridgway *et al.*, 1981) and Malawi (MacDonald *et al.*, 1983) led Cox (1988a) to amend his initial classification to include a zone of LTZ basalts and dolerites in the extreme north of the Karoo Igneous Province.

2.3.1.2 Classification of the Botswana data

As the TiO_2 - Zr bivariate plot was used to define the terms HTZ and LTZ in the literature, the initial classification of the Botswana low-K_2O lineage data was made according to these criteria (see previous section). In Fig. 2.5 TiO_2 *vs.* Zr is plotted for the mafic rocks of the low-K_2O lineage (Fig. 2.5A) together with the TiO_2 - Zr bivariate plots for the Central Lebombo (Fig. 2.5B), Northern Lebombo, Nuanetsi and Tuli regions (Fig. 2.5C) in order to facilitate the comparison between the different areas. According to generally accepted classification schemes (*e.g.* Erlank *et al.*, 1990) both HTZ and LTZ basalt and dolerites types are present in Botswana. As the Botswana data defines an apparently continuous trend (see Fig. 2.5A) from LTZ- to HTZ- type compositions, this required the definition of an additional geochemical group to include the compositions intermediate to the fields defined by the LTZ- and HTZ-type basalts. The new geochemical group is defined as having an HTLZ (high-TiO_2 and low Zr) signature.

The accepted 2.5% TiO_2 cut-off between LTZ and HTLZ/HTZ geochemical signatures divides the Botswana data midway through an apparently continuous trend, which suggests that the division at 2.5% TiO_2 is inappropriate in the classification of the Botswana data. Examination of the Botswana data demonstrated that a natural division in the geochemistry of the mafic rocks exists, such that all tholeiitic basalts with >2% TiO_2 are compositionally distinct from basalts which contain <2% TiO_2, although this is not apparent in Fig. 2.5A alone. The initial classification of the Botswana data into three geochemical groups is

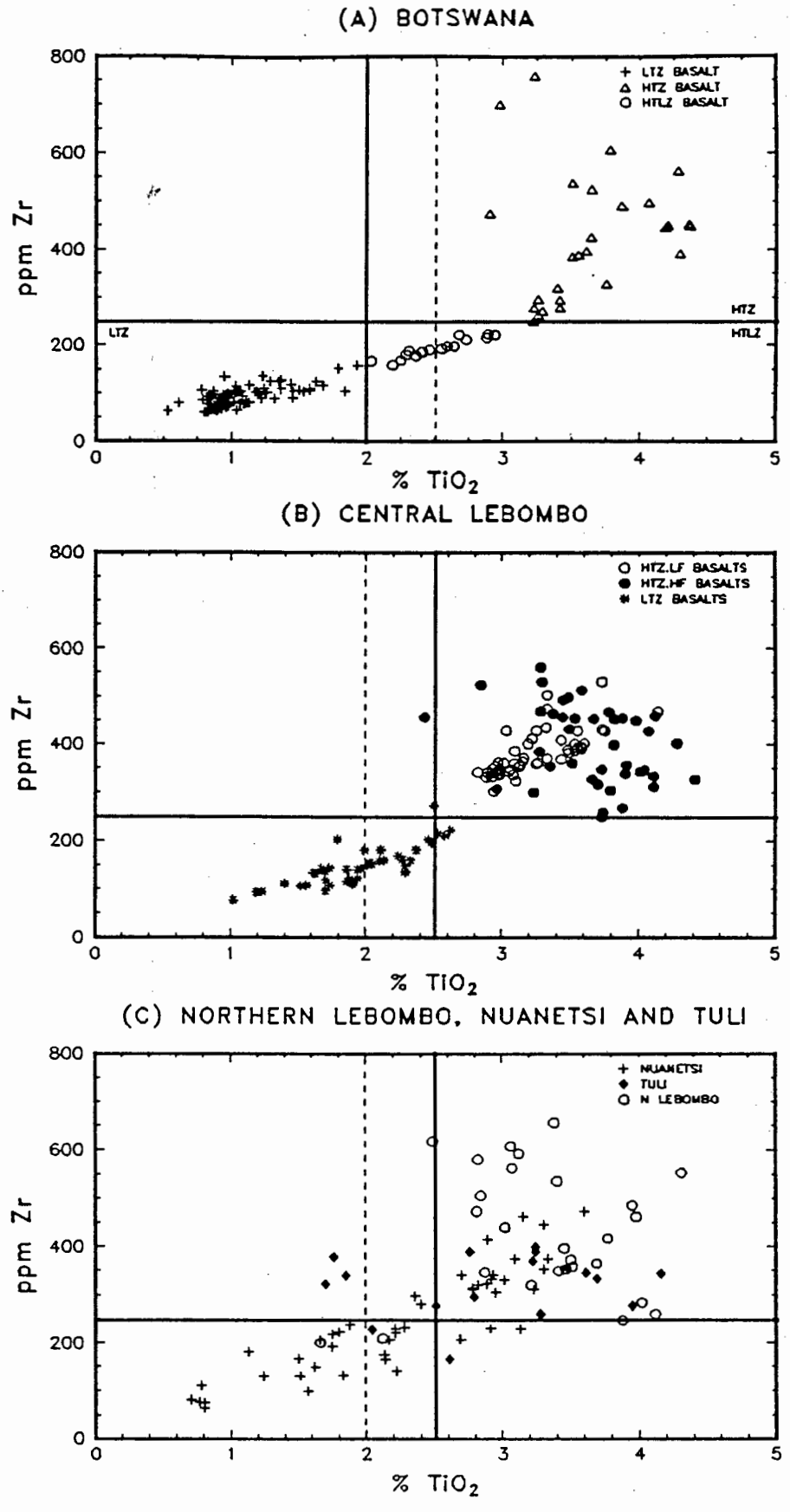

Fig. 2.5. TiO_2-Zr classification diagrams

(A) The solid lines depict the TiO_2 and Zr concentrations, defined during this study, used to classify data into LTZ-, HTLZ- and HTZ-type basalts. The dashed line is plotted according to classification schemes used in the literature (Erlank *et al.*, 1990).

(B) and (C) The solid lines represent TiO_2 and Zr concentrations after Erlank *et al.* (1990). The dashed line represents the TiO_2 content used for the classification of the Botswana data.

therefore summarised in Fig. 2.5A, with TiO_2 and Zr values of 2% and 250ppm, respectively, defining the LTZ-, HTLZ- and HTZ-quadrants. The LTZ basalts and dolerites of Botswana are recognised as containing <2% TiO_2 and <250ppm Zr while the HTZ have >2% TiO_2 and >250ppm Zr. The samples which then have >2% TiO_2 but <250ppm Zr are defined as belonging to the HTLZ group.

As fractional crystallization of tholeiitic basalts is typically accompanied by an increase in the TiO_2 concentration with continued fractionation, Mg# *vs.* TiO_2 (see Fig. 2.6) was plotted to illustrate the possible effect of low pressure fractionation on the Botswana mafic rocks. The parallel trends defined by the LTZ and HTLZ/HTZ basalts (see Fig. 2.6) demonstrates that the range in TiO_2 concentrations cannot be explained by simple low pressure fractionation from a single parent and that the division between LTZ and HTLZ/HTZ basalt types at 2% TiO_2 is justified.

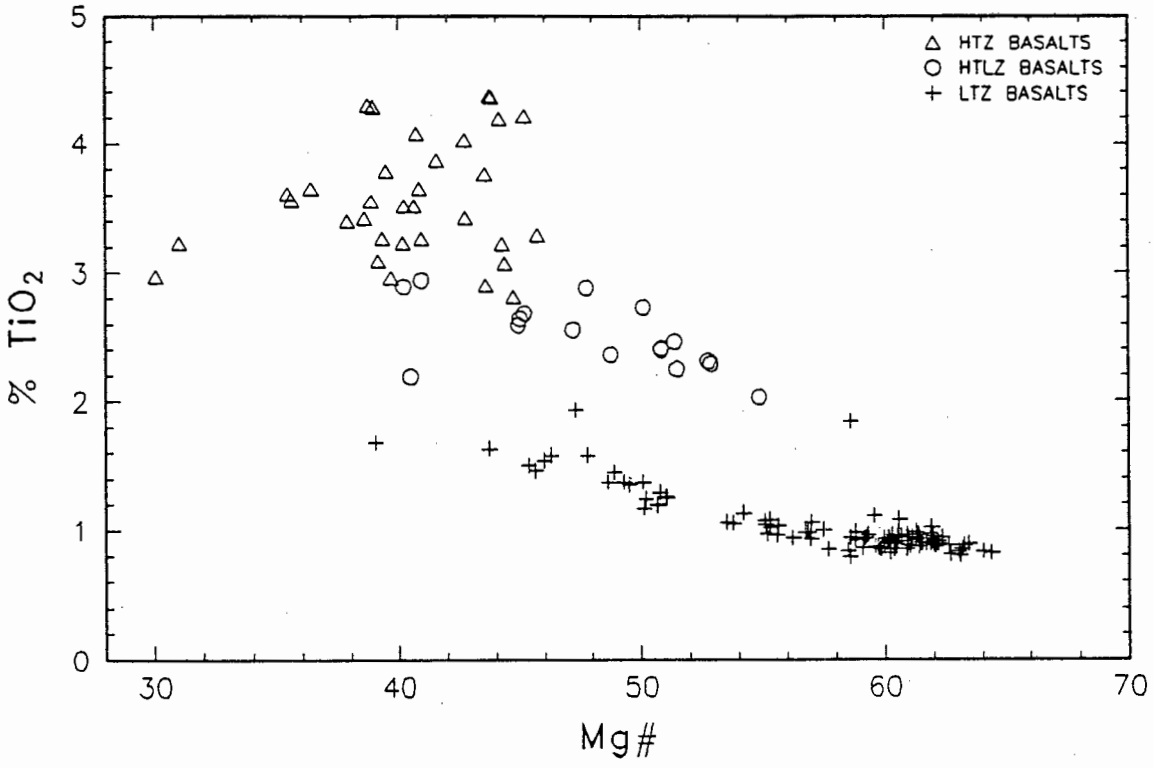

Fig. 2.6. Mg# *vs.* TiO_2 for the Botswana mafic rocks which contain <9% MgO. The geochemical groups are defined according to Fig. 2.5A.

The low-K_2O Karoo mafic rocks of Botswana have been defined as LTZ-, HTLZ- and HTZ-type basalts according to their TiO_2 and Zr concentrations only, however they can also be classified into the same geochemical groups by all TiO_2, Zr and Y inter-element ratios. In Fig. 2.7 Zr is plotted against Y for the Botswana data (Fig. 2.7A), the Central Lebombo (Fig. 2.7B) and the Northern Lebombo, Nuanetsi and Tuli areas (Fig. 2.7C). In Fig. 2.7A the line representing the Zr/Y ratio of 6 is plotted and according to the literature (Erlank

et al., 1990) all basalts with a Zr/Y ratio >6 are defined as HTZ basalts and all basalts with a Zr/Y ratio <6 are LTZ basalts by definition. In Fig. 2.7A the field defined by the Zr/Y ratio for the HTLZ basalts is seen to lie, once again, between the fields defined by Zr/Y ratios of the HTZ and LTZ basalts.

2.3.1.3 Comparison to other areas in the Karoo Igneous Province

2.3.1.3.1 Introduction

A problem with any geochemical classification scheme is that it employs only a small subset of element abundances or interelement ratios to define groups of rocks of supposedly different geochemical affinities. The Karoo mafic rocks of Botswana which define the low-K_2O lineage have proved to be an excellent example of the deceptiveness of such a tool. Although the mafic rocks which classified as HTZ- (and HTLZ-) type basalts in Botswana have elevated levels of TiO_2 and Zr (see Fig. 2.5A) and Zr/Y ratios >6 (see Fig.2.7A) and are therefore "enriched", they are defined in Fig. 2.4 as having a low-K to intermediate-K type composition and therefore correspond to the low-K_2O lineage. The HTZ (or "enriched") basalts of the "Northern Province", as defined by Cox *et al.* (1967), show a characteristic enrichment in their K_2O content relative to LTZ basalts of comparable MgO concentrations from the same area. The low K_2O concentrations suggest that the HTZ basalts of Botswana do not display all aspects of the characteristic HTZ or "enriched" signature as described by Cox *et al.* (1967). It has, however, been noted that the "enriched" and "normal" basalt compositions of the Etendeka and Paraná area cannot be differentiated by their K_2O concentrations (Erlank *et al.*, 1988).

The basalts of the Central Lebombo are known to display the characteristic HTZ- and LTZ-type behaviour and the geochemistry of the different basalt types is well documented (Sweeney, 1988; Sweeney *et al.*, 1994). The basalts of the Central Lebombo are compared to the Botswana data so that deviations of the Botswana data from characteristic geochemical behaviour can be recognised. The data of the Northern Lebombo, Nuanetsi and Tuli areas is also included for comparison, although these basalts do not display the discrete compositional fields recognised in the Central Lebombo. Three major geochemical groups are recognised within the tholeiitic basalts and their intrusive equivalents in the Central Lebombo (Sweeney, 1988; Sweeney *et al.*, 1994). The three geochemical sub-groups are defined as the LTZ (low TiO_2 (<2.7%) and low Zr (<250ppm)), the HTZ.LF (High TiO_2 (>2.5%) and Zr (>250ppm) and low total Fe_2O_3 (generally <13.5%)) and the HTZ.HF (high TiO_2 (>2.5%) and Zr (>250ppm) and high total Fe_2O_3 (generally >14.5%)) basalt types. In Fig. 2.7B the average Zr/Y ratios for the three different geochemical groups are plotted, with the LTZ basalts having an average Zr/Y ratio of 4, the HTZ.HF basalts an average Zr/Y ratio of 7 and the HTZ.LF basalts an average Zr/Y ratio of 10.

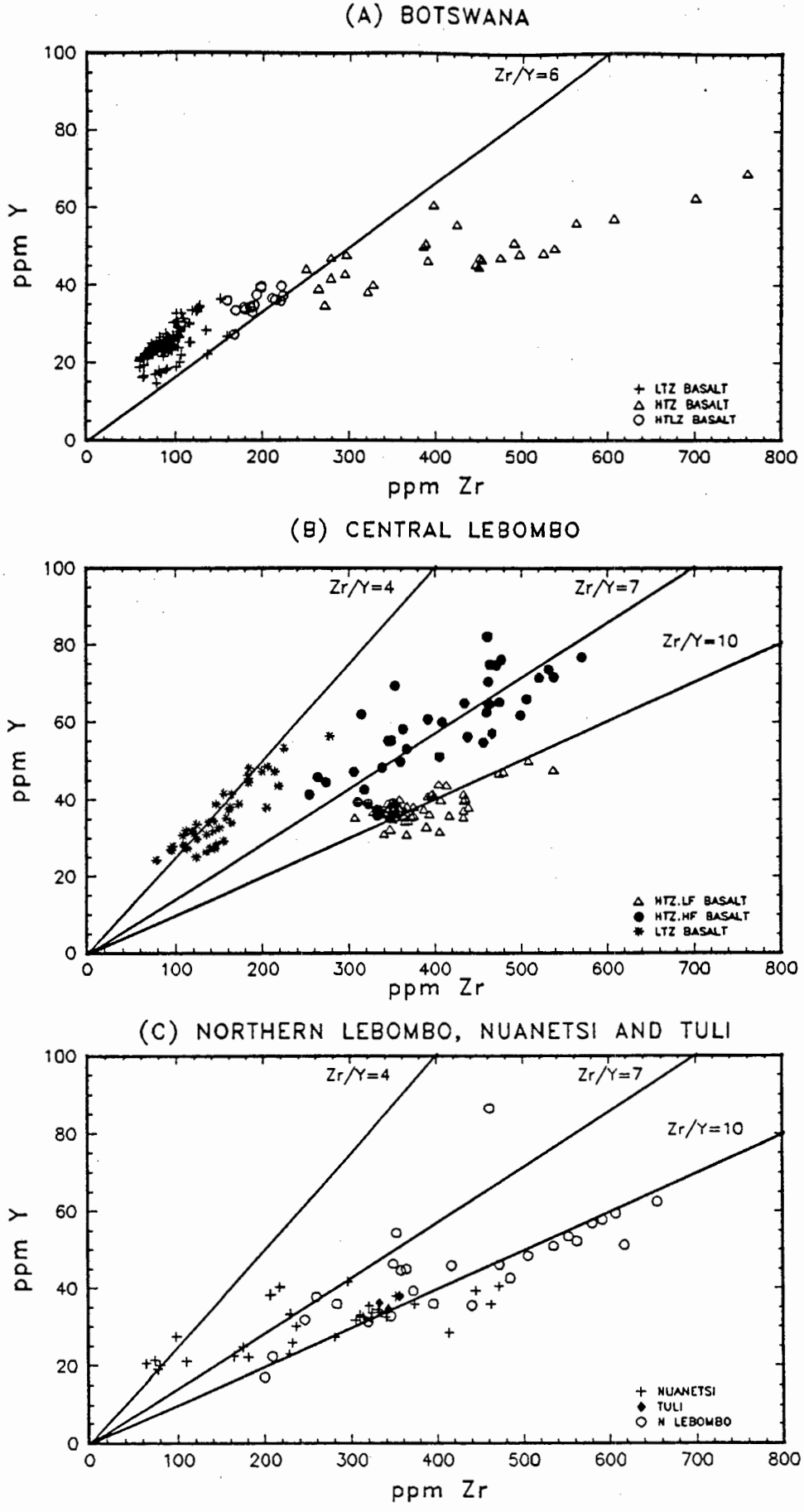

Fig. 2.7. Zr *vs.* Y bivariate plots for Botswana, the Central Lebombo and the Northern Lebombo, Nuanetsi and Tuli areas. The Zr/Y ratios are described in the text.

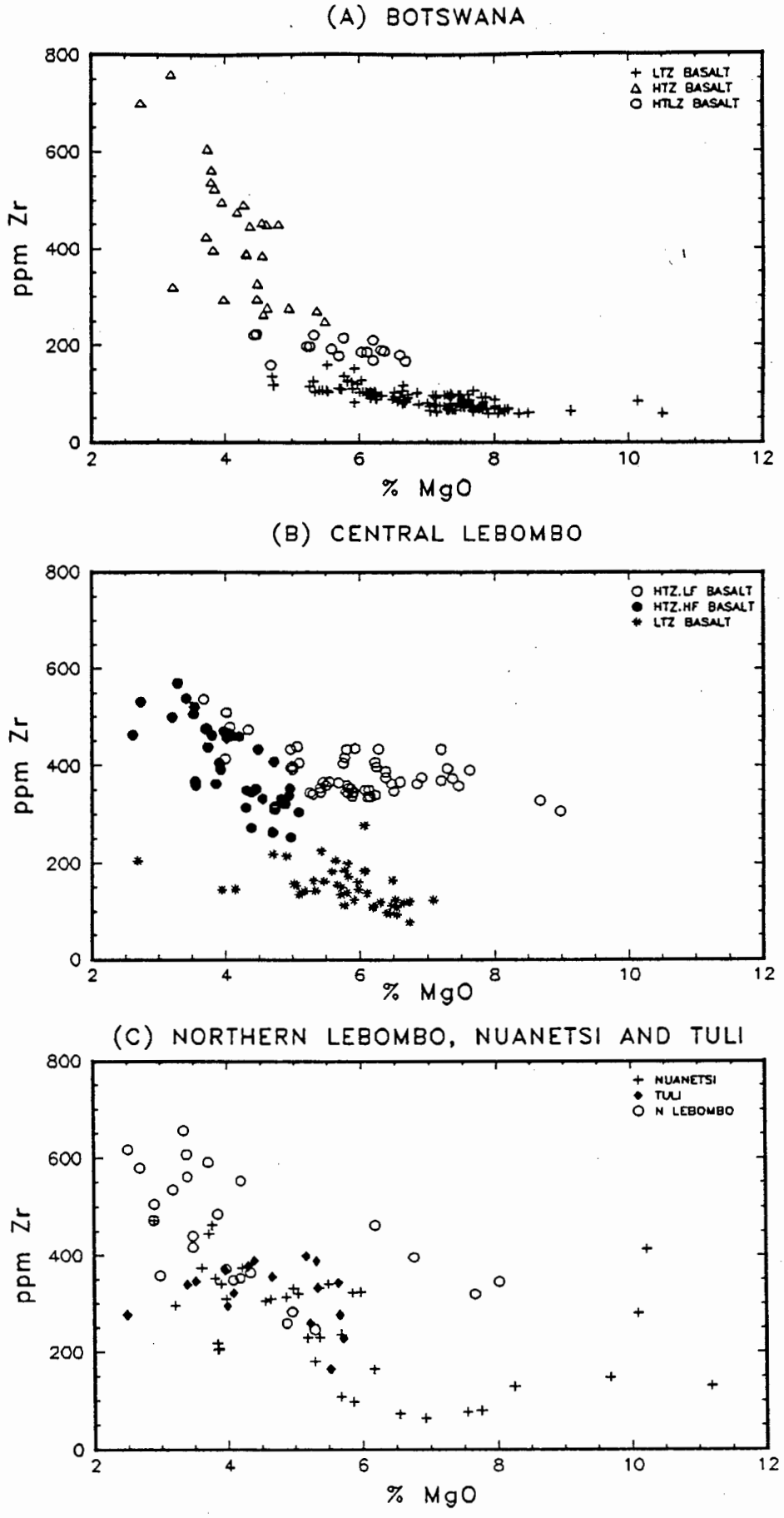

Fig. 2.8. MgO *vs.* Zr bivariate plots for Botswana, the Central Lebombo and the Northern Lebombo, Nuanetsi and Tuli areas.

2.3.1.3.2 A comparison between the Karoo basalts of Botswana and those of the Lebombo, Nuanetsi and Tuli areas

In the TiO_2 - Zr bivariate plot (Fig. 2.5A) the Botswana mafic rocks define a continuous trend from the LTZ-, through the HTLZ- into the HTZ-quadrant. This continuous range in compositions defined by the Botswana data is comparable to the compositional range shown by the data for the Northern Lebombo, Nuanetsi and Tuli and is, in contrast, very different to the discrete HTZ - LTZ compositional fields defined by the basalts of the Central Lebombo (Fig. 2.5B). In addition, no HTLZ-type basalts have been recognised in the Central Lebombo.

In Fig. 2.7 (Zr *vs.* Y) the different basalt types of the Central Lebombo defined three clearly distinct trends (Fig. 2.7B) and, in contrast, the different geochemical groups of Botswana are not characterised by unique Zr/Y ratios (see Fig. 2.7A). The LTZ basalts of Botswana have an average Zr/Y ratio of 3.41, but the value of the Zr/Y ratios varies from 2.85 to 5.90. The HTZ- and HTLZ- basalts and dolerites are characterised by an almost continuous range in Zr/Y ratios, which increase from the HTLZ basalts (Zr/Y ratio varies from 4.41 to 6.15, average Zr/Y=5.45) to the HTZ basalts (Zr/Y ratio varies from 5.62 to 11.16, average Zr/Y=8.40). The data for the Northern Lebombo, Nuanetsi and Tuli areas appears, yet again, to be more similar to the Botswana data in that no separate fields are defined by the Zr/Y ratios of the different geochemical groups, but this may be due to the scatter and scarcity of the data available.

One of the most important attributes of the HTZ-type basalts is that they are enriched in incompatible elements when compared to LTZ basalts of comparable MgO concentrations. In Fig. 2.8 Zr is plotted *vs.* MgO for the mafic rocks of Botswana (Fig. 2.8A), the Central Lebombo (Fig. 2.8B) and the Northern Lebombo, Nuanetsi and Tuli areas (Fig. 2.8C). A comparison between the three diagrams reveals the difference in behaviour of the Botswana LTZ- and HTZ-type basalts when compared to typical "normal" - "enriched" behaviour reported in the literature for the Karoo Igneous Province. The HTZ basalts of Botswana are all evolved (with <5.5% MgO) and display a considerable range in major and trace element concentrations and are characterised by a marked incompatible element enrichment relative to the LTZ- and HTLZ-type basalts of Botswana (see Fig. 2.8A). The HTZ basalts of Botswana are therefore broadly comparable with the HTZ.HF basalts of the Central Lebombo (see Sweeney *et al.*, 1994), in that both of these groups are evolved (*i.e.* typically with <5% MgO) and as neither group exhibits a characteristic HTZ-type signature, which is exemplified by the HTZ.LF type basalts of the Central Lebombo (Fig. 2.8B) and the HTZ-type basalts of the Northern Lebombo, Nuanetsi and Tuli areas (Fig. 2.8C).

The HTLZ basalts and dolerites lie at the primitive end of the trends defined for all major and trace elements *vs.* MgO of the mafic rocks with an HTZ- and HTLZ-type signature (*e.g.* see Fig. 2.6 and Fig. 2.8A). Although the HTLZ basalts and dolerites are enriched in some elements (*i.e.* TiO_2, P_2O_5, Sr, Nb and Zr) when compared to the LTZ-type basalts of similar MgO concentrations in Botswana (illustrated by Zr *vs.* MgO in Fig. 2.8A), the extent of enrichment is insignificant when contrasted with, for example, the HTZ.LF basalts of the Central Lebombo, which clearly display a marked enrichment in incompatible elements (see Zr in Fig. 2.8B) when compared to the LTZ basalts of the Central Lebombo.

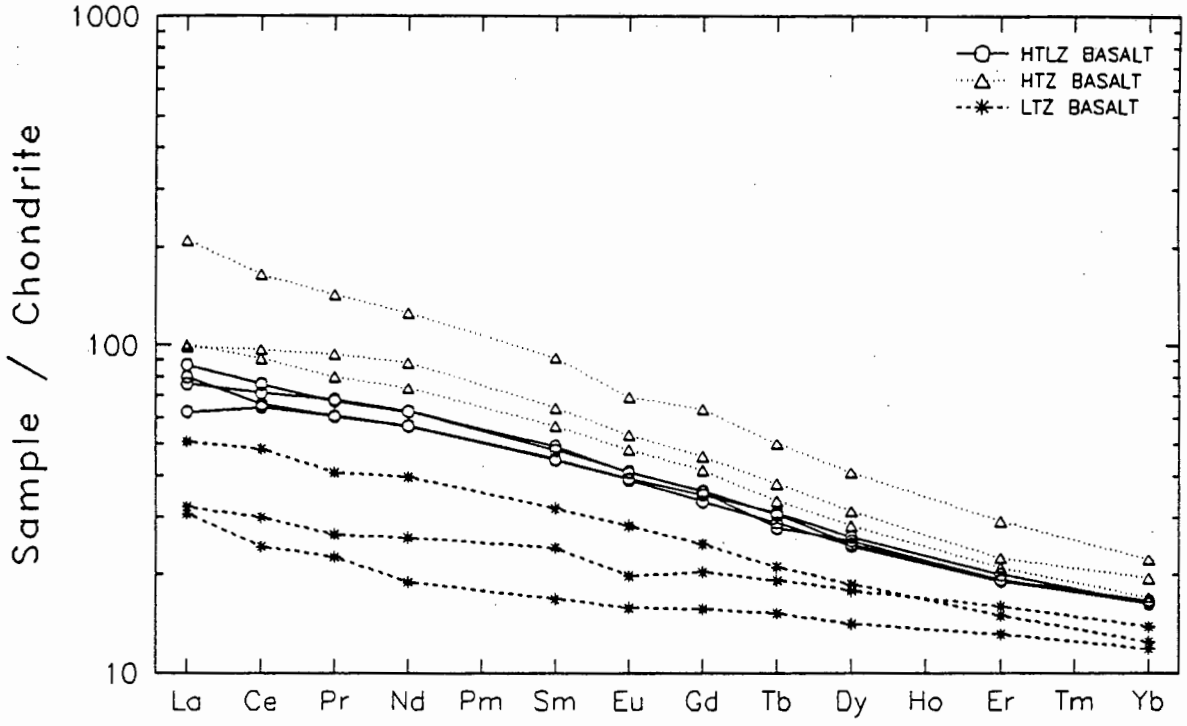

Fig. 2.9. The chondrite normalised REE concentrations for the low-K_2O lineage mafic rocks.

The REE (Rare Earth Element) patterns described by the Botswana data reflect the difference in the Botswana data compared to classical HTZ - LTZ type behaviour. The REE patterns of the Central Lebombo, Northern Lebombo, Springbok Flats and Nuanetsi are characterised by the HTZ basalts (*i.e.* the HTZ.LF basalt type for the Central and Northern Lebombo) defining a REE pattern with a significantly steeper slope in comparison to the REE pattern of the LTZ basalts from the same area (Erlank *et al.* 1990). In the Central Lebombo the HTZ.LF basalts have LREE (light REE) element concentrations of 150-200X chondritic in comparison to the 30-50X chondritic concentrations of the LREE in the LTZ basalts and both the HTZ.LF and LTZ basalts have HREE (heavy REE) concentrations of approximately 10X chondritic (Sweeney, 1988). The REE data of the mafic rocks of Botswana (see Fig. 2.9) display a progressive increase in REE concentrations (both LREE and HREE) from LTZ through HTLZ to HTZ basalt types, although the

LREE do display a greater level of enrichment when compared to the HREE. The basalts of Botswana show a range in LREE concentrations from approximately 20X chondritic in the LTZ basalts to approximately 200X chondritic concentrations in the HTZ basalts and the HREE show a range in concentrations from 10X chondritic in the LTZ basalts to 20X chondritic concentrations in the HTZ basalts. This progressive increase in HREE concentrations is not recognised in the HTZ-type basalts (exemplified by the HTZ.LF basalts of the Central Lebombo), however the HTZ.HF basalts of the Central Lebombo similarly exhibit an enrichment in HREE concentration, 15-20X chondritic, with respect to the LTZ basalts of the Central Lebombo and their REE patterns are therefore comparable to those of the HTZ basalts of Botswana.

2.3.1.4 Summary

The mafic rocks of the low-K_2O lineage are classified according to their TiO_2 and Zr concentrations into HTZ-, HTLZ- and LTZ-type basalt/dolerite groups (see Fig. 2.5A). Although the HTZ- and HTLZ-type basalts and dolerites of Botswana are enriched in some elements relative to LTZ basalts and dolerites from the same area, the style of "enrichment" is not one where incompatible element concentrations are markedly higher than those observed in the LTZ basalts at comparable MgO concentrations. Fig. 2.10 summarises the essential differences between the HTZ/HTLZ-type basalts of Botswana and the characteristic HTZ- or "enriched" signature. In Fig. 2.10A the HTZ/HTLZ-type basalts define a continuous trend with the LTZ-type basalts from low-K to intermediate-K K_2O concentrations, *i.e.* similar to the HTZ.HF basalts of the Central Lebombo in Fig. 2.10B. In contrast, the HTZ.LF basalts (with their characteristic "enriched" signature) of the Central Lebombo clearly define in Fig. 2.10B a high-K trend which is distinctly different to the trends defined by the LTZ (and HTZ.HF) type basalts. The HTLZ/HTZ basalts of Botswana have been shown to broadly resemble the whole rock geochemistry of the HTZ.HF basalts of the Central Lebombo (see section 2.3.1.3.2). The HTZ.HF basalt group is, however, characterised by a low Zr/Nb ratio (<14) when compared to both the LTZ- and HTZ.LF basalts groups from the same general area (see Fig. 2.10D after Sweeney *et al.*, 1994). Duncan *et al.* (1995), similarly, noted the presence of three chemically distinct basalt groups in the Tuli Syncline, where a group of basalts with a low Zr/Nb ratio (<12) can be compared to the HTZ.HF basalts of the Central Lebombo. The HTLZ/HTZ basalts of Botswana, however, have a high Zr/Nb ratio (see Fig. 2.10C), where three of the HTZ-type basalts and dolerites of Botswana which have a Zr/Nb ratio of <14 (*i.e.* KLB-063, -066 and -081) contain a high proportion of plagioclase or plagioclase and pyroxene phenocrysts. The HTLZ/HTZ basalts and dolerites of Botswana therefore cannot be broadly correlated, using the Zr/Nb ratio, with the HTZ.HF basalt group of the Central Lebombo or with the equivalent high-Fe groups of the Nuanetsi or Tuli areas. However, the definitions of HTZ-,

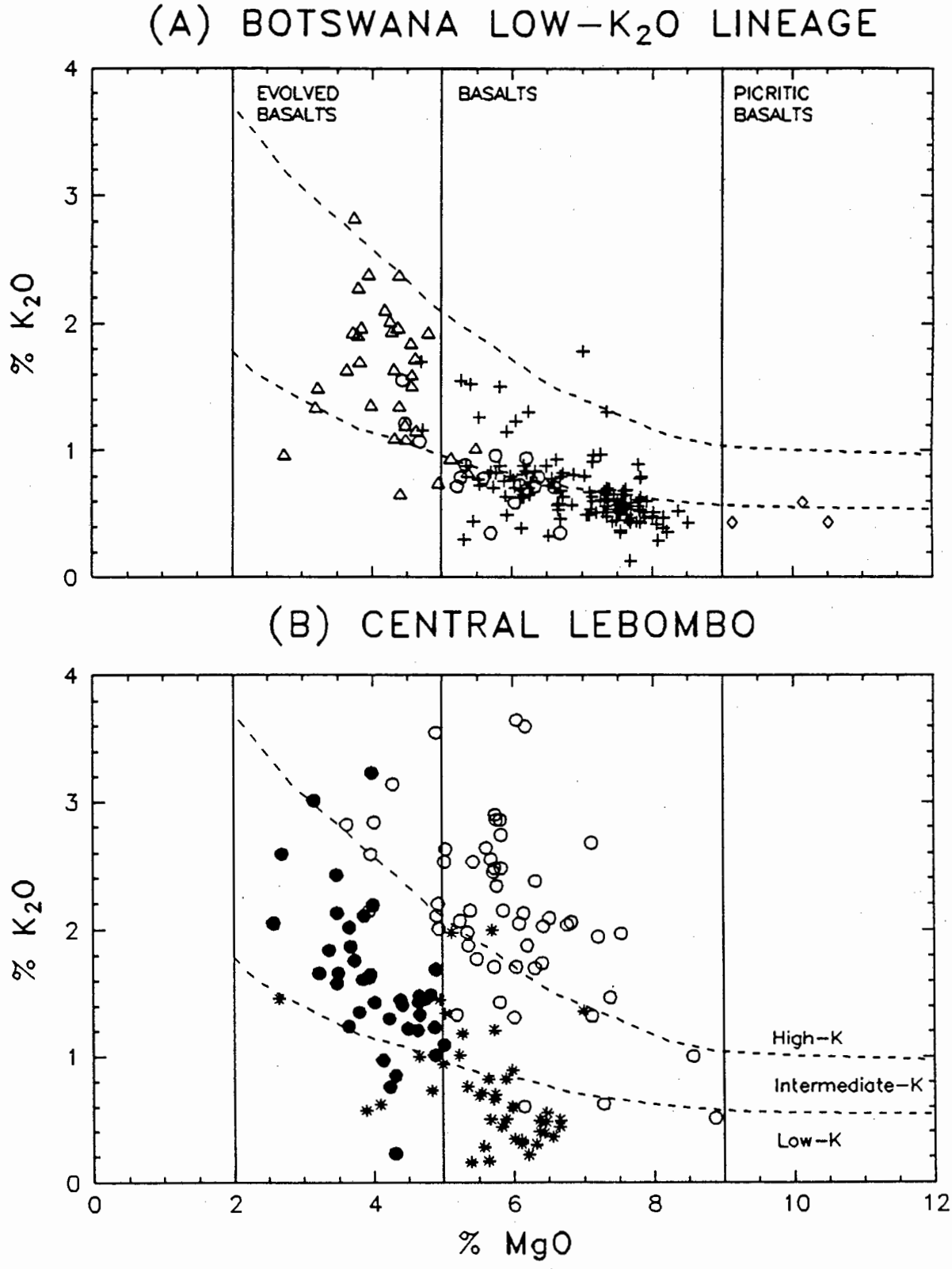

Fig. 2.10. A summary of the geochemical relationships exhibited between the different basalt groups of Botswana and the Central Lebombo. Symbols as for Fig. 2.8A & B.

(A & B) A comparison between the MgO-K_2O classification diagrams of the low-K_2O lineage of Botswana and the mafic rocks of the Central Lebombo.

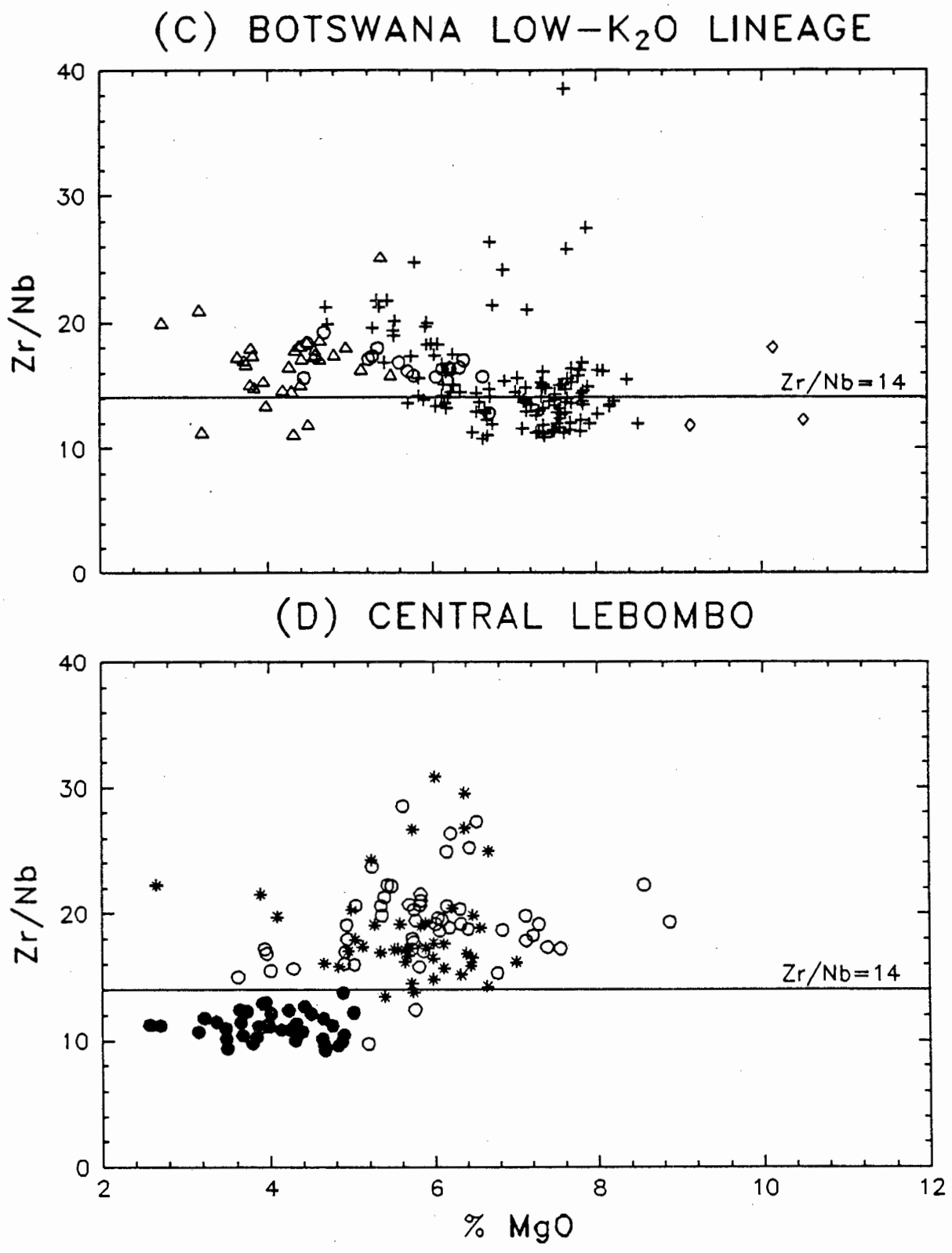

Fig. 2.10. A summary of the geochemical relationships exhibited between the different basalt groups of Botswana and the Central Lebombo. Symbols as for Fig. 2.8A & B.
(C & D) Zr/Nb *vs.* MgO for the different geochemical groups from Botswana and the Central Lebombo.

HTLZ- and LTZ-type basalt groups according to the TiO_2 and Zr concentrations are adopted for the Botswana data as they represent a useful means of separating the basaltic rocks into groups with different geochemical characteristics.

2.3.2 A COMPARISON BETWEEN THE INTRUSIVE AND EXTRUSIVE MAFIC ROCKS OF THE LOW-K_2O LINEAGE

2.3.2.1 Introduction

In the initial classification of the mafic rocks of the low-K_2O lineage into geochemical types according to their TiO_2 and Zr concentrations (see Fig. 2.5A) the outcrop character (*i.e.* whether intrusive or extrusive) was not considered, although all three of the geochemical groups include both intrusive and extrusive types. However the dolerites of Botswana are known to intrude through the lava pile in a number of places and the possible younger age of the dolerites quoted in the literature (*e.g.* Rundle, 1983) suggest that a comparison between the geochemistry of the basalts and dolerites is required.

2.3.2.2 LTZ basalts and dolerites

The LTZ basalts and dolerites both include "picritic basalts", "basalts" and "evolved basalts" according to the relevant MgO concentrations (refer to Fig. 2.4). The LTZ dolerites are characterised by a bimodal MgO concentration distribution and consequently both high-MgO LTZ picrites with 21.83-13.98 wt% MgO and LTZ dolerites (to evolved LTZ dolerites) with 7.88-4.70 wt% MgO are present. The LTZ basalts, in contrast, are characterised by a continuous range in MgO concentrations from 10.51-4.72 wt% MgO and therefore include, by definition, "picritic basalts" (subsequently referred to as low-MgO LTZ picritic basalts), "basalts" and "evolved basalts" (which are collectively referred to as the LTZ basalts).

The LTZ-type basalts of Botswana can be further subdivided into distinctive geochemical sub-groups. A group of nine basalts (KLB-023, -024, -015, -016, -179 to -182, -184), which have a LTZ-type signature, have whole rock compositions which are distinctly different to those of the other LTZ-type basalts. These nine samples are subsequently referred to as low-P_2O_5 LTZ basalts. Although these low-P_2O_5 LTZ basalts are, on average, more evolved than the LTZ-type basalts, with 6.17 and 4.72 wt% MgO, they are characterised by somewhat lower concentrations of SiO_2, Na_2O, P_2O_5, Ba and Nb and by a marked enrichment of TiO_2, Fe_2O_3*, V and Ni when compared to other LTZ-type basalts of similar MgO concentrations. In Fig. 2.11 the high TiO_2/P_2O_5 ratio of the low-P_2O_5 LTZ basalts reflects the lower P_2O_5 and increased TiO_2 concentrations in the low-P_2O_5 LTZ basalts with respect to the LTZ-type basalts.

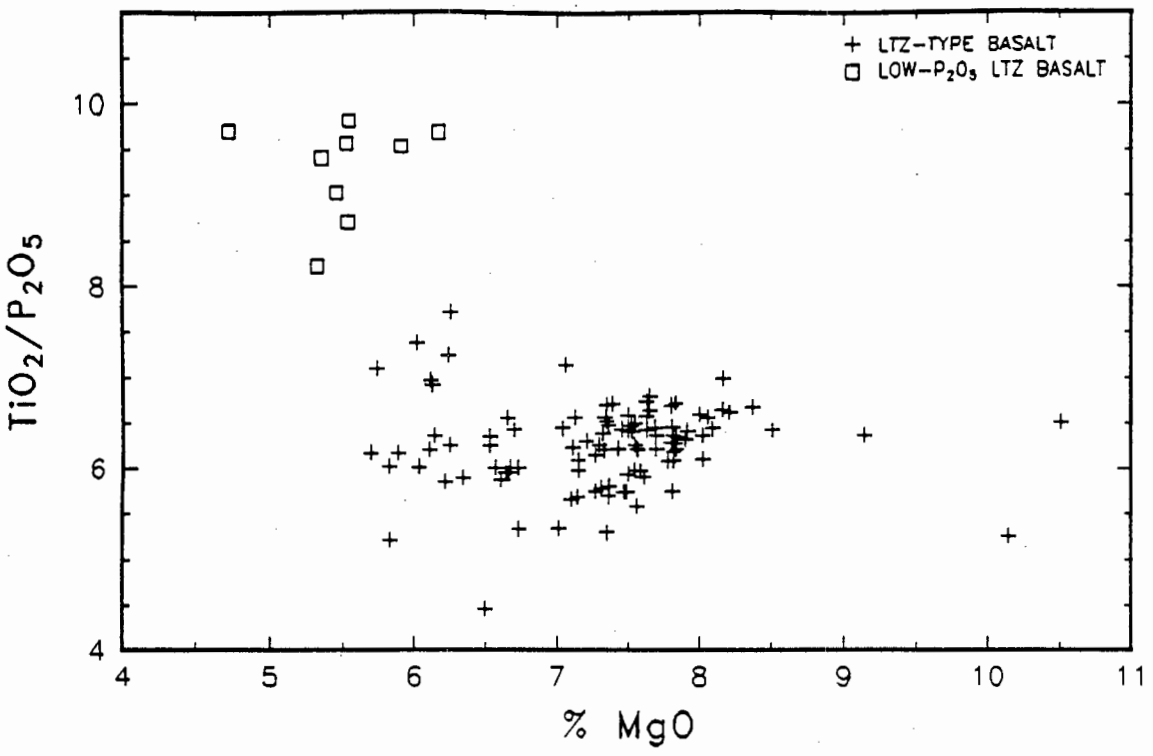

Fig. 2.11. TiO_2/P_2O_5 *vs.* MgO used to discriminate between the LTZ-type and low-P_2O_5 LTZ basalts.

The high-Na_2O basalts (see Fig. 2.3) recognised by their anomalously high Na_2O concentrations and normative mineralogy in section 2.2 are all extrusive in nature, and are all characterised by an LTZ-type signature. The high-Na_2O LTZ basalts are also characterised by, on average, lower CaO concentrations relative to the LTZ basalts (see Fig. 2.12A) and the degree of CaO depletion increases sympathetically with Na_2O enrichment (see Fig. 2.12B). These high-Na_2O LTZ basalts have whole rock compositions which are otherwise identical, but for the Na_2O and CaO concentrations, to the LTZ basalts for all major and trace element concentrations and are therefore not differentiated from the LTZ basalts. The general term LTZ-type basalt will therefore subsequently refer to the combined LTZ basalt and high-Na_2O LTZ basalt dataset.

As the difference in composition between the LTZ basalts and dolerites is fairly subtle, statistical procedures were used to emphasize, and clarify, any differences that exist between the whole rock compositions of the two LTZ outcrop types. The LTZ-type picrites (*i.e.* the high- and low-MgO LTZ picrites) were excluded from the LTZ dataset used so as to minimise the effects of fractional crystallization on the major and trace element concentrations. The statistical package SAS (Statistical Analysis System) was used for all the statistical analyses undertaken. A multivariate technique (*i.e.* each observation is characterised by a number of variables) known as discriminant function analysis (or DFA) was used, as it produces a maximum difference between the pre-defined groups (*i.e.* LTZ-type basalts and dolerites) and a minimum within group variation using a linear combination

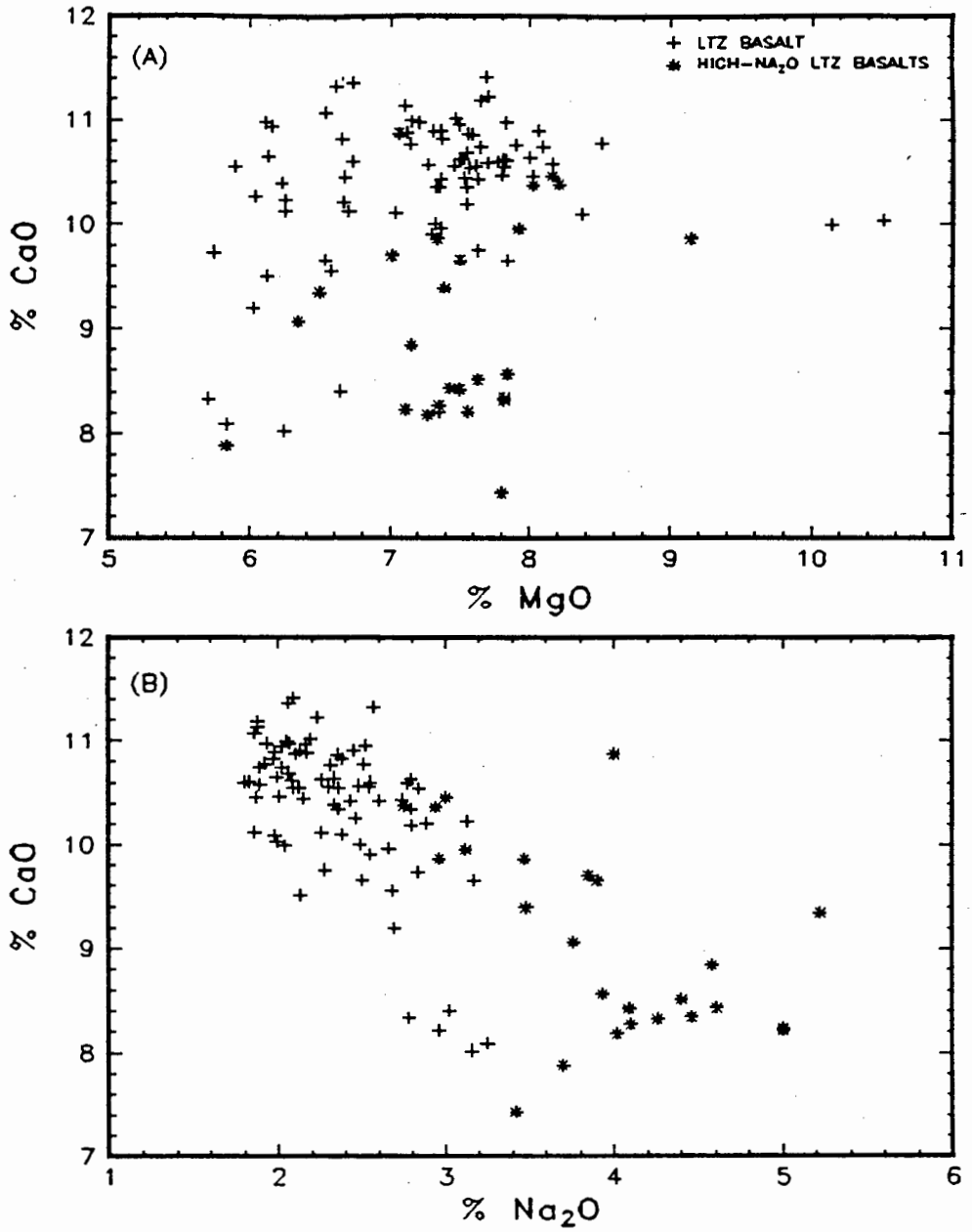

Fig. 2.12. (A) MgO *vs.* CaO and (B) Na_2O *vs.* CaO for the LTZ and high-Na_2O LTZ basalts.

of the original variables, *i.e.* oxides and trace elements (Davis, 1986). The SAS procedure **PROC DISCRIM** was used to perform the discriminant function analysis. However prior to DFA a stepwise discrimination procedure (**PROC STEPDISC**) was used to select the group of variables which best discriminate between the pre-defined groups.

The results of the stepwise DFA and the DFA computed for the LTZ-type basalts (excluding the low-P_2O_5 LTZ basalts) and the LTZ-type dolerites are summarised in Fig. 2.13 and the methods and data required for the calculation of the canonical scores are summarised in APPENDIX B. The clear separation in the fields defined by the first two canonical variables for the LTZ-type basalts and the LTZ dolerites therefore emphasises the differences in the whole rock compositions of the two LTZ outcrop types. Two of the

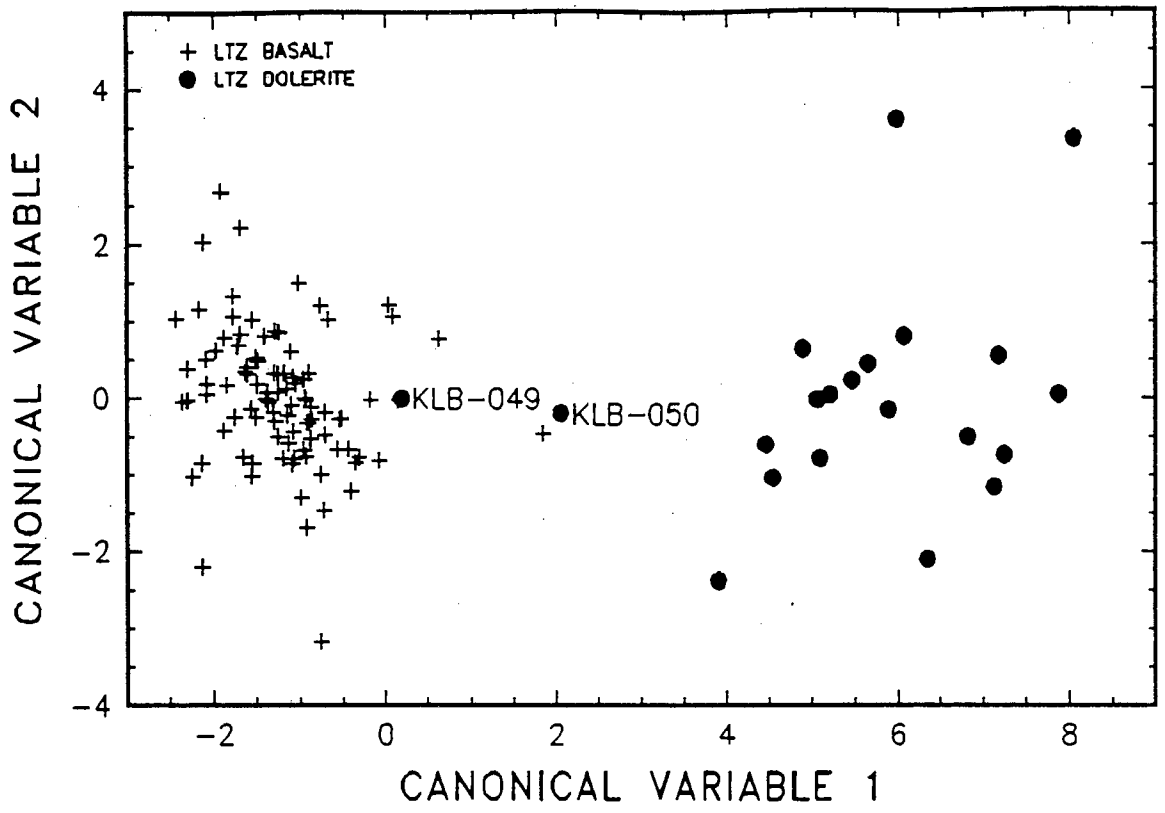

Fig. 2.13. DFA diagram for the LTZ-type basalts (*i.e.* excluding the low-P_2O_5 LTZ basalts) and the LTZ dolerites. The canonical variables are calculated using the variables Rb, K_2O, TiO_2, Y, Ba, SiO_2, Al_2O_3, Zr, P_2O_5, Nb, FeO* and MnO (selected in that order by stepwise DFA).

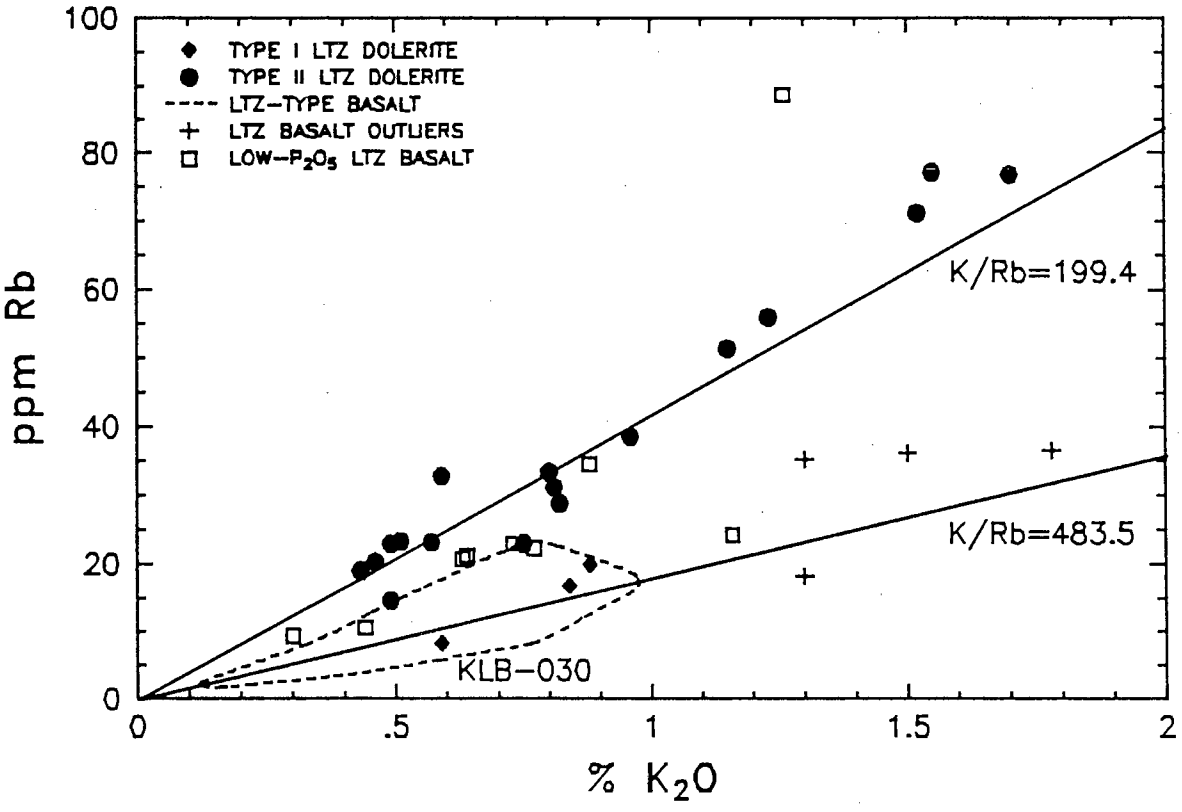

Fig. 2.14. K_2O *vs.* Rb for the LTZ basalts and dolerites. The K_2O/Rb ratios are described in the text.

LTZ dolerites (KLB-049 and -050) were "misclassified" as LTZ-type basalts during the DFA (with the posterior probability of the KLB-049 and -050 being re-classified as LTZ-type basalts as 1.000 and .6443 respectively) and these two LTZ dolerites thus have whole rock compositions which are statistically similar to the LTZ-type basalts. This statistical difference between the whole rock composition of the LTZ-type basalts and LTZ dolerites determined by DFA is reflected in Fig. 2.14 where K_2O and Rb were the first two variables selected by the stepwise DFA. The LTZ dolerites can therefore be subdivided into 2 main geochemical types. The first group, or TYPE I LTZ dolerites, includes the two misclassified LTZ dolerite samples KLB-049 and -050 and the whole rock compositions of the TYPE I LTZ dolerites are essentially identical to the LTZ-type basalts (*i.e.* compare K/Rb ratios of 415.1 and 368.5 for KLB-049 and -050 respectively with the average LTZ-type basalt K/Rb ratio of 483.5). The second group, or TYPE II LTZ dolerites, includes the majority of the LTZ dolerite samples and is clearly different to the LTZ-type basalts (reflected in the TYPE II LTZ dolerites lower average K/Rb ratio of 199.4 in Fig. 2.14. Although both K_2O and Rb concentrations are readily effected by secondary processes such as alteration, the concentrations of the immobile trace elements Zr and Y (see Fig. 2.15) reflects the behaviour of the more mobile elements. In Fig. 2.15 the Zr/Y ratios clearly differentiate between the TYPE I and TYPE II LTZ dolerites (with average Zr/Y ratios of 3.75 and 4.61 respectively). The two TYPE I LTZ dolerites have Zr/Y ratios of 3.76 and 3.73 (KLB-049 and -050 respectively), which are comparable to the LTZ-type basalts (average Zr/Y=3.365).

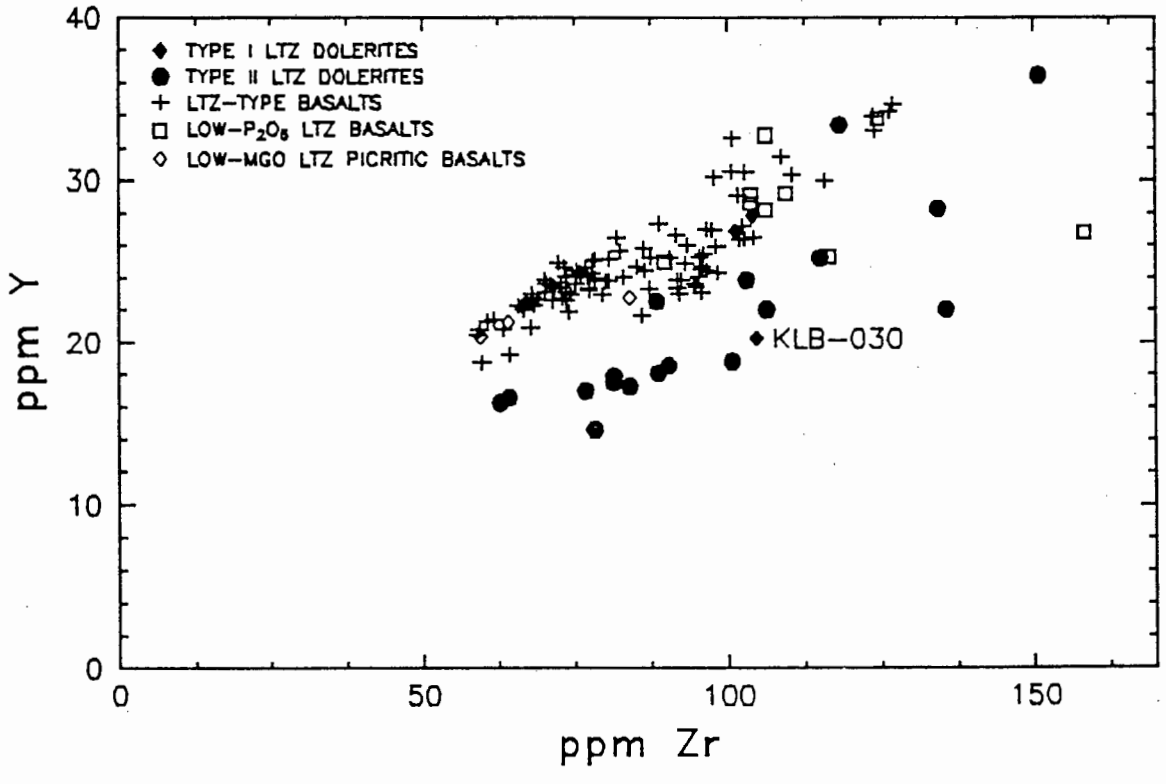

Fig. 2.15. Zr *vs.* Y for the LTZ basalts and dolerites.

The sample KLB-030, which is classified as an LTZ dolerite according to its TiO_2 (1.84 wt%) and Zr (105ppm) concentration, has a whole rock composition which is unlike either the TYPE I LTZ dolerites and therefore the LTZ-type basalts (see Fig. 2.15) or the TYPE II LTZ dolerites (see Fig. 2.14). However in Fig. 2.6 (Mg# *vs.* TiO_2) KLB-030 lies on the trend defined by the HTLZ- and HTZ-type basalts and dolerites and KLB-030 may represent a more mafic equivalent to the HTLZ/HTZ-type basalt and dolerite type.

The low-P_2O_5 LTZ basalts can be differentiated, geochemically, from the TYPE II LTZ dolerites in both Fig. 2.14 and 2.15 and the low-P_2O_5 LTZ basalts are therefore not extrusive equivalents of the TYPE II LTZ dolerite, but are a separate LTZ basalt type.

2.3.2.3 HTLZ and HTZ basalts and dolerites

The HTLZ- and HTZ-type basalts and dolerites were defined as separate geochemical groups according to their TiO_2 and Zr concentrations in section 2.3.1.2, although the two geochemical sub-groups define a continuous range in their whole rock compositions. In order to assess statistically any possible differences that may exist according to outcrop character between the whole rock chemistry of the HTLZ- and HTZ-type basalts and dolerites, the separation into HTLZ- and HTZ-type sub-groups was retained as the HTZ basalts and dolerites tend to be more evolved (with <5.5% MgO) than the HTLZ basalts and dolerites.

Although fifteen HTLZ dolerites were sampled during this study, only three HTLZ basalt samples have been recognised. These HTLZ basalts are characterised by a considerable variation in whole rock compositions (*e.g.* TiO_2 concentrations of 2.19 and 2.89 wt% and Zr concentrations of 158 and 223 ppm were determined for KLB-177 and -178 respectively). The HTLZ basalts and dolerites are therefore not differentiated according to outcrop character because of both the scarcity of data and the range in compositions exhibited by the HTLZ basalts.

A similar multivariate statistical comparison (see section 2.3.2.2) was undertaken using DFA to determine if the HTZ basalts and dolerites could be differentiated geochemically according to their outcrop character. The samples DB-14 and DB-16 sampled from the Nxai Pan borehole in northern Botswana were excluded from the HTZ dataset as the DFA analysis of the dataset which included these two samples was unsuccessful with nine of the samples misclassified. Furthermore DB-14 and DB-16 were sampled from drill chips which were collected over a metre interval and there is therefore a high possibility of contamination, which justifies their exclusion from the HTZ dataset. Fig. 2.16 summarises the results of the DFA and the data required to calculate the canonical scores are

summarised in APPENDIX B. Although the DFA was partially successful in differentiating statistically between the HTZ basalts and HTZ dolerites, three HTZ basalts were misclassified (with the posterior probabilities of KLB-070, -096 and -101 being reclassified as HTZ dolerites being .7071, .5687 and .9644 respectively) and the fields defined by the first two canonical variables for the HTZ basalts and dolerites are neither clearly defined nor well separated. The statistical differences computed for the HTZ basalts and dolerites are, however, not replicated by any inter-element ratios and it was therefore concluded that the HTZ basalts and dolerites could not be differentiated according to the outcrop character.

In summary, as neither the HTLZ- nor the HTZ-type basalts and dolerites can be differentiated by outcrop character and as the two geochemical groups define a continuum in whole rock chemistry the HTLZ- and HTZ-type basalts and dolerites are therefore collectively referred to as the HTZ-type basalts in subsequent sections.

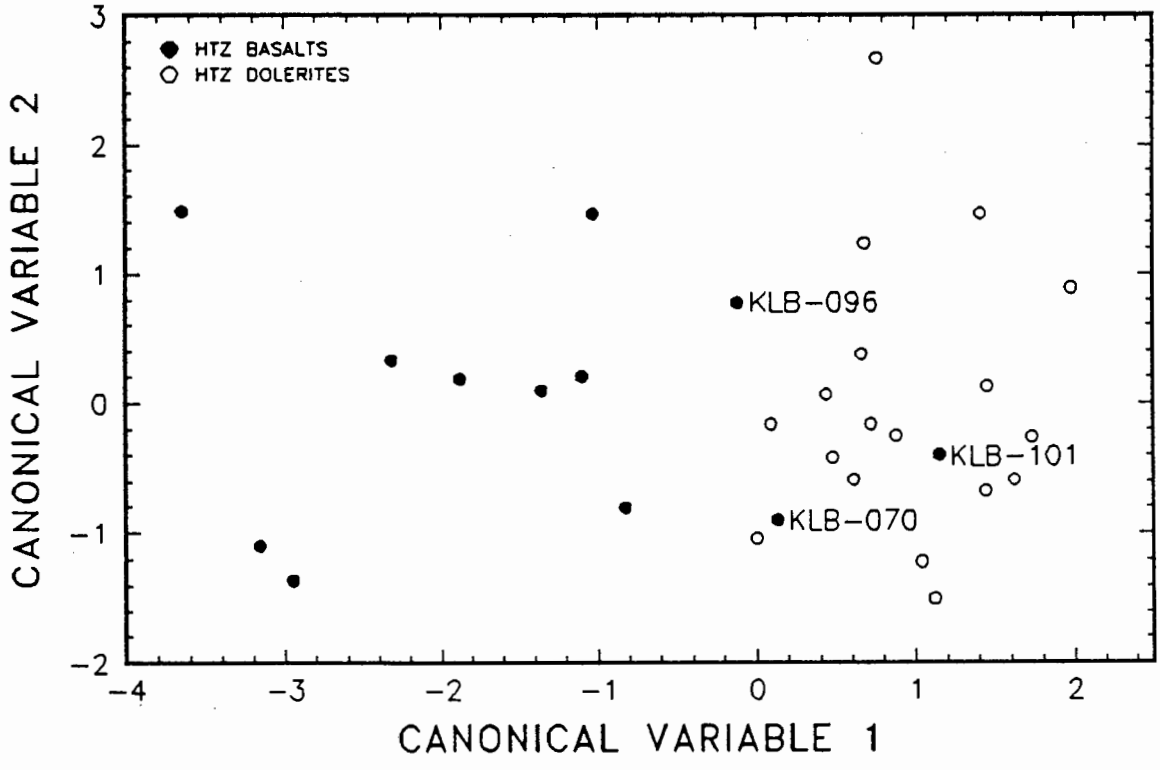

Fig. 2.16. DFA diagram for the HTZ-type basalts and dolerites. The canonical variables are calculated using the variables MgO, TiO_2, Co, Nb, P_2O_5, Zr, K_2O and Cu (selected in that order by stepwise DFA).

The HTZ-type basalts and dolerites can, however, be sub-divided into two geochemical sub-groups according to their Fe_2O_3* and TiO_2 concentrations and in Fig. 2.17A (Fe_2O_3* *vs.* TiO_2) two discrete Fe_2O_3* *vs.* TiO_2 trends are defined by these HTZ samples. A sub-group of HTZ-type basalt samples are characterised by, on average, lower Fe_2O_3* concentrations than the remaining HTZ-type basalts with comparable MgO concentrations and are

therefore subsequently referred to as the HTZ (low Fe) basalts and dolerites. The remaining HTZ-type basalts, which are subsequently referred to as the HTLZ/HTZ basalts and dolerites, have, on average, higher Fe_2O_3* concentrations than the HTZ (low Fe) basalts and dolerites with similar MgO concentrations and the HTLZ/HTZ basalts and dolerites define a relatively coherent trend of increasing Fe_2O_3* *vs.* MgO concentrations (see Fig. 2.17B). A similar bimodal distribution with respect to Fe_2O_3* concentrations has been recognised by Sweeney *et al.* (1994) in the "enriched" basalts of the Central Lebombo where the HTZ basalts with lower Fe_2O_3* concentrations (*i.e.* HTZ.LF) have a true "enriched" signature as defined by Cox *et al.* (1967). Duncan *et al.* (1995), similarly, subdivided the basalts of the Tuli Syncline into three distinct basalt groups on the basis of their Zr/Nb and Ce/Y ratios. The Zr/Nb ratio was used to subdivide the basalts into two distinct geochemical groups where those basalts with a low Zr/Nb ratio (*i.e.* < 12) can be compared with the HTZ.HF basalts of the Central Lebombo (see Fig. 2.10D). The basalts with a high Zr/Nb ratio (*i.e.* > 12) are subdivided into two distinct groups according to their Ce/Y ratio. The first high Zr/Nb type has a high Ce/Y ratio (*i.e.* >2.1) as well as high Zr and Ba concentrations and is equivalent to the HTZ.LF basalt types of the Central Lebombo. The second high Zr/Nb basalt group is characterised by a low Ce/Y ratio (*i.e* <2.1) and low Zr and Ba concentrations and is therefore equivalent to the LTZ basalt type of the Central Lebombo.

The HTZ-type basalts are characterised by a considerable range in the value of their Ce/Y ratios, from 1.0 to 3.3 (see Fig. 2.18), and therefore exhibit a range in character from the HTZ.LF to the LTZ type lineages as defined by Duncan *et al.* (1995). The HTZ (low Fe) basalt and dolerite sub-group are, however, characterised by higher values for their Ce/Y ratio (*i.e.* ≥2.0) with respect to the remaining HTLZ/HTZ basalts and dolerites (see Fig. 2.18) and the high Ce/Y ratio of the HTZ (low Fe) basalts and dolerites is therefore comparable with the high Ce/Y ratio (*i.e.* ≥2.1) of the HTZ.LF basalt type of the Tuli and Central Lebombo areas (see section 2.3.2.3). The HTZ (low Fe) basalts and dolerites, like the HTZ.LF basalts, are enriched in Ba and Zr (see Fig. 2.19) with respect to the remaining HTLZ/HTZ basalts and dolerites and the LTZ basalts of Botswana at similar MgO concentrations. The two HTZ (low Fe) basalt and dolerite samples (KLB-066 and -081) which lie in the field defined by the HTLZ/HTZ basalts and dolerites in Fig. 2.19 both have > 13% plagioclase phenocrysts and can therefore be disregarded.

The low Ce/Y ratio and somewhat lower Ba and Zr concentrations of the HTLZ/HTZ basalts and dolerites with respect to the HTZ (low Fe) basalts and dolerites therefore suggests a resemblance between the HTLZ/HTZ basalts and dolerites and the LTZ group as defined by Duncan *et al.* (1994) for the Tuli area. The HTLZ/HTZ basalts and dolerites

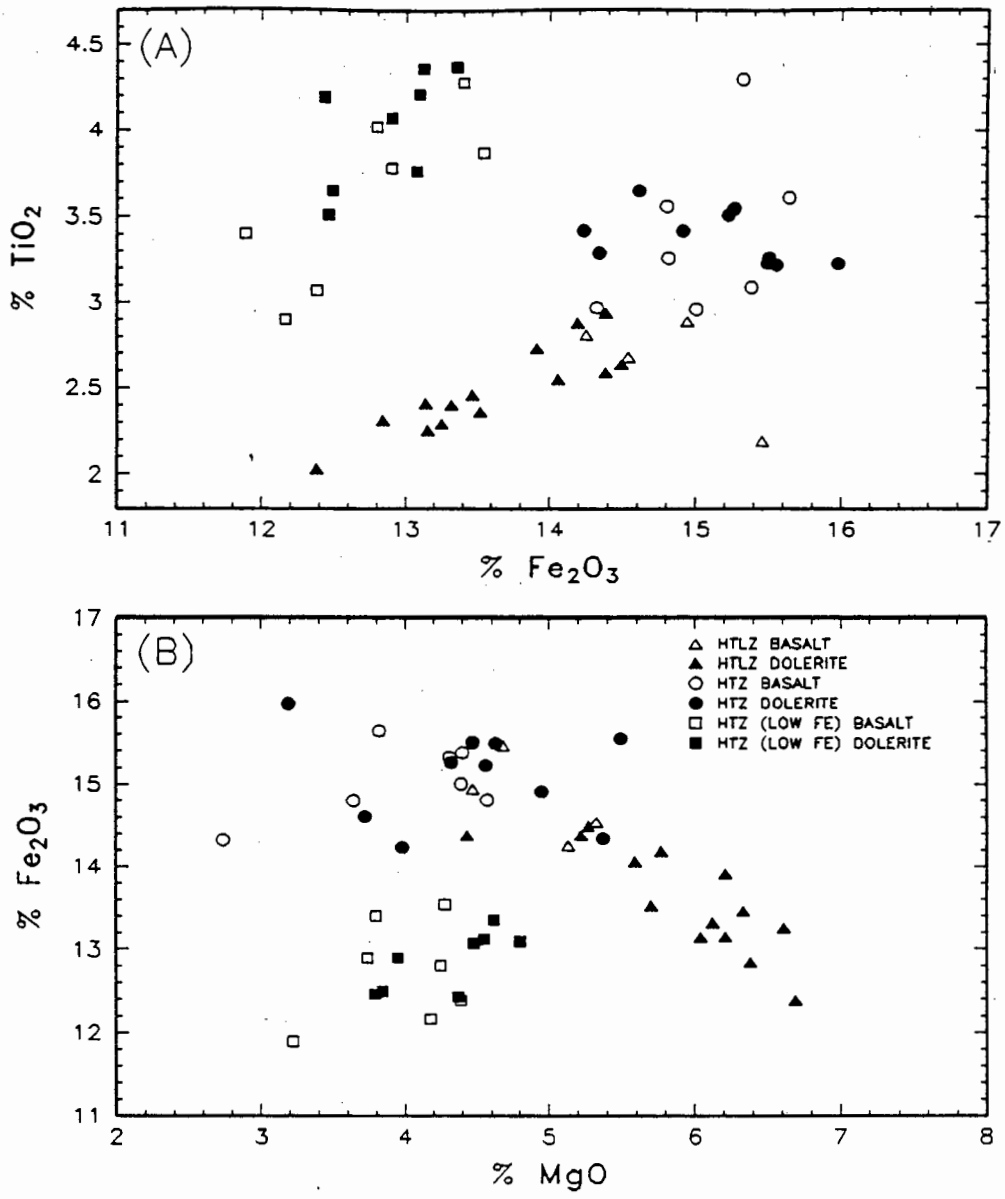

Fig. 2.17. (A) Fe_2O_3* *vs.* TiO_2 and (B) MgO *vs.* Fe_2O_3* used to classify the two HTZ-type basalt sub-groups.

however have somewhat higher Ce/Y ratio values with respect to the LTZ basalts of Botswana (see Fig. 2.18) and, furthermore, the HTLZ/HTZ basalts and dolerites have been shown to define enriched trends *vs.* MgO with respect to the LTZ basalts for some of the incompatible elements (*e.g.* see Fig. 2.6 and 2.19). The HTLZ/HTZ basalts and dolerites are therefore recognised as a separate geochemical group in Botswana. In section 2.3.1.3.2 and 2.3.1.4 it was noted that the HTZ-type basalt (and dolerite) data of Botswana clearly did not have a true "HTZ"- or "enriched"-type signature. The HTLZ/HTZ-type basalt data, however, closely resembles the HTZ.HF basalts of the Central Lebombo and Tuli areas for all major, trace and rare earth element data, except that the HTLZ/HTZ-type basalts and dolerites of Botswana all have a high Zr/Nb ratio (see Fig. 2.10C). The HTLZ/HTZ basalts and dolerites of Botswana are therefore proposed to be a lateral equivalent to this HTZ.HF basalt type, although the HTLZ/HTZ basalts and dolerites do not have the characteristic low Zr/Nb ratio.

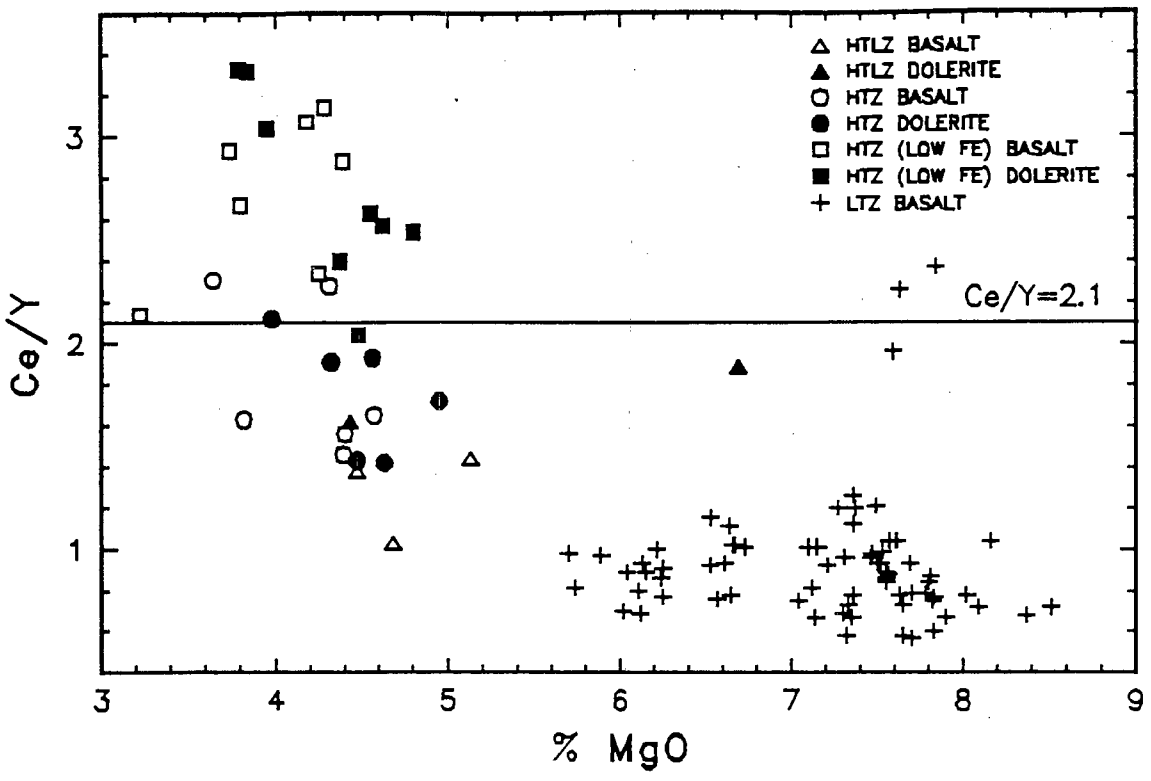

2.18. Ce/Y *vs.* MgO for the HTZ-type basalts and dolerites and the LTZ basalts. The Ce/Y ratio of 2.1 after Duncan *et al.* (1995) is described in the text.

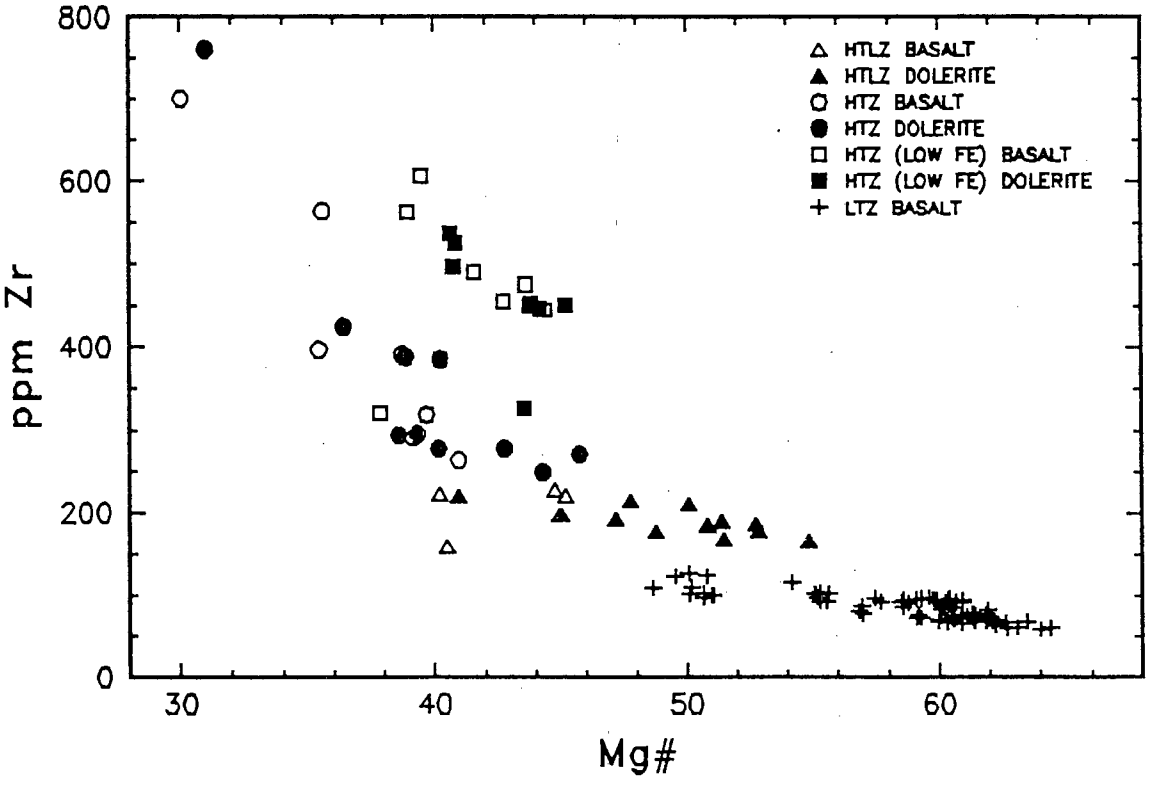

Fig. 2.19. Zr *vs.* MgO for the HTZ-type basalts and dolerites and the LTZ basalts.

2.4 HIGH-K_2O LINEAGE

The high-K_2O lineage includes, by definition, both shoshonites (with 2-5% MgO and high K_2O concentrations) and the high-K_2O picritic basalts (with >9% MgO) according to Fig. 2.4.

2.4.1 SHOSHONITES

Joplin (1964) defined shoshonites as near-silica saturated derivatives of alkali basalts, and shoshonites are enriched in K_2O, CaO and Al_2O_3 with respect to typical alkali basalts. Shoshonites characteristically contain between 7 and 8 wt% total alkalis with roughly equal proportions of Na_2O and K_2O. Both intrusive and extrusive shoshonites are characterised by a phenocryst assemblage which includes labradorite (or oligoclase), augite and olivine in a groundmass of plagioclase microlites mantled with orthoclase, augite, magnetite and a trace of serpentine and the orthoclase may range in proportion from 10 to 60% of the total feldspar population. Some types may contain glass and/or leucite (Joplin, 1964).

Although the shoshonites of Botswana lie close to the shoshonite - absarokite boundary of Bristow and Cox (1984) at 5% MgO (see Fig. 2.4), the term shoshonite is preferred for the Botswana data as the shoshonites sampled during this study are both petrographically and geochemically similar to the shoshonites sampled in the Zimbabwe portion of the Tuli Syncline by Vail *et al.* (1969) and to the definitions outlined in Joplin (1964). The shoshonites of Botswana are therefore characterised by their nepheline normative compositions (see TABLE 2.1), their high total alkali concentrations (Na_2O + K_2O varies between 6,68 and 7.50 wt%) and their high, and approximately equal, concentrations of Na_2O (2.91 to 3.86 wt%) and K_2O (3.48 to 4.14 wt%).

2.4.2 HIGH-K_2O PICRITIC BASALTS

Extensive outcrops of picritic basalts of the Letaba Formation are recognised in the Northern Lebombo, Nuanetsi and Tuli regions of the Karoo Igneous Province. These picritic basalts exhibit a range in MgO concentrations from ±9 to 24 wt% MgO, with an average MgO concentration of ±15%. Picritic basalts with >18% MgO have been regarded as cumulus-enriched as they typically contain large megacrysts and/or phenocrysts of olivine and orthopyroxene. The picritic basalts are characterised by variable and enriched abundances of K_2O, TiO_2, P_2O_5, Rb, Ba, Sr and Zr (Bristow, 1984b; Sweeney *et al.*, 1991; Ellam and Cox, 1989).

The high-K_2O picritic basalts defined in Fig. 2.4. have MgO concentrations of 19.63 and 16.18% (KLB-083 and -084 respectively) and lie within the range of MgO concentrations exhibited by the Letaba Formation. The trace and incompatible element concentrations of the high-K_2O picritic basalts similarly lie within the range of compositions defined by the Letaba Formation and the high-K_2O picritic basalts sampled in the Botswana portion of the Tuli Syncline this study therefore belong to the Letaba Formation.

	KLB-057	KLB-058	KLB-059	KLB-060	KLB-090	KLB-099	TV-48	TV-49
OR	21.5	24.5	23.6	22.3	20.6	22.1	26.0	24.7
AB	19.9	19.4	20.7	24.0	23.4	21.3	19.4	21.9
AN	19.5	18.9	17.8	18.7	15.5	16.9	18.8	17.1
NE	7.0	3.4	3.3	.3	3.9	3.6	5.3	4.3
DI	11.4	13.5	13.9	12.2	15.3	15.1	10.2	12.9
DIWO	5.7	6.8	7.0	6.2	7.7	7.6	5.1	6.4
DIEN	2.9	3.5	3.6	3.1	3.7	3.8	2.3	2.6
DIFS	2.7	3.1	3.3	3.0	3.8	3.6	2.8	3.9
OL	13.0	12.4	12.4	13.4	11.9	12.1	12.7	11.0
OLFO	6.3	6.3	6.1	6.5	5.6	5.9	5.5	4.1
OLFA	6.6	6.2	6.2	6.9	6.3	6.2	7.2	6.9
MT	1.8	1.8	1.8	2.0	2.0	1.9	1.9	2.0
IL	3.4	3.5	3.8	4.4	4.8	4.3	3.2	3.5
AP	1.8	1.8	1.8	1.8	1.8	1.8	1.5	1.6

TABLE 2.1. The CIPW norms of the shoshonites sampled during this study and by Vail *et al.*, 1969 (samples TV-48 and -49) in the Tuli Syncline. Normative compositions are calculated from data normalised to 100% on a volatile-free basis with a Fe_2O_3/FeO ratio of .15.

2.5 FELSITES

The two felsic dyke samples are defined as quartz latites with >3% K_2O and >63% SiO_2 according to the classification scheme of Mackenzie and Chappell (1972) and as a quartz latite and a high-K dacite according to the Peccerillo and Taylor (1976) classification scheme in Fig. 2.20. Although the Botswana felsic samples lie within the field defined by the Etendeka quartz latites (see Fig. 2.20), the term felsite has, however, been retained for the Botswana samples as the term quartz-latite is usually associated with extrusive rocks.

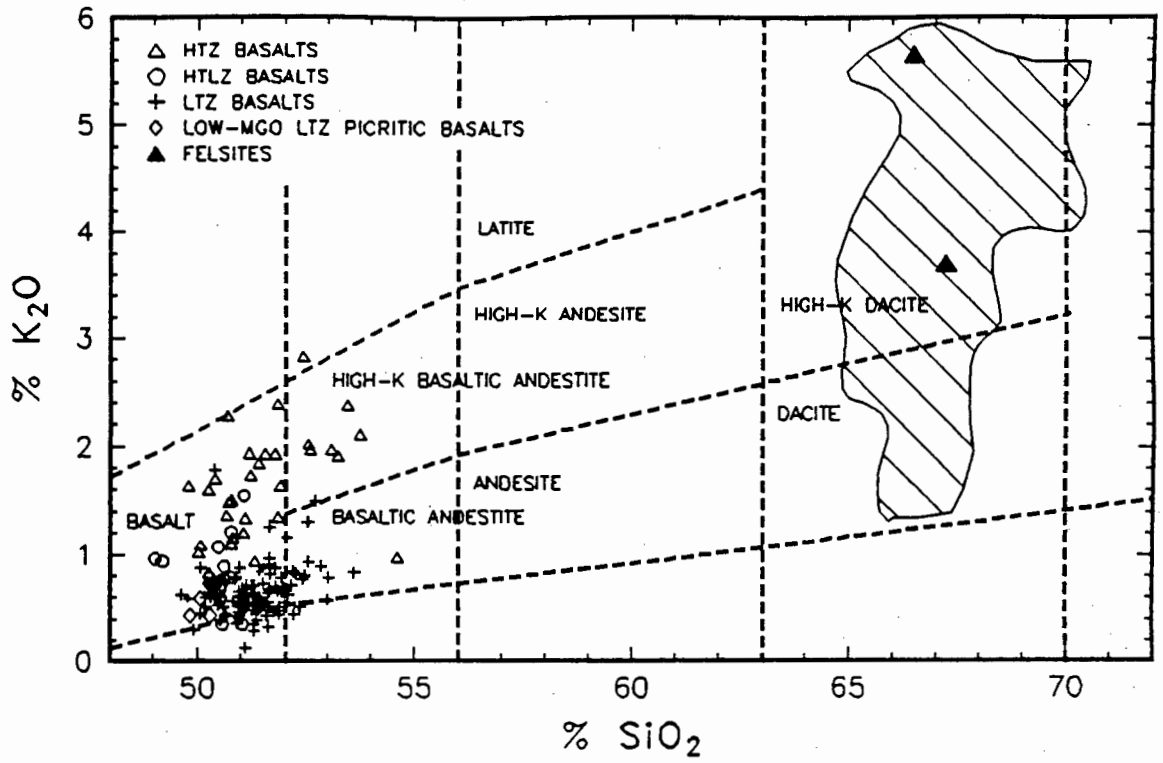

Fig. 2.20. The SiO_2-K_2O classification scheme of Peccerillo and Taylor (1976). The shaded field is defined by the quartz-latites of the Etendeka (includes both the southern Etendeka and Sarusas Quartz-Latites) after Milner (1988).

2.6 SUMMARY

The lavas and dykes in Botswana which are of presumed Karoo age can be subdivided into a number of different geochemical types utilising outcrop character and certain major and trace element concentrations and ratios. TABLE 2.2 summarises the classification scheme outlined in this chapter. TABLE 2.3 tabulates the average compositions and the standard deviations (S.D.) for each of the geochemical types which have been defined. The averages and S.D. were calculated for data (listed in full in APPENDIX D) which had all Fe expressed as Fe_2O_3* and in which the major and trace element data were normalised to 100% on a volatile-free basis.

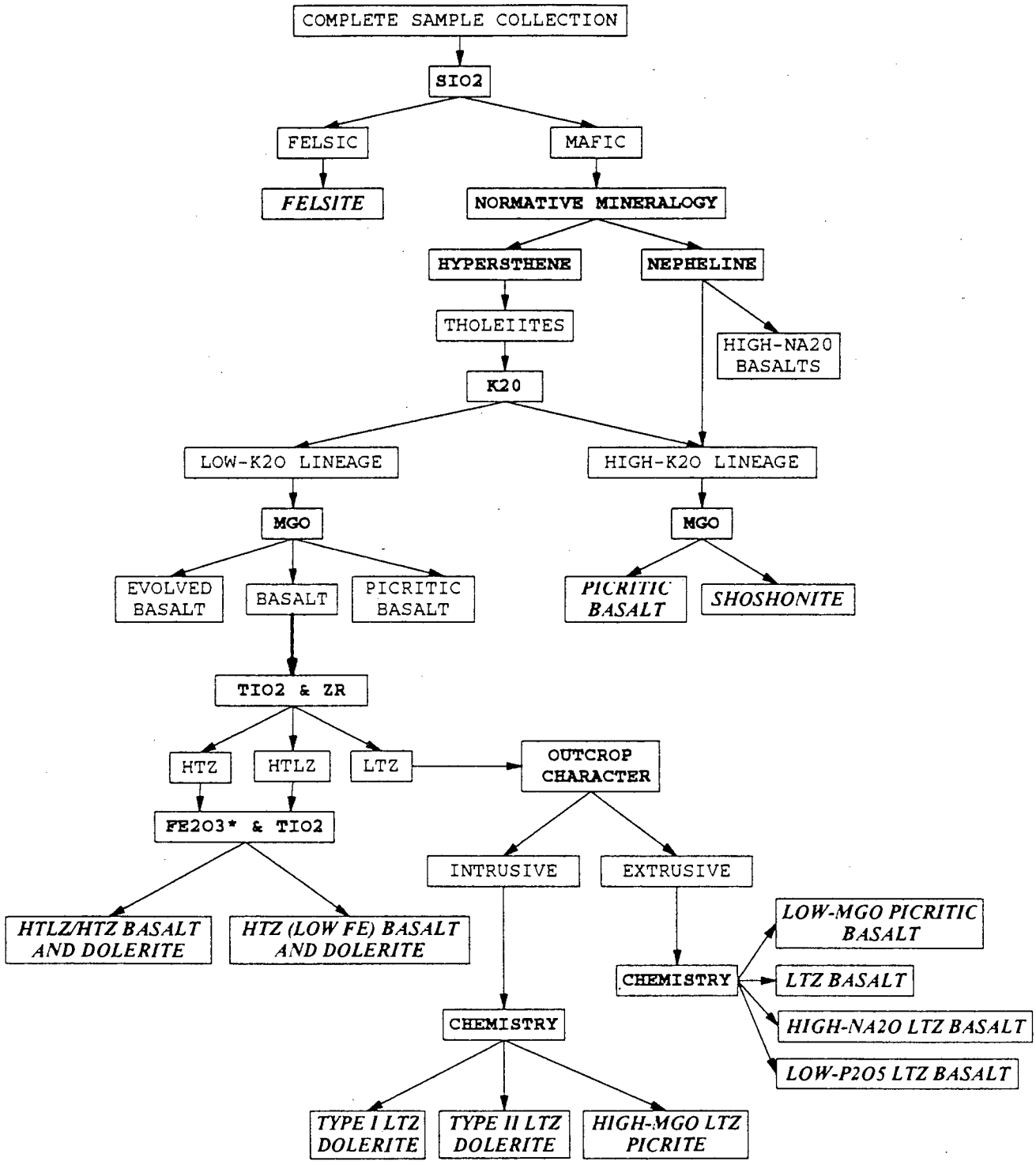

TABLE 2.2. Classification scheme used in the definition of geochemical types within the Botswana dataset. The criteria used for classification are depicted with a bold type face, whereas the geochemical sub-groups defined in this study are highlighted with an italics type face.

			HIGH-K_2O LINEAGE				LOW-K_2O LINEAGE							
	FELSITE		HIGH-K_2O PICRITIC BASALT		SHOSHONITE		LOW-MGO LTZ PICRITIC BASALT		LTZ BASALT		HIGH-NA_2O LTZ BASALT		LOW-P_2O_5 LTZ BASALT	
	N=2		N=2		N=6		N=3		N=78		N=24		N=9	
	MEAN	S.D.	MEAN	S.D.	MEAN	S.D.	MEAN	S.D.	MEAN	S.D.	MEAN	S.D.	MEAN	S.D.
SiO_2	66.86	.52	49.25	1.99	50.08	.31	50.06	.23	51.45	.69	51.30	.68	50.89	.93
TiO_2	.92	.06	2.47	.06	2.12	.29	.82	.04	.97	.14	.94	.11	1.60	.15
Al_2O_3	14.93	.13	7.99	.90	16.11	.75	14.51	.62	15.39	.54	15.43	.31	14.60	.40
Fe_2O_3	5.58	.14	12.26	.86	10.88	.60	11.61	.19	11.33	.87	10.91	.61	14.78	.79
MnO	.07	.01	.15	.01	.16	.01	.16	.04	.17	.02	.16	.02	.18	.03
MgO	1.65	.54	17.91	2.44	4.88	.11	9.93	.71	7.18	.69	7.40	.57	5.50	.40
CaO	1.99	.39	6.53	.19	7.91	.18	9.96	.09	10.39	.73	9.03	.94	9.28	1.35
Na_2O	3.09	.15	1.35	.11	3.31	.36	2.33	.54	2.35	.37	3.96	.67	2.25	.29
K_2O	4.68	1.39	1.67	.27	3.80	.24	.48	.09	.61	.21	.71	.28	.76	.31
P_2O_5	.23	.02	.42	.01	.76	.01	.14	.02	.16	.02	.15	.03	.17	.02
Rb	94	20	30	9.8	116	17	9.9	4.1	12	5.8	12	6.7	28	24
Ba	1911	517	717	72	1815	173	131	26	159	37	172	54	143	37
Sr	470	79	817	99	1225	175	172	4.7	202	28	213	58	226	50
Th	17	.7	4.1		19	2.4			2.8	.5	2.9	.7		
U	3.5	.8	3.2	.2	3.1	.8			2.1	.3	2.1	.7	2.6	.8
Zr	839	11	318	22	298	17	69	13	86	16	77	14	113	19
Nb	24	.0	20	9.0	142	16	5.0	.4	6.3	1.5	5.6	1.1	5.7	1.0
Cr	39	5.5	964	109	193	20	403	82	277	75	308	57	110	28
V	46	3.9	189	5.0	176	16	201	18	230	23	238	25	319	18
Sc	7.4	1.0	20	1.5	14	2.0	30	.1	34	2.5	34	2.2	42	6.4
Ni	20	2.6	990	163	92	7.3	172	29	91	17	91	14	77	8.4
Co	11	.6	83	12	32	2.0	61	1.8	50	3.1	49	2.5	51	3.8
Ga														
Pb	21	.5	14	1.0	12	1.7	4.2	.4	4.5	1.0	3.5	.6	3.7	.7
Zn	77	.4	113	4.3	92	5.2	83	2.7	85	10	88	19	109	5.9
Cu	24	2.4	85	1.8	179	17	68	5.5	84	24	77	20	150	24
Y	56	.9	25	1.4	28	2.6	21	1.2	25	3.1	24	2.8	29	3.0
La	104	1.7	39	3.9	112	9.0	8.0	.7	10	2.3	9.4	2.0	12	1.9
Ce	231	3.2	87	7.6	212	12	18	.6	23	8.4	21	7.7	25	4.6
Nd	114	.8	55	2.4	82	1.6	9.6	.8	13	3.8	12	5.7	17	3.2

TABLE 2.3. The average compositions (and one standard deviation) of the geochemical groups defined in this chapter.

	LOW-K_2O LINEAGE (continued)												
	HIGH-MGO LTZ PICRITE		TYPE I LTZ DOLERITE		TYPE II LTZ DOLERITE			HTLZ BASALT & DOLERITE		HTZ BASALT & DOLERITE		HTZ (LOW FE) BASALT & DOLERITE	
	N=3				N=18			N=18		N=17		N=15	
	MEAN	S.D.	KLB-049	KLB-050	MEAN	S.D.	KLB-030	MEAN	S.D.	MEAN	S.D.	MEAN	S.D.
SiO_2	50.18	1.08	51.44	51.51	52.50	1.77	49.77	50.45	.56	51.02	1.1	52.01	1.13
TiO_2	.47	.14	1.06	1.05	1.04	.30	1.84	2.52	.27	3.39	.32	3.83	.46
Al_2O_3	11.27	2.66	14.57	14.57	14.90	.77	14.99	13.85	.29	13.07	.43	13.89	.87
Fe_2O_3	10.73	1.57	12.09	11.94	11.57	1.42	12.24	13.87	.79	15.08	.51	12.80	.48
MnO	.16	.02	.20	.19	.17	.02	.17	.19	.02	.18	.01	.15	.01
MgO	16.61	4.52	6.19	6.17	6.47	.91	7.70	5.68	.71	4.27	.71	4.15	.42
CaO	8.41	1.80	10.44	10.49	10.14	.91	10.13	9.76	.60	8.46	.60	7.82	.67
Na_2O	1.71	.25	3.01	3.02	2.22	.30	2.35	2.57	.20	2.68	.25	2.67	.33
K_2O	.41	.09	.84	.88	.87	.40	.59	.82	.28	1.28	.36	1.99	.40
P_2O_5	.06	.02	.18	.17	.12	.04	.22	.29	.03	.57	.23	.69	.13
Rb	12	3.3	17	20	38	20	8.2	19	7.3	26	7.6	38	11
Ba	191	13	217	332	225	78	172	262	60	532	211	795	198
Sr	155	39	189	202	216	79	413	377	39	583	169	929	172
Th	2.5	.1			4.8	2.1		2.9	.45	4.4	1.1	5.3	1.5
U	1.6	.0			1.7	.1		2.0	.39	2.2	.8	2.0	.45
Zr	46	16	101	104	98	25	105	195	21	385	153	469	76
Nb	2.1	.5	7.2	7.9	5.1	1.5	6.4	12	1.4	22	8.1	30	3.9
Cr	2182	952	204	206	132	81	195	117	35	49	31	57	32
V	159	21	233	239	227	43	189	347	26	302	64	242	28
Sc	27	4.0	31	33	30	4.2	22	32	2.4	28	3.9	20	2.0
Ni	682	362	56	58	104	51	240	89	17	62	23	65	19
Co	79	19	44	46	54	4.9	56	47	3.5	47	10	40	3.7
Ga										26.3	5.06		
Pb	3.2	.3	2.9	2.7	5.8	2.5		3.9	1.12	6.69	3.2	8.8	2.4
Zn	70	13	87	91	89	15	77	106	9.1	132	16	128	13
Cu	56	25	99	100	90	41	156	196	35	217	48	130	47
Y	11	3.1	27	28	21	6.1	20	36	3.1	50	9.2	48	5.0
La	8.8	3.8	13	17	14	3.9		22	3.1	36	10	55	12
Ce	12	5.3	58	50	30	7.4		51	8.4	88	23	131	28
Nd	5.8	1.8	11	31	15	3.3		32	5.6	57	15	80	16

TABLE 2.3 (continued)

3 PETROGRAPHY AND MINERAL CHEMISTRY

3.1 LOW-K_2O LINEAGE

3.1.1 PETROGRAPHY

3.1.1.1 LTZ basalts and dolerites

The LTZ basalts and dolerites, as defined in Fig. 2.5A, have been sub-divided into a number of geochemical types (*e.g.* see TABLE 2.3) and where appropriate, the petrography of these geochemical types is described simultaneously.

3.1.1.1.1 LTZ-type basalts

The LTZ-type basalt sub-group includes the LTZ basalts, the high-Na_2O LTZ basalts, the low-MgO LTZ picritic basalts and the TYPE I LTZ dolerites (see section 2.3.2.2) as these sub-types define a continuous range in geochemical compositions (*i.e.* apart from the high-Na_2O and low CaO concentrations of the high-Na_2O LTZ basalts). These LTZ-type basalts (and dolerites) exhibit a variety of textural and petrological features both within and between the individual basalt units, and these variations appear to be largely independent of the whole rock composition, grain size or the relative position of the sample within the individual basalt units.

The LTZ- and high-Na_2O LTZ basalts and the TYPE I LTZ dolerites are characterised, in general, by the presence of glomeroporphyritic aggregates and/or phenocrysts of zoned plagioclase (abbreviated to "phenocryst" in subsequent TABLES). Although the LTZ- and high-Na_2O LTZ basalts typically have $<1\%$ modal glomeroporphyritic (or phenocrysts of) plagioclase (see TABLE 3.1), often as a single aggregate of plagioclase per thin section, LTZ- and high-Na_2O LTZ basalts with up to 10% (by volume) glomeroporphyritic plagioclase are recognised. In contrast to the average LTZ-type basalts, the TYPE I LTZ dolerites tend to have a higher modal proportion ($\pm$5-9.1%) of plagioclase phenocrysts, often in glomeroporphyritic aggregates, present. Pseudomorphs after pyroxene and/or olivine phenocrysts are rare and were only recognised in two very fine grained LTZ basalts (KLB-119 and -188).

The LTZ-type basalts and dolerites exhibit a range in textures from ophitic to sub-ophitic. The interstitial domains vary in texture from intergranular to intersertal, often within a

	LTZ basalts												
Sample No. (KLB-)	115	123	125	126	127	134	135	137	145	155	156	196	203
Plagioclase	41.9	43.0	49.8	41.9	47.2	49.6	37.4	42.5	38.3	40.0	45.8	39.9	36.9
Pyroxene	25.3	27.2	27.4	28.1	24.4	26.0	28.9	24.1	24.0	23.7	22.8	22.7	27.2
Mesostasis	14.1	7.3	7.3	10.6	9.4	5.4	11.1	11.8	9.3	14.5	9.4	9.3	13.4
Oxide	4.8	4.0	1.6	3.6	4.0	1.6	3.7	4.2	3.7	2.5	2.6	4.8	4.0
Olivine	4.5	7.9	6.1	5.0	3.7	1.7	6.2	5.6	6.9	1.6	5.2	7.3	4.5
"Amygdales"	9.4	10.6	7.6	10.8	11.2	12.7	11.2	8.8	16.2	12.3	14.2	13.6	14.0
Phenocryst						3.0	1.5	2.8	1.6	5.4		2.4	
%MgO	6.24	7.47	6.73	7.04	6.57	7.69	6.13	7.10	8.51	6.53	7.61	7.36	7.65

	High-Na_2O LTZ basalts				Low-MgO LTZ picritic basalts		TYPE I LTZ dolerite	Low-P_2O_5 LTZ basalts	
Sample No. (KLB-)	117	165	170	173A	128	172	049	016	023
Plagioclase	38.4	38.2	44.6	41.0	46.4	47.8	43.1	40.7	34.4
Pyroxene	23.6	26.0	23.3	18.8	33.9	20.2	26.6	25.5	23.0
Mesostasis	17.8	15.6	11.0	14.0		7.2	12.7	7.3	13.0
Oxide	5.3	4.0	3.8	4.4	3.1	1.8	3.5	9.8	10.4
Olivine	5.8	2.0	1.8	8.6	10.1	9.6	4.6	3.3	6.2
"Amygdales"	5.8	14.2	15.5	13.0	6.9	13.4	0.4	8.8	7.8
Phenocryst	3.03						9.1	4.6	5.2
%MgO	5.83	8.02	8.16	7.82	10.51	9.14	6.19	5.53	5.32

"Amygdales" refer to diktytaxitic amygdales only
%MgO is the whole rock wt% MgO (data normalised to 100%)

TABLE 3.1. Modal proportions determined by point-counting (N = 1000) for the LTZ-type basalts and dolerites.

single thin section. The predominantly ophitic textures of the LTZ-type basalts is similar to that described for the basalts of the Central Karoo area by, for example, Walker and Poldervaart (1949). The mineral assemblage in the LTZ-type basalts and dolerites invariably includes plagioclase, pyroxene (both augite and pigeonite), oxide, olivine pseudomorphs, mesostasis and diktytaxitic amygdales. Modal analyses of the LTZ-type basalts and dolerites, determined by point-counting, are tabulated in TABLE 3.1 and although the modal proportions of the mineral phases present are variable, the relative proportions are generally independent of the whole rock geochemistry (see %MgO in TABLE 3.1), although the low-MgO LTZ picritic basalts are characterised by a somewhat higher modal proportion of olivine (see TABLE 3.1), which is coarser grained than the olivine of the LTZ-type basalts (and dolerites). The angular interstices defined by plagioclase (± pyroxene) are filled by either mesostasis or outline angular "diktytaxitic" amygdales. The interstitial mesostasis is ubiquitous in the LTZ-type basalts and dolerites and has, on average, modal proportions of ± 10% (see TABLE 3.1) and is only rarely totally absent (see, for example, the low-MgO LTZ picritic basalt KLB-128). The mesostasis of the LTZ-type basalts is typically very altered and shows a textural variation from an altered glass to a cryptocrystalline matrix with microphenocrysts of oxide, plagioclase and rare pyroxene. The crystal habit of the microphenocrysts (skeletal to acicular oxides and swallowtail and hollow sections of plagioclase) are characteristic of rapid crystallization or

quenching (Cox, Bell and Pankhurst, 1979). The mesostasis of the TYPE I LTZ dolerites, however, varies from an altered glass (which contains microphenocrysts of plagioclase and oxide) to a fine feldspar, chlorite ±oxide aggregate (*i.e.* the product of either the final stages of crystallization or due to the devitrification of the mesostasis). Williams *et al.* (1954) define diktytaxitic vesicles as abundant closely spaced minute angular cavities defined by the random orientation of plagioclase laths. The plagioclase laths which project into and outline the diktytaxitic amygdales are of the same size and composition as the adjacent groundmass plagioclase. The diktytaxitic amygdales in the LTZ-type basalts (and dolerites) exhibit a wide variation in size (from ≤0.5mm to ≤5mm) and modal proportions (0.4 to 16.2% - see TABLE 3.1). The diktytaxitic amygdales usually have chlorite or zeolite margins and are filled with chlorite and/or zeolite (± rare calcite or quartz) and well defined colloform textures are common. Few spherical or sub-spherical true amygdales were seen in thin section but such amygdales are filled with chlorite, calcite, zeolite or quartz and are often associated with an increased concentration of the mesostasis in the adjacent matrix. The LTZ-type basalts are commonly cross-cut by chlorite, zeolite, calcite and/or quartz veins.

3.1.1.1.2 Low-P_2O_5 LTZ basalts

The low-P_2O_5 LTZ basalts are characterised by a phenocryst/xenocryst assemblage (see discussion on pages 71-72), usually present in glomeroporphyritic aggregates, which includes plagioclase, alkali feldspar (perthite), pyroxene and pseudomorphs after olivine. A high modal proportion of phenocrysts/xenocrysts are present, typically between ±5 to 10% (see TABLE 3.1), with a single exception, KLB-024, which contains rare phenocrysts/xenocrysts (< 1 modal%) of feldspar only.

The low-P_2O_5 LTZ basalts are all fine to very fine grained and the texture varies from intergranular through intersertal to hyalopilitic and rare sub-ophitic pyroxenes are present in the "coarser" grained samples, KLB-023 and -024. The mineral assemblage of the low-P_2O_5 LTZ basalts includes feldspar (plagioclase and alkali feldspar), pyroxene (both clinopyroxene and pigeonite), oxide, olivine pseudomorphs, mesostasis and diktytaxitic amygdales. The mineral assemblage of the low-P_2O_5 LTZ basalts and the modal proportions of the phases present (see TABLE 3.1) is similar to that of the LTZ-type basalts, although the phenocryst/xenocryst assemblage of the low-P_2O_5 LTZ basalts is distinctly different to that of the LTZ-type basalts (which typically includes only plagioclase). The low-P_2O_5 LTZ basalts however have, on average, a higher proportion of the oxide phase present with these oxides concentrated in the mesostasis. The oxides are typically very altered resulting in the characteristic Fe-staining of the mesostasis in the low-P_2O_5 LTZ basalts. The diktytaxitic amygdales of the low-P_2O_5 LTZ basalts are filled with chlorite, calcite and/or quartz and occasionally have oxide margins.

An undulating contact between basalt and quartzite (with rounded quartz grains cemented by calcite) is observed in the low-P_2O_5 LTZ basalt, KLB-179, where rounded segregations of basalt are included in the quartzite. Two red sedimentary lenses are included in the basalt interval intercepted by the borehole NG1 (see APPENDIX A and the BGR Kalahari Project (GS-17-G) Drill logs) and this undulating contact marks the contact between the upper flow margin of the basalt unit sampled by KLB-179 and the lower of the sedimentary lenses. The possible origin of these quartzite lenses (*i.e.* either xenolith or interbedded sediment) cannot be identified from the core sample.

3.1.1.1.3 LTZ dolerites

The LTZ-dolerites are characterised by a bimodal MgO distribution and the low MgO sub-group is further sub-divided into TYPE I and TYPE II LTZ dolerites (see section 2.3.2.2) where the TYPE I LTZ dolerites are geochemically and petrographically (see section 3.1.1.1.3) similar to the LTZ-type basalts.

TYPE II LTZ dolerites

Although the TYPE II LTZ dolerites have a widespread distribution in eastern Botswana, they are characterised by a broadly similar petrographic appearance and by their low grade (greenschist) metamorphic assemblages with their primary igneous textures extensively replaced by chlorite and epidote.

The TYPE II LTZ dolerites are typically aphyric. When they are sparsely phyric the phenocrysts, often in glomeroporphyritic aggregates, of plagioclase and rare pyroxene (KLB-104 only) are present in modal proportions of <3%. The plagioclase in the glomeroporphyritic aggregates is typically very altered and pseudomorphs after plagioclase (chlorite, epidote and sericite) are common. A remnant sub-ophitic texture is preserved in the TYPE II LTZ dolerites and well developed interstitial granophyric/myrmekitic-type intergrowths of quartz, plagioclase, alkali feldspar and chlorite together with free quartz (present in modal proportions of up to 4%) and rare apatite and epidote, which form, in total, up to ±10% (by volume) of the rock, are preserved in the less altered TYPE II LTZ dolerites. The plagioclase crystals adjacent to these interstitial "granophyric" domains often retain their primary euhedral outlines. An increased degree of replacement, usually chloritization (and epidote concentration) and the progressive replacement of pyroxene by amphibole and chlorite, are associated with these "granophyric" domains, which results in the characteristic patchy style of replacement seen in many of the TYPE II LTZ dolerites. The mineral assemblage of the TYPE II LTZ dolerites therefore includes plagioclase, pyroxene (both augite and pigeonite), oxide, quartz, chlorite, amphibole, epidote and the "granophyric" assemblages (plagioclase, alkali feldspar, quartz and apatite). The oxides of

the TYPE II LTZ dolerites are often very altered and pseudomorphs after oxides are common, but lamellae of oxide (ilmenite), or pseudomorphs after oxide, with a trellis-type habit, are usually visible in these oxides/oxide pseudomorphs. The oxidation of titanomagnetite at temperatures >600°C and moderate pressures results in the direct formation of ilmenite-hematite solid solution (*i.e.* oxidation exsolution) while continued oxidation (at progressively higher oxygen fugacities) results in pseudomorphic replacement of the primary titanomagnetite by rutile, titanohematite and pseudobrookite (Haggerty, 1991). According to the oxidation classification scheme outlined in Haggerty (1991) the primary titanomagnetites in the TYPE II LTZ dolerites of Botswana are therefore oxidised at temperatures >600°C to at least the C2 or C3 stage (*i.e.* from a small number of "exsolved" ilmenite lamellae in a magnetite-enriched ulvöspinel solid solution to a ulvöspinel-poor magnetite solid solution densely crowded with ilmenite lamellae along the {111} parting planes) although a C7-type complete replacement of the primary titanomagnetite is more common.

The extensive replacement of the primary igneous mineralogy and textures in the TYPE II LTZ dolerites suggests that these dolerites have undergone low grades of regional metamorphism as chlorite, actinolite, zoisite/clinozoisite (epidote) and albite assemblages are indicative of greenschist facies grades of regional metamorphism in mafic rocks (Winkler, 1979). The presence of rare biotite in some samples (*e.g.* KLB-051) suggests that metamorphic grades as high as middle greenschist facies have occurred locally (Winkler, 1979) with the biotite replacing chlorite as the metamorphic grade increases. The TYPE II LTZ dolerites are therefore distinctly different to both the TYPE I LTZ dolerites and the LTZ-type basalts of Botswana and to Karoo basalts and dolerites in general. However, in contrast, the TYPE II LTZ dolerites are noted to closely resemble the Proterozoic dolerites of Botswana and Zimbabwe (see section 1.2.2.2) which have typical mineral assemblages of plagioclase, pyroxene (augite and pigeonite), oxide and quartz and Aldiss (1989) describes a patchy style of chlorite alteration and pyroxene replacement associated with interstitial granophyric domains in the Proterozoic dolerites of the Shashe area, while Tennick *et al.* (1976) assigns a similar association to low grade regional metamorphism of the dolerite dykes associated with the Deweras basalts. The close petrographic resemblance that exists between the TYPE II LTZ dolerites and these Proterozoic dolerites of Botswana and Zimbabwe suggests that the TYPE II LTZ dolerites of this study may in fact not be Karoo aged, but that they rather belong to the Proterozoic suite of dolerites in eastern Botswana.

HIGH-MGO LTZ PICRITES

The high-MgO LTZ picrites are characterised by a mesocumulate texture with euhedral to subhedral cumulus crystals of orthopyroxene (commonly rimmed in clinopyroxene),

clinopyroxene and olivine (in KLB-072 only) with interstitial clinopyroxene and plagioclase. The clinopyroxene is recrystallised to polygonal aggregates and reaction relationships between the recrystallised clinopyroxene, and olivine in KLB-072, and the interstitial plagioclase are well developed. The recrystallised clinopyroxene is partially to totally replaced by biotite, where the biotite pseudomorphs the polygonal outlines of the recrystallised clinopyroxene. The mineral assemblage of the high-MgO LTZ picrites therefore includes orthopyroxene, clinopyroxene, biotite, plagioclase, rare green spinels, oxide and olivine (in KLB-072 only) and the modal proportions determined by point-counting are listed in TABLE 3.2.

	High-MgO LTZ picrites	
Sample No. (KLB-)	072	077
Olivine	18.4	
Orthopyroxene	35.2	39.8
Clinopyroxene	19.8	19.7
Biotite	7.8	5.4
Plagioclase	17.8	34.9
Oxide	0.5	
%MgO	21.83	14.01

TABLE 3.2. Modal proportions determined by point-counting (N = 1000) for the high-MgO LTZ picrites, where %MgO refers to the whole rock %MgO (data normalised to 100% on a volatile-free basis).

The high-MgO LTZ picrites are characterised by a petrography and mineralogy which is distinctly different to the ophitic to sub-ophitic textures and the plagioclase, clinopyroxene, olivine and oxide assemblage described in section 3.1.1.1 for the LTZ-type basalts (including the low-MgO LTZ picritic basalts) and dolerites of Botswana. Evidence, including the recrystallization of clinopyroxene into polygonal aggregates, suggests that the primary mesocumulus textures of the high-MgO LTZ picrites may have been affected by granulite grades of metamorphism, indicated by the instability of olivine and pyroxene in the presence of plagioclase. The mesocumulus textures together with the interpreted granulite grades of metamorphism of the high-MgO LTZ picrites are, however, similar to those described for the Olivine Norites and Norites of the basement complex (see section 1.2.2.1) as described by Aldiss (1983a & b). The high-MgO LTZ picrites therefore do not appear to be Karoo aged, but rather belong to the Archaean suite of Norites and Olivine Norites.

3.1.1.2 HTZ-TYPE BASALTS AND DOLERITES

The HTZ-type basalts (which include both the HTLZ/HTZ- and HTZ (low Fe)- basalt and dolerite sub-groups defined in section 2.3.2.3) are characterised by a considerable variation in their textures, petrology and mineralogy and these variations appear to be largely

independent of rock type, outcrop character or whole rock composition and the two HTZ-types are described simultaneously, where appropriate, to avoid repetition.

The HTZ-type basalts, with rare exceptions, are characterised by the ubiquitous presence of phenocrysts, both in glomeroporphyritic aggregates and as isolated individual grains. Plagioclase is the dominant phenocryst phase present in the HTZ-type basalts although the phenocryst assemblage typically also includes pyroxene (both augite and rare pigeonite) and rare pseudomorphs after olivine and oxide may be present. The modal proportions of the phenocrysts in the HTZ-type basalts is very variable, with proportions varying from <1% to >20%, as is the ratio of the different phases within the phenocryst assemblage (see TABLE 3.3). Average modal proportions of 2-5% total phenocrysts are most common with the phenocryst size typically 2 to 5mm, although plagioclase phenocryst laths with lengths of up to 35mm (see KLB-063) are present, and many of the HTZ-type basalts exhibit a seriate grain size variation, of plagioclase in particular, from microphenocryst to phenocryst.

	HTZ basalts					HTLZ basalts			HTZ dolerites				HTLZ dolerites	
Sample No. (KLB-)	014	066	088	096	114	044	100	178	031	040	062A	085	041	095
Plagioclase	42.2	31.7		34.8	49.5	39.9	39.5	42.2	38.8	42.3			12.6	36.6
Pyroxene	36.6	21.7		31.5	14.0	28.6	38.6	33.2	36.7	21.2			5.7	35.5
Olivine	0.5	0.8		3.3	7.0	1.7	0.2	1.7						3.5
Oxide	11.2	7.3		8.8	6.6	8.9	6.3	7.8	7.9	8.5				7.1
Mesostasis	7.3	16.7	87.1	8.1	16.4	13.6	5.2	7.3	22.3	25.6	97.5	95.0	69.7	16.0
"Amygdales"				1.6	2.7		0.8							
Phenocryst assemblage														
Plagioclase	2.2	21.8	6.5	10.3	2.5	7.3	8.2	7.0		2.1	1.7	3.5	9.7	1.2
Pyroxene			6.4	1.2	1.3		0.8	0.7			0.8	1.2	2.1	
Olivine												0.3		
%MgO	4.57	3.22	4.39	4.40	4.18	5.33	5.13	4.47	5.49	3.72	4.55	3.84	6.21	6.69

"Amygdales" includes both true and diktytaxitic amygdales
%MgO is the whole rock wt% MgO (data normalised to 100%)

TABLE 3.3. Modal proportions determined by point-counting (N=1000) for the HTZ-type basalts.

The HTZ (low Fe) and HTLZ/HTZ basalt and dolerite sub-groups have similar phenocryst assemblages, present in similar modal proportions, although the most phyric HTZ-type basalt samples recognised are all HTZ (low Fe) basalts and dolerites (*i.e.* KLB-066, -081 & -088 all contain ≥13% plagioclase phenocrysts, with rare anhedral olivine and pyroxene included in the plagioclase phenocrysts). The HTZ (low Fe) basalts and dolerites also tend to include a higher proportion of pyroxene in the phenocryst assemblage where these pyroxene phenocrysts are commonly present as isolated subhedral to lath-like crystals. In contrast, in at least five of the HTLZ/HTZ basalts and dolerites (KLB-044, -063, -092, -093 & -096) two distinct "phenocryst" populations are present where the plagioclase "megacrysts", with lengths ≥6mm, are considerably coarser grained than the associated phenocryst

assemblage and in a single example, KLB-096, strongly zoned glomeroporphyritic aggregates of plagioclase and pyroxene are included in the "megacryst" assemblage.

The HTZ-type basalts (and dolerites) exhibit a considerable variation in texture with these variations primarily the result of grain size, proportion of mesostasis present and the relationship between plagioclase and pyroxene and these factors appear to be relatively unaffected by either rock type or whole rock geochemistry. The most common texture observed in the HTZ-type basalts, however, varies, often within a single thin section, from intergranular to intersertal. Although the modal proportion of mesostasis present in the intersertal domains varies from ≤1% to ≥97.5%, in the extreme, where a hyalopilitic-type texture is present (see TABLE 3.3), the HTZ (low Fe) basalts and dolerites tend to have a higher modal proportion of mesostasis present (*i.e.* commonly have hyalopilitic textures). Rare sub-ophitic pyroxene may, however, be present in these intergranular domains and a single HTLZ dolerite sample, KLB-095, has an ophitic texture which is more commonly associated with the LTZ-type basalts and dolerites. The mesostasis of the HTZ-type basalts (and dolerites) similarly exhibits a considerable range in character from an altered glass to having a felted texture (which commonly includes free quartz) and the mesostasis typically includes microphenocrysts, with skeletal habits, of plagioclase, oxide, apatite and rare pyroxene. A number of the HTZ-type basalts include late stage patchy granophyric domains which include plagioclase, alkali feldspar, quartz, apatite and zeolite together with rare pyroxene and oxide. This late stage granophyre is best developed in the HTZ (low Fe) basalt and dolerite, KLB-091 and -094, where it varies in habit from patchy interstitial domains to discrete spherical segregations with diameters ≤4mm. The mineral assemblage of the HTZ-type basalts therefore includes plagioclase, augite (and rare pigeonite), oxide, apatite and mesostasis and may also include pseudomorphs after olivine, quartz, zeolite and diktytaxitic amygdales. Two distinct oxide crystal habits, both with skeletal morphologies, *i.e.* prismatic to acicular and equant, are present in the HTZ-type basalts although the acicular oxide is usually found associated with the mesostasis. TABLE 3.3 tabulates the modal analyses of the HTZ-type basalts, determined by point-counting, and clearly reflects the diversity in the petrography of the HTZ-type basalts and dolerites. Amygdales are present in both HTZ-type basalts and dolerites and are usually small in size and associated with the mesostasis, and in the HTLZ dolerite, KLB-068, lunate segments of a glassy mesostasis rich in oxide and plagioclase microphenocrysts, are included in the amygdales. Diktytaxitic amygdales are very rarely present in the HTZ-type basalts and dolerites and, where present, are always small (≤1mm) and present in low modal proportions. Both the true and diktytaxitic amygdales are filled with chlorite, zeolite and/or quartz. Chlorite and zeolite veins may cross-cut the HTZ-type basalts and in a single example, KLB-178, calcite veins are present.

The petrographic characteristics shown by the HTLZ/HTZ- and HTZ (low Fe)- basalts and dolerites define a continuous range such that the two HTZ-type basalts and dolerites cannot be differentiated by petrography alone. The HTZ.LF basalts of the Central Lebombo have clinopyroxene as the only phenocryst phase present, although plagioclase probably joins the liquidus assemblage at low MgO concentrations (<5-5.5% MgO) as rare plagioclase phenocrysts are recognised in evolved HTZ.LF basalts. In contrast, although the HTZ.HF basalts of the Central Lebombo are predominantly aphyric, rare plagioclase phenocrysts are recognised. The late crystallization of plagioclase in the HTZ.LF basalts with respect to the LTZ and HTZ.HF basalts of the Central Lebombo is therefore an important difference (Sweeney *et.al.*, 1994). As the HTZ (low Fe) basalts and dolerites of Botswana are all evolved, the order of crystallization cannot be determined, but the higher proportion of clinopyroxene phenocrysts present suggests a resemblance to the HTZ.LF basalts of the Central Lebombo. The HTLZ/HTZ basalts and dolerites range from aphyric to having a phenocryst and "megacryst" assemblage present, whereas the HTZ.HF basalts of the Central Lebombo are predominantly aphyric, although plagioclase is the dominant phenocryst phase present in both sub-groups. The predominantly intergranular to intersertal texture, together with the plagioclase, pyroxene, olivine and titanomagnetite phenocryst assemblage, of the HTZ-type basalts of Botswana are, therefore, petrographically similar to the "enriched" basalts described from the Nuanetsi (Cox *et al.*, 1967) and Lebombo (Sweeney *et al.*, 1994) areas.

3.1.1.3 SUMMARY

A number of petrographic sub-groups are recognised in the low-K_2O lineage where these sub-groups reflect broadly the differences observed in the whole-rock geochemistry. The petrographic subgroups have been defined as the LTZ-type basalts (which include the LTZ basalts, the high-Na_2O LTZ basalts, the low-MgO LTZ picritic basalts and the TYPE I LTZ dolerites), the low-P_2O_5 LTZ basalts, the TYPE II LTZ dolerites, the high-MgO LTZ picrites and the HTZ-type basalts (and dolerites).

Two of these petrographic (and geochemical) sub-groups have petrographic and mineralogical evidence which suggests that they are not Karoo aged where the metamorphic characteristics of the TYPE II LTZ dolerites are broadly comparable with the Proterozoic dolerite suite in eastern Botswana (see section 3.1.1.1.3), while the cumulate textures together with evidence of granulite grades of metamorphism in the high-MgO LTZ picrites are broadly similar to the Archaean Norites and Olivine Norites of eastern Botswana (see section 3.1.1.1.3).

Apart from these two LTZ sub-groups which do not appear to be Karoo aged a third LTZ sub-type, the low-P_2O_5 LTZ basalts, are present. The low-P_2O_5 LTZ basalts are characterised by a phenocryst assemblage which includes plagioclase, alkali feldspar (perthite), pyroxene and pseudomorphs after olivine (see section 3.1.1.1.2), which is in contrast to the plagioclase only phenocryst assemblage of the LTZ-type basalts. The low-P_2O_5 LTZ basalts are, in addition, characterised by higher modal proportions of oxide (see TABLE 3.1) than the LTZ-type basalts.

3.1.1.3.1 Comparison between the LTZ-type and HTZ-type basalts and dolerites

The LTZ-type basalts (and dolerites) typically contain only plagioclase as a phenocryst phase (pyroxene and olivine are included in the phenocryst assemblage of only two LTZ-type basalts), typically in modal proportions of ≤1% although a range from 0 to 9.1% was determined by point-counting. In contrast, the HTZ-type basalts and dolerites are characterised by a phenocryst assemblage which typically includes plagioclase and pyroxene, together with rare olivine pseudomorphs and oxide with typical modal proportions of 2-5%, although a range from 0 to >20% was determined by point-counting.

The LTZ-type basalts (and dolerites) typically have ophitic to sub-ophitic pyroxene with the interstitial domains varying in texture from intergranular to intersertal while the HTZ-type basalts and dolerites have rare sub-ophitic pyroxene, and in a single example ophitic pyroxene, and vary in texture from intergranular through intersertal to hyalopilitic. The mineral assemblage of the LTZ-type basalts and the HTZ-type basalts and dolerites are similar, although olivine which is ubiquitous in the LTZ-type basalts is not present in all of the HTZ-type basalts and dolerites and the HTZ-type basalts and dolerites are, in addition, characterised by the presence of apatite. A comparison between the modal proportions of the LTZ-type basalts and the HTZ-type basalts and dolerites (see TABLE 3.1 and 3.3) suggests a similar range in proportions for all of the phases present except for the mesostasis, oxides and the diktytaxitic amygdales. The oxides are present in greater modal proportions in the HTZ-type basalts and dolerites with a range of 6.3 to 11.2% (see TABLE 3.3) and the both acicular and equant crystal habits are present, whereas in the LTZ-type basalts (and dolerites) the oxides usually only have an equant habit and modal proportions vary from 1.6 to 5.3% (see TABLE 3.1).

In conclusion, although the LTZ-type basalts (and dolerites) and the HTZ-type basalts and dolerites exhibit characteristic petrographic and mineralogical features, the range of features is such that the LTZ-type basalts and HTZ-type basalts (and dolerites) cannot be distinguished by petrography alone.

3.1.2 MINERAL CHEMISTRY

3.1.2.1 Olivine

Anhedral interstitial pseudomorphs after olivine are present in all of the LTZ-type basalts and in many of the HTZ-type basalts and dolerites with the olivine pseudomorphed by a combination of bowlingite, iddingsite and oxide. The modal proportions of the olivine pseudomorphs present in the LTZ-type basalts is variable and a range from 1.6 to 10.1% (by volume) was determined by point-counting and the proportion of olivine pseudomorphs present in the LTZ-type basalts exhibit, in general, no direct relationship with the whole rock composition (see TABLE 3.1). Olivine pseudomorphs, where present, in the HTZ-type basalts and dolerites have modal proportions of 0.2 to 7.0%, determined by point-counting, and rare pseudomorphs after olivine are also included in the phenocryst assemblage, however the presence/absence or the proportion of olivine pseudomorphs present in the HTZ-type basalts and dolerites appears to be independent of the whole rock compositions (see TABLE 3.3).

	LTZ-type basalts					
	OLIV1C	OLIV1M	OLIV2M	OLIV2C	OLIV2M2	OLIV3
SiO_2	33.58	33.62	34.18	33.84	34.07	34.33
FEO	45.53	45.63	44.79	44.64	44.20	42.63
MNO	.73	.77	.57	.56	.61	.60
MGO	18.89	18.99	20.98	21.42	21.77	21.62
CAO	.48	.44	.50	.34	.29	.19
TOTAL	99.21	99.45	101.02	100.80	100.94	99.37
STRUCTURAL FORMULA CALCULATED TO 4 OXYGENS						
SI	.9990	1.0000	.9910	.9840	.9860	1.0020
FE	1.1330	1.1350	1.0860	1.0850	1.0690	1.0400
MN	.0190	.0190	.0140	.0140	.0150	.0150
MG	.8380	.8420	.9070	.9280	.9390	.9400
CA	.0150	.0140	.0150	.0110	.0090	.0060
SUM	3.0040	3.0100	3.0130	3.0220	3.0180	3.0030
FO	42.1	42.2	45.2	45.8	46.4	47.1
FA	57.9	57.8	54.8	54.2	53.6	52.9

TABLE 3.4. Selected olivine analyses of the LTZ-type basalts. C refers to the core and M to the margin of the individual grains with the same number in the analysis name.

SAMPLE DESCRIPTION:
OLIV1: coarse anhedral olivine (KLB-199)
OLIV2: anhedral olivine (KLB-199)
OLIV3: anhedral olivine (KLB-200) included in pyroxene

Fresh olivine, or fragments of fresh olivine, are preserved only in a single relatively unaltered LTZ-type basalt flow sampled from borehole C1. The olivine in these samples (KLB-199 and -200) is present as both inclusions in pyroxene and interstitial to plagioclase laths. The olivine in sample KLB-199 has a range in composition from $Fo_{54.3}$ to $Fo_{37.4}$ and

exhibits no apparent compositional zonation from the core to the margin within individual grains (see OLIV2 in TABLE 3.4). The composition of the olivine in KLB-200 is similar to that in KLB-199 with a range in composition from $Fo_{50.9}$ to $Fo_{42.9}$. Representative olivine compositions are summarised in TABLE 3.4 and the electron microprobe analyses of olivine are tabulated in APPENDIX C1.

If a Fe_2O_3:FeO ratio of 0.15 for the LTZ basalts is assumed (after Brooks, 1976) the Mg Numbers (Mg#), calculated from whole rock compositions normalised to 100%, of the samples KLB-199 and -200 are 60.93 and 59.20 respectively. The compositions of the olivine, calculated using a K_D of .3 (Roeder and Emslie, 1970) which would be in equilibrium with these whole rock compositions are $Fo_{83.87}$ (KLB-199) and $Fo_{82.87}$ (KLB-200). The low Fo contents in the analyzed olivine are probably the result of alteration as the predominant chemical effect associated with the alteration of olivine is an increase in the Fe:Mg ratio (Deer, Howie and Zussman, 1962). Walker and Poldervaart (1949), however, noted the presence of olivine with compositions which range from Fo_{85} to Fo_0 in the Central Karoo area, with olivine with compositions of $\geq Fo_{50}$ generally crystallizing prior to the onset of pyroxene crystallization.

3.1.2.2 Pyroxene

Pyroxene (both clinopyroxene and pigeonite) is present in all of the LTZ-type basalts and exhibits a wide variety of characteristics and the relationship between the plagioclase and the pyroxene defines the texture of the LTZ-type basalts. The pyroxenes range in habit from coarsely ophitic (≤5mm in diameter) through sub-ophitic to interstitial, often within a single basalt unit, and pyroxene may be present as microphenocrysts in the mesostasis. Fig. 3.1A summarises the results of the electron microprobe analyses of pyroxene from selected LTZ-type basalt samples (see APPENDIX C1) and representative pyroxene analyses are tabulated in TABLE 3.5. The pyroxenes of the LTZ-type basalts define a broad compositional variation from augite through sub-calcic augite to pigeonite. The augites, however, broadly define a trend of decreasing wollastonite (Wo) and enstatite (En) and an increasing ferrosilite (Fs) concentrations which is typical of fractional crystallization (or cotectic equilibrium crystallization) of tholeiitic magmas and normal zoning in individual augite grains, see TABLE 3.5, reflects a similar compositional variation from the core to the margins of individual augite grains. Pigeonite was optically identified in the majority of the LTZ-type basalts as small interstitial grains, although rare sub-ophitic and ophitic pigeonites are present and the composition of the pigeonites reflects an increase in Wo and Fs and a decrease in En concentrations with continued fractionation and normal zonation patterns (see TABLE 3.5). The composition of augite in the LTZ-type basalts broadly reflects the whole rock geochemistry with the augites having higher En contents in the more mafic

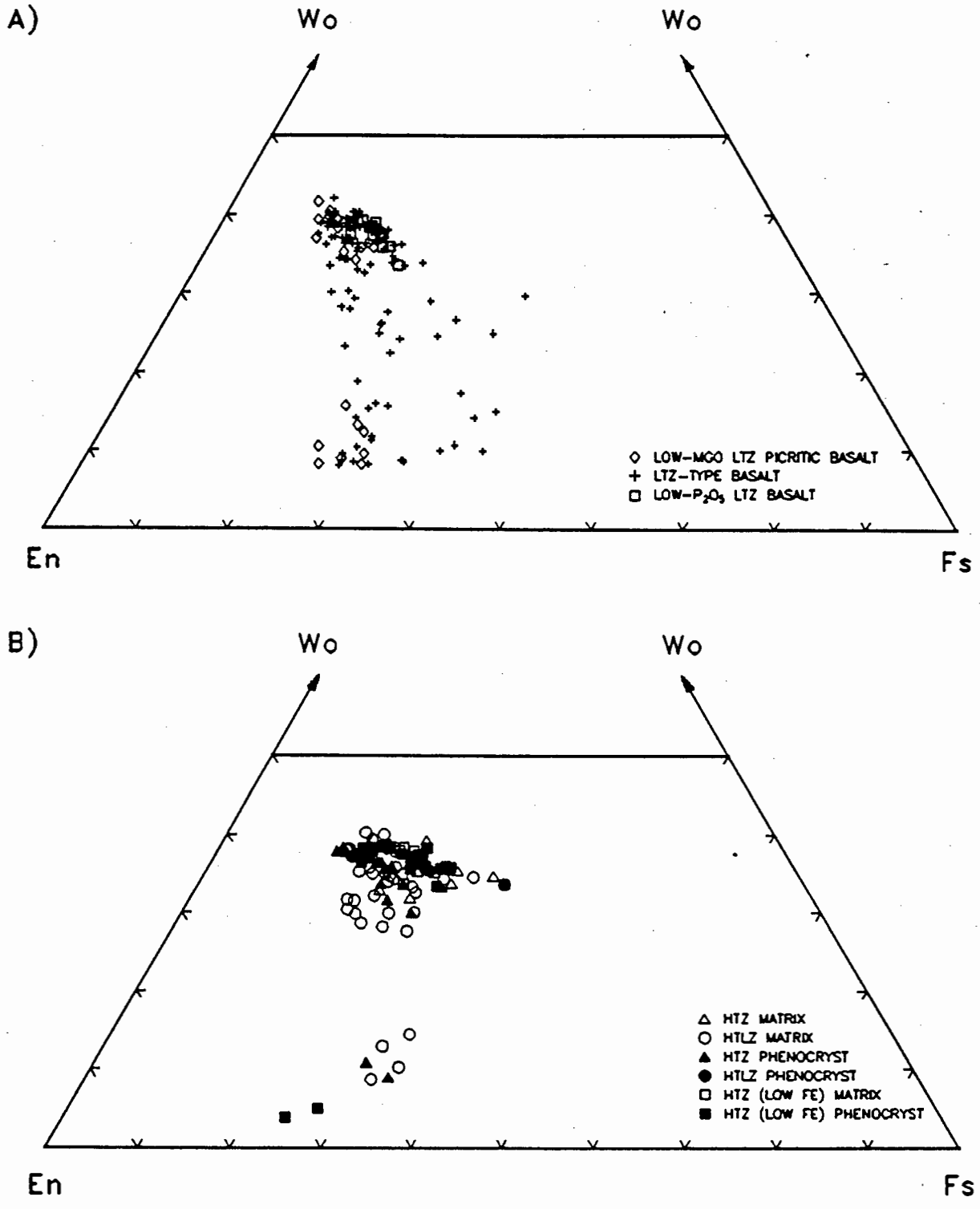

Fig. 3.1. Pyroxene compositions, in terms of the Wo, En and Fs contents, of the (A) LTZ-type basalts and dolerites and (B) HTZ-type basalts, where the matrix and phenocryst pyroxene compositions of the HTZ-type basalts are indicated with different symbols (matrix: open and phenocryst: closed).

	LTZ-type basalts									HTZ-type basalts and dolerites		
	PYX1C	PYX1M	PYX2C	PYX2M	PYX3C	PYX3M	PYX4C	PYX4H	PYX4M	PYX5C	PYX5H	PYX5M
SiO_2	53.21	52.62	53.47	52.34	53.29	52.89	52.34	52.40	50.97	50.32	49.88	50.15
TiO_2	.27	.40	.35	.50	.21	.28	.32	.36	.58	1.06	1.23	1.16
Al_2O_3	1.55	1.78	1.15	1.77	.64	.69	1.79	1.19	1.39	3.67	3.32	2.31
Cr_2O_3	.76	.14					.50			.34	.23	
FeO	6.95	9.43	9.61	10.65	17.80	19.77	7.19	9.94	18.85	9.21	11.23	16.08
MnO	.24	.30	.24	.21	.40	.43	.19	.27	.42	.30	.28	.32
MgO	18.44	18.32	18.10	17.44	23.11	21.79	16.92	16.96	15.61	15.80	15.31	16.57
CaO	18.82	17.35	17.86	17.01	4.05	4.10	19.79	18.00	11.90	19.73	18.71	13.68
Na_2O	.21	.16	.13	.14			.18	.15	.13	.28	.22	.21
TOTAL	100.45	100.50	100.91	100.06	99.50	99.95	99.22	99.27	99.85	100.71	100.41	100.48
STRUCTURAL FORMULA CALCULATED TO 6 OXYGENS												
Si	1.943	1.933	1.958	1.940	1.976	1.972	1.942	1.958	1.942	1.863	1.865	1.889
Ti	.007	.011	.010	.014	.006	.008	.009	.010	.017	.030	.035	.033
Al	.067	.077	.050	.077	.028	.030	.078	.053	.062	.160	.146	.103
Cr	.022	.004					.015			.010	.007	
Fe	.212	.290	.294	.330	.552	.616	.223	.311	.601	.285	.351	.506
Mn	.007	.009	.008	.007	.013	.013	.006	.009	.014	.009	.009	.010
Mg	1.004	1.003	.988	.964	1.277	1.211	.936	.944	.886	.872	.853	.930
Ca	.736	.683	.701	.676	.161	.164	.787	.721	.486	.783	.750	.552
Na	.015	.011	.009	.010			.013	.011	.010	.020	.016	.016
SUM	4.013	4.021	4.018	4.018	4.013	4.014	4.009	4.017	4.018	4.032	4.032	4.039
WO	37.58	34.40	35.21	34.20	8.03	8.16	40.31	36.32	24.45	40.15	38.19	27.62
EN	51.22	50.54	49.63	48.76	63.77	60.41	47.96	47.59	44.63	44.72	43.46	46.54
FS	11.20	15.07	15.16	17.04	28.19	31.42	11.73	16.09	30.93	15.13	18.35	25.84
%MgO	8.21		9.14		7.12		6.53			6.69		

TABLE 3.5. Selected pyroxene analyses of the low-K_2O lineage basalts and dolerites. C refers to core, M to the margin and H to a point between the core and the margin of the individual grains with the same number in the analysis name. (%MgO is the whole rock wt% MgO)

	HTZ-type basalts and dolerites						Low-P_2O_5 LTZ basalts		
	PYX6C	PYX6M	PYX7	PYX8	PYX9C	PYX9M	PYX10C	PYX10M	PYX11
SiO_2	51.47	51.31	51.25	51.81	52.90	51.57	51.09	51.49	51.52
TiO_2	1.13	.81	1.33	.72	.38	.98	.52	.46	.48
Al_2O_3	1.79	1.34	2.06	1.63	2.01	2.19	3.56	1.53	2.04
Cr_2O_3					.25	.18	.42		.11
FeO	12.65	15.82	12.38	18.60	8.47	11.63	8.55	12.03	10.26
MnO	.24	.38	.25	.39	.21	.26	.19	.24	.23
MgO	14.93	13.31	14.55	21.39	17.28	16.03	16.46	16.16	16.18
CaO	18.55	17.50	18.67	5.40	19.16	18.16	19.01	17.86	19.07
Na_2O	.23	.22	.24	.11	.20	.24	.26	.21	.22
TOTAL	100.99	100.69	100.73	100.05	100.86	101.24	100.06	99.98	100.11
CALCULATED TO 6 OXYGENS									
Si	1.920	1.942	1.915	1.930	1.936	1.907	1.890	1.932	1.920
Ti	.032	.023	.037	.020	.010	.027	.014	.013	.014
Al	.079	.060	.091	.071	.087	.096	.155	.068	.090
Cr					.007	.005	.012		.008
Fe	.395	.501	.387	.579	.259	.360	.265	.378	.320
Mn	.008	.012	.008	.012	.006	.008	.006	.008	.007
Mg	.830	.751	.811	1.187	.943	.884	.907	.904	.898
Ca	.742	.710	.748	.215	.751	.719	.753	.718	.761
Na	.017	.016	.018	.008	.014	.018	.018	.015	.016
SUM	4.023	4.015	4.015	4.022	4.013	4.024	4.020	4.036	4.029
WO	37.57	35.96	38.28	10.80	38.34	36.50	39.01	35.77	38.32
EN	42.05	38.04	41.50	59.53	48.10	44.83	46.98	45.04	45.22
FS	20.38	25.99	20.22	29.67	13.56	18.67	14.01	19.20	16.46
%MgO	3.74			4.32	4.40		5.35		

SAMPLE DESCRIPTION:
LTZ-TYPE BASALTS
PYX1: sub-ophitic pyroxene (KLB-171)
PYX2: sub-ophitic pyroxene (KLB-172)
PYX3: interstitial pyroxene (KLB-200)
PYX4: interstitial pyroxene (KLB-155)
HTZ-TYPE BASALTS AND DOLERITES
PYX5: sub-ophitic pyroxene (KLB-095)
PYX6: pyroxene phenocryst (KLB-152)
PYX7: sub-ophitic pyroxene (KLB-152)
PYX8: pyroxene phenocryst (KLB-067)
PYX9: pyroxene "megacryst" (KLB-096)
LOW-P_2O_5 LTZ BASALTS
PYX10: pyroxene phenocryst (KLB-015)
PYX11: interstitial pyroxene (KLB-015)

TABLE 3.5 (continued).

basalts, illustrated by a comparison between the compositions of the augite in the low-MgO LTZ picritic basalts and the LTZ-type basalts in general (see Fig. 3.1A).

Pyroxene (augite and in some examples pigeonite) is present in the matrix of all of the HTZ-type basalts and is commonly also included in the phenocryst assemblage. The matrix pyroxenes are typically present as anhedral interstitial grains or as microphenocrysts in the mesostasis although both ophitic and sub-ophitic pyroxenes are present in rare examples. The pyroxene phenocrysts range in habit from anhedral grains associated with the glomeroporphyritic aggregates of plagioclase to individual euhedral crystals. The pyroxene compositions of selected HTZ-type basalts determined by electron microprobe (see APPENDIX C1) are summarised in Fig. 3.1B and representative pyroxene compositions are tabulated in TABLE 3.5. Although augite is present in both the phenocryst assemblage and in the matrix of the HTZ-type basalts these augites are of similar compositions (see Fig. 3.1B) in both the HTLZ/HTZ- and HTZ (low Fe)-type basalt and dolerites. The pyroxene "megacrysts" from the plagioclase-pyroxene glomeroporphyritic aggregates in KLB-096 have broadly similar compositions to the augites of the HTZ-type basalts, in general, although they have the highest En contents of all the HTZ-type basalt and dolerite pyroxenes (see TABLE 3.5 and Fig. 3.1B) which lie on the broad trend (of decreasing En and Wo and increasing Fs concentrations) defined by the augite compositions. This broad trend defined by the augite compositions is often reflected in the zonation of the individual phenocryst and matrix augites. The composition of the augite in the HTZ-type basalts broadly reflects the whole rock compositions with the pyroxenes having higher En and Fs concentrations in the samples which have higher whole rock MgO concentrations (see TABLE 3.5). Although the augite zoning is usually normal, augites with intense Ca^{2+}-Mg^{2+}-Fe^{2+} zonation, particularly along grain margins, are present (see TABLE 3.5) and some of the pyroxene microphenocrysts associated with the mesostasis have lower Wo contents than the associated matrix pyroxenes. Low-Ca pyroxene compositions were obtained from only three of the HTZ-type basalts, although pigeonite was identified optically (with a pseudo-uniaxial optic figure, *i.e.* $2V \approx 0$) in many of the HTZ-type basalts. In the HTZ (low Fe) basalt, KLB-062A, both orthopyroxene and pigeonite phenocrysts are present, where the orthopyroxene analyses were obtained from two different rounded anhedral phenocryst grains. The crystallization of orthopyroxene followed by pigeonite, which have $Mg:Fe^{2+}$ ratios $\geq 70:30$, is characteristic of tholeiitic fractionation (Deer, Howie and Zussman, 1978) and with continued fractional crystallization the pigeonites define a broad trend of increasing Wo and Fs and decreasing En concentrations.

Pyroxene (augite only) is present in the matrix and as a common phenocryst phase in the low-P_2O_5 LTZ basalts and the crystal habits of the matrix pyroxenes vary from sub-ophitic

through interstitial to microphenocryst, while both anhedral pyroxene phenocrysts associated with the glomeroporphyritic plagioclase and isolated subhedral pyroxene phenocrysts are present. The matrix and phenocryst augites have similar compositions (see TABLE 3.5) and typically exhibit normal zonation patterns. The augites (both matrix and phenocryst) composition of the low-P_2O_5 LTZ basalts reflect the relatively evolved whole rock geochemistry (6.17 to 4.72% MgO) of the low-P_2O_5 LTZ basalts with respect to the LTZ-type basalts (see Fig. 3.1A).

The composition of two pyroxene assemblages (a Ca-rich and a Ca-poor pyroxene) is characteristic of early fractional crystallization of tholeiitic magmas and is associated with a miscibility gap between augite and pigeonite. Sub-calcic augites (with 15-25% Wo) are therefore either metastable or are of a mixed augite-pigeonite composition (*e.g.* the sub-calcic pyroxenes may not represent a single phase, but rather an average composition of fine spinoidal and lamellar exsolution of augite and pigeonite as seen by Secco *et al.* (1988) in sub-calcic pyroxenes from a tholeiite dyke in the Paraná). Two trends, however, have been recognised in pyroxene crystallization of tholeiitic magmas. The first trend is the result of cotectic equilibrium crystallization with pyroxenes becoming progressively enriched in the hedenbergite component with continued crystallization. The second trend is the result of quench crystallization and defines a sub-calcic augite sequence recognised in the pyroxene compositions of the groundmass, as rims to more calcic pyroxene, or in chilled tholeiitic basalts (Deer, Howie and Zussman (1978), Muir and Tilley (1964) and Smith and Lindsley (1971)). The quench trend is characterised by constant Mg concentrations with $Ca \leftrightarrow Fe^{2+}$ substitution probably reflecting metastable crystal↔liquid partition as a result of rapid crystallization (Deer, Howie and Zussman, 1978). Although many of the analyzed augite grains in the LTZ-type basalts display normal zonation patterns from the core to the margin of individual grains (*i.e.* as a result of cotectic equilibrium crystallization) strong Wo and Fs zonation patterns are present and are usually associated with sub-calcic augites or with augites which have grain margins with sub-calcic compositions. Rare interstitial pyroxenes with sub-calcic compositions are also present and they are usually closely associated with, or included in, the mesostasis. The sub-calcic pyroxene compositions of the LTZ-type basalts may therefore be attributed to quench crystallization. Some of the scatter in the HTZ-type basalt and dolerite pyroxene compositions resulting from unusual zonation at grain margins and from pyroxene microphenocryst compositions may also be attributed to quench crystallization.

The range in compositions of the pyroxenes in the LTZ-type basalts and the HTZ-type basalts broadly reflects the differences in the whole rock geochemistry of these two low-K_2O lineage sub-groups, with the pyroxenes of the more evolved HTZ-type basalts exhibiting a

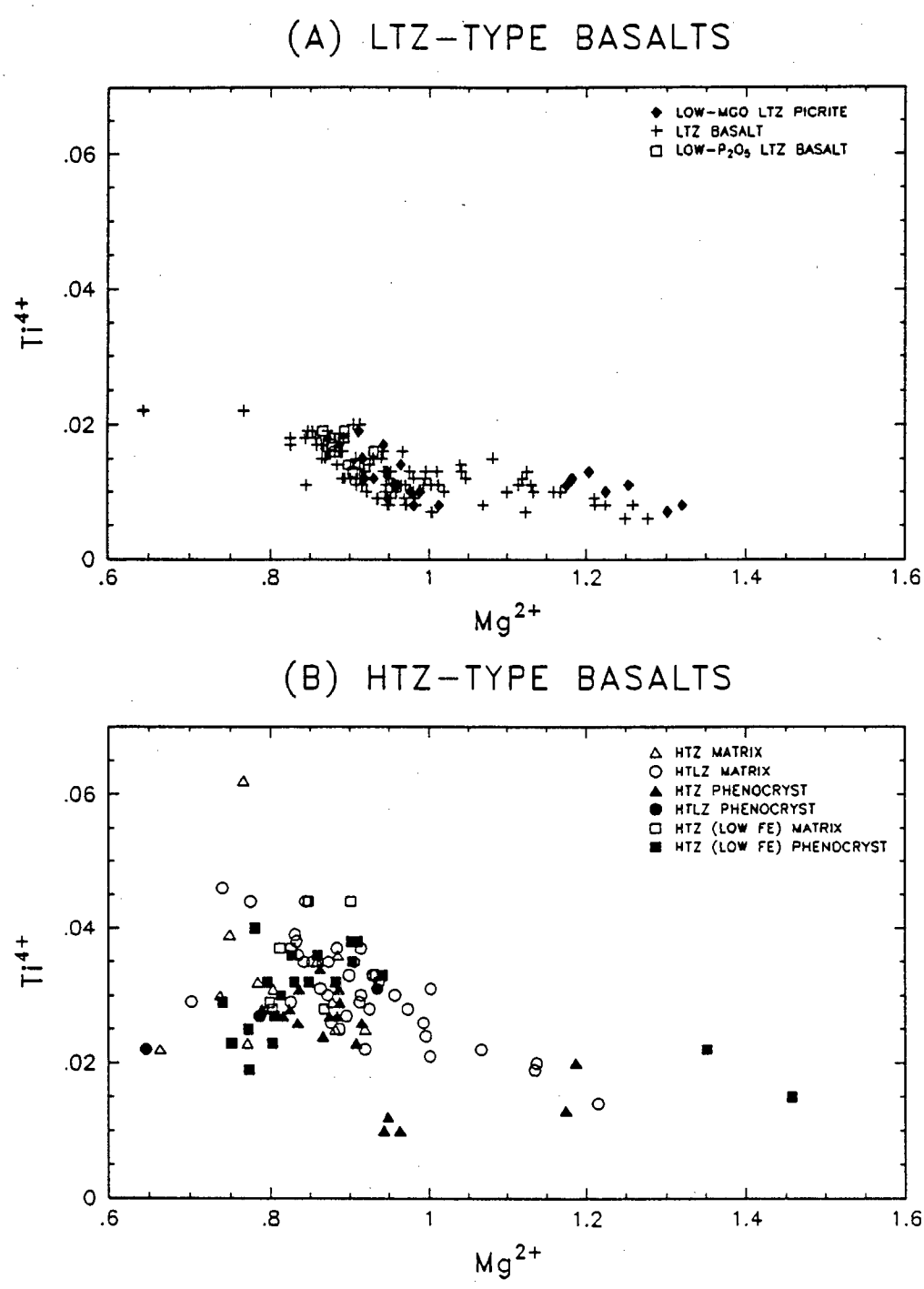

Fig. 3.2. Mg^{2+} *vs.* Ti^{4+} in the pyroxene compositions of the different low-K_2O lineage sub-groups.

greater range in their augite compositions, while the most primitive augite compositions are present in the LTZ-type basalts (see Fig. 3.1A & B and Fig. 3.2). In Fig. 3.2 the pyroxenes (both augite and pigeonite) of the LTZ-type basalts are characterised by lower Ti^{4+} concentrations at similar Mg^{2+} concentrations than the HTZ-type basalts and Ti^{4+} defines a negative trend *vs.* MgO. The pyroxene compositions of the two HTZ-type basalt sub-groups are similar and are characterised by considerable scatter in their Ti^{4+} concentrations (possibly reflecting the scatter in whole rock compositions), although the phenocryst and matrix pyroxenes have similar Ti^{4+} concentrations. In contrast to the LTZ data, the Ti^{4+} concentration of the augites in the HTZ-type basalts define no clear trend *vs.* MgO. The

low Ti^{4+} concentrations of the more evolved augite compositions (see Fig. 3.2) may reflect the appearance of magnetite/ilmenite on the liquidus of the evolved HTZ-type liquids as Sweeney *et al.* (1994) suggested for a similar positive Ti^{4+} *vs.* Mg^{2+} trend noted for pyroxenes from an HTZ.LF dolerite in the Central Lebombo. Three of the pyroxene "megacryst" analyses have lower Ti^{4+} concentrations with respect to the pyroxenes of the HTZ-type basalts, in general, and their Ti^{4+} concentrations lie within the field defined by the LTZ-type basalts. The margin of the "megacryst" pyroxene (PYX8 in TABLE 3.5) has a Ti^{4+} concentration which is similar to that of the HTZ-type basalts which suggests that either the "megacrysts" have re-equilibrated along grain margins with the HTZ-type liquids or that continued crystallization of the pyroxene from a liquid enriched in TiO_2 has occurred.

It is of interest to note that although the low-P_2O_5 LTZ basalts are enriched in whole rock TiO_2 concentrations with respect to the LTZ-type basalts (see section 2.3.2.2) this TiO_2 enrichment is not reflected in the Ti^{4+} composition of the pyroxenes.

3.1.2.3 Feldspar

Plagioclase is the most abundant mineral phase present in the LTZ-type basalts, and is found as a phenocryst phase, as microphenocrysts in the mesostasis and as the major constituent of the groundmass with the plagioclase laths defining the texture. The plagioclase of the LTZ-type basalts is twinned, according to the carlsbad, albite and pericline twin laws, and is often strongly zoned. The plagioclase is usually very altered and pseudomorphs after plagioclase of chlorite, calcite and clay minerals are common. The electron microprobe analyses of plagioclase from selected LTZ-type basalts are summarised in Fig. 3.3A & B (see APPENDIX C1) and representative plagioclase analyses are tabulated in TABLE 3.6.

The plagioclase of the groundmass in the LTZ-type basalts display a range in compositions with the anorthite (An) component of the plagioclase varying from $An_{76.6}$ to $An_{33.2}$ (see Fig. 3.3A) with the plagioclase composition of the LTZ-type basalts broadly reflecting the whole rock geochemistry with the most calcic matrix plagioclase analyzed being present in the low-MgO LTZ picritic basalts. The plagioclase in the glomeroporphyritic aggregates of the LTZ-type basalts exhibits a range in composition from $An_{75.3}$ to $An_{49.2}$ (see Fig. 3.3B) and these compositions are comparable to those recorded for the plagioclase in the matrix of the individual LTZ-type basalt samples. Unfortunately most of the electron microprobe analyses obtained for glomeroporphyritic plagioclase are from areas adjacent to the grain margins as the more calcic cores of the plagioclase are preferentially altered. The phenocrysts of plagioclase in the glomeroporphyritic aggregates are strongly zoned and frequently exhibit an increased compositional variation adjacent to the grain margins and

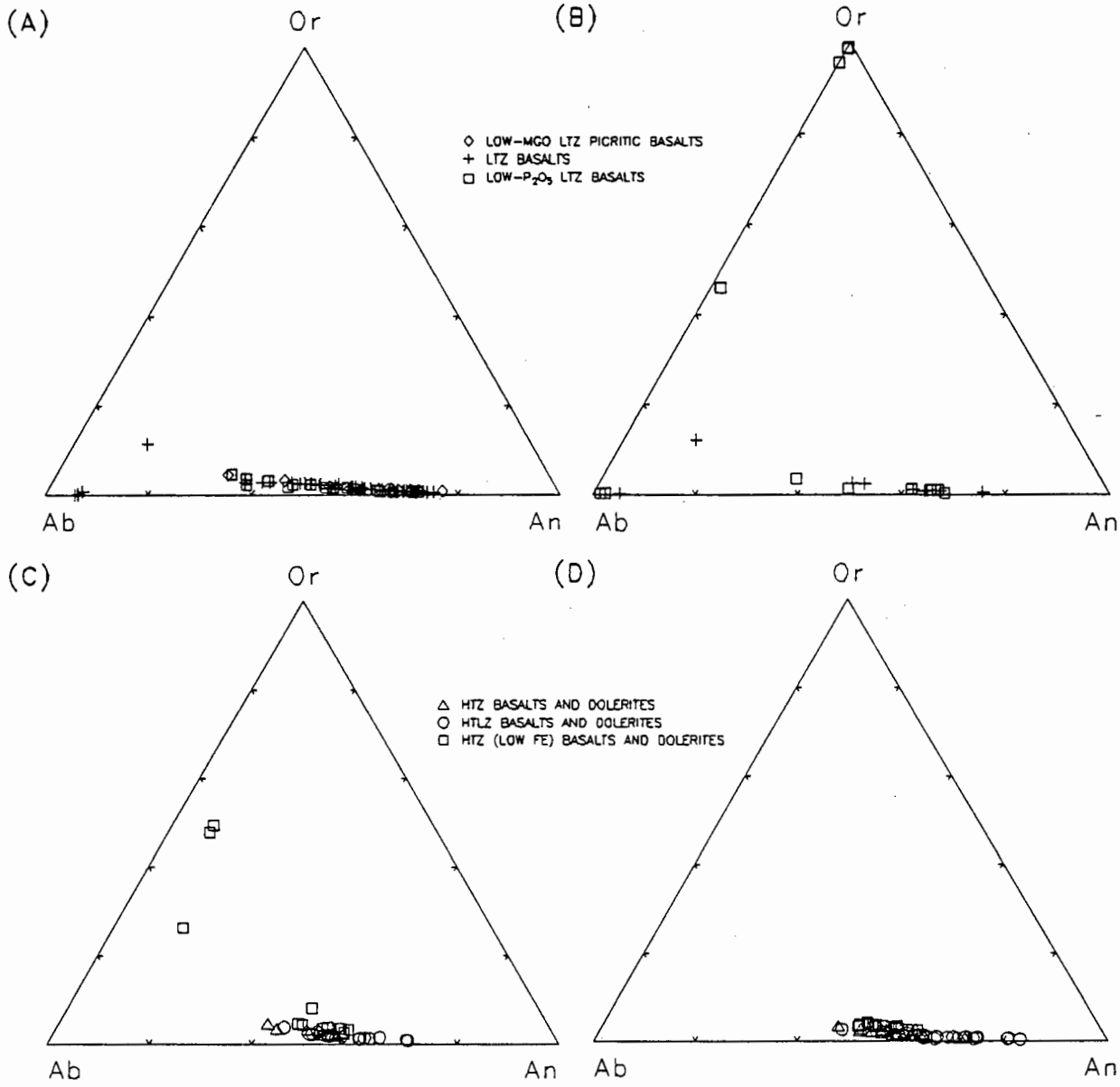

Fig. 3.3. (A) Matrix and (B) phenocryst plagioclase compositions of the LTZ-type basalts and dolerites and (C) matrix and (D) phenocryst plagioclase compositions of the HTZ-type basalts expressed in terms of the An, Ab and Or contents.

	LTZ-type basalts										HTZ-type basalts and dolerites	
	PLAG1C	PLAG1M	PLAG2C	PLAG2M	PLAG3C	PLAG3M	PLAG4	PLAG5C	PLAG5M	PLAG6	PLAG7C	PLAG7M
SiO_2	50.50	53.70	51.71	61.28	51.06	57.11	53.26	52.07	51.03	58.86	53.23	55.13
Al_2O_3	30.73	28.48	29.56	23.90	30.92	26.62	28.42	29.92	30.19	25.42	29.41	28.10
FeO	.57	.76	.56	.57	.46	.84	.61	.48	.65	.68	.58	.68
MgO	.18	.13	.20		.21	.08	.17	.20	.17		.12	.17
CaO	14.90	12.05	13.89	6.29	14.80	9.99	12.58	13.75	14.22	8.31	13.64	12.61
Na_2O	2.64	3.99	2.96	6.52	2.66	4.93	3.47	3.32	3.10	6.39	3.65	4.50
K_2O	.09	.21	.12	.72	.10	.36	.19	.13	.12	.49	.15	.25
TOTAL	99.61	99.32	99.00	99.28	100.21	99.93	98.70	99.87	99.48	100.15	100.78	101.44
STRUCTURAL FORMULA CALCULATED TO 8 OXYGENS												
SI	2.313	2.448	2.374	2.743	2.321	2.569	2.442	2.370	2.338	2.637	2.401	2.467
AL	1.659	1.530	1.599	1.261	1.657	1.411	1.536	1.605	1.631	1.342	1.563	1.482
FE	.022	.029	.021	.021	.018	.032	.023	.018	.025	.026	.022	.025
MG	.012	.009	.013		.014	.006	.011	.013	.012		.008	.012
CA	.731	.589	.683	.302	.721	.482	.618	.670	.698	.399	.659	.605
NA	.234	.352	.263	.566	.235	.430	.308	.293	.275	.555	.319	.390
K	.005	.012	.007	.041	.006	.021	.011	.008	.007	.028	.009	.014
SUM	4.976	4.969	4.960	4.934	4.972	4.951	4.949	4.977	4.986	4.987	4.981	4.995
AB	24.1	37.0	27.6	62.3	24.4	46.1	32.9	30.2	28.1	56.5	32.4	38.7
OR	.5	1.3	.7	4.5	.6	2.2	1.2	.8	.7	2.8	.9	1.4
AN	75.3	61.8	71.6	33.2	75.0	51.7	65.9	69.0	71.2	40.6	66.8	59.9

TABLE 3.6. Selected plagioclase analyses of the low-K_2O lineage basalts and dolerites. C refers to core and M to the margin of the individual grains with the same number in the analysis name.

	HTZ-type basalts and dolerites						Low-P_2O_5 LTZ basalts		
	PLAG8C	PLAG8R	PLAG9	PLAG10C	PLAG10R	PLAG11	PLAG12C	PLAG12R	PLAG13
SiO_2	48.62	53.65	55.05	54.51	55.29	56.35	51.82	56.82	66.73
Al_2O_3	32.25	28.34	28.35	28.60	28.14	27.14	30.50	27.30	19.42
FeO	.54	1.10	.73	.75	.76	.88	.61	.97	
MgO	.17	.18	.10			.07	.18	.08	
CaO	16.82	12.61	12.34	12.38	11.69	10.71	13.85	10.10	.38
Na_2O	1.87	4.11	4.44	4.22	4.54	5.11	3.53	5.66	5.95
K_2O	.08	.24	.20	.44	.55	.63	.08	.26	7.99
TOTAL	100.35	100.23	101.21	100.90	100.97	100.89	100.57	101.19	100.47
STRUCTURAL FORMULA CALCULATED TO 8 OXYGENS									
SI	2.224	2.435	2.465	2.454	2.482	2.527	2.347	2.535	2.984
TI									
AL	1.739	1.516	1.496	1.517	1.489	1.435	1.628	1.435	1.023
FE	.021	.042	.027	.028	.029	.033	.023	.036	
MN									
MG	.012	.012	.006			.005	.012	.005	
CA	.825	.613	.592	.597	.562	.515	.672	.483	.018
NA	.166	.361	.385	.368	.395	.445	.310	.489	.516
K	.005	.014	.011	.025	.032	.036	.005	.015	.456
SUM	4.992	4.993	4.982	4.989	4.989	4.996	4.997	4.998	4.997
AB	16.7	36.6	39.0	37.2	40.0	44.7	31.4	49.6	52.1
OR	.5	1.4	1.2	2.5	3.2	3.6	.5	1.5	46.0
AN	82.8	62.0	59.9	60.3	56.8	51.7	68.1	48.9	1.9

SAMPLE DESCRIPTION:
LTZ-TYPE BASALTS
PLAG1: plagioclase phenocryst (KLB-134)
PLAG2: matrix plagioclase (KLB-172) adjacent to the mesostasis
PLAG3: coarse matrix plagioclase (KLB-171)
PLAG4: matrix plagioclase (KLB-155)
PLAG5: coarse matrix plagioclase (KLB-046)
PLAG6: skeletal plagioclase (DB-19) in the mesostasis
HTZ-TYPE BASALTS AND DOLERITES
PLAG7: plagioclase "megacryst" (KLB-044)
PLAG8: plagioclase phenocryst (KLB-095)
PLAG9: matrix plagioclase (KLB-044)
PLAG10: plagioclase phenocryst (KLB-062A)
PLAG11: matrix plagioclase (KLB-114)
LOW-P_2O_5 LTZ BASALTS
PLAG12: plagioclase phenocryst (KLB-015)
PLAG13: alkali feldspar phenocryst (KLB-015)

TABLE 3.6 (continued).

the matrix plagioclase similarly has normal zonation patterns and individual plagioclase grains in a thin section often show a compositional variation which is comparable to the range of plagioclase compositions in that basalt sample. Although most plagioclase is characterised by normal zonation, rare reversed zoning of plagioclase does occur (see TABLE 3.6). The microphenocrysts of plagioclase in the mesostasis have, on average, the most evolved compositions (*i.e.* the lowest An contents) of the plagioclase in the LTZ-type basalt. Plagioclase margins immediately adjacent to the mesostasis have similar low An contents.

Albitization of the plagioclase in the matrix and in the glomeroporphyritic aggregates of the LTZ-type basalts has occurred (see Fig. 3.3A & B) in both the LTZ- and high-Na_2O LTZ basalts. This is probably as a result of the exchange of alkali and alkali earth cations between plagioclase and saline hydrothermal solutions. The equilibrium reaction controlling the albitization reaction (Lagarche, 1984) can be written as:

$$CaAl_2Si_2O_8 + 2NaCl + 4SiO_2 \rightharpoonup 2NaAlSi_3O_8 + CaCl_2$$

The equilibrium constant of the reaction at constant temperature and pressure is a function of the activities of the anorthite, albite, SiO_2 and the chloride salts. As temperature and pressure increase the plagioclase is effectively in equilibrium with more Na-rich solutions and an increase in the total concentration of the chlorides effectively shifts the reaction to the right (Lagarche, 1984). The composition of the water in the Karoo basalts is known to be locally saline and the Ntane sandstone, the Karoo basalts and the Kalahari sands are often in hydraulic continuity (section 1.2.5). These saline solutions, in the presence of free quartz, would shift the equilibrium to the right, *i.e.* promoting the albitization of the plagioclase.

Plagioclase is the dominant modal constituent in the HTZ-type basalt mineral assemblage (see TABLE 3.3) and exhibits a considerable variation in grain size with "megacrysts", phenocrysts and microphenocrysts of plagioclase co-existing with matrix plagioclase in a single thin section. Plagioclase characteristically exhibits a seriate grain size variation between microphenocryst and phenocryst. Fig. 3.3C & D summarises the compositions of plagioclase from selected HTZ-type basalts analyzed by electron microprobe (see APPENDIX C1) and representative plagioclase analyses are tabulated in TABLE 3.6.

Plagioclase phenocrysts of the HTZ-type basalts display a considerable variation in composition with a range from $An_{82.9}$ to $An_{46.2}$ and the plagioclase phenocryst compositions broadly reflect the whole rock geochemistry with the most calcic plagioclase compositions

determined from the least evolved HTZ-type basalts. The compositional range of $An_{72.2}$ to $An_{50.9}$ displayed by the "megacrysts" is included in the field defined by the plagioclase phenocrysts which suggests that the size distinction between "megacryst" and phenocryst may only be a function of sampling. The matrix plagioclase of the HTZ-type basalts exhibits a variation in composition from $An_{69.7}$ to $An_{40.7}$ and the matrix plagioclase compositions within individual thin-sections are usually more evolved than associated phenocryst plagioclase and have compositions which are comparable with the margins of the plagioclase phenocrysts. The plagioclase microphenocrysts are characterised by their more evolved compositions and rare alkali feldspar microphenocrysts are present in the mesostasis (see Fig. 3.3C). The plagioclase (both phenocrysts and matrix) is characterised by strong normal zonation patterns, often with intense zoning concentrated adjacent to grain margins, and the range in composition exhibited by individual plagioclase grains is comparable to the compositional variation of that basalt or dolerite. Although normal zonation is most common, reversed plagioclase zonation is also recognised (see TABLE 3.6).

In Fig. 3.4 the plagioclase compositions of the low-K_2O lineage define two approximately parallel trends. The vast majority of the HTZ-type basalts have plagioclase (matrix and phenocryst) compositions which are broadly comparable to the plagioclase compositions of the LTZ-type basalts, *i.e.* possibly reflecting the absence of K_2O enrichment in the whole rock compositions of the HTZ-type basalts relative to the LTZ-type basalts at similar MgO concentrations (see Fig. 2.10A). However, a trend of high Or *vs.* An concentrations is defined by both the matrix and phenocryst plagioclase compositions of three of the HTZ (low Fe) basalts (*i.e.* KLB-062A, 114- and -152). Sweeney *et al.* (1994) noted a similar parallel, but enriched, trend in the Or *vs.* An trend of the HTZ.LF- and HTZ.HF basalts with respect to the LTZ basalts of the Central Lebombo. This parallel, but enriched, trend exhibited by these plagioclase compositions suggests that, at least, these three HTZ (low Fe) basalts crystallised along a different liquid line of descent with respect to the other HTZ-type basalts and LTZ-type basalts.

In contrast to the LTZ-type basalts and the HTZ-type basalts which have plagioclase as the only feldspar in the phenocryst assemblage, alkali feldspar (typically as coarse irregular perthites), together with plagioclase, pyroxene and olivine pseudomorphs are present in the phenocryst/xenocryst assemblage of the low-P_2O_5 LTZ basalts. Although plagioclase is present as microphenocrysts, phenocrysts and as a matrix constituent of the low-P_2O_5 LTZ basalts, alkali feldspar (perthite) is included only in the phenocryst/xenocryst assemblage. The feldspar compositions of selected low-P_2O_5 LTZ basalts are summarised in Fig. 3.3A &B and representative plagioclase compositions are tabulated in TABLE 3.6. Alkali feldspar (perthite) was recognised in all of the low-P_2O_5 LTZ basalts sampled from the

borehole NG1, however no alkali feldspar (orthoclase or perthite) was recognised in the overlying HTZ-type basalts.

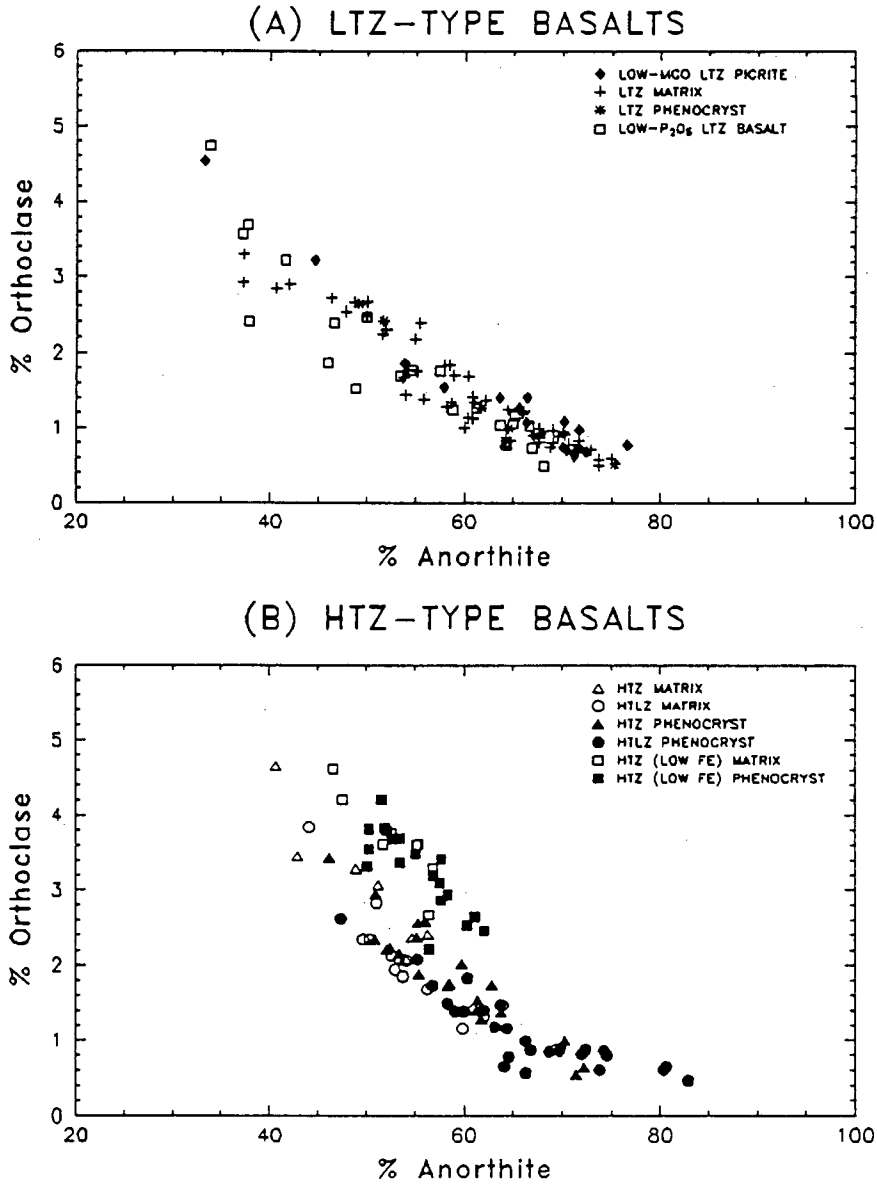

Fig. 3.4. The An *vs.* Or contents of the plagioclase compositions of the low-K_2O lineage.

Parsons and Brown (1984) consider the development of alkali feldspar in three stages, *i.e.* magmatic, post-magmatic or hydrothermal (deuteric). Magmatic alkali feldspars are the result of crystal growth from the melt, post-magmatic (or sub-solidus) alkali feldspars involve coherent exsolution of feldspars which results in the development of regular strain controlled crypto- or mesoperthites and hydrothermal (or deuteric) alkali feldspars result from feldspar-fluid interactions and give rise to coarse irregular perthites. The alkali feldspars of the low-P_2O_5 LTZ basalts are present in coarse glomeroporphyritic aggregates which include rare euhedral plagioclase laths and anhedral grains of both altered coarse, irregular perthites and rare unmixed alkali feldspar (see TABLE 3.6) and remnant albite twins are occasionally preserved in the perthites. The association of euhedral plagioclase and alkali

feldspar phenocrysts in the glomeroporphyritic aggregates suggests that the alkali feldspars in the low-P_2O_5 LTZ basalts do not result from the low temperature alteration of plagioclase and must therefore have either a xenocrystic or an intratelluric origin. Although the alkali feldspar (perthite) phenocrysts exhibit no evidence of disequilibrium, *e.g.* resorption, which is a characteristic feature of xenocrysts, it is unlikely that they result from primary magmatic processes in tholeiitic magmas. However, the coarse irregular nature of the perthites, and their association with adjacent altered glomeroporphyritic plagioclase, suggests that the perthites are the result of late stage alkali feldspar (and not plagioclase) - hydrothermal (or deuteric) fluid interactions and the origin of these alkali feldspar phenocrysts in the low-P_2O_5 LTZ basalts is therefore somewhat ambiguous.

3.1.2.4 Fe-Ti oxides

The Fe-Ti oxides of the LTZ-type basalts are present as small anhedral to skeletal interstitial grains in the matrix and as microphenocrysts and tiny anhedral blebs in the mesostasis. The microphenocryst morphologies are very variable and skeletal (usually a cruciform type), anhedral and acicular varieties are found. Titanomaghemite is the dominant Fe-Ti oxide present in the LTZ-type basalts and pseudobrookite is found only as rare acicular microphenocrysts in the mesostasis. Ilmenite and titanomaghemite are commonly both present in the HTZ-type basalts. The ilmenite commonly has an acicular to prismatic habit and is usually found within or adjacent to the mesostasis, while the titanomaghemite is generally present as interstitial equant crystals. The primary ilmenite/titanomagnetite ratio in igneous rocks depends largely on the prevailing oxygen fugacities, SiO_2 activities and the initial bulk composition of the magma (Haggerty, 1976) and the higher proportion of ilmenite in the HTZ-type basalts therefore reflects the relative enrichment in the whole rock TiO_2 concentrations of the HTZ-type basalts with respect to the LTZ-type basalts. Fig. 3.5 summarises the results of the electron microprobe analyses of the Fe-Ti oxides from selected LTZ-type and HTZ-type basalts, with FeO, Fe_2O_3 and TiO_2 recalculated to 100 percent, and selected analyses are tabulated in TABLE 3.7.

Titanomaghemites lie in the field defined by the Fe_2TiO_4, $FeTiO_3$, Fe_3O_4 and Fe_2O_3 end members in Fig. 3.5 (after Haggerty, 1976) and their compositions result from the oxidation of titanomagnetites (*i.e.* spinels with Fe_2TiO_4 - Fe_3O_4 solid solution compositions). The oxidation of titanomagnetite to titanomaghemite occurs at low temperatures ($<600°C$) and pressures and the formation of titanomaghemite is promoted by the presence of water, usually of a supergene origin (Lindsley, 1976). Although water is thought to act only as a catalyst to the oxidation reaction, both hydroxides and free H_2O may be included in the cation-deficient spinel structure of the titanomaghemites (Lindsley, 1976). The low totals ($\pm$ 95) of the oxide analyses can therefore be attributed to the high degree of oxidation of

the titanomaghemites and the possible inclusion of water in the crystal lattice. The increased alteration of the titanomaghemites is associated with a decrease in the TiO_2 and an increase in the SiO_2, CaO and calculated Fe_2O_3 concentrations (illustrated for the LTZ-type basalts in Fig. 3.5). Pseudobrookite is the final product (*i.e.* R7) resulting from the oxidation of ilmenite-haematite$_{ss}$ and is present only as rare tiny acicular (and anhedral) microphenocrysts in the mesostasis and as very rare interstitial grains in the matrix of the LTZ-type basalts. The pseudobrookite compositions typically include a high proportion of non-ternary components (*i.e.* MgO, SiO_2, CaO and Al_2O_3), but the recalculated pseudobrookite analyses are included in Fig. 3.5.

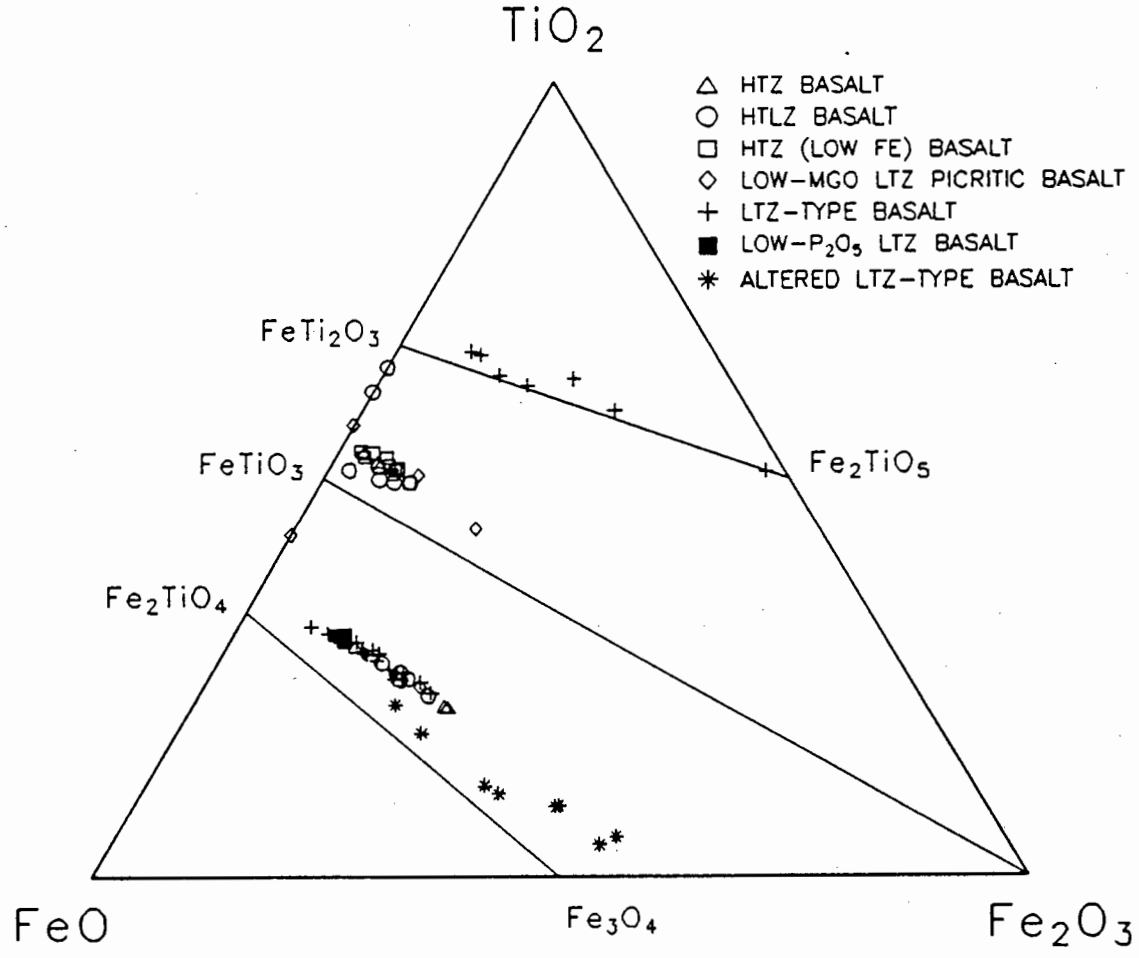

Fig. 3.5. The Fe-Ti oxide compositions analyzed in the various sub-groups of the low-K_2O lineage.

	LTZ-type basalts			HTZ-type basalts and dolerites		
	OXID1	OXID2	OXID3	OXID4	OXID5	OXID6
SiO_2	.34	.22			.16	.21
TiO_2	28.81	24.77	23.26	51.67	24.81	48.59
Al_2O_3	1.58	1.42	1.47	.24	2.20	.38
Cr_2O_3	.1					
FeO	55.54	51.04	49.86	41.74	51.19	41.73
Fe_2O_3	7.24	15.60	21.95	3.68	16.34	7.68
MnO	.76	.86	.56	.51	.65	.53
MgO	.28		.66	1.99	.93	.66
CaO	.21	.44			.09	.13
TOTAL	94.85	94.35	97.75	99.84	96.38	99.92
OXYGEN	4	4	4	3	4	3
SI	.014	.009			.006	.005
TI	.866	.779	.722	.980	.757	.943
AL	.075	.070	.071	.007	.105	.011
CR	.0					
FE	2.074	2.276	2.402	.951	2.236	1.049
MN	.026	.031	.020	.011	.022	.012
MG	.016		.041	.075	.056	.026
CA	.009	.020			.004	.004
SUM	3.082	3.184	3.256	2.024	3.186	2.050

TABLE 3.7. Selected Fe-Ti oxide analyses of the low-K_2O lineage basalts and dolerites.

SAMPLE DESCRIPTION:
LTZ-type basalts
OXID1: anhedral interstitial titanomaghemite (KLB-115)
OXID2: anhedral interstitial titanomaghemite (KLB-046)
OXID3: skeletal interstitial titanomaghemite (KLB-199)
HTZ-type basalts and dolerites
OXID4: skeletal equant ilmenite (KLB-152)
OXID5: skeletal equant titanomaghemite (KLB-095)
OXID6: fine acicular ilmenite (KLB-095)

3.1.2.5 Summary

The LTZ-type basalts (excluding the low-P_2O_5 LTZ basalts) are characterised by their mineral chemistry which is both typical with respect to LTZ-type basalts of the Karoo Igneous Province and, in general, to normal low pressure fractionation of tholeiitic magmas. In contrast, the HTZ-type basalts exhibit considerable diversity in their mineral chemistry of plagioclase and pyroxene, in particular. The presence of orthopyroxene, the rare low Ti^{4+} cores to the pyroxene "megacrysts" with respect to the typical Ti^{4+} concentration in the pyroxenes of the HTZ-type basalts and the sub-parallel trends defined by the An and Or contents of the plagioclase compositions in the HTZ-type basalts suggests a complex petrological history for the HTZ-type basalts, which therefore can not result from a simple single liquid-line-of-descent.

3.2 HIGH-K_2O LINEAGE

3.2.1 PETROGRAPHY

The high-K_2O lineage, as defined in Fig. 2.4, includes the shoshonites and the high-K_2O picritic basalts sub-groups.

3.2.1.1 Shoshonites

The shoshonites have a phenocryst assemblage which includes olivine, clinopyroxene and possibly feldspar (both plagioclase and alkali feldspar), where the feldspar is present in aggregates of ≤6mm. The seriate grain size distribution of the feldspars, in particular, obscures the distinction between groundmass and phenocryst, but the phenocryst assemblage is estimated to have modal proportions of <5 percent and the phenocryst size seldom exceeds ±5mm. The olivine and clinopyroxene phenocrysts typically have euhedral outlines and the clinopyroxene is strongly zoned, which is reflected in the increased purple coloration of the clinopyroxene phenocrysts towards the grain margins. The plagioclase and alkali feldspar in the feldspar aggregates are usually finer grained than the associated olivine and clinopyroxene phenocrysts and the plagioclase, which is usually strongly zoned, is often mantled by alkali feldspar, although both euhedral laths and anhedral grains of alkali feldspar are present in these feldspar aggregates.

The groundmass texture of the shoshonites varies from holocrystalline intergranular to hyalopilitic and has a mineral assemblage which includes olivine, clinopyroxene (often with a strong purple coloration), plagioclase, alkali feldspar, oxide, apatite, zeolite (±leucite/analcite), blue-green hornblende and may include mesostasis. Modal analyses, determined by point-counting, for three of the shoshonites are tabulated in TABLE 3.8, where no distinction between phenocryst or matrix phases was made. The mesostasis exhibits a considerable variation in modal abundances, with a range from 0 to 67.9% (by volume) and the mesostasis typically contains abundant skeletal clinopyroxene, olivine, feldspar, apatite and blue-green hornblende. Although the mesostasis is absent in some samples, apatite, zeolite and hornblende are concentrated in interstitial granular feldspar aggregates which probably represent the final stages of crystallization.

The shoshonites sampled during this study are indistinguishable petrographically from the shoshonites of southwest Zimbabwe as described by Vail *et al.*, 1969.

	Shoshonites			High-K_2O picritic basalts		
Sample No. (KLB-)	057	058	060	083	084	Letaba Fmt.
Olivine	5.9	5.4	3.9	36.1	31.1	17.7-46.1
Clinopyroxene	19.2	19.2	8.2	14.5	17.4	20.3-34.7
Feldspar	50.1	43.6	18.5			
Oxide	5.5	3.6	1.5	5.3	6.9	5.3-12.8
Mesostasis	10.4	28.2	67.9	44.1	44.6	20.2-37.7
"Other"	8.8					

Where mesostasis includes microphenocryts/microlites and accessory phases
"Other" includes zeolite and leucite/analcite

TABLE 3.8. Modal proportions determined by point-counting (N=1000) for the high-K_2O lineage sub-groups.

3.2.1.2 High-K_2O picritic basalts

The high-K_2O picritic basalts sampled during this study have two distinct phenocryst assemblages. KLB-083 has anhedral to subhedral phenocrysts, often in aggregates, of olivine only (≤3mm in diameter) and is therefore equivalent to the 1-P type of the Letaba Formation (Bristow, 1980; 1984b and Vail *et al.*, 1969). In contrast, KLB-084, has phenocrysts of subhedral to anhedral olivine (≤1.5mm) and clinopyroxene (≤1mm) and is therefore equivalent to the 2-P type of Bristow (1980; 1984b) and Vail *et al.* (1969). The hyalopilitic to microcrystalline matrix of the high-K_2O picritic basalts contains abundant sheaves of plagioclase microlites, anhedral clinopyroxene, skeletal acicular oxides, apatite and rare altered glass. Modal analyses, determined by point-counting, are tabulated in TABLE 3.8, together with the range in modal proportions quoted by Bristow (1984b) for the Letaba Formation picritic basalts with similar whole rock compositions and mineral assemblages. For more detailed petrographic descriptions of the Letaba Formation picritic basalts, which are considered equivalent to the high-K_2O picritic basalts (see section 2.4.2) see Bristow (1980; 1984b) and Vail *et al.* (1969).

3.2.2 MINERAL CHEMISTRY

3.2.2.1 Olivine

Olivine compositions were determined by electron microprobe analysis for a single shoshonite and a single high-K_2O picritic basalt (see APPENDIX C2) and representative olivine compositions are tabulated in TABLE 3.9.

The phenocryst and matrix olivine of the shoshonite are characterised by a similar range in compositions, *i.e.* $Fo_{68.7}$-$Fo_{60.2}$ and $Fo_{66.6}$-$Fo_{60.7}$ respectively. Both the phenocryst and matrix olivine exhibit normal zonation patterns of decreasing Fo contents towards the grain

margins, and the compositional zonation is commonly most intense immediately adjacent to the grain margin. These olivine compositions are somewhat more evolved than the compositions of $\pm Fo_{78}$ determined optically by Vail *et al.* (1969) using the extinction angle of olivine phenocrysts in the shoshonites of southwest Zimbabwe.

The olivine phenocrysts of the high-K_2O picritic basalts exhibit a range in compositions from $Fo_{83.4}$ to $Fo_{76.1}$ and the olivine is characterised by continuous normal zonation (*i.e.* decreasing Fo contents) from the core to the margin (see TABLE 3.9). A similar compositional range of $Fo_{89.3}$ to $Fo_{76.5}$, with normal zonation in the order of 2-7%Fo, is reported by Bristow (1980; 1984b) for the olivine phenocrysts of the Letaba Formation picritic basalts. The matrix olivine of the high-K_2O picritic basalts tend to have more evolved compositions than the associated phenocrysts with a range in compositions from $Fo_{78.7}$ to $Fo_{72.8}$, and in a single example normal zonation of $Fo_{78.7}$ to $Fo_{77.1}$ was determined for a matrix olivine of the high-K_2O picritic basalts.

	Shoshonites				High-K_2O picritic basalts				
	OLIV1C	OLIV1M	OLIV2C	OLIV2M	OLIV3C	OLIV3H	OLIV3R	OLIV4C	OLIV4M
SiO_2	37.73	36.39	37.17	36.25	39.12	38.36	38.18	38.81	37.77
TiO_2				.07					
FeO	27.48	33.76	29.28	33.39	15.70	20.60	21.56	19.39	21.19
MnO	.46	.52	.44	.56	.18	.20	.28	.25	.25
MgO	34.67	29.27	33.44	29.37	43.98	40.48	39.53	41.36	41.06
CaO	.45	.44	.42	.43	.28	.28	.27	.27	.25
NiO	.28	.23	.22		.28	.26	.27	.32	.21
TOTAL	101.07	100.61	100.98	100.07	99.54	100.18	100.09	100.49	100.73
STRUCTURAL FORMULA CALCULATED TO 4 OXYGENS									
Si	.999	1.000	.994	1.001	.995	.991	.992	.994	.975
Ti				.001					
Fe	.608	.776	.655	.771	.334	.445	.469	.415	.457
Mn	.010	.012	.010	.013	.004	.004	.006	.005	.005
Mg	1.369	1.199	1.334	1.209	1.667	1.559	1.531	1.579	1.579
Ca	.013	.013	.012	.013	.008	.008	.007	.007	.007
Ni	.006	.005	.005		.006	.005	.006	.007	.004
SUM	3.005	3.005	3.010	3.008	3.014	3.012	3.011	3.010	3.027
FO	68.66	60.18	66.56	60.65	82.92	77.41	76.11	78.70	77.17
FA	31.34	39.82	33.44	39.35	17.08	22.59	23.89	21.30	22.83

TABLE 3.9. Selected olivine analyses of the high-K_2O lineage. C refers to core, M to the margin and H to a point between the core and the margin of the individual grains with the same number in the analysis name.

SAMPLE DESCRIPTION:
SHOSHONITE
OLIV1: subhedral olivine phenocryst (KLB-099)
OLIV2: matrix olivine (KLB-099)
HIGH-K_2O PICRITIC BASALT
OLIV3: subhedral olivine phenocryst (KLB-083)
OLIV4: matrix olivine (KLB-083)

3.2.2.2 Pyroxene

Pyroxene is present as both a phenocryst phase and as a groundmass constituent of the shoshonites, but is present only in the phenocryst assemblage of a single high-K_2O picritic basalt (KLB-084). The pyroxene compositions of the high K_2O lineage, determined by electron microprobe analysis (see APPENDIX C2), are summarised in Fig. 3.6 and representative pyroxene analyses are tabulated in TABLE 3.10.

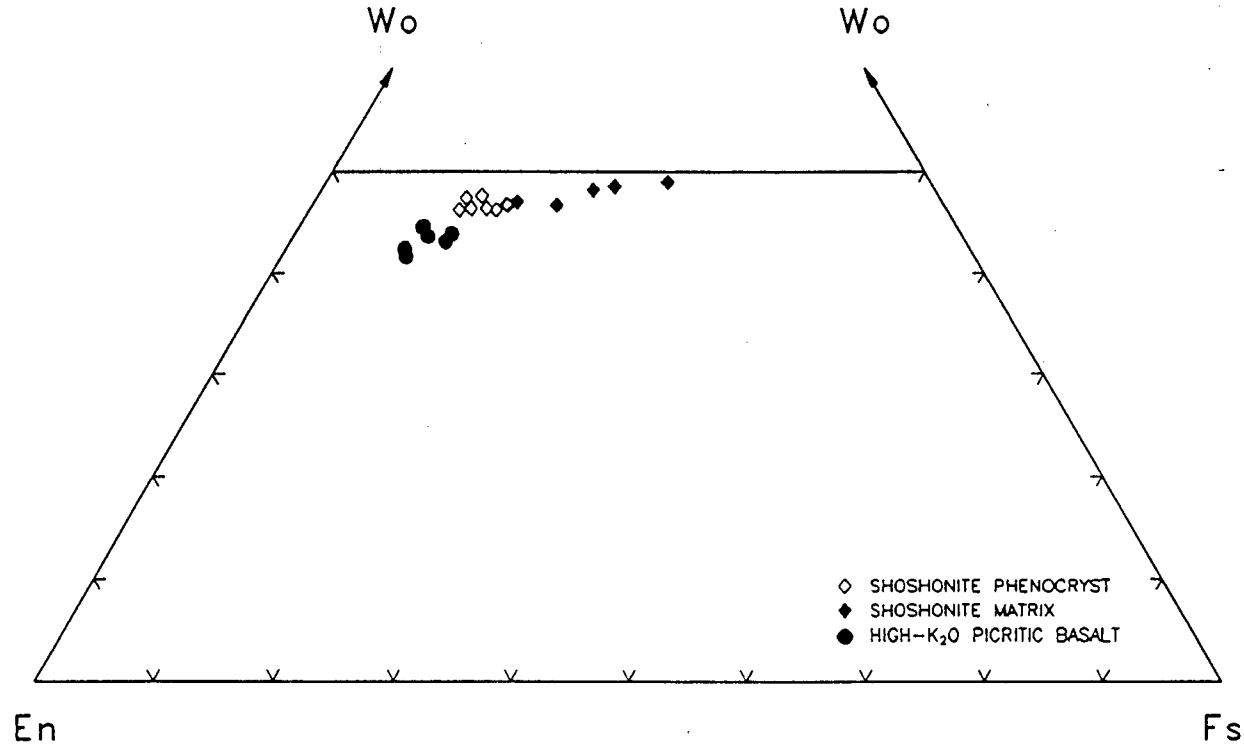

Fig. 3.6. Pyroxene compositions of the high-K_2O lineage in terms of the Wo, En and Fs contents.

The pyroxene phenocrysts of the shoshonites exhibit a range in compositions from $En_{41.2}Wo_{46.2}$ to $En_{36.8}Wo_{46.7}$ and the clinopyroxenes of the shoshonites have a high Wo component in their compositions (see Fig. 3.6) when compared to the clinopyroxene of the tholeiitic basalts and dolerites (see Fig. 3.1A & B) and these salitic compositions are typical of alkali basalts (Deer, Howie and Zussman, 1978). Although the clinopyroxene phenocrysts are characterised by compositional zonation, with increasing Wo and Fs and decreasing En contents, from the core to margin (see TABLE 3.10), the degree of zonation is usually more intense adjacent to the grain margins. The increased purple coloration of the clinopyroxene phenocrysts towards the grain margins reflects the elevated Ti^{4+} concentrations associated with the intense compositional zonation of the grain margins. The matrix clinopyroxenes of the shoshonites tend to be more evolved than the associated clinopyroxene phenocrysts with a range in composition from $En_{35.9}Wo_{47.0}$ to $En_{22.2}Wo_{48.9}$ and consequently have, on average, higher Ti^{4+} concentrations than the clinopyroxene phenocrysts, which in turn, results in the intense purple coloration of the matrix clinopyroxene. The compositional zonation

pattern of increasing Wo and Fs components of the clinopyroxene compositions, together with the high Wo content of the clinopyroxene in the shoshonites are characteristic of alkali basalts and therefore serve as a means of differentiating the shoshonites from the associated LTZ-type and HTZ-type basalts in Botswana and southwest Zimbabwe.

	Shoshonites						High-K_2O picritic basalts	
	PYX1C	PYX1H	PYX1M	PYX2C	PYX2M	PYX3C	PYX4C	PYX4M
SiO_2	49.72	48.84	47.93	47.63	47.58	46.13	51.10	48.78
TiO_2	1.37	1.82	2.57	2.62	2.25	3.56	1.40	2.00
Al_2O_3	3.50	4.33	4.55	4.55	3.56	5.38	1.90	4.23
Cr_2O_3	.15	.25					.55	
FeO	7.67	8.16	9.86	10.06	12.95	11.83	6.36	7.85
MnO	.15	.15	.16	.19	.29	.25	.12	.15
MgO	14.39	13.76	12.54	12.12	9.35	10.79	17.00	14.84
CaO	22.44	22.14	22.10	22.07	21.68	21.39	20.42	20.93
Na_2O	1.00	.47	.48	.57	.88	.63	.25	.32
TOTAL	100.39	99.92	100.19	99.81	98.54	99.96	99.10	99.10
STRUCTURAL FORMULA CALCULATED TO 6 OXYGENS								
Si	1.855	1.831	1.810	1.808	1.855	1.765	1.902	1.836
Ti	.038	.051	.073	.075	.066	.102	.039	.056
Al	.154	.191	.202	.203	.163	.243	.083	.187
Cr	.004	.007					.016	
Fe	.239	.256	.311	.319	.422	.379	.198	.247
Mn	.005	.005	.005	.006	.009	.008	.004	.005
Mg	.800	.769	.705	.686	.543	.615	.943	.832
Ca	.897	.889	.894	.897	.906	.877	.814	.844
Na	.072	.034	.035	.042	.066	.047	.018	.024
SUM	4.064	4.033	4.035	4.036	4.030	4.036	4.017	4.031
WO	46.20	46.35	46.67	47.01	48.15	46.66	41.55	43.77
EN	41.23	40.08	36.82	35.94	28.89	32.76	48.14	43.16
FS	12.57	13.57	16.51	17.05	22.96	20.58	10.31	13.07

TABLE 3.10. Selected pyroxene analyses of the high-K_2O lineage. C refers to core, M to the margin and H to a point between the core and the margin of the individual grains with the same number in the analysis name.

SAMPLE DESCRIPTION:
SHOSHONITE
PYX1: coarse pyroxene phenocryst (KLB-099)
PYX2: interstitial pyroxene (KLB-099)
PYX3: interstitial pyroxene (KLB-099)
HIGH-K_2O PICRITIC BASALT
PYX4: interstitial pyroxene (KLB-083)

Although clinopyroxene is present as a phenocryst phase in the high-K_2O picritic basalt KLB-084, no pyroxene phenocryst compositions were determined, but the matrix clinopyroxenes of the high-K_2O picritic basalt, KLB-083, exhibit a range in compositions from $En_{48.1}Wo_{37}$ to $En_{43.2}Wo_{43.8}$ (see Fig. 3.6) and the clinopyroxenes exhibit a compositional zonation of decreasing En and increasing Wo and Fs contents from the core to grain margins (see TABLE 3.10). Clinopyroxene compositions reported by Bristow (1980; 1984b)

for the Letaba Formation picritic basalts are characterised by a narrow compositional range (*i.e.* $En_{53}Wo_{37}$ to $En_{46}Wo_{44}$) with the most magnesian compositions determined from clinopyroxene phenocrysts and from clinopyroxene which mantles orthopyroxene. The clinopyroxene compositions determined during this study are similar to those determined by Bristow (1980; 1984b) although the compositions of the grain margins tend to be more evolved.

3.2.2.3 Feldspar

The shoshonites are characterised by a feldspar assemblage which includes both plagioclase and alkali feldspar and although both the plagioclase and alkali feldspar exhibit a seriate grain size distribution, coarser grained aggregates of feldspar have been included in the phenocryst assemblage. In contrast, plagioclase is present only as tiny microlites in the mesostasis of the high-K_2O picritic basalts. The plagioclase compositions determined by electron microprobe analyses (see APPENDIX C2) of the high K_2O lineage are summarised in Fig. 3.7 and representative plagioclase analyses are tabulated in TABLE 3.11.

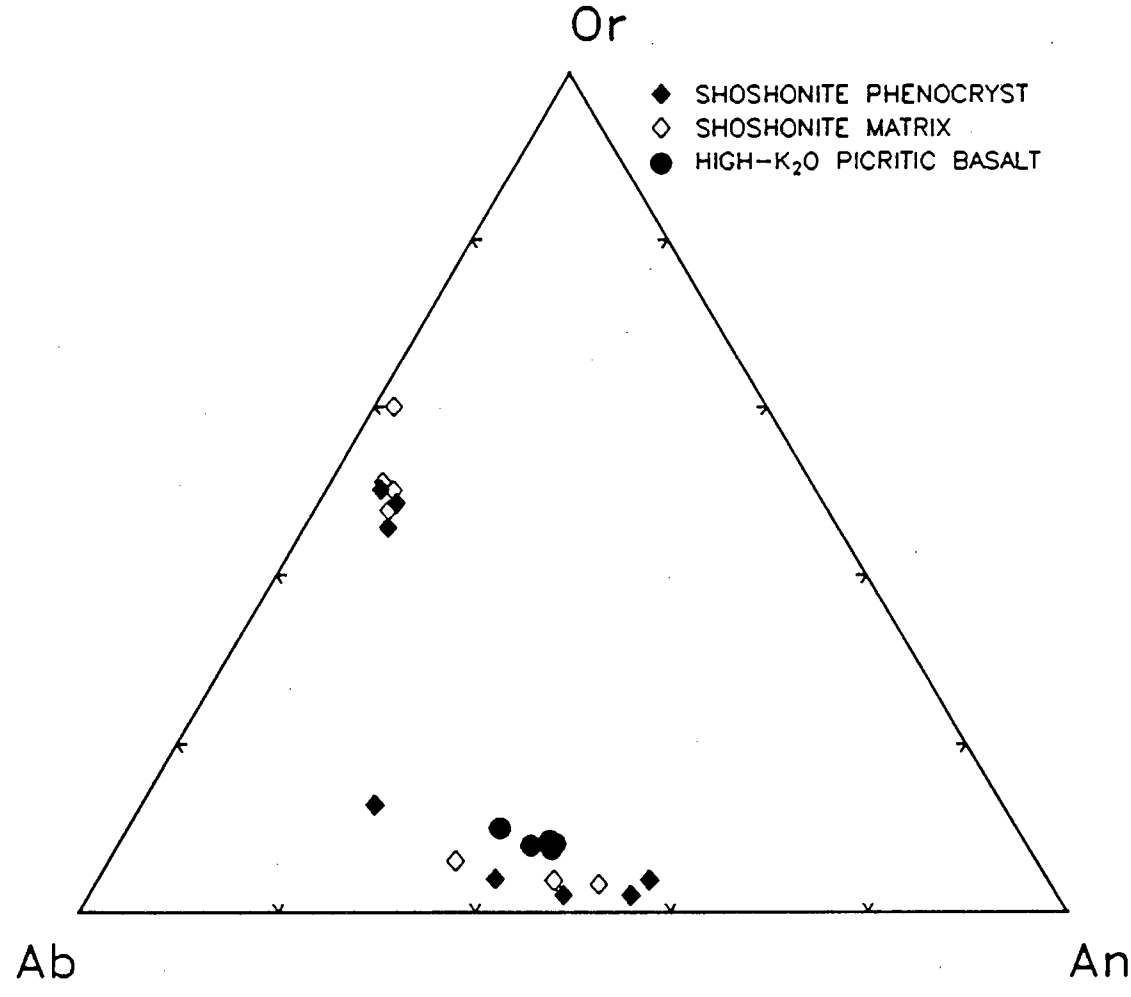

Fig. 3.7. Plagioclase compositions of the high-K_2O lineage in terms of the An, Ab and Or contents with the plagioclase phenocrysts depicted with open symbols and the matrix plagioclase with closed symbols.

The shoshonites exhibit a considerable variation in plagioclase compositions with a range from $An_{55.9}Ab_{40.3}$ to $An_{23.3}Ab_{63.8}$ (see Fig. 3.7). The phenocryst and groundmass plagioclase have similar compositions although the plagioclase phenocrysts exhibit a greater range in composition and both the phenocryst and matrix plagioclase exhibit normal zonation patterns (see TABLE 3.11). Vail *et al.* (1969) report similar compositions for the plagioclase of the shoshonites from southwest Zimbabwe with maximum symmetrical extinction angles in the zones normal to (010) indicating labradoritic compositions. In contrast to the plagioclase compositions, the alkali feldspars (both phenocryst and groundmass) of the shoshonites exhibit a narrower range in compositions from $Or_{45.6}Ab_{45.9}$ to $Or_{60.0}Ab_{38.0}$ (see Fig. 3.8) and the groundmass and phenocrysts have comparable compositions (*i.e.* as seen for plagioclase compositions). Unfortunately the alkali feldspar is more altered than the plagioclase and analyses from fresh grains were difficult to obtain, however a single alkali feldspar phenocryst is zoned with the K_2O and Na_2O concentrations increasing towards the grain margins (see TABLE 3.11).

	Shoshonites						High-K_2O picritic basalts
	PLAG1C	PLAG1M	PLAG2C	PLAG2M	PLAG3C	PLAG3M	PLAG4
SiO_2	56.03	56.03	65.29	66.33	54.61	54.92	57.22
Al_2O_3	27.90	27.03	20.04	19.73	28.74	28.49	25.79
FeO	.46	.50	.16	.21	.50	.58	.78
MgO	.08	.08	.04		.08	.12	.20
CaO	10.49	9.41	1.63	1.16	11.36	11.22	8.63
Na_2O	5.19	5.64	4.94	5.11	4.53	4.87	5.31
K_2O	.59	.64	8.36	8.77	.66	.35	1.42
TOTAL	100.74	99.33	100.46	101.31	100.48	100.55	99.35
STRUCTURAL FORMULA CALCULATED TO 8 OXYGENS							
Si	2.511	2.542	2.933	2.957	2.461	2.471	2.597
Al	1.473	1.445	1.061	1.037	1.526	1.510	1.379
Fe	.017	.019	.006	.008	.019	.022	.029
Mg	.005	.005	.003		.005	.008	.014
Ca	.504	.458	.078	.055	.549	.541	.420
Na	.451	.496	.430	.442	.396	.425	.467
K	.033	.037	.479	.499	.038	.020	.082
SUM	4.994	5.002	4.990	4.998	4.994	4.997	4.988
AB	45.62	50.08	43.55	44.36	40.28	43.09	48.19
OR	3.39	3.75	48.51	50.08	3.86	2.04	8.50
AN	51.00	46.17	7.94	5.57	55.86	54.87	43.30

TABLE 3.11. Selected plagioclase analyses of the high-K_2O lineage. C refers to core, M to the margin and H to a point between the core and the margin of the individual grains with the same number in the analysis name.

SAMPLE DESCRIPTION:
SHOSHONITE
PLAG1: matrix plagioclase (KLB-099)
PLAG2: alkali feldspar phenocryst (KLB-099)
PLAG3: plagioclase phenocryst (KLB-099)
HIGH-K_2O PICRITIC BASALT
PLAG4: matrix plagioclase (KLB-083)

Plagioclase is present typically as sheaves of microlites and as rare fine laths in the mesostasis of the high-K_2O picritic basalts and the compositions determined for plagioclase range from $An_{44.1}Ab_{47.7}$ to $An_{37.5}Ab_{50.5}$. Plagioclase is present as rare skeletal crystals in the glassy picritic basalts, is a common matrix phase in the evolved picritic basalts and is only very rarely present as a phenocryst phase in the picritic basalts of the Letaba Formation and the plagioclase has compositions which range from $An_{67}Ab_{30}$ to $An_{56}Ab_{40}$ (Bristow, 1980; 1984b). Although the plagioclase compositions of the high-K_2O picritic basalts are more evolved than those quoted by Bristow (1980; 1984b) they are similarly characterised by relatively high K_2O concentrations, *i.e.* 1.26 to 1.72% K_2O, when compared to, for example, the plagioclase compositions of the shoshonites in Fig. 3.7.

3.2.2.4 Fe-Ti Oxides

The Fe-Ti oxide compositions of the high-K_2O lineage determined by electron microprobe analyses (see APPENDIX C2) are summarised in Fig. 3.8 and representative oxide analyses are tabulated in TABLE 3.12.

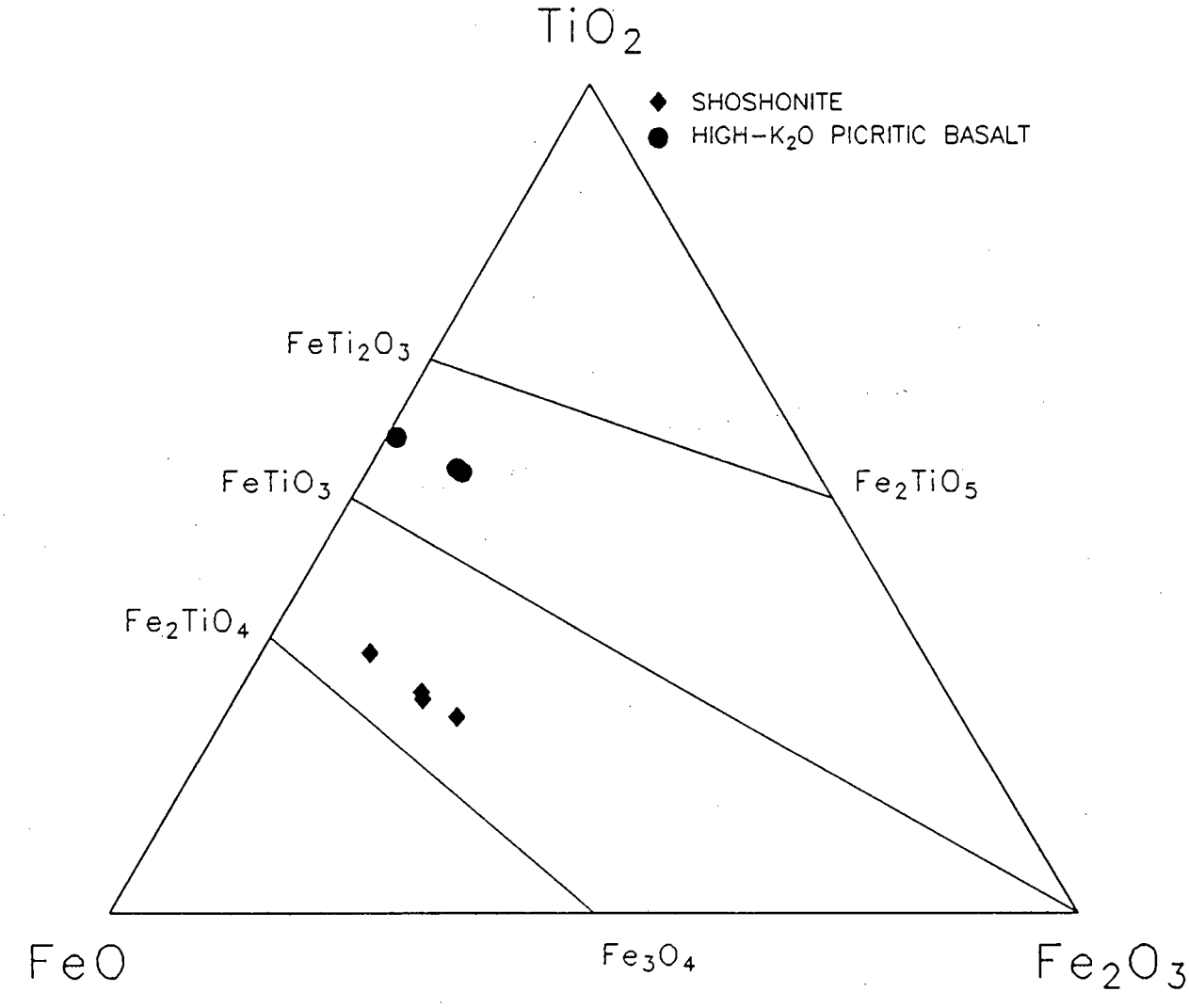

Fig. 3.8. The Fe-Ti oxide compositions of the high-K_2O lineage with Fe_2O_3, FeO and TiO_2 recalculated to 100%.

Titanomaghemite is the only Fe-Ti oxide present in the shoshonites (see Fig. 3.8) and the titanomaghemites typically have rounded anhedral to blocky habits. The titanomaghemites, similar to those observed in the LTZ-type and HTZ-type basalts (see section 3.1.2.4), are the result of low temperature (<600°C) and pressure oxidation of titanomagnetite. The ilmenites of the high-K_2O picritic basalts commonly have acicular (skeletal) habits and are concentrated in the mesostasis. The ilmenites of the high-K_2O picritic basalt have high MgO concentrations (4.11 to 5.47% MgO) similar to those reported by Bristow (1980; 1984b) for the ilmenites of the Letaba Formation picritic basalts.

	Shoshonites		High-K_2O picritic basalts	
	OXID1	OXID2	OXID3	OXID4
SiO_2		.09		
TiO_2	25.36	22.39	50.17	49.65
Al_2O_3	.81	.96	.37	.37
Cr_2O_3			.13	
FeO	51.83	49.33	34.84	34.49
Fe_2O_3	17.94	22.75	8.66	9.33
MnO	1.18	1.28	.38	.41
MgO			5.47	4.95
CaO	.05	.10	.07	
TOTAL	97.17	96.89	100.08	99.21
OXYGEN	4	4	3	3
Si		.004		
Ti	.785	.709	.940	.945
Al	.039	.048	.011	.011
Cr			.003	
Fe	2.341	2.460	.888	.908
Mn	.041	.046	.008	.009
Mg			.203	.187
Ca	.002	.005	.002	
SUM	3.208	3.272	2.055	2.060

TABLE 3.12. Selected Fe-Ti oxide analyses of the high-K_2O lineage.

SAMPLE DESCRIPTION:
SHOSHONITE
OXID1: anhedral titanomaghemite (KLB-099)
OXID2: skeletal titanomaghemite (KLB-099)
HIGH-K_2O PICRITIC BASALT
OXID3: anhedral ilmenite (KLB-083)
OXID4: skeletal ilmenite (KLB-083)

3.3 FELSITES

3.3.1 PETROGRAPHY AND MINERAL CHEMISTRY

The two felsite samples are porphyritic to glomeroporphyritic and the fine grained holocrystalline matrix has a felted texture and includes fine-grained equant to blocky oxides. The phenocryst assemblage of the felsites includes feldspar, clinopyroxene, rare oxide and

possibly olivine (in KLB-080 only) although, unfortunately, the felsite samples are very altered and the phenocryst assemblage is therefore commonly replaced by secondary mineral phases. Elongated euhedral hexagonal prisms of apatite are commonly associated with the glomeroporphyritic aggregates. The modal proportions of the phenocryst assemblage determined by point-counting are 4.8 and 7.3 for KLB-080 and -082 respectively and clinopyroxene is more abundant than plagioclase in the phenocryst assemblage (including fresh, altered and pseudomorphed grains) of both felsite samples.

Rare rounded anhedral brown chlorite and oxide pseudomorphs associated with both plagioclase and pyroxene (and their associated pseudomorphs) in the glomeroporphyritic aggregates of KLB-080 may represent rare altered olivine phenocrysts.

The clinopyroxene phenocrysts (≤3mm) tend to have subhedral to rounded outlines and are altered to, or pseudomorphed by, green chlorite and calcite and the clinopyroxene tends to be less altered than the associated feldspar. Clinopyroxene compositions from unaltered clinopyroxene phenocrysts in KLB-080, determined by electron microprobe analysis (see APPENDIX C3), are summarised in Fig. 3.9A and representative clinopyroxene analyses are tabulated in TABLE 3.13. The clinopyroxene exhibits a range in compositions from $En_{48.1}Wo_{38.9}$ to $En_{38.5}Wo_{38.9}$ and individual pyroxene grains are zoned with both the En and Wo contents decreasing towards the grain margins, although the trace element concentrations (Ti^{4+} and Al^{3+}) are more variable and may either increase or decrease in concentration towards the grain margins of the individual clinopyroxene phenocrysts.

The feldspar phenocrysts are all very altered and are commonly pseudomorphed by sericite together with rare chlorite and calcite. The feldspar phenocryst laths, with lengths varying from .25 to 2mm, characteristically have remnant euhedral to subhedral outlines although the grain margins may be blurred by alteration. Remnant carlsbad and rare lamellar twins are frequently preserved in the altered feldspar phenocrysts. The feldspar compositions determined by electron microprobe analysis (see APPENDIX C3) of the altered feldspar phenocrysts are summarised in Fig. 3.9B and representative feldspar compositions are tabulated in TABLE 3.13. The feldspar phenocrysts exhibit a considerable range in compositions from oligoclase ($An_{25.9}Ab_{65.1}$) to orthoclase ($Or_{95.1}Ab_{4.7}$), although the orthoclase and albite end-member compositions probably represent perthites resulting from either post-magmatic exsolution or from the hydrothermal alteration of alkali feldspar (see section 3.1.2.3 and Parsons and Brown, 1984) and the alkali feldspar compositions therefore range from $Or_{70.4}Ab_{29.4}$ to $Or_{39.2}Ab_{58.7}$. As the feldspars are very altered it is impossible to determine either the nature of the alkali feldspar (*i.e.* whether it has an intratelluric (as either discrete phenocryst or as overgrowths on plagioclase), xenocrystic or hydrothermal

origin) or its relationship to the plagioclase.

The Fe-Ti oxides (titanomagnetites) of the phenocryst assemblage are all very altered and the compositions therefore include high SiO_2 and CaO concentrations ($<7\%$), illustrated by the single titanomagnetite composition, determined by electron microprobe analysis, which is included in TABLE 3.13.

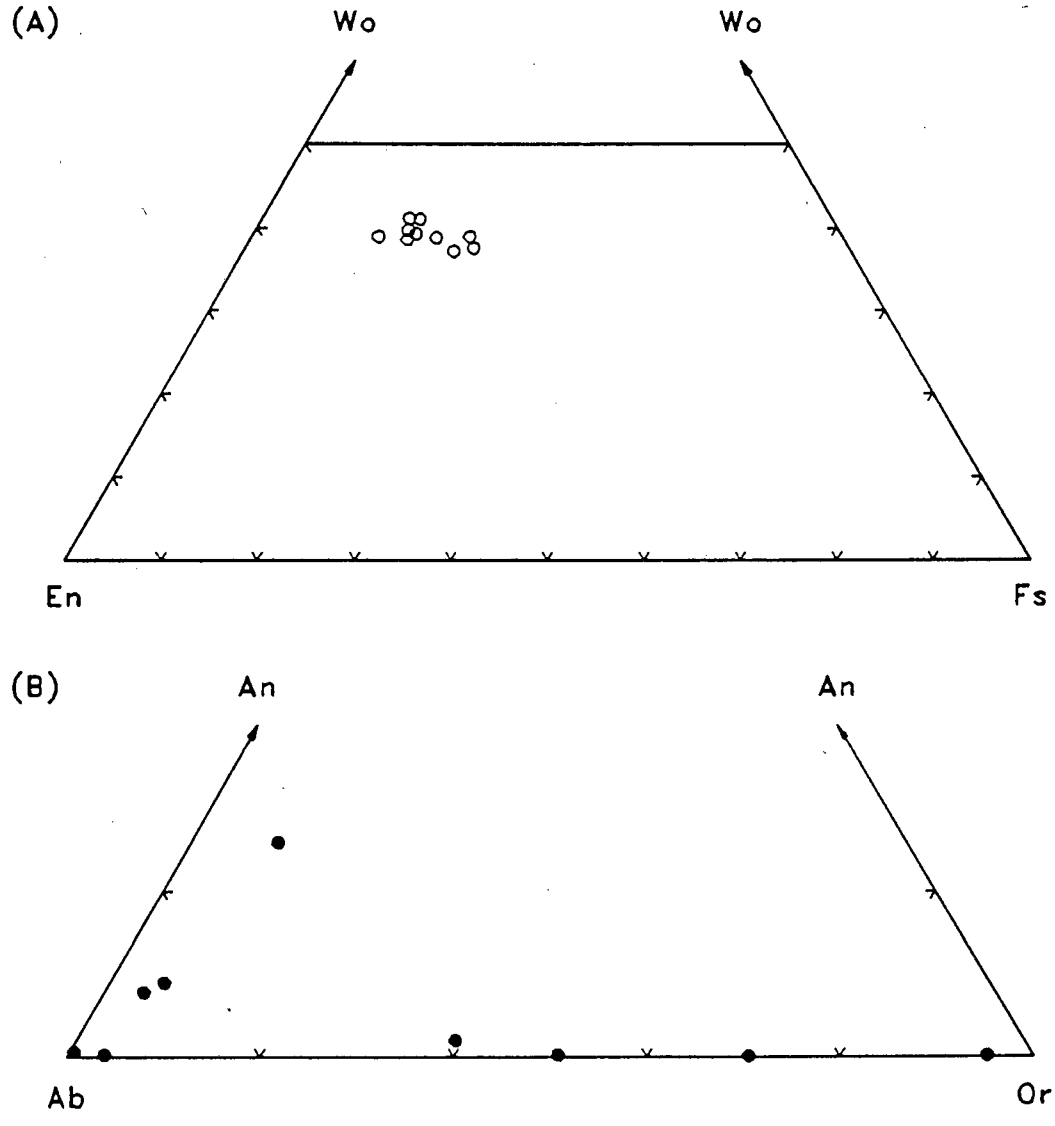

Fig. 3.9. (A) Pyroxene and (B) plagioclase phenocryst compositions of the Felsites.

	Felsites									
	PYX1C	PYX1M	PYX2C	PYX2M	PLAG1	PLAG2C	PLAB2M	PLAG3A	PLAG3B	OXID1
SiO_2	51.01	49.89	49.82	50.36	61.90	67.17	66.08	65.41	66.25	8.76
TiO_2	1.20	1.33	1.45	.60						23.22
Al_2O_3	2.42	3.62	3.17	1.77	24.32	21.46	18.80	18.40	18.51	2.26
Cr_2O_3	.15		.16							.12
FEO	9.69	11.50	9.80	13.73	.37	.16	1.80	.21	.32	52.71
Fe_2O_3										2.48
MnO	.15	.15	.18	.31						2.28
MgO	15.59	14.41	14.63	13.43	.05		.42			
CaO	19.35	18.50	19.58	18.90	4.92	1.54	.41	.05	.05	7.99
Na_2O	.25	.39	.31	.20	6.83	9.63	6.31	.50	3.25	
K_2O					1.44	.69	6.39	15.56	11.86	
TOTAL	99.81	99.79	99.10	99.30	99.83	100.65	100.21	100.13	100.24	99.82
OXYGEN	6	6	6	6	8	8	8	8	8	4
Si	1.905	1.877	1.880	1.926	2.751	2.923	2.967	3.007	3.007	.310
Ti	.034	.038	.041	.017						.618
Al	.106	.161	.141	.080	1.274	1.101	.995	.997	.990	.094
Cr	.004		.005							.004
Fe	.303	.362	.309	.439	.014	.006	.068	.008	.012	1.627
Mn	.005	.005	.006	.010						.068
Mg	.868	.808	.823	.766	.003		.028			
Ca	.774	.746	.792	.775	.234	.072	.020	.003	.003	.303
Na	.018	.028	.023	.015	.588	.813	.549	.045	.286	
K					.081	.038	.366	.912	.687	
SUM	4.017	4.025	4.020	4.028	4.945	4.953	4.993	4.972	4.985	3.025
WO	39.71	38.83	41.02	38.93						
EN	44.51	42.07	42.65	38.49						
FS	15.77	19.10	16.33	22.58						
AB					65.07	88.07	58.74	4.67	29.35	
OR					9.01	4.13	39.15	95.06	70.38	
AN					25.92	7.80	2.11	.27	.27	

SAMPLE DESCRIPTION:
PYX1: anhedral pyroxene phenocryst
PYX2: subhedral pyroxene phenocryst
PLAG1: plagioclase phenocryst
PLAG2: alkali feldspar phenocryst
PLAG3A & B: two analyses from a single alkali feldspar phenocryst
OXID1: titanomagnetite

TABLE 3.13. Selected phenocryst analyses of the felsite sample KLB-080. C refers to the core and M to the margin of the individual grains with the same number in the analysis name.

3.3.2 COMPARISON TO OTHER KAROO FELSIC ROCKS

The rhyolites of the Lebombo are all porphyritic with phenocryst proportions ranging from 10-30% (average of ± 15-25%) and the phenocryst assemblage typically includes plagioclase, clinopyroxene (ferroaugite), magnetite, quartz, alkali feldspar, apatite, zircon, olivine and very rare ilmenite and pigeonite whereas the rhyolites of the Nuanetsi are essentially aphyric (Cleverly *et al.*, 1984). Alkali feldspar is present as overgrowths around plagioclase in many of the rhyolites and is only present as a discrete phenocryst phase in the more evolved rock types (*e.g.* the Oribi Beds with 72-76% SiO_2).

The phenocryst assemblage of the intermediate Pronksberg Dacite and Belmore Andesite of the Central Karoo area includes hypersthene, plagioclase, rare Fe-Ti oxides and several percent of cordierite is present in the Pronksberg Dacite (Marsh and Eales, 1984).

The felsite dykes of Botswana with a phenocryst assemblage of clinopyroxene, plagioclase and alkali feldspar (and associated perthites) together with titanomaghemite and accessory apatite are therefore comparable to the Lebombo rhyolites although the Lebombo rhyolites tend to have a higher proportion of phenocrysts where plagioclase is the dominant phenocryst phase present.

4 WHOLE ROCK GEOCHEMISTRY

The Botswana Karoo data set (which also includes samples from the Tuli Syncline of southwest Zimbabwe) currently contains whole rock data (including major and trace elements) for 198 samples, of which new analyses for 128 samples were undertaken during this study. Major and trace element data was obtained by XRF analysis at UCT according to the analytical techniques outlined in Duncan *et al.* (1984b) and le Roex (1985). The whole rock compositions for the Botswana dataset, which have all Fe as Fe_2O_3*, are tabulated in APPENDIX D.

4.1 LOW-K_2O LINEAGE

4.1.1 LTZ-TYPE BASALTS (AND DOLERITES)

The LTZ-type basalts (and dolerites) are sub-divided (as discussed in Chapter 2) into a number of geochemical sub-groups, *i.e.* the low-MgO LTZ picritic basalts, the LTZ basalts, the high-Na_2O LTZ basalts, the TYPE I LTZ dolerites and the low-P_2O_5 LTZ basalts. The whole rock geochemistry of the various groups will be described simultaneously, where appropriate, to avoid unnecessary repetition. TABLE 4.1 summarises the mean, maximum, minimum and standard deviation of the major and trace element compositions for all of the various LTZ-type basalt (and dolerite) sub-groups and the average composition of the Lesotho Formation basalt type of the Central Karoo area is included in TABLE 4.1 to aid comparison between the different basalt types from the two areas. The major and trace element concentrations of all of the LTZ-type basalts (and dolerites) are plotted *vs.* MgO in Fig. 4.1A & B.

4.1.1.1 Major element geochemistry

The LTZ-type basalts (and dolerites) as a single group are characterised by a considerable range in major element geochemistry with the MgO concentration varying from a maximum of 10.51 wt% in the low-MgO LTZ picritic basalts to a minimum of 4.72 wt% in the low-P_2O_5 LTZ basalts. As noted previously the LTZ- and high-Na_2O LTZ basalts have similar major element compositions apart from the higher Na_2O and lower CaO concentrations of the high-Na_2O LTZ basalts, and the major element composition of the TYPE I LTZ dolerites clearly lie within the field defined by the major element concentrations of the LTZ

	LOW-MGO LTZ PICRITIC BASALT					LTZ BASALT					HIGH-NA_2O LTZ BASALT				
	MEAN	MIN	MAX	S.D.	N	MEAN	MIN	MAX	S.D.	N	MEAN	MIN	MAX	S.D.	N
SiO_2	50.06	49.83	50.28	.23	3	51.45	50.05	53.61	.69	78	51.30	50.06	52.84	.68	24
TiO_2	.82	.78	.86	.04	3	.97	.79	1.37	.14	78	.94	.83	1.37	.11	24
Al_2O_3	14.51	14.02	15.22	.62	3	15.39	13.56	16.56	.54	78	15.43	14.68	15.98	.31	24
Fe_2O_3	11.61	11.40	11.78	.19	3	11.33	10.12	13.65	.87	78	10.91	10.17	13.46	.61	24
MnO	.16	.12	.19	.04	3	.17	.14	.23	.02	78	.16	.13	.21	.02	24
MgO	9.93	9.14	10.51	.71	3	7.18	5.70	8.51	.69	78	7.40	5.83	8.21	.57	24
CaO	9.96	9.86	10.03	.09	3	10.39	8.02	11.41	.73	78	9.03	7.43	10.87	.94	24
Na_2O	2.33	1.99	2.96	.54	3	2.35	1.80	3.25	.37	78	3.96	2.75	5.22	.67	24
K_2O	.48	.43	.59	.09	3	.61	.13	1.50	.21	78	.71	.36	1.78	.28	24
P_2O_5	.14	.12	.16	.02	3	.16	.12	.25	.02	78	.15	.12	.23	.03	24
Rb	9.9	6.9	15	4.1	3	12	1.8	36	5.8	78	12	5.2	37	6.7	24
Ba	131	113	149	26	2	159	62	270	37	75	172	101	373	54	23
Sr	172	169	177	4.7	3	202	107	353	28	78	213	144	382	58	24
Th					0	2.8	2.3	3.8	.5	13	2.9	2.3	4.0	.7	5.0
U					0	2.1	1.7	2.8	.3	10	2.1	1.7	3.3	.7	5.0
Zr	69	60	84	13	3	86	59	126	16	78	77	59	127	14	24
Nb	5.0	4.7	5.4	.4	3	6.3	3.3	9.5	1.5	75	5.6	4.5	8.9	1.1	24
Cr	403	345	497	82	3	277	123	424	75	78	308	156	412	57	24
V	201	182	218	18	3	230	191	292	23	78	238	216	329	25	24
Sc	30	30	31	.12	2	34	29	41	2.5	71	34	30	40	2.2	23
Ni	172	139	189	29	3	91	54	124	17	78	91	62	115	14	24
Co	61	59	62	1.8	3	50	44	61	3.1	78	49	44	52	2.5	24
Pb	4.2	3.9	4.5	.40	2	4.5	2.7	7.1	1.0	51	3.5	2.8	4.6	.6	13
Zn	83	80	85	2.7	3	85	66	118	10	78	88	75	164	19	24
Cu	68	63	74	5.5	3	84	42	162	24	78	77	37	153	20	24
Y	21	20	23	1.2	3	25	19	34	3.1	78	24	19	35	2.8	24
La	8.0	7.5	8.5	.73	2	10	5.8	17	2.3	71	9.4	5.5	14	2.0	23
Ce	18	17	18	.64	2	23	12	61	8.4	71	21	13	51	7.7	23
Nd	9.6	9.0	10	.81	2	13	7.1	35	3.8	71	12	7.7	36	5.7	23

TABLE 4.1. Average whole rock compositions of the LTZ-type basalts (and dolerites). Data for Lesotho Formation from Microfiche Card 2A attached to Duncan *et al.* (1984b).

	TYPE I LTZ DOLERITE		LOW-P_2O_5 LTZ BASALT					LESOTHO FORMATION (CENTRAL AREA)				
	KLB-049	KLB-050	MEAN	MIN	MAX	S.D.	N	MEAN	MIN	MAX	S.D.	N
SiO_2	51.44	51.51	50.89	49.62	52.22	.93	9	51.50	49.71	53.71	.78	49
TiO_2	1.06	1.05	1.60	1.45	1.93	.15	9	.95	.86	1.13	.06	49
Al_2O_3	14.57	14.57	14.60	13.90	15.07	.40	9	15.69	14.03	16.98	.53	49
Fe_2O_3	12.09	11.94	14.78	13.86	16.58	.79	9	10.96	10.12	11.93	.43	49
MnO	.20	.19	.18	.13	.22	.03	9	.16	.13	.23	.02	49
MgO	6.19	6.17	5.50	4.72	6.17	.40	9	7.01	6.08	7.91	.53	49
CaO	10.44	10.49	9.28	6.03	10.77	1.35	9	10.69	9.06	11.54	.61	49
Na_2O	3.01	3.02	2.25	1.96	2.96	.29	9	2.17	1.38	2.93	.32	49
K_2O	.84	.88	.76	.30	1.26	.31	9	.70	.30	1.13	.21	49
P_2O_5	.18	.17	.17	.15	.22	.02	9	.16	.10	.20	.02	49
Rb	17	20	28	9.3	89	24	9	12	4.2	52	8.7	49
Ba	217	332	143	92	200	37	9	177	77	280	46	47
Sr	189	202	226	137	309	50	9	192	115	256	31	49
Th								1.27	.9	1.5	.26	4
U			2.6	1.9	3.9	.8	6	.29	.2	.3	.0485	4
Zr	101	104	113	90	158	19	9	94	78	120	12.4	49
Nb	7.2	7.9	5.7	4.9	8.3	1.0	9	4.9	2.4	8.0	1.39	49
Cr	204	206	110	69	155	28	9	283	33	377	61	49
V	233	239	319	288	337	18	9	240	204	289	19	49
Sc	31	33	42	33	54	6.4	9	33	29	42	2.9	36
Ni	56	58	77	61	91	8.4	9	94	52	120	15.4	49
Co	44	46	51	45	56	3.8	9	48	43	52	2.5	49
Pb	2.9	2.7	3.7	3.1	4.6	.7	4	2.9	2.5	3.3	.4	4
Zn	87	91	109	100	118	5.9	9	86	69	101	9.5	49
Cu	99	100	150	114	178	24	9	87	68	130	11.5	49
Y	27	28	29	25	34	3.0	9	24	21	31	2.0	49
La	13	17	12	9.3	16	1.9	9					
Ce	58	50	25	18	33	4.6	9					
Nd	11	31	17	14	24	3.2	9					

TABLE 4.1 (continued).

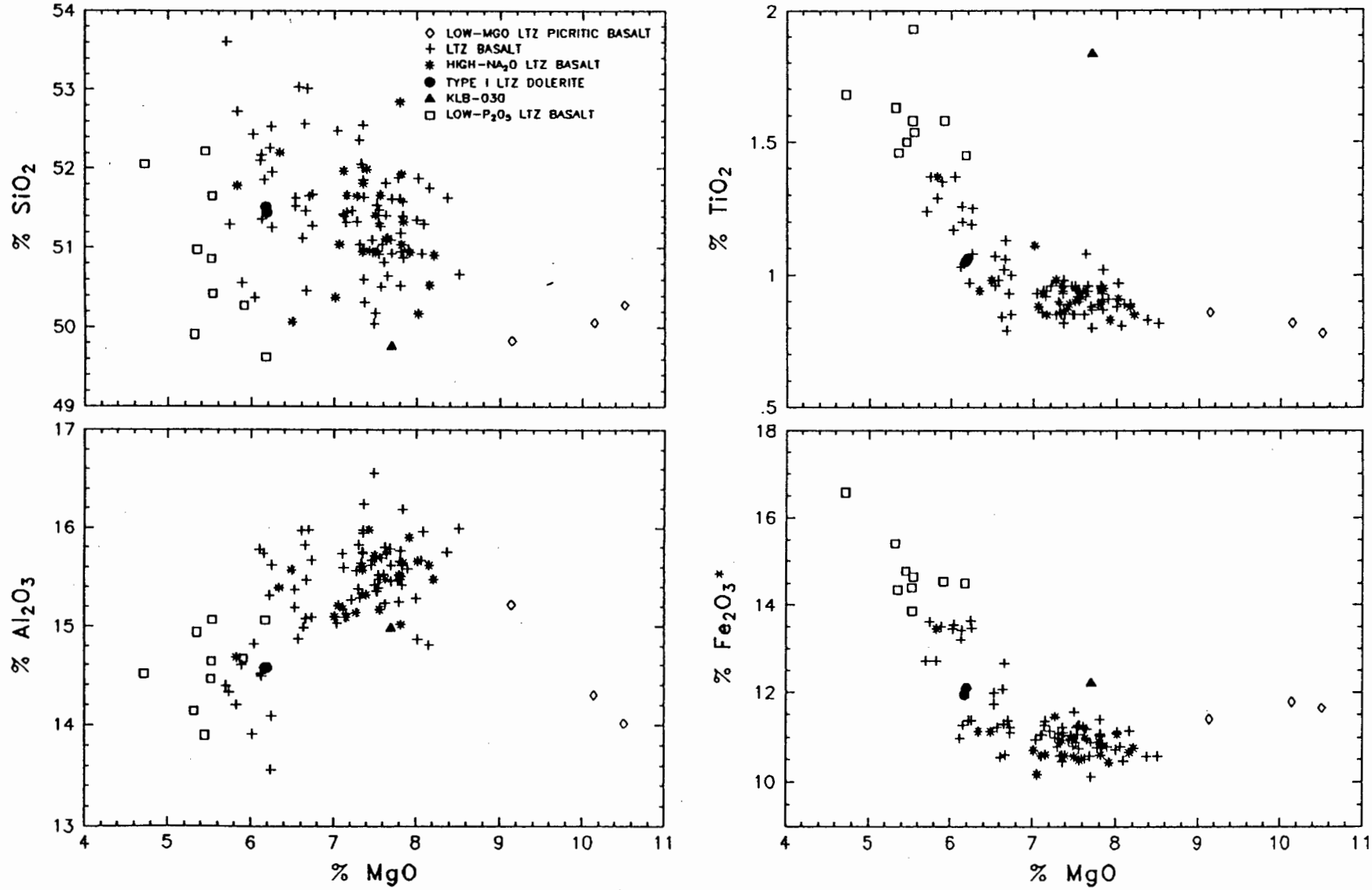

Fig. 4.1A. Major element variation diagrams plotted *vs.* MgO for the LTZ-type basalts (data normalised to 100% volatile-free with all Fe as Fe_2O_3*).

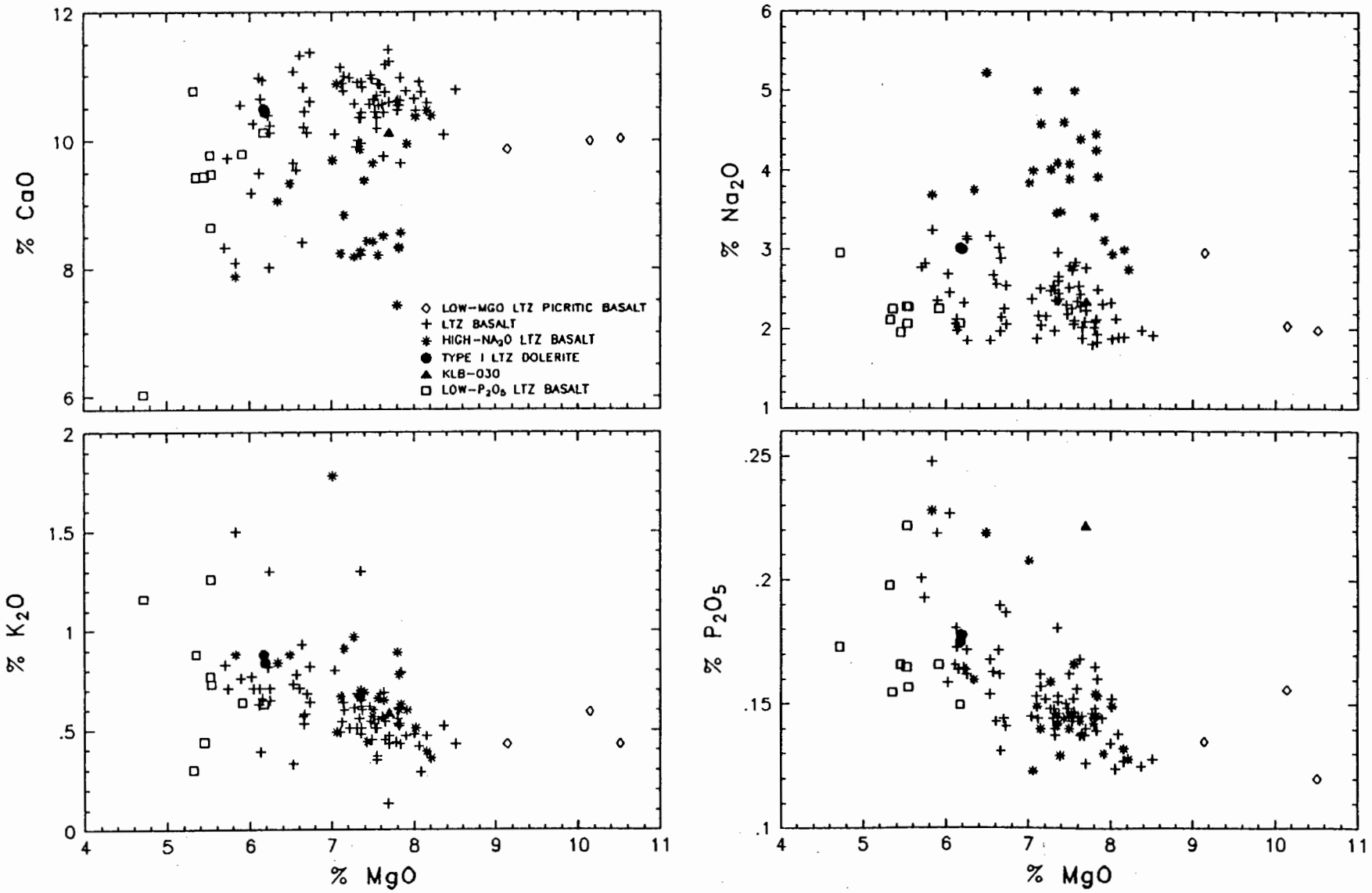

Fig. 4.1A (continued).

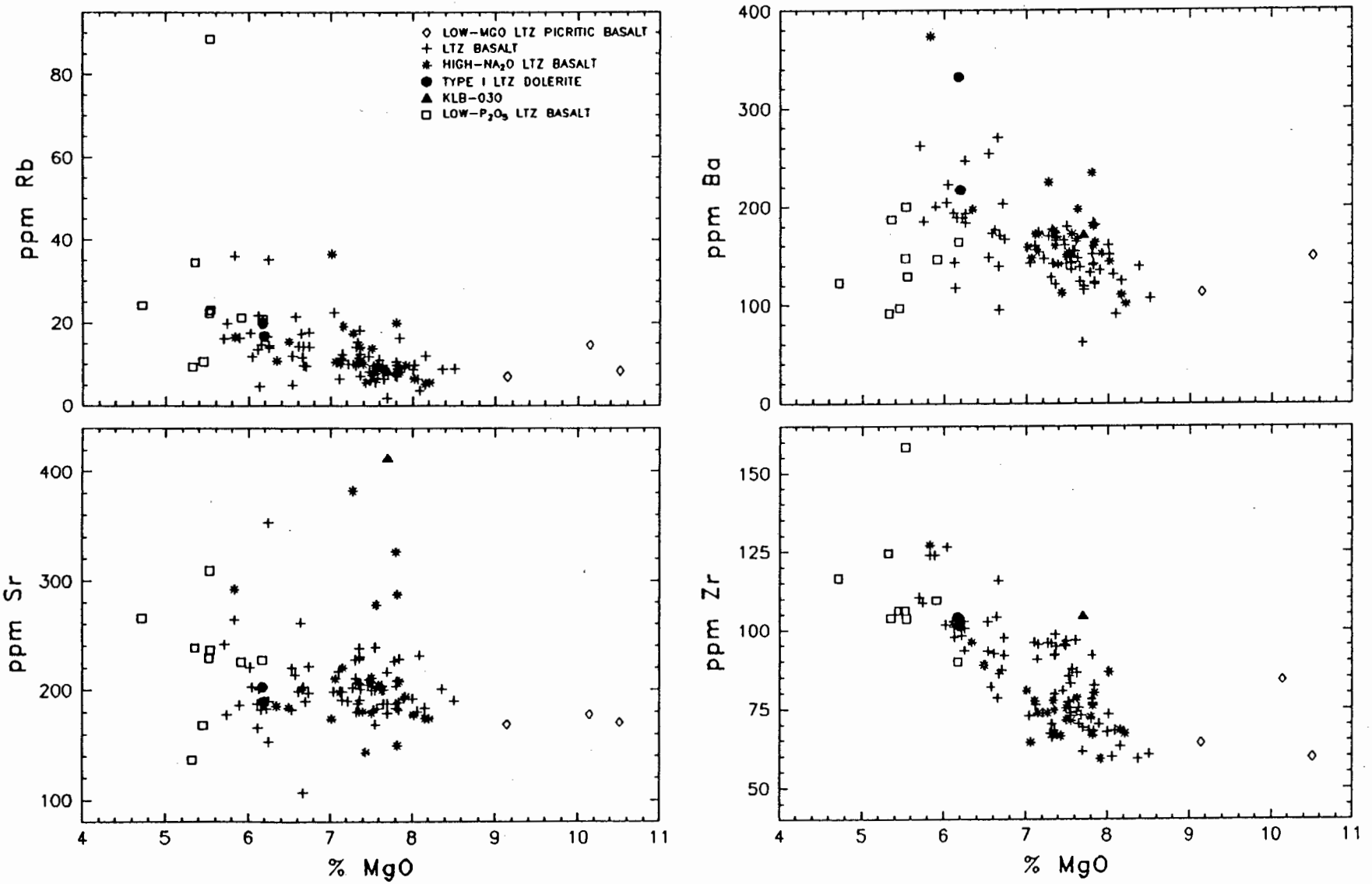

Fig. 4.1B. Trace element variation diagrams plotted *vs.* MgO for the LTZ-type basalts (data normalised to 100% volatile-free).

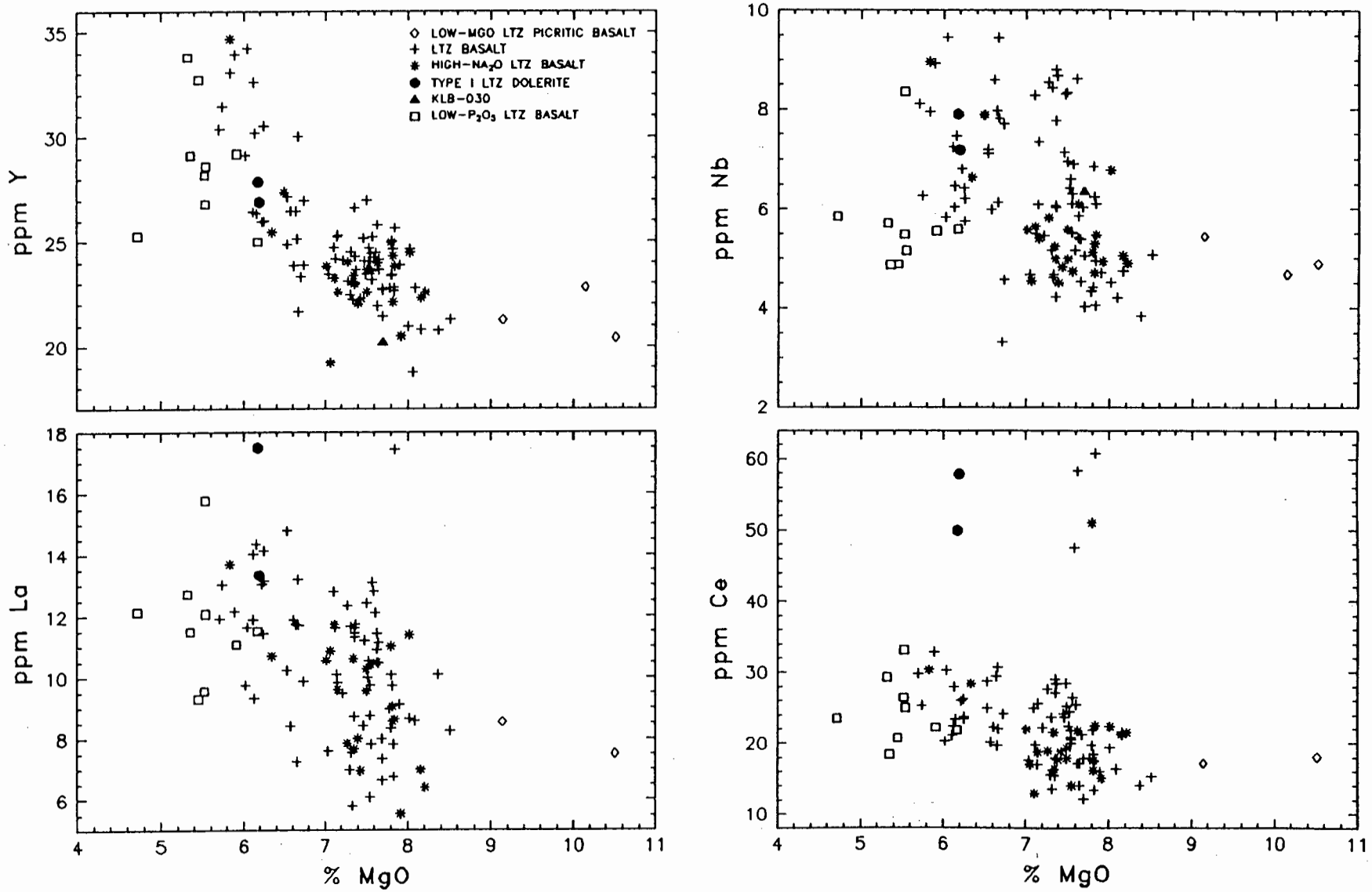

Fig. 4.1B (continued).

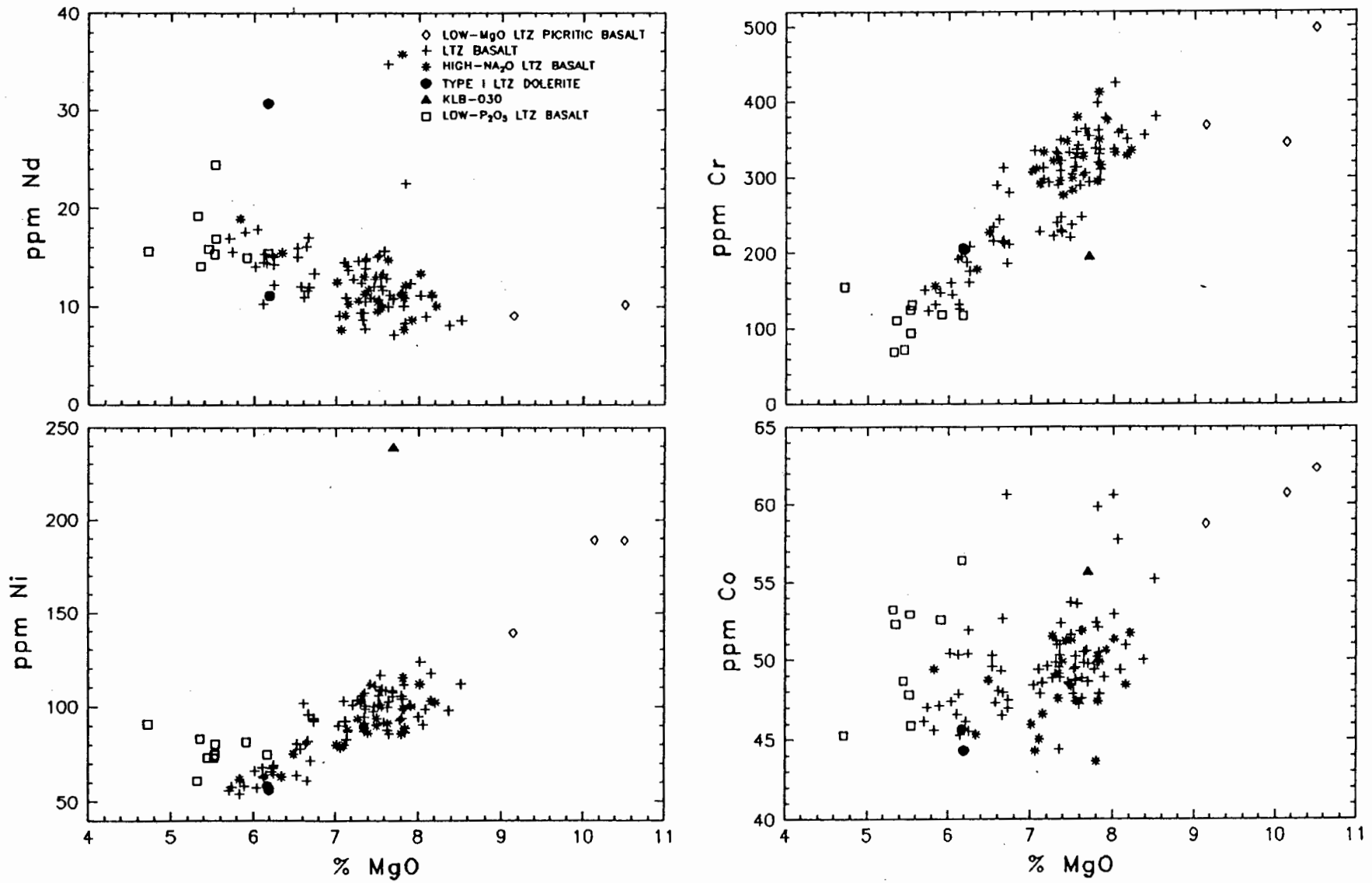

Fig. 4.1B (continued).

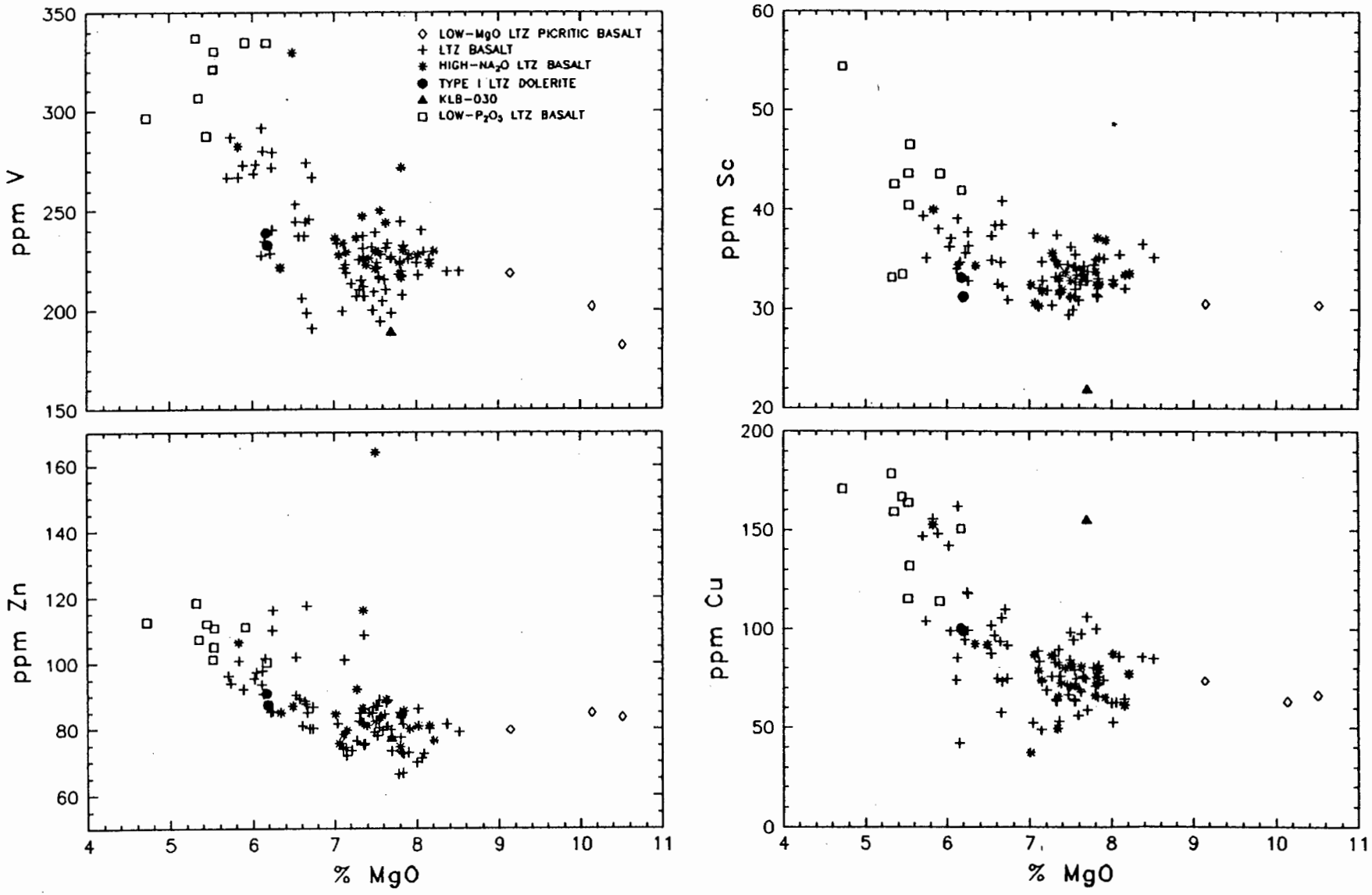

Fig. 4.1B (continued).

basalts (see Fig. 4.1A). The major element characteristics of the LTZ basalts are therefore also applicable to these sub-groups.

The most striking feature of the whole rock geochemistry of the LTZ basalts of Botswana is their remarkable similarity to the composition of the Lesotho Formation basalts of the Central Karoo area with the means of the major element concentrations being almost identical (see TABLE 4.1 and Fig. 4.2) although the LTZ basalts do exhibit a greater range in MgO concentrations (5.71-8.51 wt%) with respect to a range in MgO concentration of 6.08 to 7.91 wt% observed for the Lesotho Formation basalts (Marsh and Eales, 1984). The LTZ basalts are, however, characterised by a relatively narrow compositional range for many elements (see the small S.D. values in TABLE 4.1), similar to that described for the Lesotho Formation basalts (Marsh and Eales, 1984), although the greater range in the MgO concentrations of the LTZ basalts is reflected in a greater range of the TiO_2 (0.79-1.37%), Fe_2O_3* (10.12-13.2%), CaO (8.02-11.41%) and K_2O (0.13-1.5%) concentrations, in particular. Although the major element concentrations, especially SiO_2 and CaO, display considerable scatter in Fig. 4.1A, TiO_2, Fe_2O_3*, Na_2O, K_2O and P_2O_5 define relatively coherent negative correlation trends against MgO. Al_2O_3, in particular, shows two clear trends above and below 9% MgO. The scatter in CaO data points disguises any clearly defined trend although samples do show a general decrease in concentration with decreasing MgO. Below ±6% MgO the trends defined by the major element concentrations *vs.* MgO kink such that the degree of enrichment or depletion (in the case of Al_2O_3 and CaO) is more marked.

The three low-MgO LTZ picritic basalts have major element compositions which are similar to the more mafic LTZ-type basalts, although, in contrast to the LTZ-type basalts, the low-MgO LTZ picritic basalts appear to define a negative trend of increasing Al_2O_3 and CaO concentrations with decreasing MgO in Fig. 4.1A which attest to the importance of olivine in the relationship, whether by accumulation or fractional crystallization, between the low-MgO LTZ picritic basalts and the LTZ basalts. The relatively low CaO concentration (9.86%) of the low-MgO LTZ picritic basalt with the lowest MgO concentration (9.14%) probably reflects a similar Ca-Na type exchange as noted for the high-Na_2O LTZ basalts (see Fig. 2.12A & B and section 3.1.2.3) as it has a higher Na_2O concentration (*i.e.* similar to the high-Na_2O LTZ basalts) than the other low-MgO LTZ picritic basalts.

The low-P_2O_5 LTZ basalts have the most evolved compositions of the LTZ-type basalts (and dolerites) with between 6.17 and 4.72 wt% MgO (mean of 5.5 %) and these low-P_2O_5 LTZ basalts lie on the evolved end of the trends defined by the major element concentrations of the LTZ-type basalts and dolerites in Fig. 4.1A. The low-P_2O_5 LTZ basalts tend to have lower SiO_2, Na_2O and P_2O_5 and higher TiO_2 and Fe_2O_3* concentrations

when compared to the evolved LTZ-type basalts. The higher TiO_2/P_2O_5 ratio of the low-P_2O_5 LTZ basalts (see Fig. 2.11) is a useful discriminant between the low-P_2O_5 LTZ basalts and the LTZ-type basalts.

The sample KLB-030 which is classified as having a LTZ-type signature with <2% TiO_2 (*i.e.* 1.84%) and <250ppm Zr (*i.e.* 105ppm) is included in Fig. 4.1A for completion, although KLB-030 has a distinctly different major element chemistry as it is clearly enriched in TiO_2, P_2O_5 and Fe_2O_3* with respect to the LTZ-type basalts and the low-P_2O_5 LTZ basalts.

4.1.1.2 Trace element geochemistry

The trace element compositions of the various LTZ-type basalt sub-groups mirror their major element compositions with the resemblance in the trace element concentrations of the LTZ basalts, high-Na_2O LTZ basalts and TYPE I LTZ dolerites (see Fig. 4.1B) reflecting their major element compositions. The remarkable similarity noted between the major element compositions of the LTZ basalts and the Lesotho Formation basalts of the Central Karoo area is likewise reflected in their trace element compositions (see TABLE 4.1 and Fig. 4.2). Cr and Ni define coherent positive trends against MgO, and Co shows a broad decrease in concentration with decreasing MgO concentration. The incompatible elements (Rb, Ba, Zr, Nb & Cu and the LREE (La, Ce and Nd) define negative trends against MgO although the scatter in the Rb and Ba concentrations are presumably the result of alteration. The scatter in the Nb and LREE concentrations, however, probably reflect the difficulties in precise analytical determinations at low concentrations by XRF analysis (Duncan *et al.*, 1984b). Y and Zn also show a negative correlation with MgO and the lower levels of enrichment displayed by these elements may reflect their partitioning into clinopyroxene in the fractionating assemblage. In contrast, Sr, which is characterised by a range in concentrations, and Sc show no correlation with MgO in Fig. 4.1B.

The trace element concentrations of the low-MgO LTZ picritic basalts are similar to the more mafic LTZ basalts, although the low-MgO LTZ picritic basalts are enriched in Ni (and Co), and although the low-MgO LTZ picritic basalts display a considerable scatter in Cr concentrations, the apparent change in the slope direction defined by low-MgO LTZ picritic basalts in the Cr *vs.* MgO plot corresponds with the major element evidence of the importance of olivine in the relationship between the low-MgO LTZ picritic basalts and the LTZ basalts.

The low-P_2O_5 LTZ basalts and the more evolved LTZ basalts similarly have comparable trace element compositions, the low-P_2O_5 LTZ basalts are, however, enriched in Ni (and Co) and are somewhat depleted in Ba and Nb when compared to the LTZ basalts and

furthermore the low-P_2O_5 LTZ basalts show a marked enrichment in V and Cu (*i.e.* imitating the TiO_2 and Fe_2O_3* enrichment of their major element concentrations) with respect to the LTZ basalts.

The trace element composition of KLB-030 is again distinctly different to the LTZ-type basalts (and dolerites) and the low-P_2O_5 LTZ basalts as KLB-030 is clearly enriched in Sr, Ni, Cu (and Zr) and somewhat depleted in Y, Cr, V and Sc with respect to the LTZ-type basalts (see Fig. 4.1B).

4.1.1.3 Rare earth elements

The REE data available for the LTZ-type basalts, obtained by ion chromatography at UCT, were discussed in section 2.3.1.3.2 and are plotted in Fig. 2.9. They are tabulated in TABLE 4.2, together with the average (and standard deviation) REE compositions of the Lesotho Formation basalts of the Central Karoo area (A.R. Duncan, *pers. comm.*, 1995). The LTZ basalt (KLB-017) has a lower concentration of both LREE and HREE when compared to the low-P_2O_5 LTZ basalts (KLB-015 and -016) and the chondrite normalised LTZ-type basalts are characterised by relative LREE enrichment patterns (see La/Yb_N in TABLE 4.2). The LREE enrichment patterns of the low-P_2O_5 LTZ basalts are very variable (La/Yb_N ratio varies from 2.31 to 4.06) and the slope of the LTZ basalt (La/Yb_N=2.57) is included in this range. The chondrite-normalised REE patterns of the LTZ-type basalts of Botswana are similar to those defined by the Lesotho Formation basalts of the Central Karoo area which have LREE concentrations of ±25-30X chondritic, HREE concentrations of 10-12X chondritic and a LREE enrichment with La/Yb_N variations of 2.46 to 3.29 (Marsh and Eales, 1984).

	LTZ BASALT	LOW-P_2O_5 LTZ BASALT		LESOTHO FORMATION	
	KLB-017	KLB-015	KLB-016	MEAN	S.D.
La	7.25	7.61	12.0	10.3	1.4
Ce	14.9	18.3	29.5	24.6	3.2
Pr	2.15	2.52	3.88	3.01	.37
Nd	8.85	12.1	18.5	13.4	1.4
Sm	2.58	3.70	4.87	3.37	.33
Eu	0.92	1.15	1.64	1.10	.09
Gd	3.23	4.19	5.11	3.89	.20
Tb	0.57	0.72	0.79	0.64	.04
Dy	3.60	4.55	4.75	4.02	.27
Er	2.18	2.65	2.49	2.60	.16
Yb	2.02	2.36	2.12	2.40	.14
La/Yb_N	2.57	2.31	4.06	3.06	

TABLE 4.2. The REE data for the LTZ-type basalts (concentrations in ppm).

4.1.1.4 Sr-isotopes

A single radiogenic Sr isotopic analysis of a LTZ-type basalt (R.A. Armstrong, *pers. comm.*, 1994) shows an initial $^{87}Sr/^{86}Sr$ ratio of 0.70591 (age corrected to 190Ma) for KLB-045. The R_o for KLB-045 lies within the range in initial $^{87}Sr/^{86}Sr$ ratios of 0.70495 -0.70696 determined for the Lesotho Formation basalts (Bristow *et al.*, 1984).

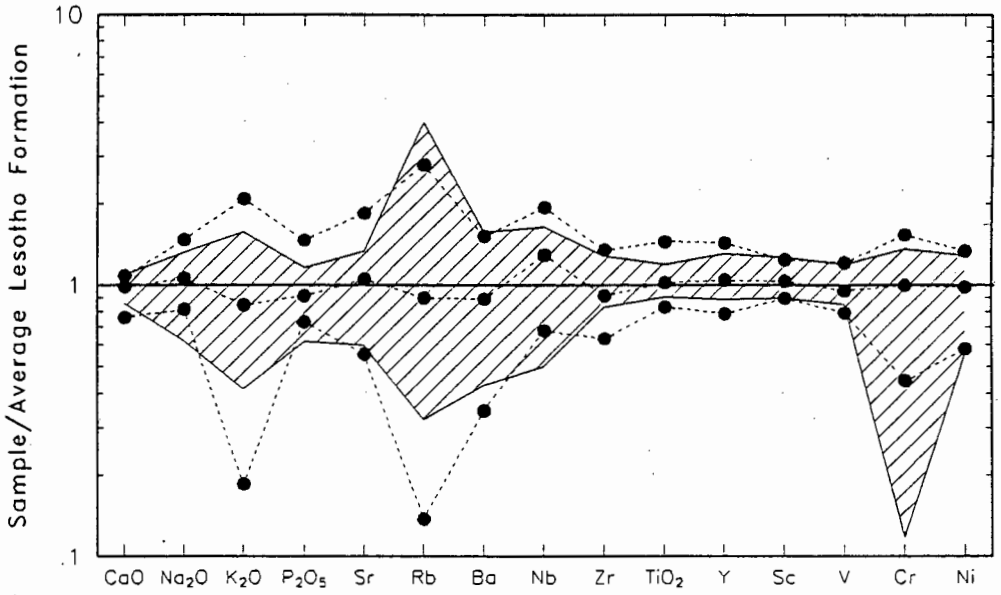

Fig. 4.2. Mean, maximum and minimum concentrations of selected variables of the LTZ basalt type (N=78) normalised to the average Lesotho Formation basalts composition (dashed lines). The range in composition shown by the Lesotho Formation basalts (see text) are similarly normalised to average Lesotho Formation basalt compositions (shaded field).

4.1.1.5 Summary

The LTZ-type basalts (*i.e.* excluding the low-P_2O_5 LTZ basalts) define a relatively coherent compositional group which have whole rock compositions (both the average and range in element concentrations) which are remarkably similar to those of the Lesotho Formation basalts of the Central Karoo area. This resemblance between the LTZ basalts and the Lesotho Formation basalts of the Central Karoo area is summarised in Fig. 4.2 where the mean, minimum and maximum concentrations of selected elements of the LTZ basalts of Botswana are normalised to the average concentrations in the Lesotho Formation basalts (see dashed lines in Fig. 4.2) and, for comparison, the range in Lesotho Formation basalt compositions (data from Microfiche Card 2A attached to Duncan *et al.*, 1984b) are similarly normalised to the average Lesotho Formation composition (see the shaded field in Fig. 4.2). The REE and isotope compositions of the LTZ basalts are comparable with those reported in the literature for the Central Karoo area. This compositional homogeneity therefore suggests a considerably more widespread distribution of the Lesotho/LTZ basalt type. The two TYPE I LTZ dolerites resemble, both petrographically and geochemically, the LTZ-type

basalts and are the only intrusive equivalents to this basalt type recognised in Botswana.

The whole rock compositions of the low-P_2O_5 LTZ basalts typically define the evolved end of the relatively coherent compositional trends in the MgO bivariate plots of Fig. 4.1A & B, but can be clearly distinguished from the LTZ basalts using some inter-element ratios (*e.g.* TiO_2/P_2O_5 *vs.* MgO in Fig. 2.11).

4.1.1.6 Within and between flow heterogeneities

The original composition of the LTZ-type basalt may be obscured by a number of magmatic or post-magmatic processes. Magmatic processes such as fractional crystallization, flowage differentiation, cumulus enrichment, compensated crystal settling and migration and concentration of late stage residual liquids and volatiles will produce within-flow heterogeneities which may be further effected by late stage low temperature secondary processes such as surface weathering, hydrothermal alteration and amygdale formation (Marsh and Eales, 1984; Peate, 1989; Cox, Bell and Pankhurst, 1979).

Plenty of evidence is available to support the importance of late stage hydrothermal activity in the LTZ-type basalts, including the ubiquitous amygdales (both true and diktytaxitic), the albitization of plagioclase, the low temperature oxidation of titanomagnetite to titanomaghemite, complete replacement of olivine and the alteration of plagioclase, pyroxene and the mesostasis. As these secondary post-magmatic processes would have modified the original composition of the LTZ basaltic magmas, the geochemical effects need to be evaluated. The LTZ-type basalts of Botswana were sampled from a number of different drill cores, often with two or more samples collected from within a single basalt unit (in a vertical section) and therefore within-flow and within-core variations can be evaluated.

A similar study was undertaken by Marsh and Eales (1984) to assess the effects of alteration on the composition of Lesotho Formation basalts in the Central Karoo area and they defined a coefficient of variation with C.V. = range X 100/mean and a C.V. with a value of 20 was arbitrarily chosen to distinguish between highly variable and less variable element concentrations. Marsh and Eales (1984) conclude that Na_2O, K_2O, Rb, Ba, Sr and Cu were the elements most susceptible to mobilization during the alteration of the Lesotho Formation basalts. A comparable study undertaken by Peate (1989) obtained similar results with the elements Na_2O, K_2O, Rb, Ba and Sr affected most by the alteration of the Paraná basalts. TABLE 4.3 summarises the coefficients of variation calculated for within-flow variations for the LTZ-type basalts of Botswana. In contrast to the results obtained by Marsh and Eales (1984) the LTZ basalts of Botswana are characterised, on average, by large

within-flow variations with C.V. values of >20 recorded for most element concentrations in at least one basalt flow. However the similarity in whole rock composition of the LTZ-type basalts of Botswana and the Lesotho Formation basalts of the Central Karoo area suggests that the elements Na_2O, K_2O, Rb, Ba, Sr and Cu would be most effected by alteration and the high C.V. values (see TABLE 4.3) calculated for these elements, together with CaO, in those basalt flows which are relatively unaffected by primary magmatic differentiation processes (*i.e.* reflected in low MgO concentration variations) supports this suggestion with the high within-flow variability of the CaO concentration in the LTZ-type basalts of Botswana (see high C.V. values in TABLE 4.3), in part, the result of the albitization of plagioclase (see section 3.1.2.3). The relatively high C.V. values calculated for Nb in these LTZ-type basalts probably reflect imprecision in the XRF analysis (see section 4.1.1.2) and not increased mobilization due to alteration. In contrast the elements TiO_2, Zr, Nb, Y, V, Co, Zn and some REE (*i.e.* the high field strength or HFS elements) are known to be relatively immobile and are not affected by post-magmatic processes (Marsh and Eales, 1984; Peate, 1989) and the high within-flow C.V. values calculated for these elements in some cases (*e.g.* KLB-126 to -128) must therefore reflect the effects of primary magmatic differentiation.

Fig. 4.3A-C summarises the within-core concentration variations for the elements Rb, Mg# and Zr *vs.* depth in the borehole P11, which is drilled in the Nata Sub-basin to the NE of the former Lake Makgadikgadi (see Fig. 5.1). The wide range in concentrations which are measured for Rb in P11 (see Fig. 4.3A) with the Rb concentrations varying from 1.79-35.22 ppm (*i.e.* a within core C.V. value calculated = 239.64) reflect, to some degree, the within-flow Rb variations due to alteration. The broad increase in Rb concentrations towards the top of the borehole, however, suggests that progressive magmatic differentiation is also involved in the within and between flow Rb variations. The wide variation in the Mg# and the Zr concentrations *vs.* depth in Fig. 4.3B & C, respectively, support the suggestion that primary magmatic processes are also involved in the within and between flow heterogeneities. The progressive fractionation of the LTZ-type basalts in the vertical stratigraphy of the borehole P11 is seen in other boreholes drilled in Botswana (*e.g.* Zr *vs.* depth for borehole P8) and Cox and Hornung (1966) and Pemberton (1978) similarly noted the that more fractionated basalts tend to be stratigraphically higher in a vertical section through the Lesotho Formation basalts of the Central Karoo area.

KLB-	115& 116	119& 120	121& 122	124& 125	126- 128	157& 158	166& 167	17&18 187&188	199& 200	201& 202	19&20 204
TiO_2	1.69	9.96	10.23	7.32	22.22	2.33	1.09	10.96	6.59	1.04	14.77
MgO	3.59	5.79	0.30	0.90	49.00	1.23	0.53	10.23	0.84	2.78	2.56
CaO	13.60	20.76	19.45	8.34	5.56	3.07	0.95	24.40	0.09	0.10	5.62
Na_2O	16.07	12.21	4.40	4.28	29.36	1.21	3.58	64.49	59.32	7.22	22.61
K_2O	51.21	7.79	54.79	9.84	55.22	17.86	7.55	50.54	9.71	9.35	9.02
Rb	69.23	28.57	19.35	38.30	80.12	33.98	15.38	92.96	9.52	11.53	19.59
Ba	18.98	16.08	95.89	2.37	19.35	1.75	3.92	14.63	5.94	0.66	16.09
Sr	46.42	18.02	84.01	1.99	22.68	1.47	0.55	10.62	5.38	6.02	2.11
Zr	0.98	13.56	10.91	6.74	30.69	2.06	2.33	7.87	17.14	1.38	12.00
Nb	9.84	15.90	16.09	1.29	25.00	3.47	4.44	5.45	20.00	2.25	16.53
Y	6.67	12.50	14.29	8.70	26.08	4.26	-	8.70	8.70	8.33	13.24
Cr	0.62	4.05	0.93	0.47	55.66	10.66	4.80	13.22	6.30	6.33	11.80
Ni	2.99	1.77	1.23	2.11	93.28	3.81	2.79	10.43	17.54	15.65	8.77
Cu	17.62	39.02	12.00	1.34	62.79	-	23.53	14.67	4.71	29.03	48.78

TABLE 4.3. The co-efficients of variation (C.V.) calculated for the LTZ-type basalts in which two or more samples were collected form within a single flow unit.

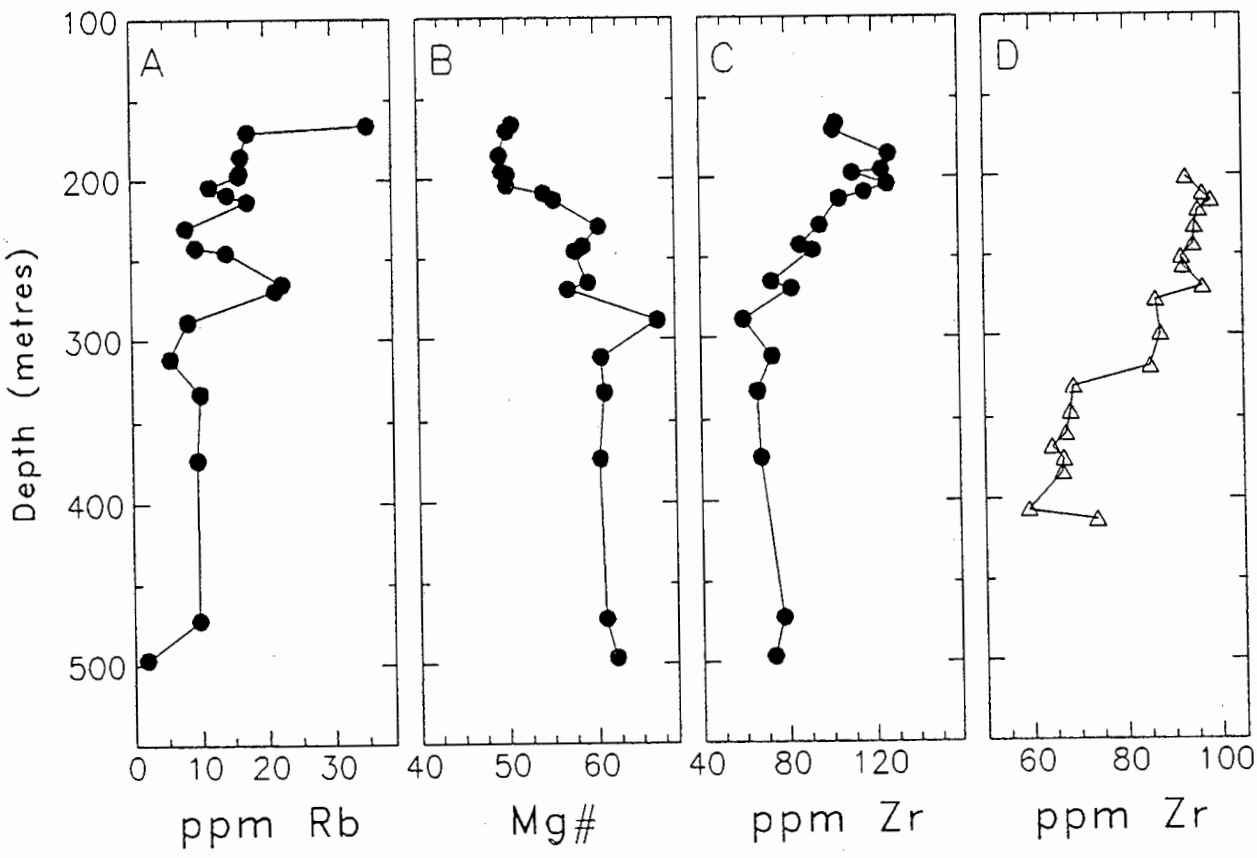

Fig. 4.3. (A)- (C) Rb, Mg# and Zr *vs.* depth for the data from the borehole P11 and (D) Zr *vs.* depth for the data from the borehole P8.

4.1.2 LTZ DOLERITES

The LTZ dolerites can be sub-divided, geochemically and petrographically into three distinct groups, *i.e.* the TYPE I LTZ dolerites, the TYPE II LTZ dolerites and the high-MgO LTZ picrites.

4.1.2.1 TYPE II LTZ dolerites

The TYPE II LTZ dolerites are characterised by their metamorphic petrography, which resembles that of the Proterozoic dolerites of Botswana and Zimbabwe (see section 3.1.1.1.3) and in section 2.3.2.2 it was shown that the whole rock compositions of the TYPE II LTZ dolerites can be differentiated statistically, using discriminant function analysis, from the LTZ-type basalts of Botswana (see also Fig. 2.13; 2.14 & 2.15).

The whole rock data for the TYPE II LTZ dolerites is tabulated in APPENDIX D and the mean, minimum, maximum and S.D. of the major and trace element concentrations of the TYPE II LTZ dolerites are listed in TABLE 4.4. As the TYPE II LTZ dolerites of Botswana are characterised by distinct whole rock compositions and are petrographically similar to the Proterozoic dolerites, it would be worthwhile to compare the compositions of the TYPE II LTZ dolerites to the Proterozoic dolerites of Botswana and Zimbabwe. Unfortunately no XRF whole rock data is available in the literature for these Proterozoic dolerites, but some major element compositions of various Proterozoic dolerites and basalts from Zimbabwe are summarised in TABLE 4.5. The major and trace element concentrations of the TYPE II LTZ dolerites are plotted *vs.* MgO in Fig 4.4A & B. The major element compositions of the Proterozoic dolerites and basalts which have all Fe as Fe_2O_3* and are normalised to 100% on a volatile-free basis are included in Fig. 4.4A together with the compositions of the TYPE I LTZ dolerites and the compositional fields defined by the major element concentrations of the LTZ basalts (see Fig. 4.1A & B).

The TYPE II LTZ dolerites are characterised by their considerable scatter in major element concentrations and show considerable variations in the within-dyke major element geochemistry with, for example, MgO showing a considerable range in concentrations from the centre to the margin of individual dykes (*i.e.* from 7.16 wt% (KLB-051) to 5.93 wt% (KLB-052) and from 7.64 wt% (KLB-103) to 4.70 wt% (KLB-104) respectively) although the MgO concentrations are relatively unchanged from the core (KLB-110) to the margin (KLB-109) of a third TYPE II LTZ dolerite dyke (7.68 to 7.60 wt% MgO respectively). The decrease in the MgO concentration from the centre to the margin of the individual TYPE II LTZ dolerite dykes is associated with variable increases in SiO_2 and K_2O concentrations and a decrease in the CaO concentrations in the dyke margins although Fe_2O_3*, TiO_2, Al_2O_3,

	TYPE II LTZ DOLERITE				
	MEAN	MIN.	MAX.	S.D.	N
SiO_2	52.50	49.15	56.05	1.78	18
TiO_2	1.04	.53	1.79	.30	18
Al_2O_3	14.90	13.81	16.69	.77	18
Fe_2O_3	11.57	9.08	14.95	1.42	18
MnO	.17	.13	.22	.02	18
MgO	6.47	4.70	7.88	.91	18
CaO	10.14	8.48	11.98	.91	18
Na_2O	2.22	1.79	2.79	.30	18
K_2O	.87	.43	1.70	.40	18
P_2O_5	.12	.06	.22	.04	18
Rb	38	15	77	20	18
Ba	225	108	402	78	18
Sr	216	125	342	79	18
Th	4.8	2.3	8.9	2.1	12
U	1.7	1.7	2.0	.1	9
Zr	98	63	151	25	18
Nb	5.1	2.0	8.3	1.5	18
Cr	132	40	281	81	18
V	227	172	347	43	18
Sc	30	21	37	4.2	18
Ni	104	44	221	51	18
Co	54	45	69	4.9	18
Pb	5.8	2.7	11	2.5	15
Zn	89	56	118	15	18
Cu	90	51	221	41	18
Y	21	15	36	6.1	18
La	14	8.8	21	3.9	17
Ce	30	19	43	7.4	17
Nd	15	10	22	3.3	17

TABLE 4.4. Average whole rock compositions of the TYPE II LTZ dolerites.

Na_2O and P_2O_5 exhibit little variation in concentration. The within-dyke major element variation of the TYPE II LTZ dolerites therefore can not be explained by normal tholeiitic fractionation processes.

The major element composition of the TYPE II LTZ dolerites is similar to that of both the LTZ-type basalts (and dolerites) and the Proterozoic dolerites and basalts of Zimbabwe, although the TYPE II dolerites are somewhat depleted in P_2O_5 with respect to the LTZ basalts and show a greater range in K_2O and P_2O_5 concentrations. The whole rock compositions of the Proterozoic basalts and dolerites resemble the TYPE II dolerite compositions in that they also show a considerable range and scatter in major element concentration and show no Fe_2O_3* or TiO_2 correlations with MgO. The TYPE II LTZ dolerites are generally lower in P_2O_5 compared to the Proterozoic dolerites and basalts at similar MgO concentrations, although the P_2O_5 concentrations of the two Deweras dolerites are similar to those of the TYPE II LTZ dolerites. The scatter in the major element concentrations exhibited by the Proterozoic dolerites and basalts may be affected by

	DEWERAS DOLERITES			PLUMTREE	UMKONDO		MASHONALAND DOLERITES				DEWERAS BASALTS					
	69-89	G543	GODZI				HARARE		EASTERN HIGHLANDS		1	2	3	4	5	6
					MEAN N = 16	S.D.	MEAN N = 3	S.D.	MEAN N = 7	S.D.						
SiO_2	50.86	52.05	50.72	51.55	53.0	.78	49.72	1.81	50.44	1.13	46.27	49.00	50.30	49.94	49.19	48.72
TiO_2	1.87	1.47	0.85	1.63	0.77	.22	1.39	.95	2.13	.63	1.56	1.40	1.07	1.28	1.11	1.44
Al_2O_3	14.20	12.89	16.11	13.74	15.31	1.64	16.50	4.78	15.31	2.31	15.25	14.31	14.75	15.01	14.07	15.55
Fe_2O_3	2.42	1.77	1.25	3.08	1.33	.54	1.22	.41	3.15	.86	1.72	3.46	3.21	2.79	3.55	2.23
FeO	11.21	12.48	7.67	9.98	8.25	1.22	10.96	2.93	9.56	1.43	10.98	9.68	8.55	8.84	8.67	9.40
MnO	.21	.21	.16	.20	.17	.03	.13	.02	.23	.08	.17	.19	.21	.08	.19	.17
MgO	5.54	4.81	8.58	4.98	6.39	1.53	5.1	4.29	4.18	.81	7.50	6.24	5.73	5.79	7.35	6.84
CaO	9.00	8.83	11.10	8.95	10.22	.69	9.73	3.53	9.06	.91	9.38	9.09	10.19	10.10	9.10	8.94
Na_2O	2.45	2.65	1.98	2.85	2.06	.35	3.08	1.30	2.48	.3	2.82	2.89	2.95	2.52	3.08	2.96
K_2O	1.00	.80	.50	.54	1.11	.27	.71	.36	1.16	.24	.51	.74	.70	.54	.63	.17
P_2O_5	.25	.14	.09	.22	.15	.18	.16	.1	.26	.19	.16	.20		.25	.12	.18
H_2O+	1.07	1.40	.93	2.08	1.18	.75	.77	.56	1.25	.68	3.94	3.12	.2	2.34	3.09	3.33
H_2O-	.15	.28	.20								.03	.03	.19	.14	.12	.22
REF:	2	2	2	3	3		3		3		1	1	1	1	1	1

REFERENCES:

1: Bliss, N.W. (1971).

2: Tennick, F.P. and Phaup, A.E. (1976).

3: Wilson, J.F., Jones, D.L. and Kramers, J.D. (1987).

TABLE 4.5. Major element concentrations of various Proterozoic-aged basalts and dolerites from Zimbabwe.

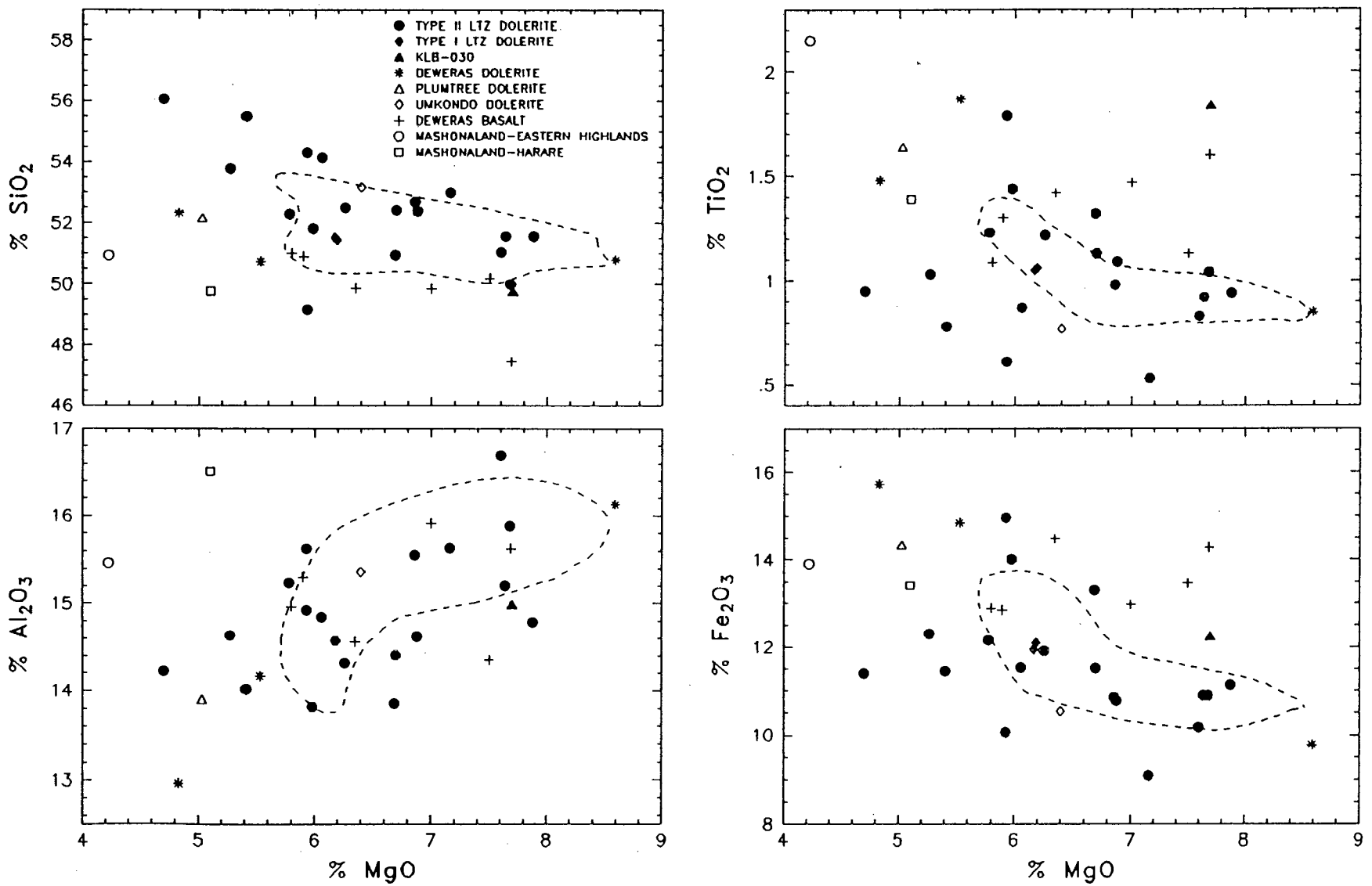

Fig. 4.4A. Major element variation diagrams plotted *vs.* depth for the TYPE II LTZ dolerites, the Proterozoic-aged basalts and dolerites of Zimbabwe (data normalised to 100% volatile-free with all Fe as Fe_2O_3*) together with the fields described by the major element compositions of the LTZ-type basalts.

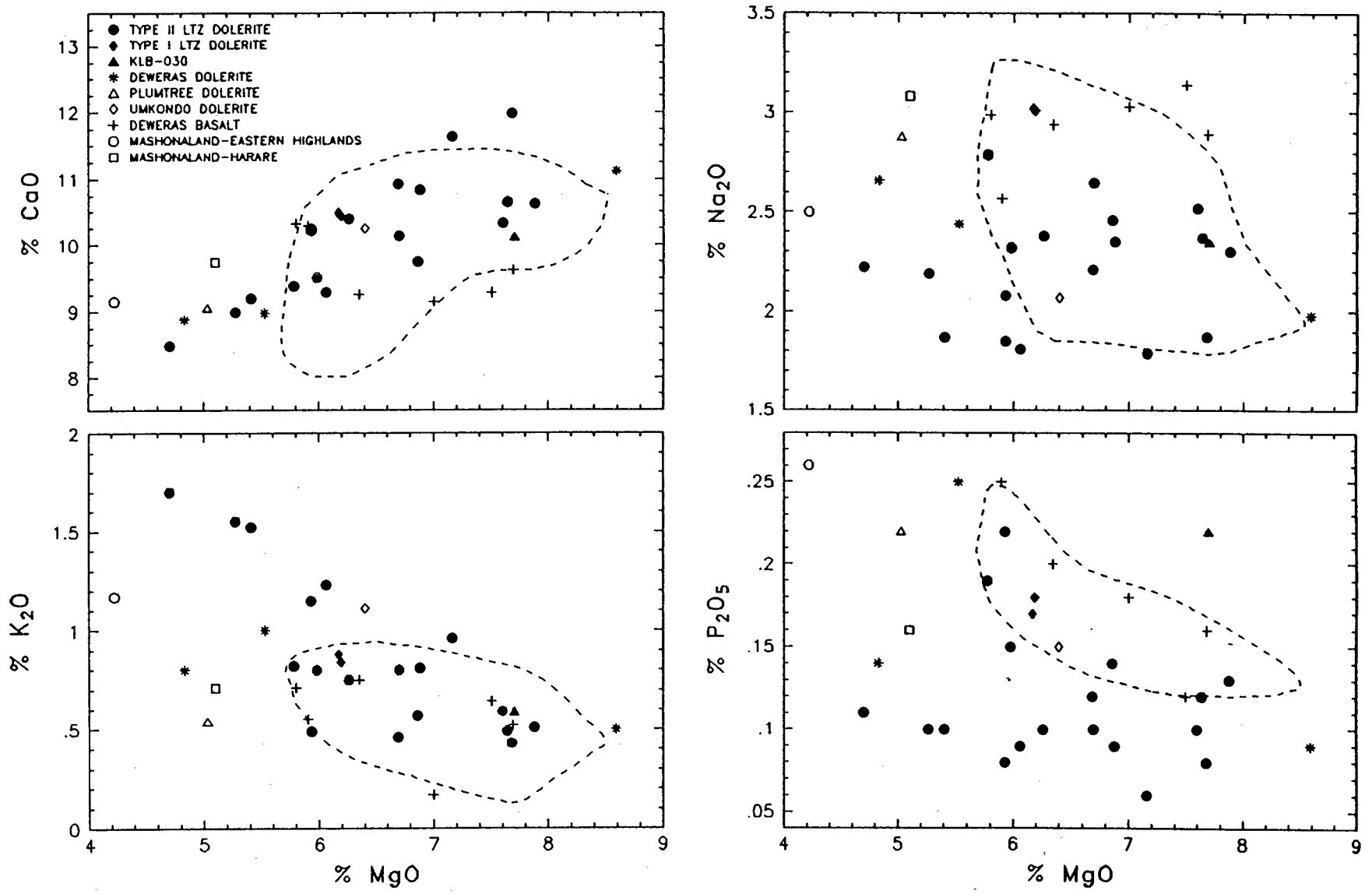

Fig. 4.4A (continued).

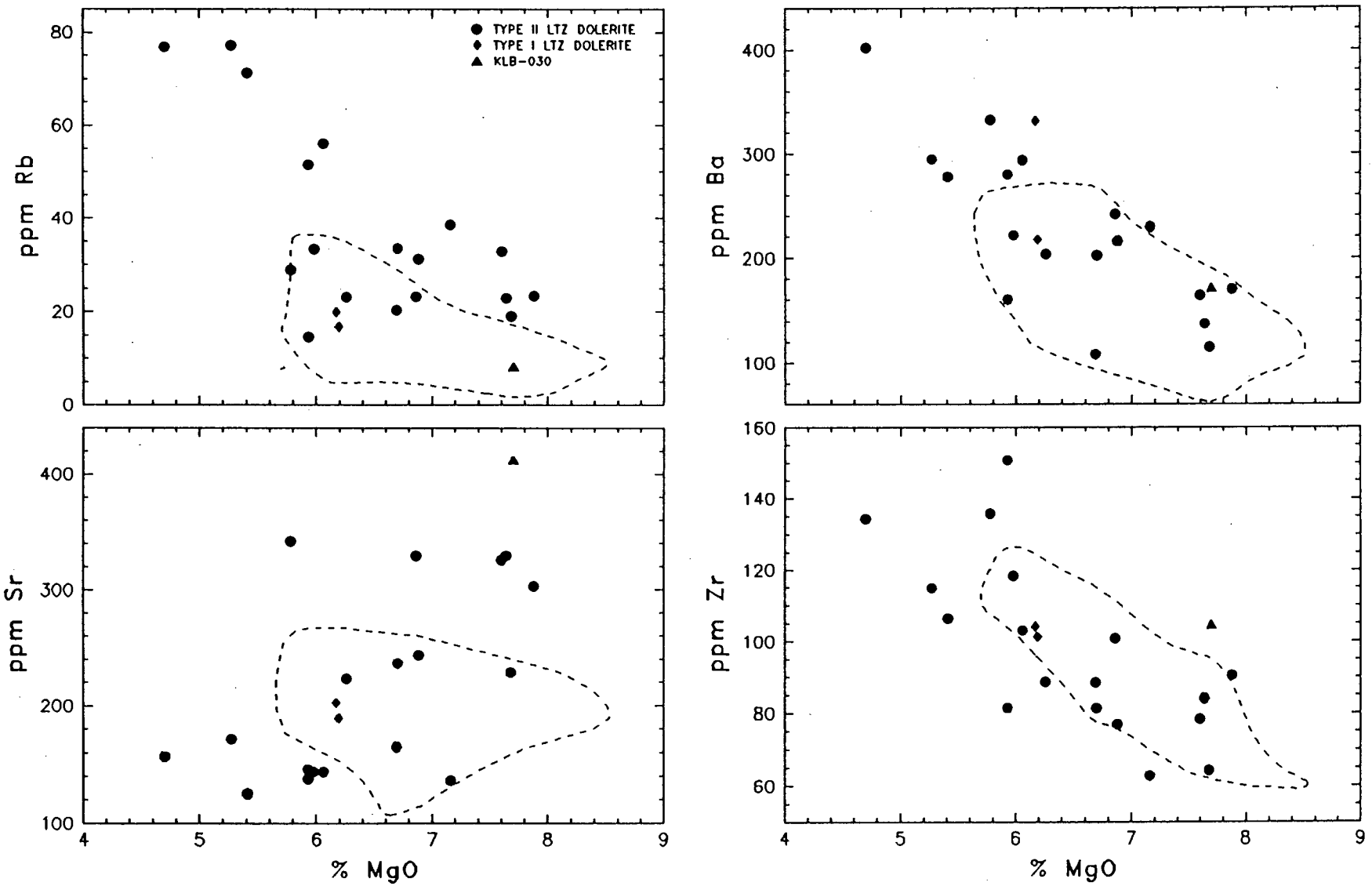

Fig. 4.4B. Trace element variation diagrams plotted *vs.* MgO for the TYPE II LTZ dolerites together with the fields described by the trace element compositions of the LTZ-type basalts.

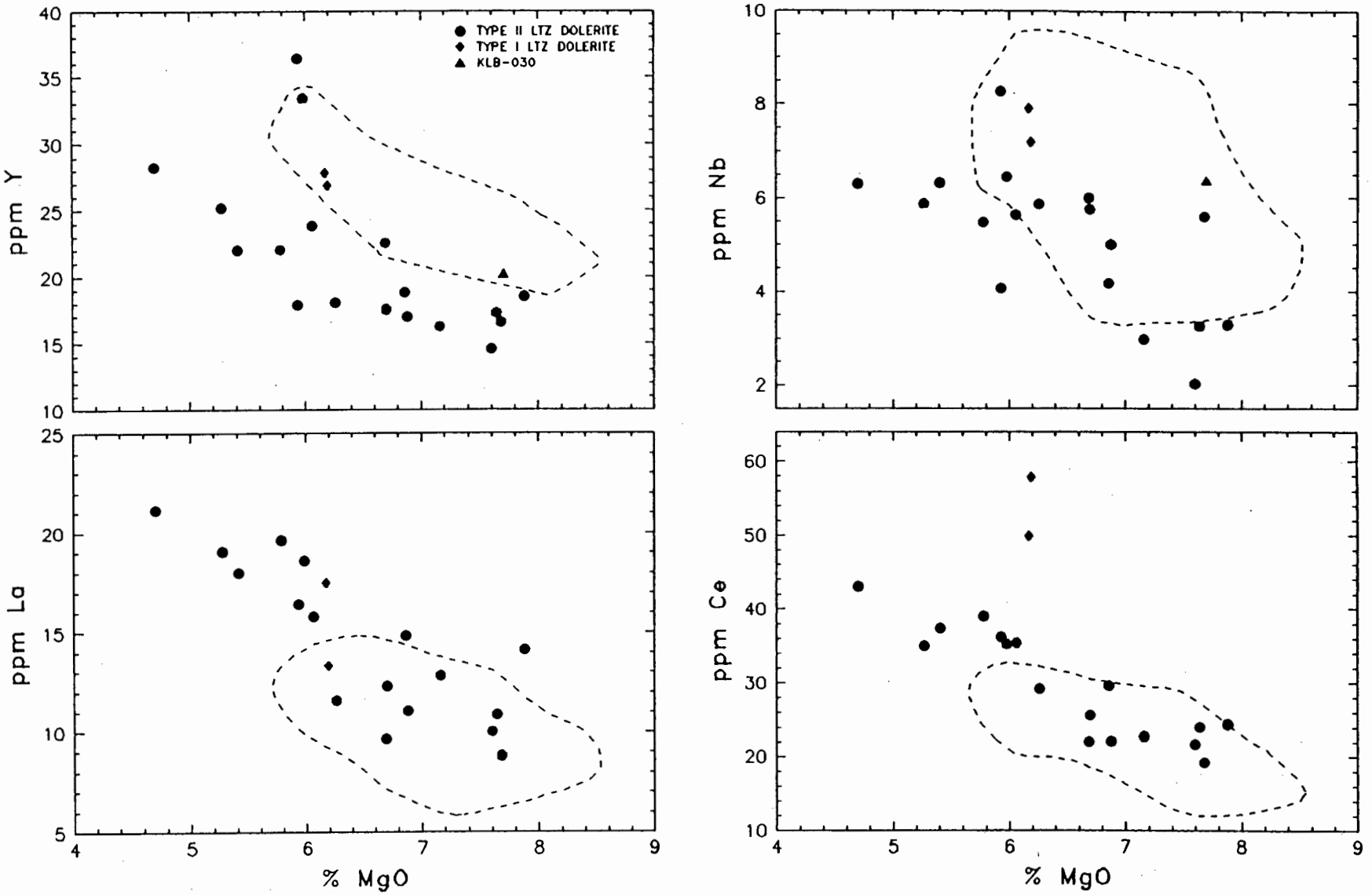

Fig. 4.4B (continued).

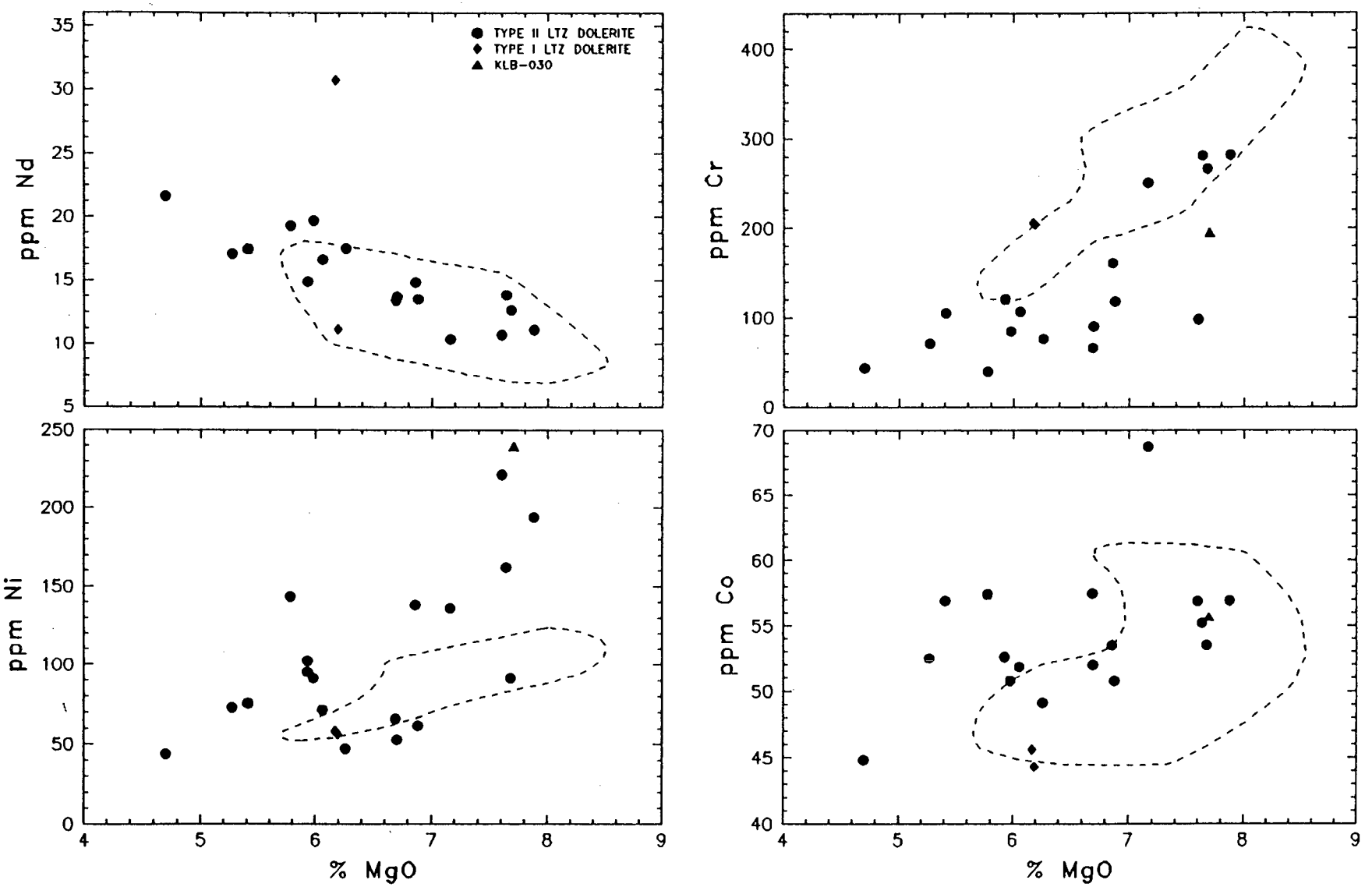

Fig. 4.4B (continued).

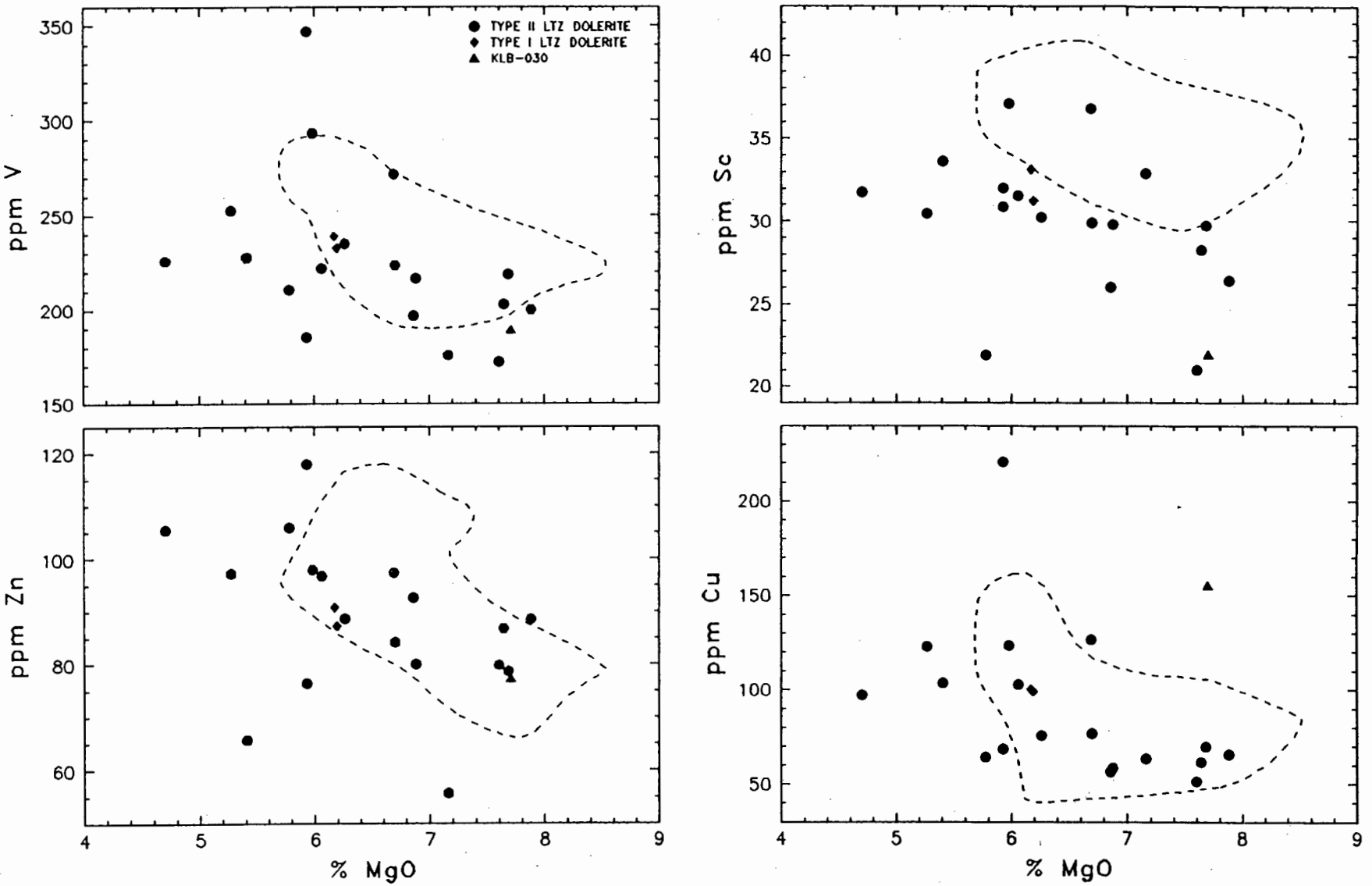

Fig. 4.4B (continued).

inter-laboratory errors and by the different analytical techniques used to obtain the major element concentrations of the Proterozoic dolerites and basalts.

Although the TiO_2/P_2O_5 ratio of the TYPE II LTZ dolerites is variable (5.13 to 10.57), the average value of 9.17 is higher than that of the LTZ basalts (average of 6.27) and similarly the TiO_2/P_2O_5 ratio of the majority of the Proterozoic basalts and dolerites of Zimbabwe are also greater than those of the LTZ basalts (see Fig. 4.5). This suggests that the TYPE II LTZ dolerites and the Proterozoic basalts and dolerites may have similar geochemical signatures although more detailed geochemical studies are required as no trace element data are available for the Proterozoic dolerites and basalts to either support or disprove the observed correlations in the major element geochemistry. The similarities in the major element chemistry as well as the petrographic resemblance between the TYPE II LTZ dolerites and the Proterozoic dolerites and basalts of Botswana and Zimbabwe support the suggestion that the TYPE II LTZ dolerites are not Karoo aged but belong rather to the Proterozoic suite of dolerites and basalts of Botswana and Zimbabwe.

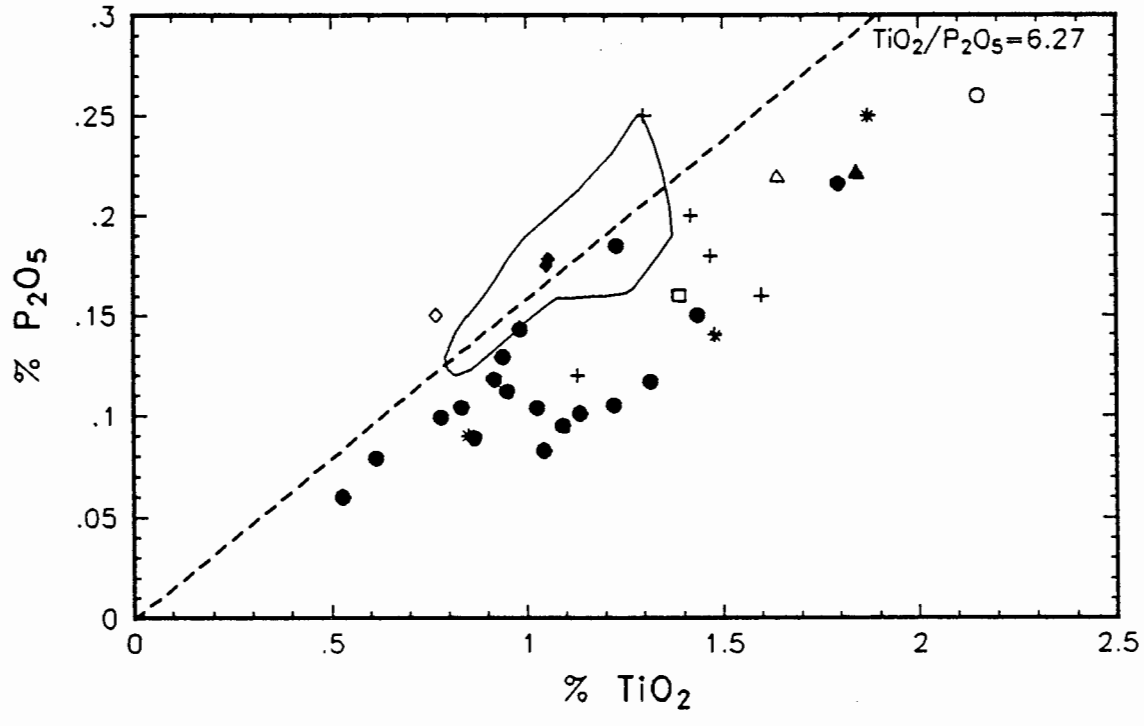

Fig. 4.5. TiO_2 *vs.* P_2O_5. A possible means of discrimination between the TYPE II LTZ dolerites, the Proterozoic basalts and dolerites and the LTZ basalt type. The LTZ basalt type, with a mean TiO_2/P_2O_5 ratio of 6.27, is indicated by the outlined field. Symbols as for Fig. 4.4A & B.

The differences observed in the major element geochemistry of the TYPE II LTZ dolerites and the LTZ basalts (for example the higher TiO_2/P_2O_5 ratios of the TYPE II LTZ dolerites in Fig. 4.5) are reflected in the trace element geochemistry of the TYPE II LTZ dolerites, although subtle differences between some of the trace element concentrations may be

obscured by the scatter in the data of the MgO variation diagrams in Fig. 4.4B. The TYPE II LTZ dolerites are, on average, enriched in Rb, Ni and Co and depleted in Cr, Y, Sc and V with respect to the LTZ basalts of similar MgO concentrations and the TYPE II LTZ dolerites are characterised by a greater range (and scatter) of trace element concentrations (see Fig. 4.4B). The pre-definition of the TYPE II LTZ dolerites according to their distinctive metamorphic petrography is therefore supported by their whole rock geochemistry (both major and trace elements) and the TYPE II LTZ dolerites and the LTZ basalt can be differentiated by a number of inter-element ratios (*e.g.* TiO_2 *vs.* P_2O_5 (Fig. 4.5), K_2O *vs.* Rb (Fig. 2.14 and Zr *vs.* Y (Fig. 2.15)). Although the large-ion-lithophile elements (K_2O, Rb and Ba) may be redistributed during low grades of metamorphism, the elements TiO_2, Y, Zr, Sc and the REE are generally accepted to be immobile during low grades of metamorphism (BVSP, 1981) and as the TYPE II LTZ dolerites are heterogeneously enriched and depleted in both compatible and incompatible element concentrations with respect to the LTZ basalts (see, for example, the different Zr/Y ratios in Fig. 2.15) it is unlikely that the TYPE II LTZ dolerites are related to the LTZ basalts by any igneous processes.

Although KLB-030 has a whole rock composition which is similar to the TYPE II LTZ dolerites for many of the trace and major element concentrations (see Fig. 4.4A & B) it is enriched in TiO_2, P_2O_5, Zr, Sr and Cu and depleted in Rb and Sc with respect to the TYPE II LTZ dolerites and in Fig. 2.14 KLB-030 has a distinctly higher K/Rb ratio (595.7) than the TYPE II LTZ dolerites (K/Rb ranges from 149.5 to 279.3).

4.1.2.2 High-MgO LTZ picrites

Although Karoo cumulus-textured dolerites with MgO concentrations ranging from ±9 to <40% MgO have been recognised in the Central Karoo area (*e.g.* Eales and Marsh, 1979) the distinct cumulate petrography of the High-MgO LTZ picrites, which include a high modal proportion of biotite (see section 3.1.1.1.3), suggests that the high-MgO LTZ picrites belong rather to the Archaean suite of Norites and Olivine Norites described (*e.g.* Aldiss, 1983a & b) from the adjacent basement complex (see section 1.2.2.1) and are therefore not Karoo aged. The whole rock compositions of these high-MgO LTZ picrites are listed in TABLE 4.6 and unfortunately, as no whole rock compositions of the Norites and Olivine Norites were available in the literature for comparison, the more detailed geochemical studies which are required to determine the relationship between the high-MgO LTZ picrites and the Norites and Olivine Norites are beyond the scope of this study.

	KLB-072	KLB-077	KLB-078
SiO_2	48.94	50.90	50.71
TiO_2	.45	.34	.61
Al_2O_3	8.36	13.58	11.86
Fe_2O_3	11.93	8.95	11.31
MnO	.17	.14	.17
MgO	21.83	14.01	13.98
CaO	6.41	9.92	8.89
Na_2O	1.43	1.81	1.90
K_2O	.43	.31	.49
P_2O_5	.05	.04	.08
Rb	12	8.3	15
Ba	192	177	204
Sr	111	186	168
Th	2.6		2.4
U	1.6	1.5	1.6
Zr	51	27	58
Nb	2.4	1.5	2.5
Cr	3279	1683	1582
V	145	149	182
Sc	23	27	31
Ni	1099	466	479
Co	101	65	71
Pb	3.1		3.4
Zn	77	55	77
Cu	53	32	82
Y	11	7.6	14
La	11	4.5	11
Ce	16	6.0	15
Nd	5.8	4.0	7.7

TABLE 4.6. The whole rock compositions of the high-MgO LTZ picrites.

4.1.3 HTZ-TYPE BASALTS AND DOLERITES

In section 2.3.1.2 the HTLZ and HTZ sub-groups were defined according to the TiO_2 and Zr classification scheme (see Fig. 2.5A) although the whole rock data of the two sub-groups showed no natural division in either the TiO_2 or Zr concentrations and in sections 2.3.2.3 it was shown that the basalts and dolerites of the HTLZ- and HTZ-type subgroups have comparable whole rock compositions. The HTZ-type basalts can, however, be subdivided into the HTZ (low Fe)- and the HTLZ/HTZ- basalt and dolerite sub-groups (see section 2.3.2.3 and Fig. 2.17). TABLE 4.7 summarises the average major and trace element concentrations of the HTLZ/HTZ- and HTZ (low Fe)- basalt and dolerite sub-groups and the sample KLB-030, which has a possible HTLZ-type signature is included in TABLE 4.7. The major and trace element concentrations of the HTZ-type basalt and dolerite sub-groups, together with sample KLB-030, are plotted *vs.* MgO in Fig. 4.6A & B where the basalts and dolerites are differentiated by open and closed symbols, respectively. The fields defined by the LTZ basalts (where the obvious outliers are excluded (see Fig. 4.1A & B)) are also included in Fig. 4.6A & B to aid comparison between these two major geochemical sub-groups of the low-K_2O lineage.

	HTLZ BASALT					HTLZ DOLERITE					HTZ BASALT				
	MEAN	MIN.	MAX.	S.D.	N	MEAN	MIN.	MAX.	S.D.	N	MEAN	MIN.	MAX.	S.D.	N
SiO_2	50.79	50.46	51.32	.38	4	50.36	49.03	51.06	.58	14	51.43	49.80	54.60	1.62	7
TiO_2	2.64	2.19	2.89	.31	4	2.49	2.03	2.94	.25	14	3.40	2.96	4.30	.48	7
Al_2O_3	13.65	13.43	13.97	.25	4	13.91	13.42	14.31	.27	14	13.08	12.73	13.68	.33	7
Fe_2O_3	14.80	14.25	15.46	.53	4	13.61	12.38	14.49	.64	14	15.04	14.32	15.64	.44	7
MnO	.21	.19	.24	.02	4	.18	.16	.20	.01	14	.18	.17	.20	.01	7
MgO	4.90	4.47	5.33	.40	4	5.90	4.43	6.69	.62	14	3.98	2.74	4.57	.64	7
CaO	9.19	8.87	9.59	.30	4	9.92	8.30	10.60	.56	14	8.18	7.11	8.89	.61	7
Na_2O	2.49	2.38	2.60	.09	4	2.59	2.13	2.91	.22	14	2.74	2.34	3.27	.29	7
K_2O	1.03	.89	1.21	.14	4	.76	.35	1.55	.29	14	1.36	.66	1.70	.40	7
P_2O_5	.31	.24	.34	.05	4	.29	.24	.33	.03	14	.62	.39	1.03	.25	7
Rb	26	16	36	9.7	4	17	9.9	33	5.6	14	29	16	39	7.9	7
Ba	295	255	329	31	4	253	171	425	63	14	612	371	1004	259	7
Sr	381	273	446	75	4	376	340	429	26	14	608	402	876	189	7
Th	3.2	2.5	3.8	.7	3	2.7	2.4	3.0	.2	6	4.5	3.6	6.6	1.2	5
U	2.0				1	2.0	1.7	2.7	.5	4	2.6	1.8	4.1	1.0	5
Zr	208	158	228	33	4	191	167	221	16	14	418	264	701	159	7
Nb	12	8.2	14	2.4	4	12	10	14	1.1	14	25	15	35	9.0	7
Cr	95	88	113	12	4	123	54	170	37	14	51	7.3	130	41	7
V	355	335	366	14	4	345	279	397	29	14	287	147	373	75	7
Sc	34	31	39	3.5	4	32	29	36	1.9	14	27	19	34	4.8	6
Ni	79	67	96	12	4	91	58	123	18	14	62	20	94	25	7
Co	50	47	56	4.1	4	46	41	53	2.9	14	51	41	82	14	7
Ga											29.8				1
Pb	5.7	4.5	7.0	1.7	2	3.6	2.8	5.1	.7	11	8.6	5.1	16	3.8	6
Zn	116	112	117	2.6	4	103	88	114	8.0	14	136	121	154	13	7
Cu	161	127	221	41	4	206	147	247	27	14	218	174	274	37	7
Y	38	36	40	1.9	4	35	27	40	3.1	14	53	39	63	9.3	7
La	21	17	24	3.8	3	23	21	24	2.3	2	39	25	58	13	6
Ce	49	37	58	10	3	55	51	58	4.7	2	94	65	145	30	6
Nd	32	24	37	6.5	3	33	28	37	6.5	2	61	43	92	19	6

TABLE 4.7. Average whole rock compositions of the HTLZ-, HTZ- and HTZ (low-Fe)- basalts and dolerites.

	HTZ DOLERITE					HTZ (LOW FE) BASALT					HTZ (LOW FE) DOLERITE					KLB-030
	MEAN	MIN.	MAX.	S.D.	N	MEAN	MIN.	MAX.	S.D.	N	MEAN	MIN.	MAX.	S.D.	N	
SiO_2	50.73	50.01	51.56	.45	10	52.11	50.68	53.76	1.28	7	51.91	50.06	53.25	1.06	8	49.77
TiO_2	3.38	3.22	3.65	.15	10	3.62	2.90	4.28	.51	7	4.02	3.51	4.37	.33	8	1.84
Al_2O_3	13.07	12.29	14.24	.51	10	14.08	13.16	16.58	1.14	7	13.73	13.19	15.01	.57	8	14.99
Fe_2O_3	15.11	14.23	15.97	.57	10	12.72	11.89	13.54	.62	7	12.86	12.43	13.35	.36	8	12.24
MnO	.19	.17	.21	.01	10	.15	.14	.17	.01	7	.15	.13	.16	.01	8	.17
MgO	4.47	3.19	5.49	.72	10	3.98	3.22	4.39	.42	7	4.30	3.79	4.80	.39	8	7.70
CaO	8.66	7.89	9.63	.54	10	7.59	6.91	8.94	.64	7	8.02	7.45	9.53	.67	8	10.13
Na_2O	2.63	2.20	3.01	.23	10	2.88	2.58	3.33	.28	7	2.48	1.98	2.84	.27	8	2.35
K_2O	1.22	.75	1.93	.34	10	2.15	1.49	2.83	.41	7	1.85	1.09	2.39	.36	8	.59
P_2O_5	.54	.38	1.11	.22	10	.71	.44	.87	.15	7	.68	.51	.84	.12	8	.22
Rb	24	17	40	7	10	38	24	57	12	7	38	20	54	11	8	8.2
Ba	476	336	845	160	10	834	442	1027	207	7	760	430	1048	197	8	172
Sr	565	368	923	161	10	946	759	1110	114	7	913	575	1218	217	8	413
Th	4.3	3.0	6.1	1.0	8	5.4	3.7	7.3	1.3	7	5.2	2.3	6.9	1.6	8	
U	1.8	1.8	1.9	.0	.0	2.3	1.7	3.3	.6	6	1.8	1.8	2.1	.1	8	
Zr	362	249	761	152	10	479	320	606	92	7	461	327	538	65	8	105
Nb	20	11	36	7.2	10	31	28	36	3.1	7	29	25	36	4.5	8	6.4
Cr	48	6.3	100	25	10	59	24	148	45	7	55	33	89	20	8	195
V	312	200	415	56	10	232	194	256	23	7	252	202	285	31	8	189
Sc	28	24	33	3.5	8	19	17	22	1.9	7	21	18	25	2.0	8	22
Ni	61	23	99	22	10	57	31	92	19	7	71	45	93	18	8	240
Co	44	36	54	5.3	10	39	34	45	3.5	7	41	35	45	3.8	8	56
Ga	22.7				1											
Pb	5.2	3.0	7.2	1.5	8	9.7	3.7	12	2.9	7	7.9	5.6	9.8	1.5	7	
Zn	129	110	172	19	10	125	102	142	13	7	131	101	147	13	8	77
Cu	217	148	304	56	10	121	52	212	56	7	138	103	227	38	8	156
Y	48	35	69	9.3	10	49	38	57	6.6	7	46	40	50	3.0	8	20
La	33	24	39	6.2	6	58	37	68	12	7	53	33	70	13	8	
Ce	82	67	97	15	6	135	82	168	30	7	128	82	165	28	8	
Nd	53	44	63	8.1	6	83	52	102	17	7	78	52	98	15	8	

TABLE 4.7 (continued).

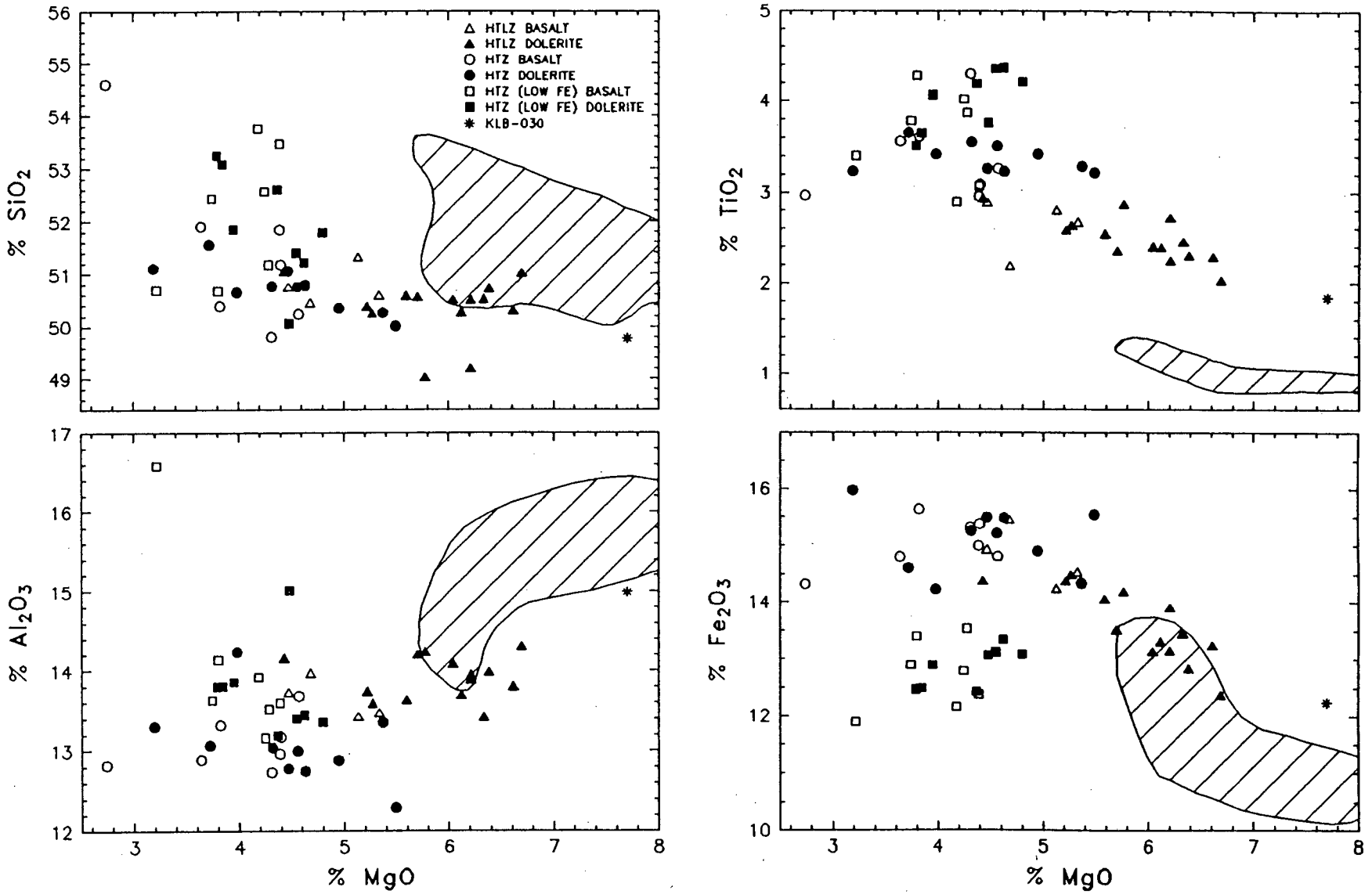

Fig. 4.6A. Major element variation diagrams plotted *vs.* MgO for the HTLZ-, HTZ- and HTZ (low Fe)- basalts and dolerites (data normalised to 100% volatile-free with all Fe as Fe_2O_3*). The shaded field indicates the data values for the LTZ basalts.

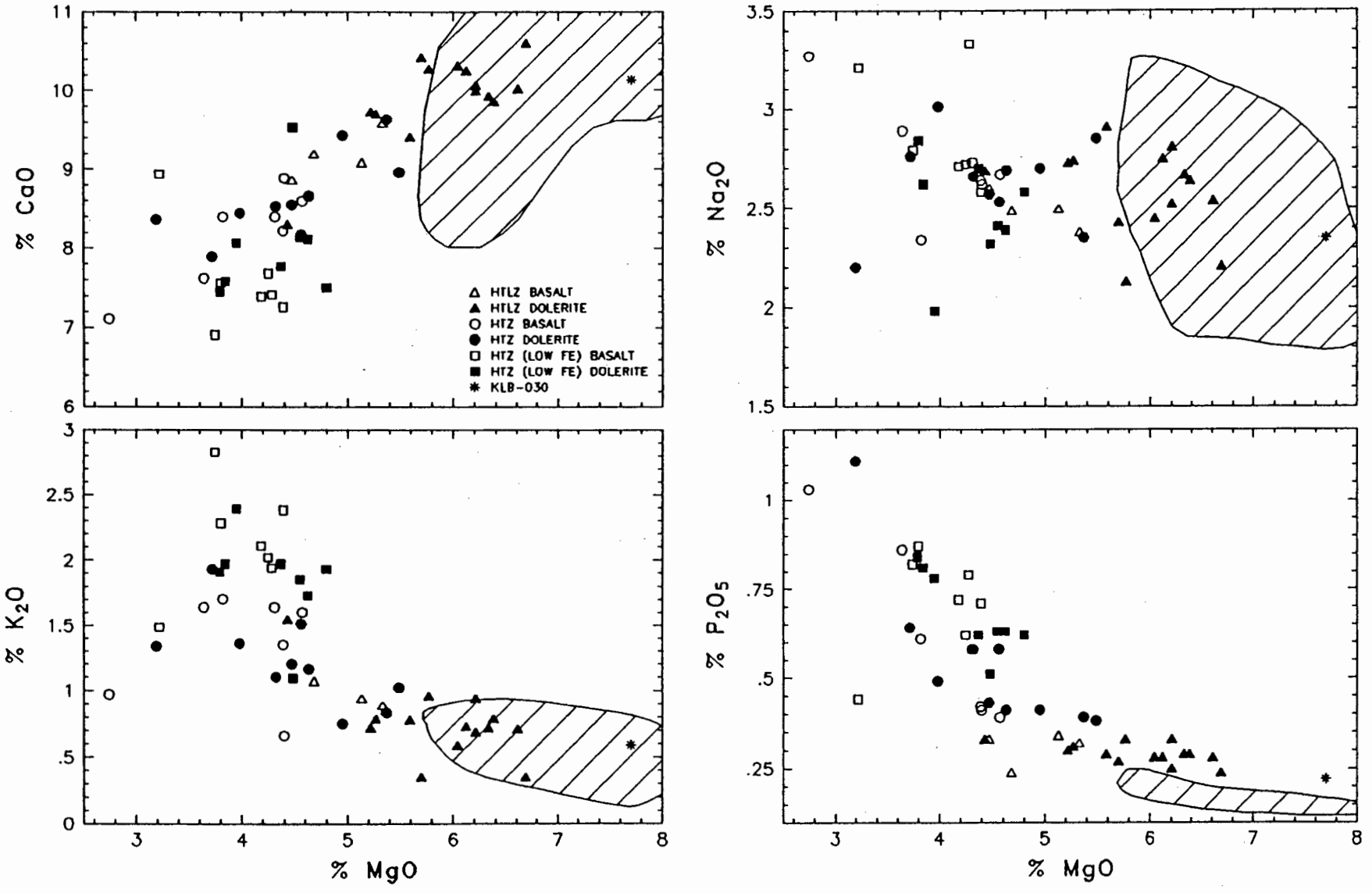

Fig. 4.6A (continued).

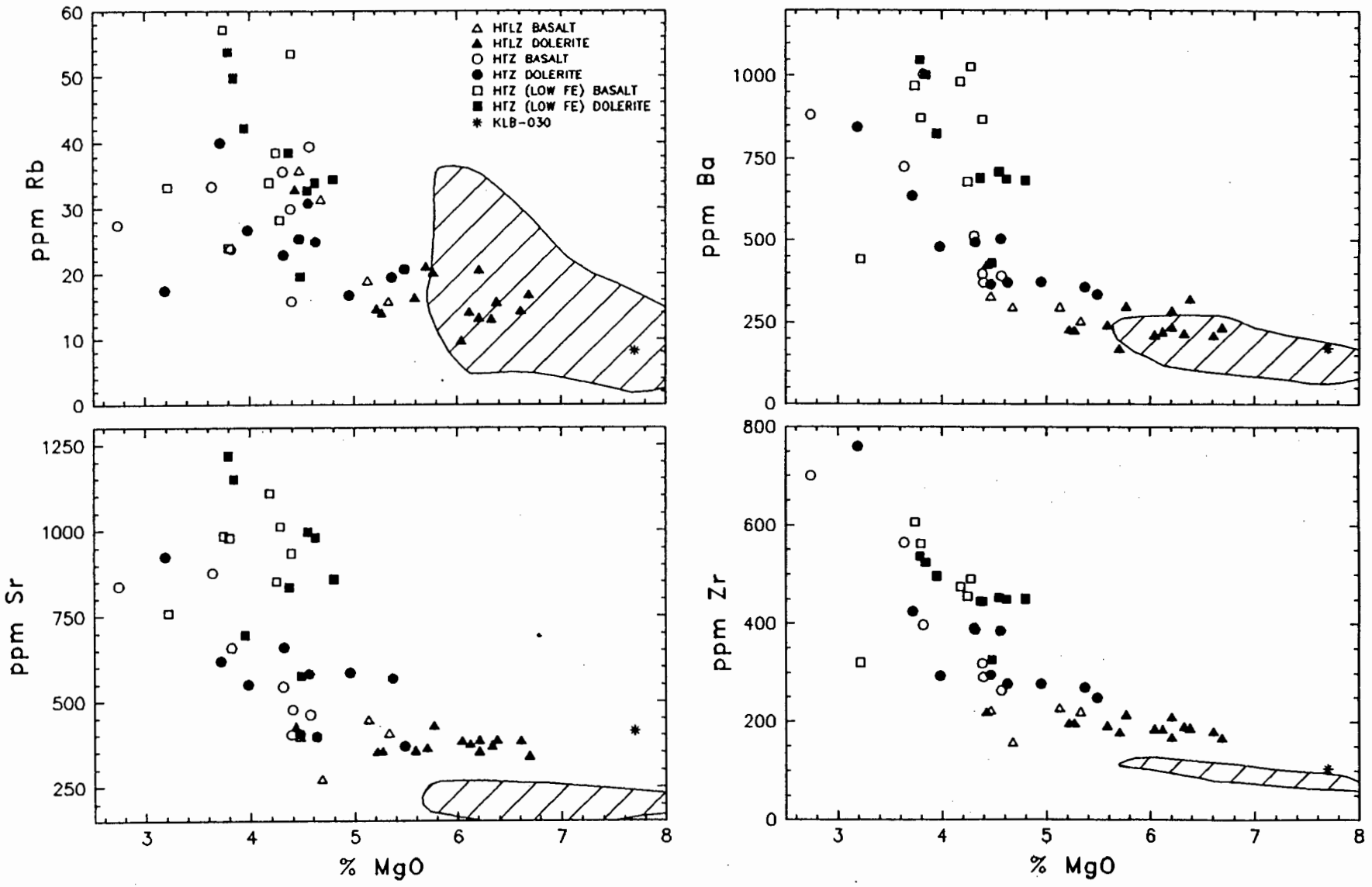

Fig. 4.6B. Trace element variation diagrams plotted *vs.* MgO for the HTLZ-, HTZ- and HTZ (low Fe)- basalts and dolerites (data normalised to 100% volatile-free). The shaded field indicates the data values for the LTZ basalts.

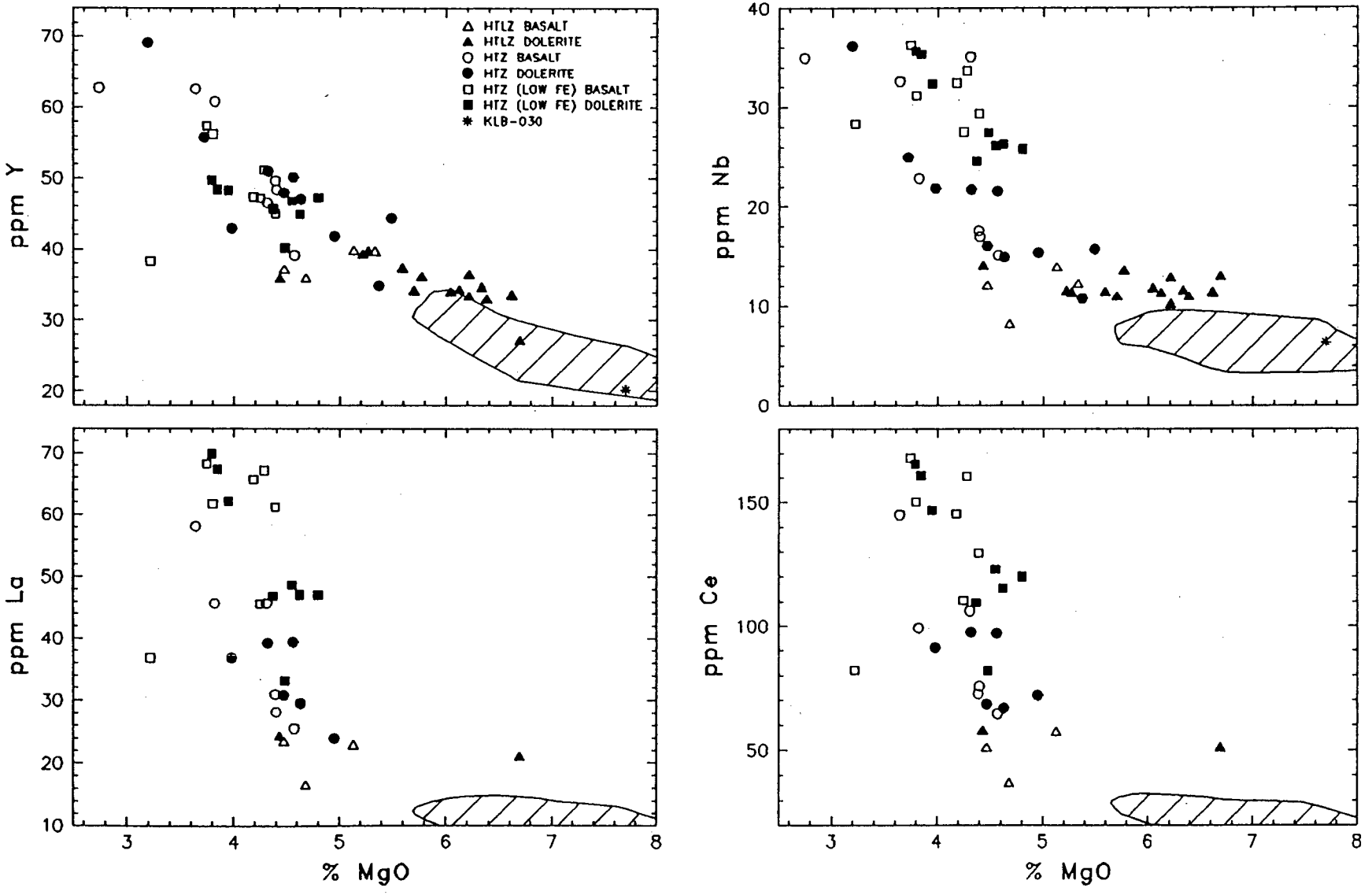

Fig. 4.6B (continued).

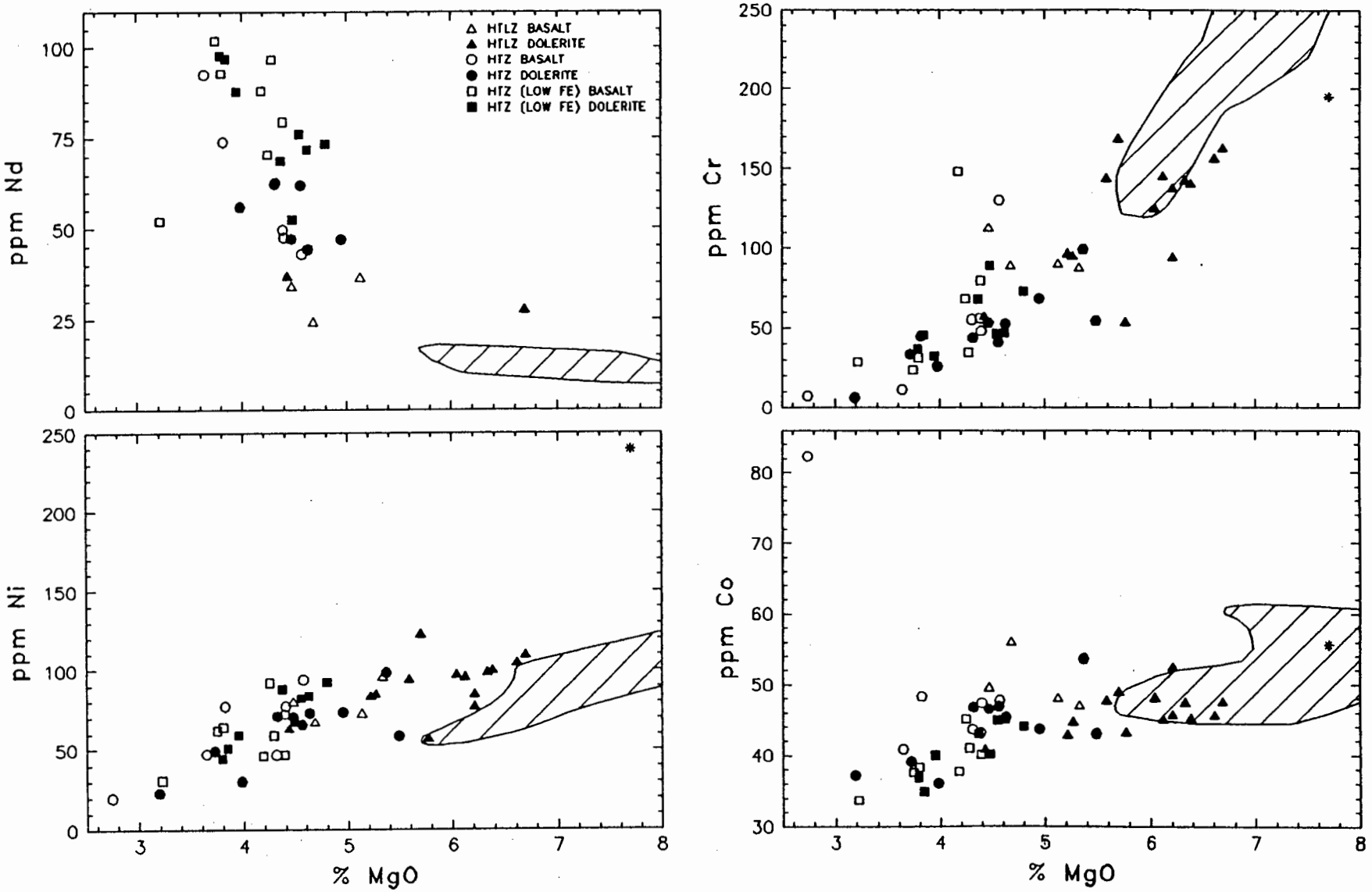

Fig. 4.6B (continued).

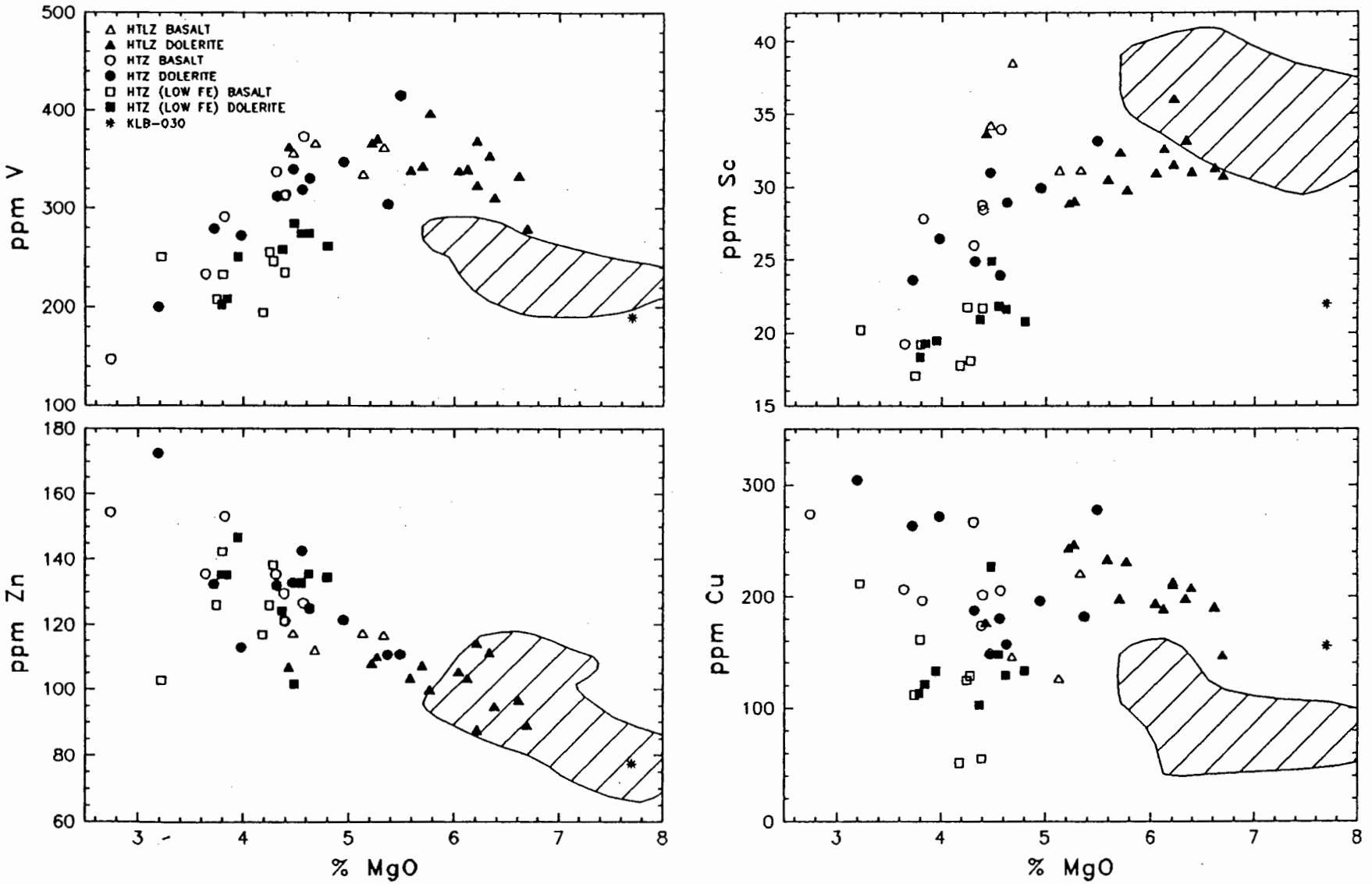

Fig. 4.6B (continued).

4.1.3.1 Major element geochemistry

The HTZ-type basalts and dolerites typically show evolved whole rock geochemistry with 6.69 to 3.19 wt% MgO. Although the HTLZ/HTZ basalts and dolerites (*i.e.* excluding the HTZ (low Fe) basalts and dolerites) define a continuous range in their major element compositions in Fig. 4.6A, the HTLZ basalts and dolerites are less evolved than the HTZ-type samples, with a range in MgO concentrations from 6.69 to 4.43 wt%. The HTLZ basalts and dolerites define a relatively coherent group of samples with a narrow range in their major element compositions (see small S.D. values in TABLE 4.7). In contrast, the HTZ basalts and dolerites are characterised by both the considerable scatter and range in their major element compositions (see Fig. 4.6A). The HTZ basalts and dolerites all have <5.5% MgO and could therefore be classified as evolved basalts according to the Bristow and Cox (1984) classification scheme (see section 2.2). The HTZ-type basalts and dolerites, as a group, define relatively coherent correlation trends *vs.* MgO with the TiO_2, Fe_2O_3*, K_2O and P_2O_5 concentrations showing a marked increase in concentration with decreasing MgO concentrations, the CaO concentrations decreasing with decreasing MgO concentrations and SiO_2, Al_2O_3 and Na_2O show a considerable scatter in concentration and define no clear trends against MgO in Fig. 4.6A, although Al_2O_3 shows a broad decrease in concentration with decreasing MgO concentrations.

The HTZ (low Fe) basalts and dolerites are all evolved with between 4.80 and 3.22 wt% MgO and are depleted in Fe_2O_3* with respect to the evolved HTLZ/HTZ basalts and dolerites where the Fe_2O_3* concentration of these HTZ (low Fe) basalts and dolerites does not define any correlation against MgO (see Fig. 4.6A). Although the major element compositions (apart from the lower Fe_2O_3* concentrations) of the HTZ (low Fe) basalts and dolerites are broadly similar to the remaining HTLZ/HTZ basalts and dolerites the HTZ (low Fe) basalts and dolerites define, on average, parallel but somewhat enriched (TiO_2, K_2O and P_2O_5) and depleted (CaO) trends with respect to the HTLZ/HTZ basalts and dolerites of similar MgO concentrations. Furthermore, although the HTZ (low Fe) basalts and dolerites are characterised by scattered Al_2O_3 concentrations, the Al_2O_3 concentrations of the HTZ (low Fe) basalts and dolerites, in contrast to the HTLZ/HTZ basalts and dolerites, show a broad increase in concentration with decreasing MgO concentrations.

The sample KLB-030, although considerably more mafic than the HTZ-type basalts and dolerites in general, with 7.7 wt% MgO, lies at the mafic end of the trends defined by all of the major elements *vs.* MgO concentrations of the HTZ-type basalts in Fig. 4.6.

4.1.3.2 Trace element geochemistry

The HTLZ basalts and dolerites are characterised by a relatively narrow range in trace element concentrations, whereas the HTZ basalts and dolerites are characterised by both a considerable scatter and range in their trace element concentrations (see Fig. 4.6B). All HTZ-type basalts and dolerites, treated as a single group, define trends of increasing Rb, Ba, Sr, Zr, Nb, Y, LREE, Zn and Cu with decreasing MgO, and decreasing Cr, Ni and Co with decreasing MgO concentrations. The V (and possibly Sc) concentrations of the HTLZ/HTZ basalts and dolerites initially increase in concentration, but below ±5% MgO the V and Sc show a decrease in concentration with decreasing MgO concentrations.

The trace element compositions of the HTZ (low Fe) basalts and dolerites closely resemble the HTLZ/HTZ basalts and dolerites, although the HTZ (low Fe) basalts and dolerites define a roughly parallel, but somewhat enriched trend for Ba, Sr, Zr, Nb and the LREE *vs.* MgO, *i.e.* reflecting the major element behaviour of TiO_2, K_2O and P_2O_5 and the HTZ (low Fe) basalts and dolerites are somewhat depleted in V and Cu with respect to the evolved HTLZ/HTZ basalts and dolerites (*i.e.* reflecting their lower Fe_2O_3* concentrations), and neither V nor Cu define a correlation against MgO.

The trace element composition of KLB-030 lies at the mafic end of the trends defined by the trace element concentrations of the HTLZ/HTZ basalts and dolerites *vs.* MgO in Fig. 4.6B, where the relatively low Sc concentration is in agreement with the suggested change at ±5% MgO in the Sc trend of the HTLZ/HTZ basalts and dolerites (from negative to positive) with decreasing MgO concentrations.

4.1.3.3 Rare earth elements

REE data is presently available for only the HTLZ/HTZ basalts and dolerites, but not for the HTZ (low Fe) basalts and dolerites, and was obtained using ion chromatography at UCT. The REE data is tabulated in TABLE 4.8, together with the range in REE compositions (determined by spark-source mass spectrography) quoted by Sweeney (1988) for the HTZ.HF and HTZ.LF basalt groups of the Central Lebombo. The REE data for the HTLZ/HTZ basalts and dolerites (and LTZ-type basalts) are plotted in Fig. 2.9 and discussed in detail in section 2.3.1.3.2. The chondrite-normalised REE patterns of the HTLZ/HTZ basalts and dolerites (see Fig. 2.9) are all LREE enriched (see La/Yb_N in TABLE 4.8) and show a progressive increase in both the LREE and HREE concentrations and relative LREE enrichment from the HTLZ- to HTZ-type basalts. Both the range in REE concentrations and relative LREE enrichment of the HTLZ/HTZ basalts and dolerites is similar to that of the HTZ.HF basalts of the Central Lebombo (see TABLE 4.8), whereas the HTZ.LF basalts of the Central Lebombo have considerably greater absolute

LREE concentrations and relative LREE enrichment.

	HTLZ				HTZ			HTZ.HF	HTZ.LF
(KLB-)	-028	-041	-042	-037	-014	-040	-056	RANGE	RANGE
La	18.9	20.6	18.0	14.8	23.8	49.7	23.4	28.2 - 54.0	46.0 - 57.0
Ce	40.3	46.4	43.6	39.4	55.7	101.0	59.3	68.4 - 122	110 - 139
Pr	5.77	6.39	6.47	5.73	7.57	13.60	8.90	9.56 - 16.5	13.5 - 18.3
Nd	26.4	29.2	29.25	26.5	34.4	58.7	41.19	44.3 - 72.4	59.2 - 72.0
Sm	6.83	7.53	7.32	6.88	8.65	14.00	9.83	10.6 - 15.9	12.9 - 13.6
Eu	2.26	2.37	2.39	2.28	2.79	4.02	3.09	2.98 - 4.13	3.63 - 3.86
Gd	6.87	7.41	7.34	7.20	8.56	13.10	9.44	10.2 - 13.0	9.5 - 10.1
Tb	1.08	1.14	1.04	1.16	1.26	1.88	1.42	1.6 - 2.21	1.37 - 1.46
Dy	6.22	6.33	6.48	6.65	7.19	10.40	7.94	8.9 - 12.7	7.1 - 7.71
Er	3.17	3.19	3.20	3.32	3.49	4.84	3.73	3.9 - 5.80	2.95 - 3.30
Yb	2.79	2.84	2.77	2.78	2.91	3.80	3.32	3.3 - 4.76	2.09 - 2.73
La/Yb_N	4.86	5.20	4.66	3.82	5.87	9.38	5.05	4.25 - 11.74	12.08 - 21.99

TABLE 4.8. The REE data for the HTLZ/HTZ basalts and dolerites (concentrations in ppm).

4.1.3.4 Within dyke heterogeneities

Only five of the HTZ-type dolerites and none of the HTZ-type basalts had more than a single sample collected from individual dykes (or flows) and therefore it is difficult to assess the effects of either magmatic or post-magmatic processes on the original compositions of the HTLZ/HTZ basalts and dolerites.

In all five of these dolerite dykes the MgO concentration varies by < 0.5 wt% MgO from the centre to the margin of the individual HTZ-type dolerite dykes, where either the centre or the margin may have a slightly more mafic compositions, and in a single example both HTLZ- (KLB-068) and HTZ- (KLB-067) samples were collected from a single dyke. Although the MgO variations from the centre to the margin of the individual HTZ-type dolerites is small, the major and trace element concentrations may show a slightly greater variation (K_2O, Rb, Ba, Cr and Ni in particular) where these variations reflect both the effects of alteration and typical tholeiitic fractionation. Samples collected from the chill margin of three different dykes are variably enriched in plagioclase (and pyroxene) phenocrysts, often in glomeroporphyritic aggregates, with respect to the samples collected from the centre of the individual dykes, which in a single example was aphyric, and this suggests that phenocryst accumulation may have occurred along the dyke margins, but the concentration of plagioclase is not reflected in the Al_2O_3, CaO or Sr concentrations which remain approximately constant from the centre to the margin of the individual dykes.

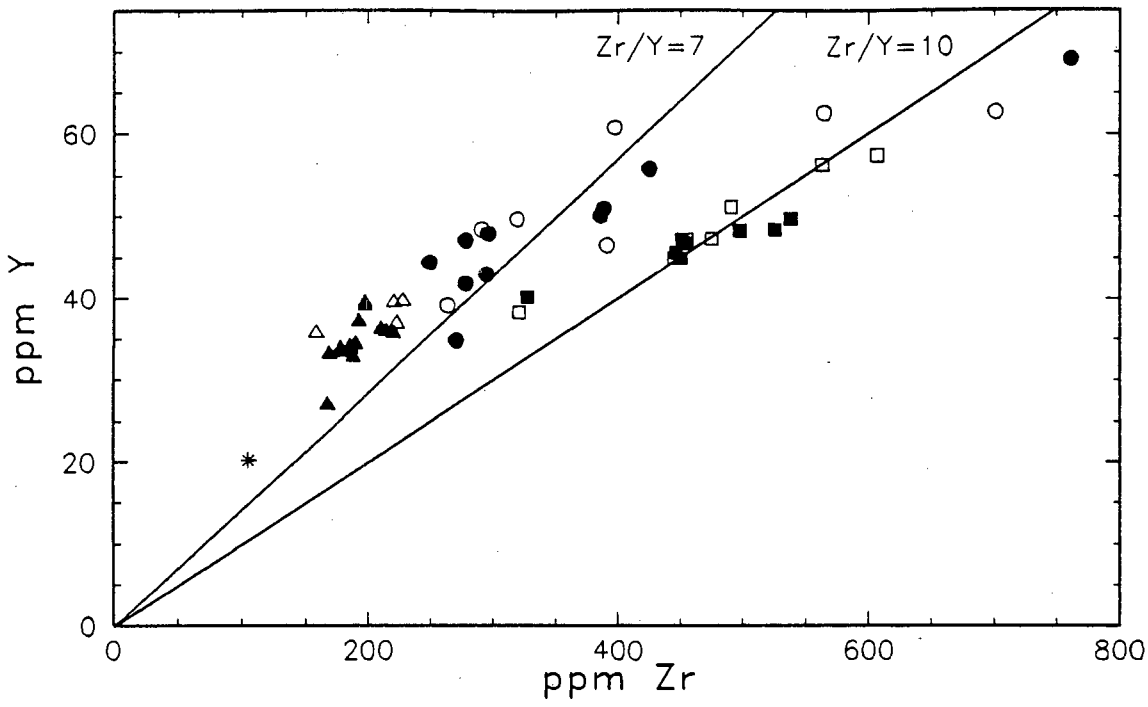

Fig. 4.7. Zr *vs.* Y for Botswana HTZ-type basalts and dolerites. The average Zr/Y ratios of the HTZ.HF (=7) and HTZ.LF (=10) type basalts of the Central Lebombo (see Fig. 2.7B) are also included. Symbols as for Fig. 4.6A & B.

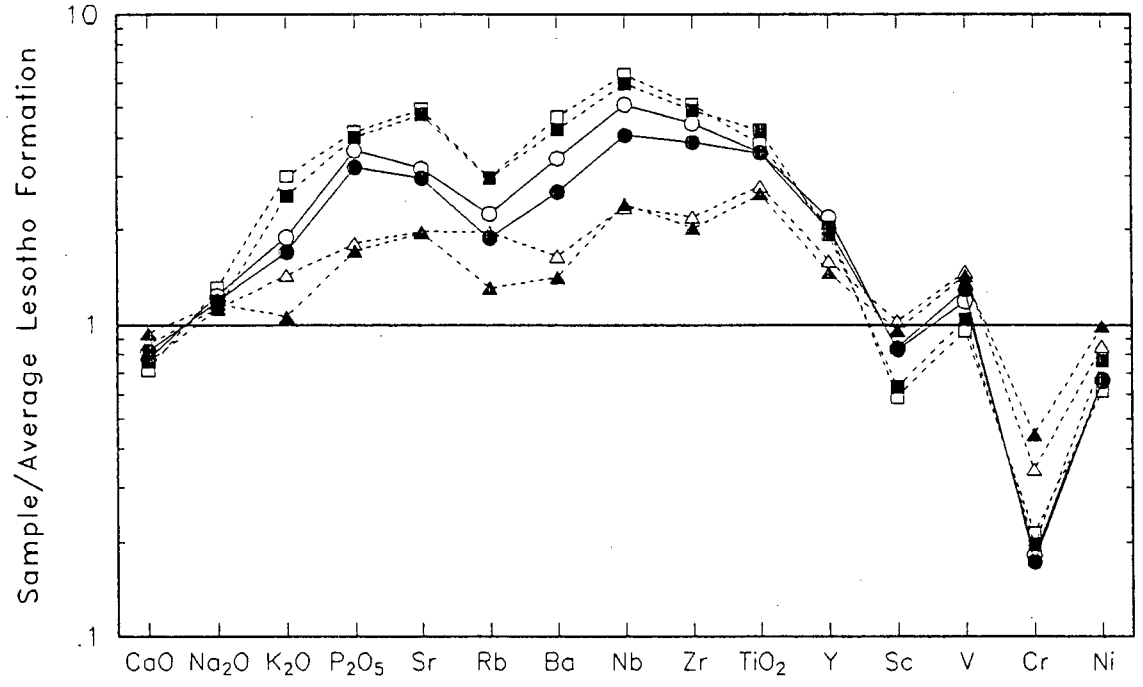

Fig. 4.8. Average concentrations of selected variables of the HTLZ-, HTZ- and HTZ (low Fe)- basalt and dolerite compositions normalised to the average Lesotho Formation basalt composition. Symbols as for Fig. 4.6A & B.

4.1.3.5 Summary

Two distinct "HTZ" geochemical types have been recognised in the "enriched" basalts of the Karoo Igneous Province. Sweeney *et al.* (1994) noted that the bimodal distribution of Fe_2O_3* concentrations within the "HTZ" basalts of the Central Lebombo was reflected in the Zr/Y ratio, where the low-Fe_2O_3* HTZ (or HTZ.LF) basalts had an average Zr/Y ratio of 10 whereas the high-Fe_2O_3* HTZ (or HTZ.HF) basalts generally have <5% MgO, an average Zr/Y ratio of 7 and, in particular, are characterised by a low and relatively constant Zr/Nb ratio of 11±2 and although Cox and Bristow (1984) noted the presence of high Fe_2O_3* HTZ-type basalts in the Nuanetsi area, the HTZ suite in that area has not been sub-divided into separate geochemical sub-groups. In a study of the Tuli area, Duncan *et al.* (1995) sub-divided the basalts into three geochemical types according to the Zr/Nb and Ce/Y ratios (see section 2.3.2.3). The enriched basalts of Botswana can similarly be sub-divided into two HTZ-types, although the discrimination between types is ill-defined. The HTZ (low Fe) basalt and dolerite type of Botswana, although very evolved with between 4.80 and 3.22% MgO, closely resembles the HTZ.LF basalt type of the Karoo Igneous Province in that the HTZ (low Fe) basalt type is depleted in Fe_2O_3* (as well as CaO, Cu and V), is somewhat enriched in TiO_2, P_2O_5, K_2O, Ba, Sr, Zr, Nb and the LREE with respect to the HTLZ/HTZ basalts and dolerites of similar MgO concentrations, has a high Ce/Y ratio (see Fig. 2.18) and in Fig. 4.7 (compare to Fig. 2.7B) the HTZ (low Fe) basalts and dolerites have, on average, higher Zr/Y ratios (means of 9.7 and 9.9 respectively). The two HTZ (low Fe) samples which have a somewhat lower Zr/Y ratio both contain ≥15% phenocrysts of plagioclase. The HTLZ/HTZ basalts and dolerites can similarly be compared to the HTZ.HF basalt type of the Central Lebombo in that they all have evolved compositions (with <6.69% MgO), are characterised by a considerable range in major, trace and rare earth element concentrations, have similar Zr/Y ratios (see Fig. 4.7), although the HTLZ basalts and dolerites have somewhat lower Zr/Y ratios (means of 5.4 and 5.5 respectively). The HTLZ/HTZ basalts and dolerites, however, do not have the low Zr/Nb ratio which is characteristic of the HTZ.HF basalts (see Fig2.10C & D) in the Central Lebombo.

Fig. 4.8 summarises both the relationships between the HTZ-type basalt and dolerite sub-groups and the LTZ basalts, where the average concentration of selected variables in the HTZ-type basalt and dolerite sub-groups are normalised to the average concentrations in the Lesotho Formation basalts (compare to Fig. 4.2). The HTLZ/HTZ- and HTZ (low Fe)-basalt and dolerite sub-groups show a progressive enrichment of K_2O, P_2O_5, Sr, Rb, Ba, Nb, Zr, TiO_2 and Y and depletion of CaO, Sc, V, Cr and Ni respectively (see Fig. 4.8).

The HTZ-type basalts and dolerites have a more evolved whole rock geochemistry than the

LTZ basalts of Botswana (a range in MgO concentrations of 6.69 to 3.19% and 8.51 to 5.71% respectively) and the HTZ-type basalts and dolerites and LTZ basalts commonly define a continuous compositional trend with decreasing MgO concentrations (*e.g.* see K_2O, Ba and Y *vs.* MgO in Fig. 4.6) and therefore the HTZ-type basalts and dolerites do not have a true "enriched" signature as defined by Cox *et al.*, 1967) although the HTZ-type basalts and dolerites do show a considerably greater enrichment in K_2O (.35-2.83 wt%), Rb (9.9-40ppm) and Ba (171-1004ppm) with decreasing MgO concentrations with respect to the LTZ basalts. The HTZ-type basalts and dolerites, as a single group define parallel but enriched trends of TiO_2, P_2O_5, Fe_2O_3*, Sr, LREE, Ni, Cu and V *vs.* MgO with respect to the LTZ basalts and Zr and Nb are also somewhat enriched in the HTZ-type basalts and dolerites with respect to the LTZ basalts, whereas the HTZ-type basalts and dolerites are depleted in SiO_2, Al_2O_3, CaO, Cr and Sc with respect to the LTZ basalts of similar MgO concentrations.

KLB-030 is has a whole rock composition which lies at the mafic end of the trends defined by both the major and trace element concentrations of the HTLZ/HTZ basalts and dolerites in Fig 4.6 A & B and, therefore clearly lies on a similar liquid-line-of-descent to these HTZ-type basalts and dolerites. KLB-030, like the HTZ-type basalts and dolerites, is clearly enriched in TiO_2, Fe_2O_3*, P_2O_5, Sr, Ni and Cu and depleted in Cr and Sc with respect to the LTZ basalts. KLB-030 however has similar Zr, Nb and somewhat lower Y concentrations than the LTZ basalts.

4.2 HIGH-K_2O LINEAGE

The high-K_2O lineage of Botswana includes both shoshonites and high-K_2O picritic basalts (see Fig. 2.4 and section 2.4) where the high-K_2O picritic basalts are considered equivalent to the Letaba Formation picritic basalts of the Karoo Igneous Province. Rare shoshonite and absarokitic type compositions have been recognised in the Lebombo, Nuanetsi and Tuli areas (*e.g.* Vail *et al.*, 1969; Cox and Bristow, 1984). These rock types have been related to the Letaba Formation Picritic basalts by fractionation within the K-rich lineage, using as a representative example, the differentiated Chilembeni olivine monzonite intrusion (Cox and Bristow, 1984). The whole rock compositions of the high-K_2O picritic basalts and the average composition of the shoshonites sampled during this study are listed in TABLE 4.9 together with some examples of the high-K lineage rock compositions from the Nuanetsi, Tuli and Northern Lebombo areas. The average shoshonite composition of Joplin (1964) is also included, for comparison, in TABLE 4.9. The data used for the calculation of the means (and S.D.) of the Letaba Formation picritic basalts was obtained from Microfiche Card 2B attached to Duncan *et al.* (1984b). The major and selected trace element

	HIGH-K_2O PICRITIC BASALTS		LETABA FORMATION		SHOSHONITES (BOTSWANA)				SHOSHONITES				CHILEMBENI INTRUSION	
	KLB-083	KLB-084	MEAN	S.D.	MEAN	MIN.	MAX.	S.D.	(1)	(2)	(3)	(4)	(1)	(2)
SiO_2	47.85	50.66	49.54	1.12	50.08	49.57	50.34	.31	50.35	50.71	50.37	51.42	48.50	46.06
TiO_2	2.43	2.51	2.94	.33	2.12	1.78	2.52	.29	1.70	1.85	3.76	1.08	3.54	4.49
Al_2O_3	7.35	8.63	8.44	1.23	16.11	15.38	17.46	.75	17.35	16.60	15.54	16.51	16.19	10.17
Fe_2O_3	12.86	11.65	12.39	1.05	10.88	10.22	11.67	.60	10.84	11.55	12.92	12.63	11.17	14.69
MnO	.16	.14	.15	.02	.16	.15	.17	.01	.13	.12	.16	.20	.12	.15
MgO	19.63	16.18	15.40	3.07	4.88	4.69	4.99	.11	4.08	3.39	3.48	3.52	3.59	11.23
CaO	6.40	6.67	7.21	1.07	7.91	7.71	8.13	.18	7.08	7.42	5.89	7.14	9.11	7.91
Na_2O	1.42	1.27	1.55	.44	3.31	2.91	3.86	.36	3.46	3.53	2.12	3.49	3.00	1.97
K_2O	1.48	1.86	1.93	.72	3.80	3.48	4.14	.24	4.40	4.18	5.14	3.41	3.20	2.39
P_2O_5	.41	.43	.45	.09	.76	.74	.78	.01	.62	.66	.62	.60	1.48	.60
Rb	23	37	43	20	116	90	140	17	120	1214	116		67	52
Ba	768	666	889	290	1815	1597	2018	173	2192	2088	2482		1437	997
Sr	887	746	961	219	1225	986	1416	175	1352	1306	1213		2412	1263
Th	4.1		1.6	1.5	19	15	21	2.4						
U	3.3	3.0	.7	.1		3.1	1.8	3.9	.8					
Zr	303	334	369	82	298	280	321	17	322	340	413		513	415
Nb	26	13	19	6.6	142	120	160	16	135	14	15		28	26
Cr	1041	887	912	182	193	158	212	20			28			
V	193	186	197	35	176	158	196	16			225			
Sc	19	21	21	3.0	14	12	17	2.0						
Ni	1105	875	805	245	92	79	98	7.3			72		42	572
Co	92	75	79	17	32	29	35	2.0	37	31	50			
Pb	14	13	31	42	12	9.9	14	1.7						
Zn	117	110	109	8.6	92	86	101	5.2	87	84	135		86	123
Cu	83	86	79	17	179	159	202	17			207		147	116
Y	24	26	27	3.7	28	25	32	2.6			45		56	34
La	42	36	44	5.7	112	100	124	9.0						
Ce	93	82	107	14	212	196	226	12						
Nd	57	53	63	10	82	80	84	1.6						
N			70		6							7	3	3

SHOSHONITES:
(1) TV-48 and (2) TV-49 Tuli Syncline, Zimbabwe. Vail *et. al.*, 1969.
(3) O-169 Balule Road, Olifants River, Cox and Bristow, 1984.
(4) Average shoshonite of Joplin, 1964
CHILEMBENI INTRUSION:
Average leucocratic (1) and mafic (2) olivine monzonite, Cox and Bristow, 1984.

TABLE 4.9. Whole rock compositions of the high-K_2O lineage rocks of Botswana and the Karoo Igneous Province.

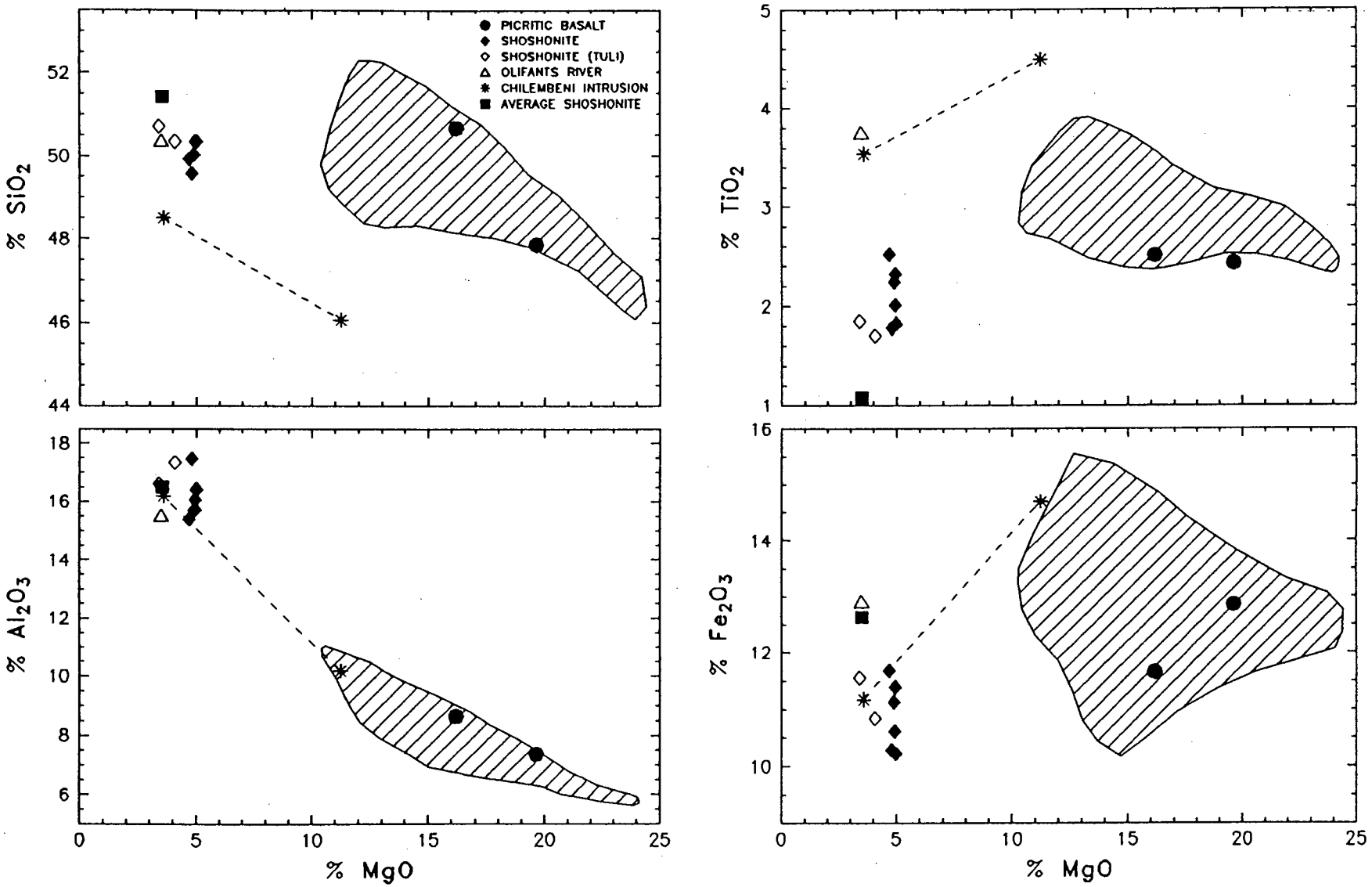

Fig. 4.9A. Major element variation diagrams plotted *vs.* MgO for the high-K_2O lineage examples listed in TABLE 4.9 (data normalised to 100% volatile-free with all Fe as Fe_2O_3*).

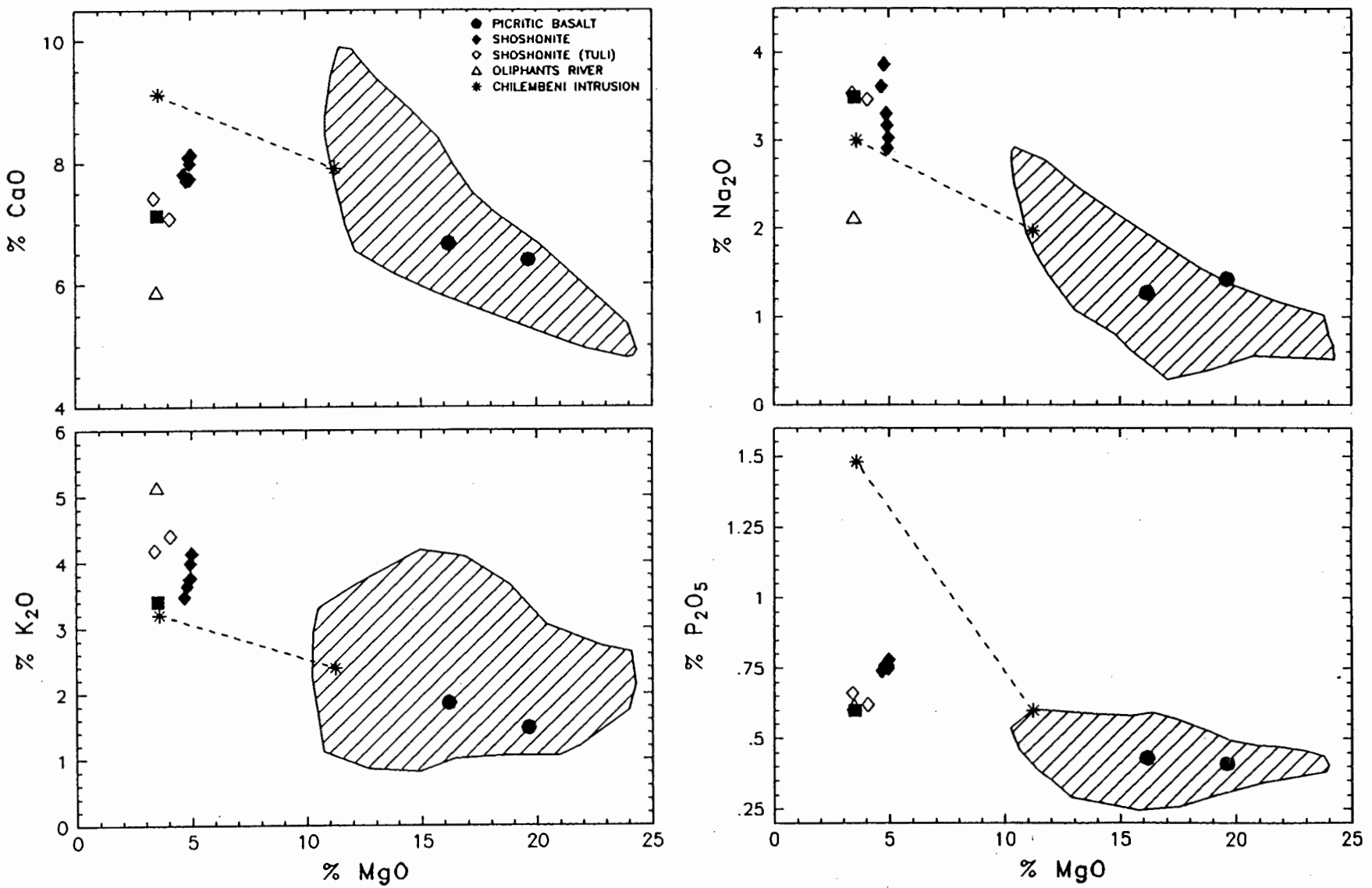

Fig. 4.9A (continued).

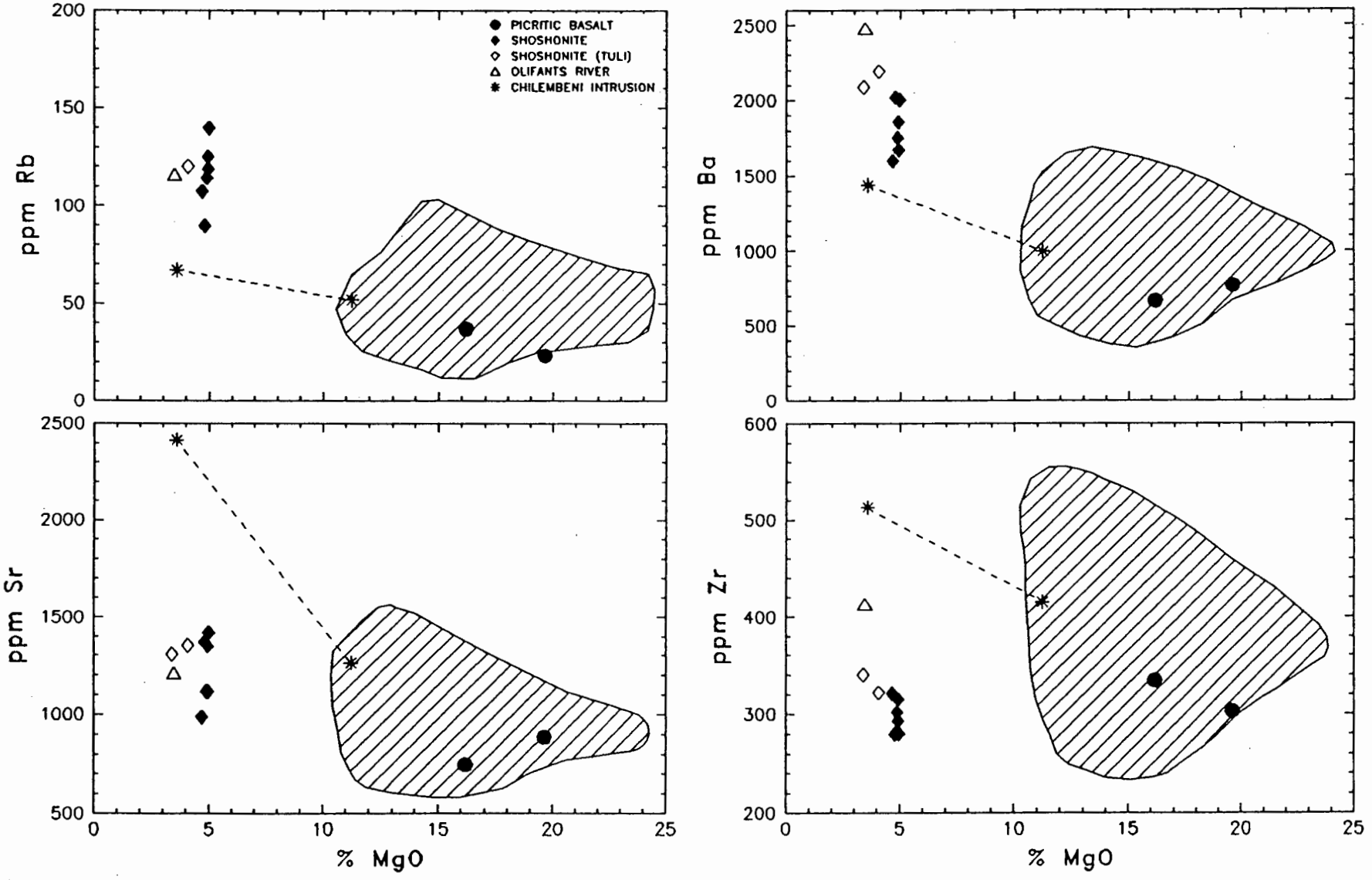

Fig. 4.9B. Trace element variation diagrams plotted *vs.* MgO for the high-K_2O lineage (data normalised to 100% volatile-free).

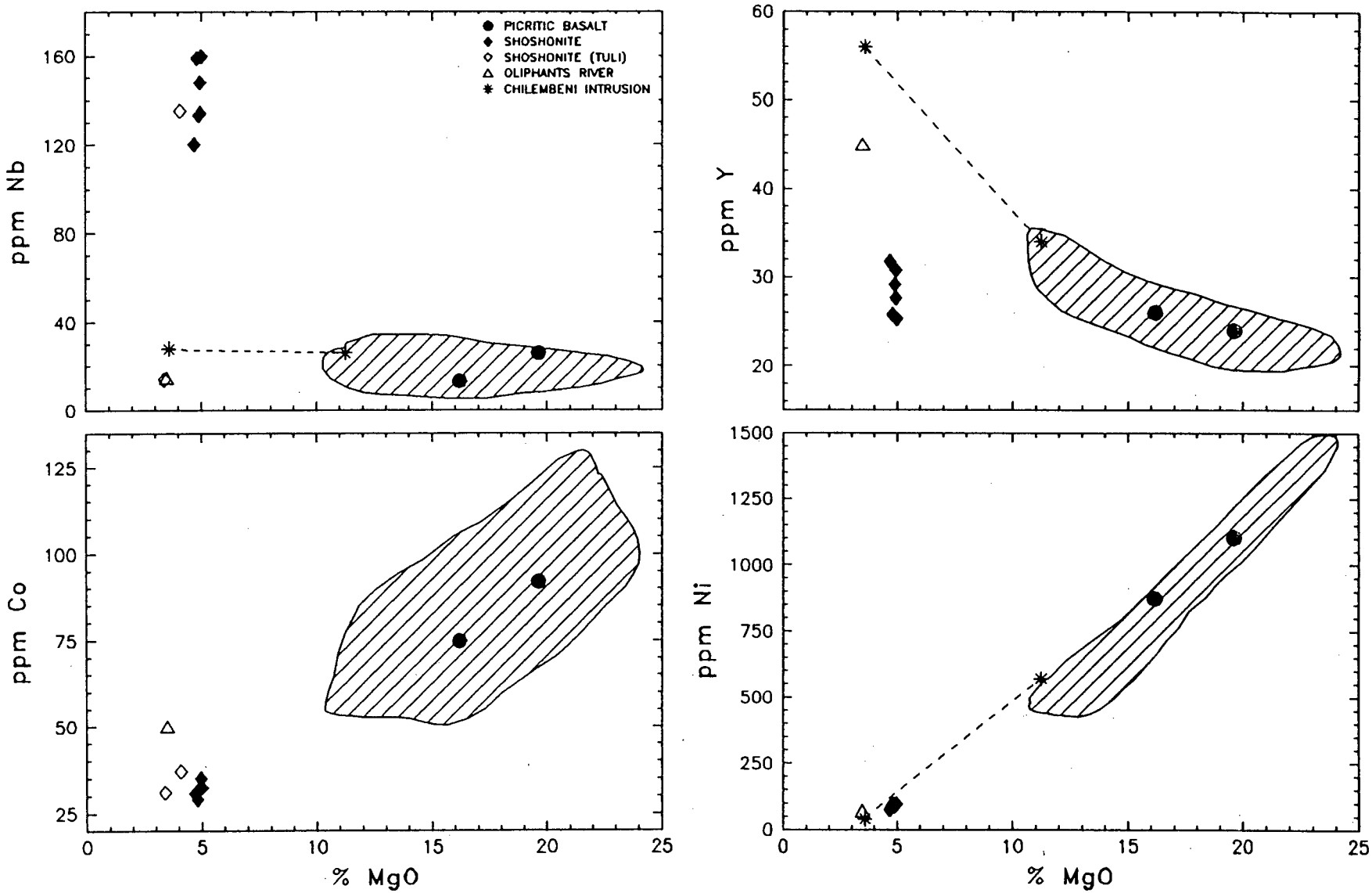

Fig. 4.9B (continued).

concentrations (where available) of the high-K lineage compositions listed in TABLE 4.9 are plotted *vs.* MgO in Fig. 4.9A & B where the compositional trend reported for the Chilembeni olivine monzonite is shown together with the fields defined by the compositional range of Letaba Formation picritic basalts (see shaded fields in Fig. 4.9A & B). The data listed in TABLE 4.9 and plotted in subsequent figures has all Fe as Fe_2O_3* and is normalised to 100% on a volatile-free basis.

4.2.1 HIGH-K_2O PICRITIC BASALTS

The high-K_2O picritic basalts sampled in the Tuli Syncline of Botswana have a whole rock geochemistry which is essentially identical to that of the Letaba Formation picritic basalts and in Fig. 4.9A & B the major and trace element concentrations of the high-K_2O picritic basalts lie within the fields defined by the compositional range of the Letaba Formation picritic basalts. The whole rock geochemistry of the Letaba Formation picritic basalts has been discussed in detail in the literature (*e.g.* Bristow, 1984b; Cox *et al.*, 1984; Ellam and Cox, 1989) and is therefore only briefly described here. The high-K_2O picritic basalts, like the Letaba Formation picritic basalts, are characterised by enriched, but variable, concentrations of TiO_2, K_2O, P_2O_5, Sr, Rb, Zr and Nb with respect to picritic basalts of similar MgO concentrations from other areas and none of these incompatible elements define coherent trends against MgO. The major element compositions of the Letaba Formation picritic basalts are reported to define coherent negative trends for Al_2O_3, CaO and Na_2O *vs.* MgO, whereas SiO_2 and Fe_2O_3* show considerable scatter in their concentrations and the trace elements Ni, Cr, Co and Y similarly define coherent trends *vs.* MgO where the behaviour of Y is therefore decoupled from Zr and Nb (see Fig. 4.9B).

4.2.2 SHOSHONITES

The Botswana shoshonites are characterised by the high, variable, and approximately equal concentrations of Na_2O and K_2O (2.91-3.86% and 3.48-4.14% respectively) and the major and trace element concentrations, apart from Nb, of the Botswana shoshonites are very similar to those reported for the shoshonites sampled in the Tuli area by Vail *et al.* (1969). However, the Botswana shoshonites have higher MgO concentrations (4.69-4.99%) than the Tuli shoshonites (3.39-4.08% MgO) and exhibit a greater range in major and trace element concentrations (see TABLE 4.9 and Fig. 4.9A & B). The Tuli shoshonites (this study and Vail *et al.*, 1969) both have major element compositions which are remarkably similar to the average shoshonite composition of Joplin (1964), although they are somewhat enriched in TiO_2 and depleted in Fe_2O_3* and SiO_2 with respect to his average composition.

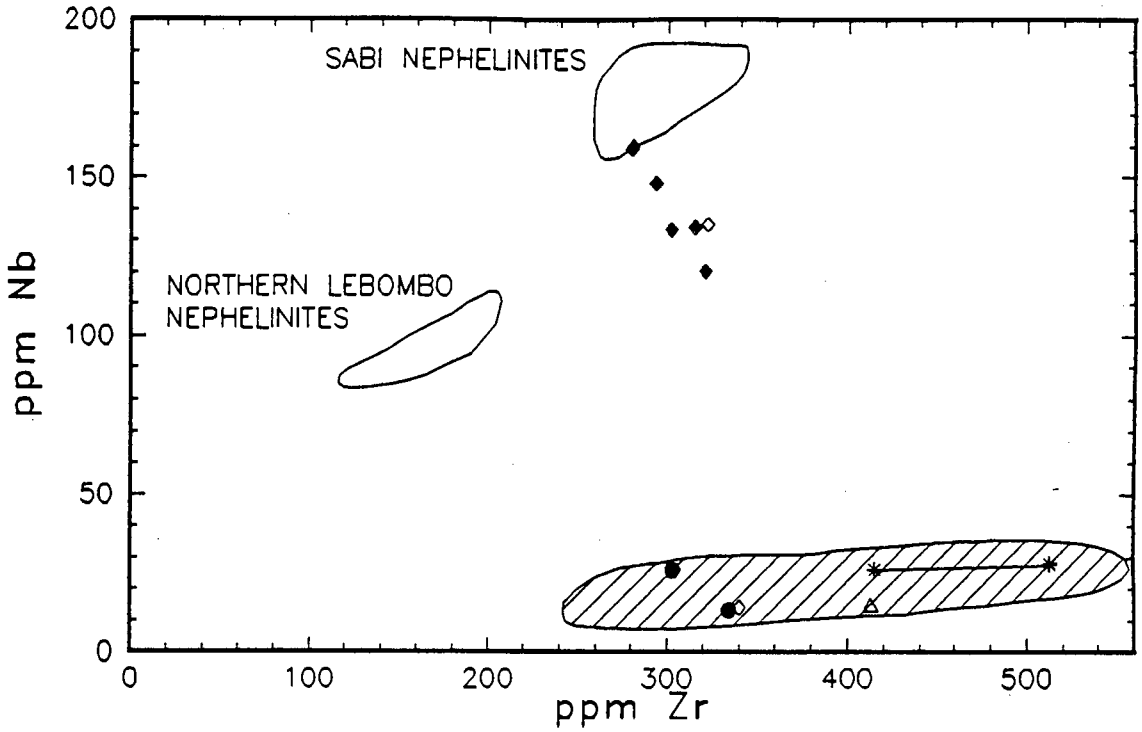

Fig. 4.10. Zr *vs.* Nb for the high-K_2O lineage. The fields defined by the Northern Lebombo and Sabi nephelinites (Bristow, 1984a) are included for comparison and symbols as for Fig. 4.11A & B.

The Tuli shoshonites, however, show a considerable range in Nb concentrations (14 to 160ppm), but the Tuli shoshonite TV-49 (14ppm Nb) is significantly depleted in Nb with respect to the Botswana shoshonites, which have a range in Nb concentrations of 120-160ppm and the Tuli shoshonite, TV-48, which has 135ppm Nb. The average Chilembeni leucocratic and mafic olivine monzonites and the Balule road shoshonite have Nb concentrations in the range of 15-28ppm (comparable with the Tuli shoshonite TV-49) and are therefore similarly significantly depleted in Nb with respect to the Botswana shoshonites and the single Tuli shoshonite, TV-48. The high Nb concentrations of the Botswana (and Tuli: TV-48) shoshonites, reflected in their low Zr/Nb ratios with respect to the other Karoo shoshonites and the Letaba Formation picritic basalts, are similar to the high Nb concentrations and low Zr/Nb ratios of the Mashikiri Formation nephelinites (see Fig. 4.10).

Radiogenic Sr isotopic analyses (R.A. Armstrong, *pers. comm.*, 1994) for two shoshonite samples, KLB-058 and -090, yielded initial $^{87}Sr/^{86}Sr$ ratios of 0.70550 and 0.70532. It is noteworthy that these initial Sr-isotope ratios closely resemble those quoted by Bristow *et al.* (1984) for the Mashikiri nephelinites (0.70510 to 0.70687) where six of the eight initial $^{87}Sr/^{86}Sr$ ratios lie between 0.70510 and 0.70551.

4.3 FELSITES

The two felsite samples collected from two different dykes in eastern Botswana are the only unequivocal Karoo acid igneous rocks found in Botswana (see section 1.2.3.3.1). The whole rock compositions of these two felsite samples are listed in TABLE 4.10 and their normative compositions are listed in TABLE 4.11. As only two felsite compositions are currently available no inter-element variation diagrams have been plotted.

4.3.1 WHOLE ROCK GEOCHEMISTRY

The two felsite samples exhibit little variation in their SiO_2 concentration (66.5 - 67.23 wt%), but are otherwise characterised by a considerable variation in their major element geochemistry with, for example, a variation in MgO concentration of 1.27 - 2.03 wt% and K_2O concentrations of 3.7 and 5.6 wt% (see TABLE 4.10). In contrast, the trace element compositions (excluding Rb, Ba and Sr) of the two felsites are similar which may suggest a uniform felsic magma type. The variation in the major element geochemistry and the range in the concentrations recorded for the more mobile elements, including Rb (80 - 108ppm), Ba (1545 - 2276ppm) and Sr (414 - 525ppm), together with the petrographic evidence of extensive alteration (see section 3.3.1), suggests that the observed compositional differences between the two felsite samples reflect, to some extent, the effect of alteration. The observed compositional differences may also reflect a variation in the modal proportion of the phenocryst assemblage (with clinopyroxene as the dominant phenocryst phase) as KLB-082 has 7.3 modal% phenocrysts and a MgO concentration of 2.03 wt% whereas KLB-080, which has 4.8 modal% phenocrysts has a MgO concentration of 1.27 wt%.

A single radiogenic Sr isotopic analysis for KLB-080 (R.A. Armstrong, *pers. comm.*, 1994) shows an initial $^{87}Sr/^{86}Sr$ ratio of 0.70957 (age corrected to 190Ma).

4.3.2 COMPARISON TO OTHER KAROO FELSIC VOLCANICS

Two essentially different petrogenetic felsic magma types have be recognised in the Karoo Igneous Province where the one felsic magma type is a product of partial melting of ancient crustal rocks and the other felsic magma type has been interpreted (*e.g.* Cleverly *et al.*, 1984; Betton and Cox, 1979) to result from decompressive melting of still-hot underplated basaltic material (Karoo age) in areas of crustal thinning (*i.e.* rift environment). The felsic magma type with a presumed crustal origin is characterised by an isotopic signature which is typical of crustal rocks and is commonly found interbedded with basalt. Examples of this felsic magma type include the minor intermediate rocks of the Central Karoo area, *i.e.* the

Belmore Andesite and the Pronksberg, Dikkop and Roodehoek Dacites (Marsh and Eales, 1984) which have a range in initial $^{87}Sr/^{86}Sr$ ratios of 0.7094 - 0.7130 and the Mkutshane Beds of the Central Lebombo area (Cleverly *et al.*, 1984) which have an initial $^{87}Sr/^{86}Sr$ ratio which is >0.715. In contrast, the felsic magma type which is a presumed product of decompressive melting of underplated basaltic material is characterised by a mantle-like isotopic composition and is seldom found interbedded with basalt, *e.g.* the Lebombo rhyolites which have typical initial $^{87}Sr/^{86}Sr$ ratios of 0.7044±2, 0.7048±1 and 0.7085±6 (Jozini rhyolites of the Southern Lebombo and Swaziland; Central and Northern Lebombo and Nuanetsi rhyolites respectively - Bristow *et al.*, 1984). Cox (1988a) suggests that the two felsic magma types can be differentiated according to the relative enrichment/depletion of the alkali elements (K, Rb) and the high field strength elements (Zr, Nb and Y). This difference is exemplified by the Rb/Nb ratio with the felsic magmas of crustal origin being characterised by high and variable Rb/Nb ratios (*i.e.* >5.5) whereas the Lebombo and Nuanetsi rhyolites (*i.e.* excluding the Mkutshane Beds) have average Rb/Nb ratios of ≤2.

The whole rock compositions of some examples of both felsic magma types are listed in TABLE 4.12. The whole rock compositions of the Botswana felsite samples when compared to compositions of the rhyolitic and intermediate rock types of the Karoo Igneous Province as a whole, suggest that the Botswana felsite compositions more closely resemble the compositions of the Lebombo and Nuanetsi rhyolites (particularly with respect to the Zr, Nb and Y concentrations) as the Botswana felsites are relatively enriched in these elements with respect to both the intermediate rocks of the Central Karoo area and the Mkutshane beds of the Central Lebombo area (see TABLE 4.10 and TABLE 4.12). However, the initial $^{87}Sr/^{86}Sr$ ratio of 0.70957 of KLB-080 is greater than typical mantle-like isotopic signatures of the Lebombo Rhyolites and the Rb/Nb ratio of the felsites (4.5 and 3.3 for KLB-080 and -082 respectively) lie approximately between the values typical of the two felsic magma types. As the Rb concentrations of the Botswana felsites appear to have been modified by alteration the validity of these ratios is somewhat questionable.

	FELSITE	
	KLB-080	KLB-082
SiO_2	66.50	67.23
TiO_2	.88	.96
Al_2O_3	15.02	14.84
Fe_2O_3	5.48	5.68
MnO	.06	.08
MgO	1.27	2.03
CaO	1.71	2.26
Na_2O	3.20	2.98
K_2O	5.66	3.70
P_2O_5	.22	.24
Rb	108	80
Ba	2276	1545
Sr	525	414
Th	18	17
U	2.9	4.1
Zr	847	831
Nb	24	24
Cr	35	43
V	43	49
Sc	6.7	8.1
Ni	18	22
Co	12	11
Pb	21	22
Zn	77	78
Cu	22	25
Y	56	57
La	106	103
Ce	233	229
Nd	115	113

TABLE 4.10. The whole rock compositions of the Felsites.

	FELSITE	
	KLB-080	KLB-082
QZ	18.5	25.7
COR	1.0	2.4
OR	33.4	21.8
AB	27.1	25.3
AN	7.1	9.6
HY	9.3	11.3
HYEN	3.2	5.1
HYFS	6.1	6.3
MT	.9	1.0
IL	1.7	1.8
AP	.5	.6

TABLE 4.11. The CIPW normative compositions of the Felsites. CIPW norms calculated with a Fe_2O_3*/FeO ratio of 0.15.

	PRONKSBERG DACITE		ROODEHOEK DACITE		JOZINI FMT. (ZULULAND)		MKUTSHANE BEDS		NUANETSI RHOLITES	
	MEAN	S.D.	MEAN	S.D.	MEAN	S.D.	MEAN	S.D.	MEAN	S.D.
SiO_2	65.40	.16	66.35	.36	70.68	1.65	69.82	3.20	71.57	2.86
TiO_2	.78	.01	.78	.01	.50	.15	.90	.34	.44	.24
Al_2O_3	17.13	.12	16.01	.08	12.65	.42	12.14	.11	12.89	.78
Fe_2O_3	6.35	.08	6.03	.16	6.34	.86	6.81	1.60	5.23	1.24
MnO	.17	.01	.16	.01	.10	.03	.08		.09	.05
MgO	2.36	.08	2.49	.09	.35	.17	.47	.16	.40	.24
CaO	2.77	.17	2.56	.25	1.47	.60	2.33	.87	1.39	.85
Na_2O	3.38	.19	2.49	.18	3.16	.41	3.74	.29	2.89	.91
K_2O	1.44	.09	2.95	.13	4.61	.55	3.55	.22	5.03	.76
P_2O_5	.21	.01	.19	.01	.14	.06	.18	.06	.08	.09
Rb	146	32	123	4	130	24	97	20.2	157	29
Ba	761	20	650	31	1475	266	559	63	1640	464
Sr	323	15	256	17	153	27	181	41	85	32.1
Zr	203	3	227	3	1085	56	293	61	763	127
Hf	4.7	.45			26.6	2.6	8.2	2.57	19.6	.7
Nb	13	.7	11	.7	84	5.1	14	2.9	102	13
Cr	54	2.6	86	5.8	7.5	1.66			13	1.6
V	68	6.5	91	5.4	6.2	2.33			5.4	4.08
Sc					13	2.3			10	
Ni	28	1.5	23	2.0	3.8				4.5	
Co	19	.6	20	1.0	5.2	2.08			6.5	.45
Pb	27	.6			22	2.7	210	188	20	3.6
Zn	97	2.7	87	3.9	135	17			112	23
Cu	27	1.2	22	2.2	8.8	3.12			6.3	2.32
Y	31	1.2	31	1.0	129	60	42	9.5	83	14.6

TABLE 4.12. Examples of average whole rock composition (and standard deviation) of some Karoo Igneous Province felsic magma types from the Central, Lebombo and Nuanetsi areas. (All data from Duncan *et al.*, 1984a).

5 DISTRIBUTION OF BASALTS AND DOLERITES IN BOTSWANA

5.1 INTRODUCTION

The distribution of the basalts and dolerites sampled in Botswana is briefly described according to the different geochemical sub-groups defined in chapter 2 and the stratigraphic relationships between the different geochemical sub-groups and the geochemistry of the dyke swarm are then discussed in more detail. A more comprehensive description of the sample collection, including locality information, is included in APPENDIX A.

5.2 LOW-K_2O LINEAGE

5.2.1 LTZ BASALTS AND DOLERITES

A total of 138 basalts and dolerites sampled in Botswana are classified as having a LTZ-type signature according to the criteria defined in Chapter 2 (*e.g.* see Fig. 2.5A). The distribution of the LTZ-type basalts and dolerites in Botswana is summarised in Fig. 5.1, with LTZ-type basalts and dolerites present in the Central Kalahari Sub-basin, in the north and northeast of Botswana, in western Botswana and in eastern Botswana, however no LTZ samples (neither basalt nor dolerite) were sampled in the Botswana portion of the Tuli Syncline.

5.2.1.1 LTZ-type basalts

The LTZ-type basalts include, by definition (see chapter 2), four separate geochemical sub-groups, *i.e.* the LTZ basalts, the high-Na_2O LTZ basalts, the low-MgO LTZ picritic basalts and the low-P_2O_5 LTZ basalts.

All but two of the LTZ-type basalts were core samples collected from 22 different boreholes. The two basalt outcrop samples, KLB-054 and -055, were sampled from a road-cutting on the Serowe-Orapa road in the Central Kalahari Sub-basin (see Fig.5.1). As the majority of the LTZ-type basalts were sampled from thirteen different boreholes, only these borehole names, and not the sample numbers, have been included in Fig. 5.1.

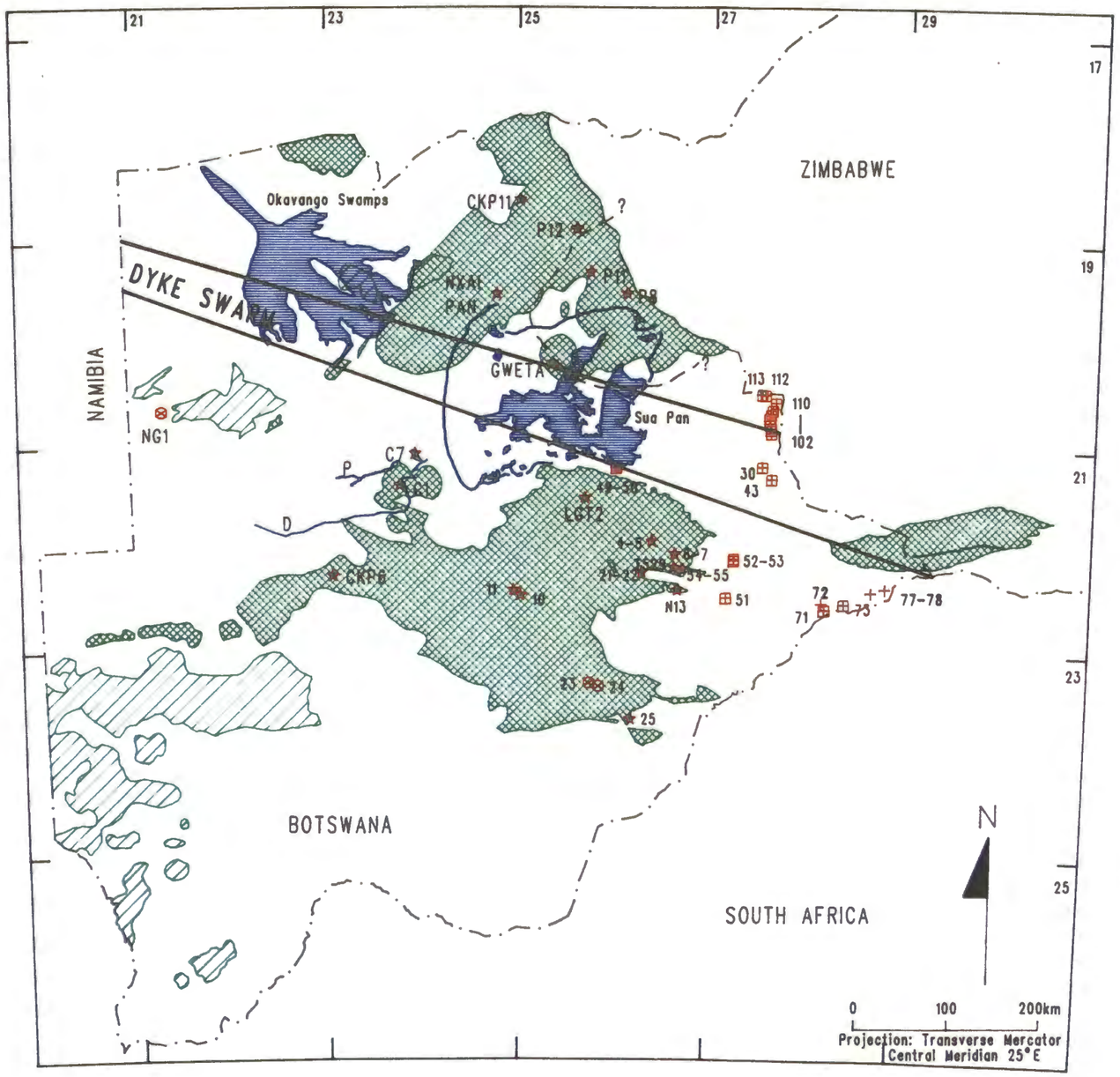

Fig. 5.1. The distribution of LTZ-type basalts and dolerites in Botswana

LEGEND

- Pans and swamps
- Basalts
- Sills

KAROO

- ★ LTZ-TYPE BASALT
- ⊗ LOW-P2O5 LTZ BASALT
- ■ TYPE I LTZ DOLERITE
- ⊞ TYPE II LTZ DOLERITE
- \+ HIGH-MGO LTZ PICRITE

- Shoreline of former Lake Makgadikgadi
  P: Passarge Mekgacha
  D: Deception Mekgacha
- Approximate northern limit of Letaba Picrites in the Tuli Syncline (Zimbabwe)
- Postulated position of the Nata Sub-basin
- International boundary

BOREHOLE (locality)	SAMPLE NUMBERS	BASALT INTERVAL	TOTAL BASALT THICKNESS
*P8 (19°24′S;26°02′E)	KLB-152 to -175	155.7-433.87m *144.0-433.87 (Smith, 1984)*	278.17m
*P11 (19°15′S;25°45′E)	KLB-114-134	129.6-499.55m	369.95m
P12 (18°46′S;25°38′E)	KLB-135 to -150	41.5-359.05m *11.5-360.7m (Smith, 1984)*	317.55m
NXAI PAN (19°31′36′′S;24°46′E)	DB-14,-16,-19,-20	136-503m	>367m
CKP11 (18°36′S;25°06′E)	KLB-019,-020, -201 to -205	31-100.78m *32-117m (Meixner and Peart, 1984)*	>69.78m
*GWETA (20°16′19′′S;25°13′25′′E)	KLB-195	160.25-180.23m	>19.98m
*CKP6 (22°17′S;23°04′E)	KLB-017,-018,-185 to -189	72.5-178.66m *77.3-178.9m (Meixner and Peart, 1984)*	106.16m
*C1 (21°24′S;23°46′)	KLB-196 to -200	104.10-264.4m *93-248m (Coates et. al., 1979)*	>160.3m
*C7 (21°06′S;23°57′E)	KLB-206 to -209	64-160.3m	96.3m
*LGT2 (21°31′10′′S;25°41′23′′E)	KLB-045 to -048	(44.2-95.3m)	>51.1m
T529 (22°12′S;26°38′E)	KLB-210 to -214	11-270.5m *11.28-251.92m (Smith, 1984)*	>259.5m
N13 (22°25′S;26°46′E)	KLB-026 & -027	(33.8-61.8m)	>28m
NG1 (20°39′S;21°18′E)	KLB-014 to -016, -177 to -184	67.6-103.25m	>36.65m

TABLE 5.1. Summary of borehole data.

TABLE 5.1 summarises some of the details available for thirteen of the boreholes sampled during this study (*i.e.* for those boreholes from which more than two basalt samples were collected), including the sample numbers for the basalts sampled from each borehole, the depth to the top and bottom of the basalt interval (from the surface to the initial basalt intersection and then to either the base of the drilling interval or to the basalt/sandstone contact) and the total thickness of basalt penetrated during drilling. The depths of the basalt interval in the boreholes P8, P11, CKP11, CKP6, C1 and T529, quoted by Meixner and Peart (1984), Smith (1984) and Coates *et al.* (1979), are shown in italics in TABLE 5.1 as they differ from the depths logged during this study.

The boreholes in which high-Na_2O LTZ basalts were sampled are marked with an asterisk in TABLE 5.1 where the high-Na_2O LTZ- and LTZ-basalt types are interbedded in the stratigraphic sections sampled by boreholes in both the Central Kalahari Sub-basin and in northeast Botswana (see Fig. 5.3). The location of some of the major salt pans and playa lakes, the fossil remnants of the former Lake Makgadikgadi, and the Passarge and Deception fossil drainage systems are included in Fig. 5.1. The distribution of the boreholes

in which high-Na_2O LTZ basalts are present therefore appears to be a function of their proximity to the drainage systems associated with the former Lake Makgadikgadi as preserved in the Kalahari Beds. Although KLB-055 is not located adjacent to the above fossil drainage systems, its high-Na_2O LTZ signature may reflect the close proximity of the basalt outcrop to minor pans preserved in the Kalahari Beds as the adjacent borehole T529 is located in the Serwe Pan (Smith, 1984).

The low-MgO LTZ picritic basalts have whole rock compositions which are geochemically continuous with the LTZ- and high-Na_2O LTZ basalts (the low-MgO LTZ picritic basalt KLB-172 has a Na_2O concentration which is comparable to that of the high-Na_2O LTZ basalts). Two of these low-MgO LTZ picritic basalts are interbedded with the LTZ- and high-Na_2O LTZ basalts in the stratigraphic sections in two boreholes (*i.e.* P11 and P8) drilled in the Nata Sub-basin of northeast Botswana (see Fig. 5.3). In the borehole P11 the low-MgO LTZ picritic basalt (KLB-128) is sampled from a single thick flow (53.2m from top to bottom flow margins) in which two other samples (KLB-126 and -127) have LTZ basalt type compositions. In contrast, the low-MgO LTZ picritic basalt sample, KLB-172, was sampled from a relatively narrow flow (9.44m) which was interbedded with basalt flows which all have high-Na_2O LTZ basalt compositions.

The low-P_2O_5 LTZ basalts define a geochemically distinct group with respect to the remaining LTZ-type basalts (see section 2.3.2.2). Seven of the nine low-P_2O_5 LTZ basalts were sampled from the borehole NG1, which was drilled through an outlier of Karoo basalt in western Botswana. These low-P_2O_5 LTZ basalts are present in the lower $\pm$15m of the basalt interval intercepted by the borehole NG1 (where the total basalt interval intercepted was 35.65m). Although two possible low-P_2O_5 LTZ flow units were logged in the basalt interval of NG1 (see APPENDIX A), the basalt is very altered, and all seven of these low-P_2O_5 LTZ basalt samples, collected from NG1, are most likely representative of a single flow unit (where the apparent flow margins may indicate flow lobes within a single unit). The remaining two low-P_2O_5 LTZ basalts were, however, sampled from two adjacent boreholes (K2 and K3 with sample numbers KLB-023 and -024 respectively) drilled in the southeast of the Central Kalahari Sub-basin (see Fig. 5.1).

5.2.1.2 LTZ-type dolerites

5.2.1.2.1 TYPE I LTZ dolerites

The two TYPE I LTZ dolerites were sampled from two adjacent dolerite dykes which outcrop along the southern margin of the Sua Pan, *i.e.* just along the southern margin of the

main dyke swarm and adjacent to the northern margin of the Central Kalahari Sub-basin (see Fig. 5.1).

5.2.1.2.2 TYPE II LTZ dolerites

The collection of the TYPE II LTZ dolerites was limited to eastern Botswana and to the eastern edge of the Central Kalahari Sub-basin. TYPE II LTZ dolerites are found to the north of, within and to the south of the major dyke swarm. The dykes south of the dyke swarm range in thickness from ±5m to ±30m and their strike ranges from WNW, *i.e.* parallel to the average strike of the dyke swarm, to approximately E-W, *i.e.* approximately parallel to the axis of the Tuli Syncline (see APPENDIX A). A single TYPE II LTZ dolerite, KLB-043, was collected within the outcrop area of the main dyke swarm from a narrow dolerite dyke with an approximate E-W strike. North of the dyke swarm the TYPE II LTZ dolerites sampled are, on average, ≥10m wide and display a variation in strike direction from N100E to N025E. A set of TYPE II LTZ dolerite dykes were collected in the Tshesebe area, where they defined prominent topographic features with strike directions which range from NNE to ENE (*i.e.* a strike direction which varies considerably from the WNW strike of the dyke swarm and the average strike of the TYPE II LTZ dolerite dykes sampled during this study). These dolerites dykes were sampled in the same general area in which Wilson *et al.* (1987) suggest a Proterozoic rather than a Karoo age for the dolerite dykes (see section 1.2.2.2).

The country rock into which the TYPE II LTZ dolerites were intruded could not be observed in the field due to the poor outcrop exposure in eastern Botswana, but according to the Geological Map of the Republic of Botswana, 1:1 000 000 (Geological Survey of Botswana, 1984) the TYPE II LTZ dolerites are intruded into the quartzo-feldspathic gneisses and granites of the Archaean basement, which are host to a variety of mafic intrusions, which include Archaean amphibolites, metagabbros, serpentinites, ultramafic schists, peridotites and pyroxenites and dolerite sills which have been assigned ages which range from ±1255Ma to ±590Ma to late Karoo ages. As discussed in chapters 2 to 4, a combination of geochemical, petrographic and field evidence suggests that the TYPE II LTZ dolerites belong to the Proterozoic suite of intrusive dolerites in eastern Botswana, with at least some of these dolerite dykes in northeast Botswana possibly representing a western extension of the Plumtree Dyke Swarm (see section 1.2.2.2).

5.2.1.2.3 High-MgO LTZ picrites

The three high-MgO LTZ picrites were collected in the field just to the south of the Tuli Syncline in eastern Botswana. Two of these high-MgO LTZ picrites were sampled from dykes with widths of >19m and >35m (KLB-072 and -078 respectively) with strike

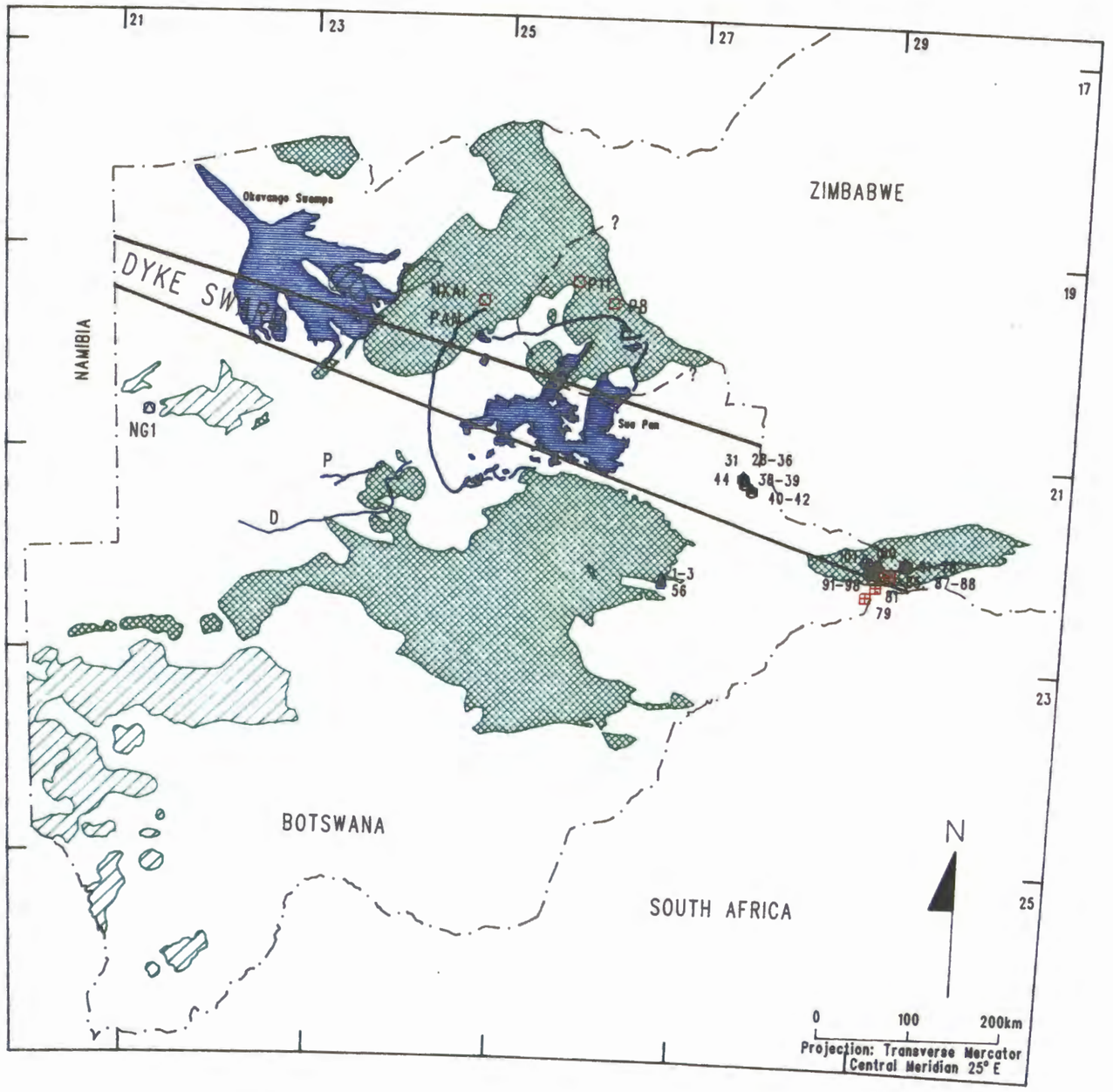

Fig. 5.2. The distribution of HTZ-type basalts and dolerites in Botswana

LEGEND

- Pans and swamps
- Basalts
- Sills

KAROO

- HTLZ BASALT
- HTLZ DOLERITE
- HTZ BASALT
- HTZ DOLERITE
- HTZ (LOW FE) BASALT
- HTZ (LOW FE) DOLERITE

Shoreline of former Lake Makgadikgadi
P: Passarge Mekgacha
D: Deception Mekgacha
Approximate northern limit of Letaba Picrites in the Tuli Syncline (Zimbabwe)
Postulated position of the Nata Sub-basin
International boundary

directions which ranged from ±NW-SE (KLB-072) to ±N-S (KLB-078). The third high-MgO LTZ picrite was sampled from a mafic pod which had poor outcrop exposure.

Aldiss (1983a & b) report the presence of petrographically similar Olivine Norites in the Semolale and Tsetsebjwe areas (*i.e.* to the north and northeast of the sample localities) where the Olivine Norites are typically present as irregularly curved sub-horizontal bodies intruded into the basement gneisses (see section 1.2.2.1) of the Limpopo Mobile Belt. The country rock could only be identified for KLB-078, which was intruded into a gneiss of the Archaean basement. These close petrographic and spatial relations therefore suggest that the high-MgO picrites are probably related to the Olivine Norites and are not Karoo aged.

5.2.2 HTZ-TYPE BASALTS AND DOLERITES

A total of 50 basalts and dolerites sampled in Botswana and in the Tuli Syncline of southeast Zimbabwe are defined as having an HTZ-type signature and the distribution of the HTZ-type basalts and dolerites is summarised in Fig. 5.2. The distribution of the HTLZ- and HTZ-type basalts and dolerites is described concurrently as they define a continuous range in geochemical compositions and samples with both an HTLZ- (KLB-068) and an HTZ- (KLB-067) type signature were collected from a single dolerite dyke in southwest Zimbabwe (see Fig. 5.2).

5.2.2.1 HTLZ/HTZ basalts

Basalts with an HTLZ/HTZ-type geochemical signature were sampled from the Tuli Syncline area, from the Central Kalahari Sub-basin and from western Botswana (see Fig. 5.2).

At least six different basalt flows with an HTLZ/HTZ-type signature were sampled in the Tuli Syncline. Due to the poor outcrop exposure in eastern Botswana neither the extent nor the thickness of individual flows could be determined, however KLB-100 was sampled from a basalt flow which defined a ±1km wide horseshoe-shaped ridge (clearly visible in the northwest corner of the 1988 1: 50 000 aerial photograph MOT 25 (161)). A single HTZ basalt KLB-002 has been recognised in the Central Kalahari Sub-basin. KLB-002 is a core sample from the borehole S326 drilled in the Serwe Pan to the north of Serowe and although no HTZ/HTLZ basalts were sampled from the adjacent borehole T529, only five samples were collected from the basalt interval. Both HTLZ- (KLB-177 and -178) and HTZ- (KLB-014) type basalts were sampled from the borehole NG1 which was drilled through an outlier of Karoo basalts in western Botswana.

5.2.2.2 HTLZ/HTZ dolerites

The collection of dolerites has been essentially limited to the eastern Botswana and Tuli areas due to poor outcrop exposure elsewhere in Botswana. The majority of the HTLZ/HTZ dolerites were sampled from within the main concentration of dykes associated with the dyke swarm in eastern Botswana and the Tuli Syncline areas (see Fig. 5.2). The only HTLZ/HTLZ dolerites sampled during this study which were not located within the dyke swarm were collected in the Serowe area along the southeastern margin of the Central Kalahari Sub-basin. One of these HTZ dolerites (KLB-056) was sampled from a dolerite sill. As the outcrop exposure in Botswana is generally very poor, the identification of the country rock into which the dolerites are intruded is difficult to ascertain and few HTLZ/HTZ dolerites are known to intrude basalt. In the Tuli area, two roughly parallel dolerite dykes are intruded into basalt. KLB-001, sampled in the Serowe area, is the only HTLZ/HTZ dolerite which is known to intrude basalt in the Central Kalahari Sub-basin.

The dolerite sample, KLB-030, has a LTZ-type signature as defined in Fig. 2.5A, but has a geochemical composition which is more similar to that of the HTLZ basalts and dolerites. KLB-030 was sampled from a narrow dyke, with a width of ±30cm, which was intruded into the northeast chill margin of a large dolerite dyke (samples KLB-028, -029 and -032) which has an HTLZ-type geochemistry (see Fig. 5.2).

5.2.2.3 HTZ (low Fe) basalts

HTZ (low Fe) basalts were sampled in the Tuli area and from three different boreholes (*i.e.* Nxai Pan, P11 and P8) in northeast Botswana (see Fig. 5.2). At least three different HTZ (low Fe) basalt flows were sampled in the Tuli area where two of these basalts (KLB-066 and -088) are characterised by their high modal proportions of plagioclase phenocrysts. As noted for the HTLZ/HTZ-type basalts, the extent and thickness of individual HTZ (low Fe) basalt flow units is obscured by the poor outcrop exposure in eastern Botswana.

5.2.2.4 HTZ (low Fe) dolerites

The only HTZ (low Fe) dolerites sampled during this study were only collected from within the Tuli Syncline area (see Fig. 5.2). Two of these HTZ (low Fe) dolerites were intruded into basalt, where KLB-091 was collected from a set of roughly parallel dolerites which intruded both basalt and dolerite, similar evidence of several generations of intrusion within the dyke swarm has been noted in the literature (*e.g.* Green, 1966; Aldiss 1983a & b; Clark and Machacha, 1982).

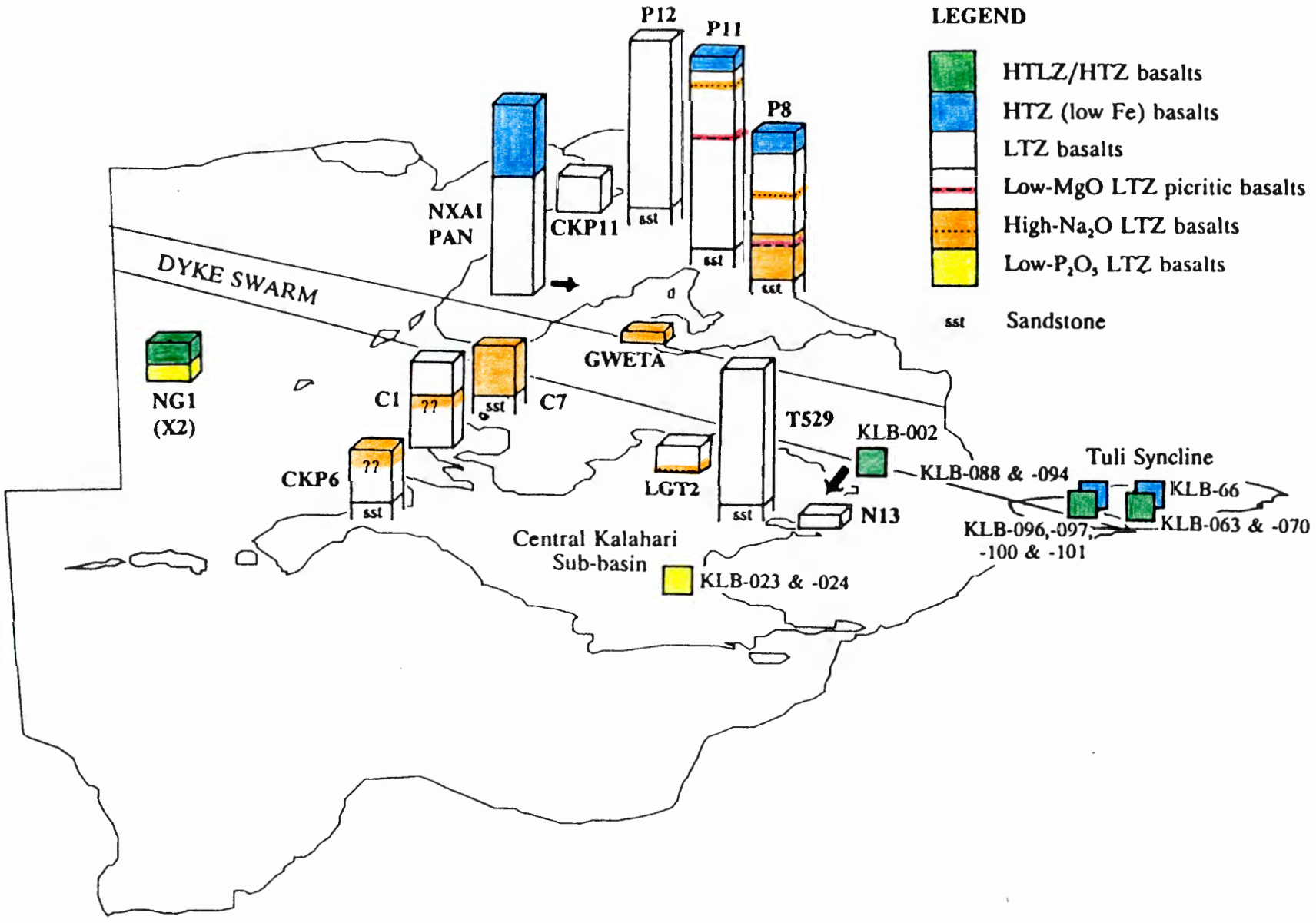

Fig. 5.3. A summary of the stratigraphy and distribution of the low-K_2O lineage basalt types in Botswana where the basalt outcrop localities are represented as squares for each rock type and the borehole stratigraphy is summarised in columns, where 1mm is equivalent to 10m. The stratigraphic columns are extended only where the contact between the base of the lava pile and the underlying sediments is intercepted by the borehole. In the boreholes CKP6 and C1 the exact thickness of the high-Na_2O LTZ basalt interval is not known as in both boreholes samples with a high-Na_2O LTZ- and LTZ-type composition were collected from within a single flow unit.

5.2.3 STRATIGRAPHIC RELATIONSHIP BETWEEN THE GEOCHEMICAL TYPES

Fig. 5.3 summarises the stratigraphy of the individual boreholes logged and illustrates the stratigraphic relationships between the different geochemical sub-groups. The HTZ-type basalts sampled from outcrop and the low-P_2O_5 LTZ basalts sampled from the southern margin of the Central Kalahari Sub-basin are included (square symbol) in Fig. 5.3 in order to give a more comprehensive picture of basalt distribution in Botswana.

In the Central Kalahari Sub-basin LTZ-type basalts dominate the lava pile (see Fig. 5.1) where high-Na_2O LTZ basalts are found interbedded with LTZ basalts in four of the stratigraphic sections (see Fig. 5.3). Only a single basalt sample, KLB-002, with an HTLZ/HTZ-type signature is present in the Central Kalahari Sub-basin and the stratigraphic relationship between this basalt and the voluminous LTZ-type basalts is not known. The thickness of the lava pile in the Central Kalahari Sub-basin is very variable (see TABLE 5.1 and Fig. 5.3) and a maximum thickness of >800m of basalt is intercepted by the Shadishadi borehole, which is drilled to the north of the Zoetfontein fault in the south of the Central Kalahari Sub-basin (see section 1.2.3.2.1). Three of the boreholes sampled in the Central Kalahari Sub-basin intercepted the base of the lava pile and in all cases the LTZ-type basalts overly Ntane sandstone (see TABLE 5.1) where Smith (1984) reports that the basalts in the borehole T529 overly metamorphosed Ntane sandstone (included in Fig. 5.3 as the core was not logged in any detail during this study).

In northeast Botswana the LTZ-type basalts similarly dominate the lava pile in all of the boreholes sampled where a thickness of >278m of LTZ-type basalt was intercepted by four of these boreholes. Low-MgO LTZ picritic basalts and high-Na_2O LTZ basalts are interbedded with the LTZ basalts in the two boreholes drilled in the Nata Sub-basin (P8 and P11). In three of the boreholes of northeastern Botswana (P8, P11 and Nxai Pan) HTZ (low Fe) basalts overlie the LTZ-type basalts in the stratigraphic columns (see Fig. 5.3). The thickness of this HTZ (low Fe) basalt is very variable and in the borehole P11 (with a basalt interval of 369.95m intercepted) a single thick basalt flow (26.1m from the top to bottom flow margins) had an HTZ signature while ±139m of basalt appear to have an HTZ signature in the Nxai Pan borehole (a minimum thickness of 367m of basalt intercepted), as the total Gamma reading had a constantly high value of ±100 API above ±275m (see APPENDIX A). In the borehole P8 four separate sedimentary layers (1.71m of red-brown sandstone, ±30cm of sandstone, 47cm of grey siltstone and ±20cm of red-brown sandstone) are interbedded with the basalts in the top 57.3m of the basalt interval (*i.e.* above the basalts with an LTZ-type signature). The three Shell Coal boreholes (P8, P11 and P12) intercepted the base of the lava pile and in all three cases the LTZ-type basalts are in contact with the

underlying sediments, *i.e.* Ntane sandstone in the borehole P11 and P12 and in the borehole P8 approximately 1m of sediment, predominantly siltstone, lies between the basalts and the rocks of the basement and according to Meixner and Peart (1984) the basalts of the borehole CKP11 overlie schists of the Ghanzi-Chobe basement.

In the borehole NG1 of western Botswana approximately 17m of HTLZ/HTZ basalt overlies what appears to be a single low-P_2O_5 LTZ basalt flow. The BGR Kalahari Project (GS-17-G) Drill log notes the presence of two sedimentary layers (1.3m and 43cm of red-brown sandstone) intercalated with the HTLZ/HTZ basalts of NG1, where the lower sedimentary lens appears to mark the change from a low-P_2O_5 to an HTLZ/HTZ type chemistry of the basalts (see APPENDIX A).

The HTZ-type basalts (*i.e.* both the HTLZ/HTZ and HTZ (low Fe) basalts) are therefore found stratigraphically above the LTZ-type basalt types in Botswana and the presence of these sedimentary layers interbedded between the LTZ and HTZ-type basalts and within the HTZ-type basalt interval in the boreholes P8 and NG1) suggests that periods of erosion and deposition occurred, at least locally, prior to, and during, the extrusion of the HTZ-type basalts.

The overall stratigraphy of the tholeiitic basalts of the Karoo Igneous Province, in general, can be summarised (after Marsh *et al.*, 1995) as follows:

HTZ.HF basalts
LTZ basalts (Lebombo-type)
HTZ.LF basalts
LTZ basalts (Lesotho-type)

The Lesotho LTZ type basalts are at the base of the lava pile and the HTZ.HF basalts are therefore youngest, although the age differences between the base and the top of the lava pile appear negligible. The stratigraphy of the basalts of Botswana follow this general pattern, although no Lebombo LTZ-type basalts are found in Botswana. However, although the HTLZ/HTZ basalts of Botswana do not have the distinctive low Zr/Nb ratio of the HTZ.HF basalt type of the Tuli and Central Lebombo areas, the resemblances in geochemistry and stratigraphic position support a correlation between the HTLZ/HTZ basalts of this study and the HTZ.HF basalts of the Central Lebombo and Tuli areas.

5.2.4 THE DYKE SWARM

The vast majority of the dykes collected from within the dyke swarm had an HTLZ/HTZ-type geochemical signature, where only HTLZ/HTZ dolerites were sampled from the dyke swarm of eastern Botswana (see Fig. 5.2). The relationship between the two TYPE I LTZ dolerites, which were sampled adjacent to the southern margin of the dyke swarm in the Central Kalahari Sub-basin (see Fig. 5.1), and the actual dyke swarm is not known as unfortunately no details regarding strike, width or country rock were available for these two TYPE I LTZ dolerite dykes. Both HTLZ/HTZ-type and HTZ (low Fe)-type dolerites were sampled from the Tuli Syncline area, but the relationship between these dolerite dykes and the dyke swarm is not known. It is possible that some of these dolerites may have been feeders to the lava pile prior to the intrusion of the dyke swarm where Duncan (*pers. comm.*, 1994) noted that the distribution of the HTZ.LF type dolerites of Tuli Syncline area (*i.e.* equivalent to the HTZ (low Fe) dolerites of this study) is restricted to the outcrop area along the southwestern margin of the Tuli Syncline of the HTZ.LF basalts.

A strike direction of ±W to WNW was measured, where a strike reading was possible, for all of the HTLZ/HTZ dolerites collected within the dyke swarm. Although the strike length of the HTLZ/HTZ dolerites was typically obscured by poor outcrop at least two of the HTZ dolerites could be traced for ≥8km along their strike length in the 1988 1:50 000 aerial photographs. Similarly, the strike of the HTZ (low Fe) dolerites, where observed, was predominantly ±WNW (parallel to the strike of the dyke swarm), however, a single set of roughly parallel HTZ (low Fe) dolerites had a local strike of N10E. A strike length of ≥8km for a single HTZ (low Fe) dolerite could be traced in the 1988 1:50 000 aerial photographs. The HTZ-type dolerites are known to intrude basalt in the Tuli Syncline and, in a single example, in the Central Kalahari Sub-basin and K-Ar age determinations (see section 1.2.3.4) for the dolerites sampled in both the Central Kalahari Sub-basin and in the Tuli Syncline range from 162±3 to 140Ma (after Rundle, 1983 and Coates *et. el.*, 1979), although these younger ages probably reflect Ar loss from the samples. These younger ages recorded for the dolerites suggests that at least some of the HTZ-type basalts and dolerites in Botswana and the Tuli Syncline may be considerably younger than the underlying ±180Ma basalts (see section 1.2.3.4). The quiet periods associated with local erosion and deposition prior to, and during, the eruption of the HTZ-type basalts appears to support this possible younger age for some of the HTZ-type basalt and dolerites. The scattered distribution of HTZ-type basalts in Botswana and their position at the top of the stratigraphic sections suggests that the HTZ-type magma may have had a more extensive distribution in Botswana prior to post-Karoo erosion.

More detailed sampling and geochronological studies are required in order to ascertain the relative age of the dyke swarm in Botswana, but as the dolerites of the dyke swarm have a predominantly, if not exclusively, HTLZ/HTZ-type geochemistry, evidence suggests that the intrusion of the dyke swarm occurred after the extrusion of the LTZ- and HTZ (low Fe)-type basalts. The basalts and dolerites with an HTLZ/HTZ-type signature have essentially identical compositions (see section 2.3.2.3) which suggests that the intrusion of these dolerite dykes associated with the dyke swarm could plausibly have acted as feeders to the rare HTLZ/HTZ basalts which have a diverse distribution in Botswana.

5.3 HIGH-K_2O LINEAGE

The high-K_2O lineage includes both high-K_2O picritic basalts and shoshonites (see Fig.2.4). These high-K_2O lineage samples were all collected within the Tuli Syncline and no high-K_2O lineage examples have been recognised elsewhere in Botswana.

The high-K_2O picritic basalts were collected from along the southern margin of the basalt outcrop in the Tuli Syncline, *i.e.* within the general area in which Vail *et al.* (1969) noted the presence of olivine-rich basalts. The high-K_2O picritic basalts were extruded onto a remnant dunefield topography of aeolian sandstone, preserved as the Tsheung formation (a lateral equivalent to the Ntane Sandstone). The high-K_2O picritic basalts therefore lie at the base of the lava pile in the Tuli area as do the Letaba picritic basalts of the Nuanetsi and Northern Lebombo areas (Bristow, 1984b).

Four of the shoshonite samples (KLB-057 to -060) were collected from a single dyke in the Tuli area of southeastern Zimbabwe. This 10-30m wide shoshonite dyke has an approximate E-W strike direction and a strike length of ±33km and is cross-cut by a minimum of seven faults (with strike directions which range from ±NNW to ±NE) according to the Rhodesia Geological Series 1: 100 000 maps of the Tuli and Mazunga areas, which accompany the Short Report No. 40 (Geological Survey of Rhodesia, 1974). The shoshonite dyke crosses the Pazhi (Ipayi) River in the same general area in which Vail *et al.* (1969) collected the shoshonite samples TV-48 and -49, although KLB-057 to -060 were sampled ±7 to 10km to the west. The two remaining shoshonites were collected from within the Tuli Syncline in Botswana. One of these shoshonites was collected from a dyke with a strike of N100E, *i.e.* parallel to the strike of the dyke swarm, while the other was sampled from a float block in a dry river bed, with the source outcrop probably to the north of the sample location.

5.4 FELSITES

The felsite dykes are located along the southern margin of the Tuli Syncline in eastern Botswana which suggests that their host rock is possibly Tsheung Formation sandstone, although no country rock was observed in the field. Both felsite dykes are visible as positive topographic features in the 1988 1:50 000 aerial photograph MOT 29 (333) with strike directions of ±N65E and approximately due north and strike lengths of 2km and 3.5km (KLB-080 and -082 respectively). These two dykes are the only examples of Karoo felsic magmatism noted in Botswana (see section 1.2.3.3.2) or in the Tuli Syncline of Zimbabwe (Vail *et al.*, 1969).

6 PETROGENESIS

6.1 LOW-K_2O LINEAGE

6.1.1 LTZ-TYPE BASALTS

The LTZ-type basalts have been shown (see chapters 2 and 4) to include a number of geochemical sub-groups and the possible relationships that exist between these sub-groups and the dominant LTZ basalt composition are described before the LTZ basalt petrogenesis is discussed.

6.1.1.1 Low-MgO LTZ picritic basalts

In section 4.1.1 it was noted that the major and trace element whole rock composition of the low-MgO LTZ picritic basalts indicated that olivine accumulation or fractional crystallization played an important role in the relationship between the low-MgO LTZ picritic basalts and the LTZ basalt type. Eales and Marsh (1979), however, proposed that all of the high-MgO tholeiitic magma compositions present in the Central Karoo area (found predominantly as intrusive dolerites) could be related to the average Stormberg- (or Lesotho-) type magma composition by the accumulation of olivine as the Ni/Mg and Mg/Fe ratios determined for the olivine compositions in these high-MgO tholeiites were incompatible with the equilibrium of the olivine in a high-MgO liquid. The remarkable similarity in the whole rock composition of the LTZ-type basalts of Botswana and the Lesotho-type basalt of the Central Karoo area (see section 4.1.1) and the noted absence of primary high-MgO liquids in the Central Karoo area, suggests that the low-MgO LTZ picritic basalts are most likely to be related to the LTZ basalt type by accumulation processes. As only pseudomorphs after olivine are preserved in the LTZ-type basalts (*i.e.* including the low-MgO LTZ picritic basalts) the possible equilibrium or disequilibrium relationships between the olivine and respective whole rock compositions could not be determined. However a cumulus origin for the low-MgO LTZ picritic basalts is supported by both the geochemistry and petrography of these low-MgO LTZ picritic basalts (see section 3.1.1.1.1 and 4.1.1). For example, in a single 53.2m thick basalt flow unit sampled from the borehole P11, the MgO concentration shows a variation from 7.04 through 6.57 to 10.51 wt% in a vertical section (KLB-126 to -128 respectively) with the three samples (KLB-126, -127 & -128) collected from 10.83-11.02m, 15.15-15.30m and 34.4-34.70m, respectively, below the upper flow margin. This variation in MgO concentrations is reflected in the

modal proportions of the olivine pseudomorphs present, where 10.1 and 3.7 modal% olivine pseudomorphs were determined by point-counting for KLB-128 and KLB-127 respectively. The sympathetic enrichment of Ni, Cr and Co and depletion of the incompatible trace elements (*e.g.* Rb and Zr in Fig. 4.3A & C) relative to MgO in this single basalt flow are in qualitative accord with a possible cumulus enrichment process occurring towards the base of the flow with an associated loss of phenocrysts from the upper part of the flow. The incompatible trace elements Ba, Cu and Zn do not show the expected depletion in concentration in KLB-128 relative to KLB-126, possibly reflecting the susceptibility of these elements to alteration processes (see section 4.1.1.5).

Quantitative modelling of the low-MgO LTZ picritic basalts by cumulus enrichment of the LTZ-type basalt is hampered by a lack of data and sample control, and the initial low-MgO LTZ picritic basalt composition, prior to cumulus enrichment, is not known. If the composition of the basalt sample KLB-126 is used as an estimate of the original liquid composition; justifiable as it has a whole rock composition which is similar to the average LTZ basalt type, the composition of KLB-128 can be modelled by cumulus enrichment. TABLE 6.1 tabulates the best major element model obtained for KLB-128 by cumulus enrichment of KLB-126, using the least squares linear approximation method of Bryan *et al.* (1969). The major element model is slightly improved by the addition of titanomagnetite to the cumulus assemblage, but this is inconsistent with the trace element models. The input data used in the model had all Fe as Fe_2O_3* and was normalised to 100% volatile-free. As only pseudomorphs after olivine were present in this basalt flow and as the few olivine compositions obtained during this study for the LTZ-type basalts appear to have been re-equilibrated (see section 3.1.2.1) an olivine composition (*i.e.* core of olivine phenocryst 4, JP-17) from the Lesotho-type basalt of the Central Karoo area was used (data obtained from the microfiche cards in the Geological Society of South Africa Special Publication No. 13, 1984). The plagioclase (PLAG3B) and augite (CPX2A) compositions used in the model are microprobe analysis of minerals in KLB-128 (see APPENDIX C).

The modelled trace element concentrations in crystal accumulation processes can be determined, assuming surface equilibrium, using the le Roex and Reid (1978) modification of the Gast (1968) equation, which is:

$$C_a/C_a^o = (1-F^D)/(1-F)$$

where: C_a is the average concentration of the element a in a suite of perfectly zoned minerals

C_a^o is the concentration of the element a in the original liquid

F is weight fraction of liquid remaining

D is the bulk distribution co-efficient for the element a

le Roex and Reid (1978) note that for successful quantitative trace element accumulation models it is necessary to assume: (1) A homogenous distribution of phenocrysts in the magma and (2) that all of the phenocrysts migrate to the enriched zone at that instant when the weight fraction of liquid remaining equals F. These assumptions allow the maximum value of F to be estimated using the equation:

$$F = 1\text{-}M(V_1/V_2)$$

where: M is the weight fraction of phenocrysts added to the cumulus enriched zone (obtained from the major element model)

V_1 is the volume of the cumulus enriched zone

V_2 is the volume of the magma from which the cumulus crystals are derived.

The ratio V_1/V_2 can be estimated by the respective thicknesses of the two volumes if it is assumed that the direction of phenocryst migration is predominantly vertical. The concentration of the trace elements in the cumulus enriched zone can then be calculated using the equation:

$$C_a^c = C_a^o(1\text{-}M) + (C_a * M)$$

Only three samples are available from the basalt flow and thus the relative thickness of the possible cumulus enriched zone cannot be determined without further sampling. For similar reasons the different physical processes that may be involved in accumulation (*e.g.* flowage differentiation or gravity settling) cannot be identified. The concentration of trace elements listed in TABLE 6.1 for the model composition were calculated using the distribution coefficients listed in TABLE 6.2, assuming that 30% of the basalt flow was cumulus enriched as an estimated 30% accumulation gives the most satisfactory model of trace element concentrations. An increase in the relative thickness of the cumulus enriched zone results in a decrease of the value of F and gives even less satisfactory trace element model concentrations. Although there is a relatively good correlation between the model composition and KLB-128 for the compatible elements (Ni, Cr and Co), the model incompatible element concentrations correlate less well with KLB-128. The less than satisfactory correlations may be due to invalid assumptions in the quantitative trace element model and it is also a possibility that a reaction between the accumulated crystals and the liquids occurred (Gast, 1968).

The assumption that 30% accumulation occurred, however, suggests that gravity settling could only be an important process if the lower chill margin of the basalt flow was at least 2.84m thick and was excluded from the accumulation process, otherwise KLB-128 is not included in the cumulus enriched zone. The major element model also requires the presence of augite in the phenocryst assemblage, but augite is very rarely seen as a phenocryst phase in the LTZ basalts and flowage differentiation may therefore be an

	INPUT DATA					MODEL	
	KLB-126	Olivine	Plag.	Augite	KLB-128	Component	%
SiO_2	52.48	37.00	50.6	53.03	50.28	KLB-126	69.48
TiO_2	.93			.28	.78	OLIVINE	12.49
Al_2O_3	15.03		30.96	1.86	14.02	PLAGIOCLASE	11.21
Fe_2O_3*	10.94	27.79	.84	7.13	11.65	AUGITE	6.82
MnO	.16				.19		
MgO	7.04	35.21	.1	17.99	10.51		
CaO	10.10		14.93	19.54	10.03		
Na_2O	2.38		2.44	.17	1.99		
K_2O	.80		.13		.43		
P_2O_5	.14				.12		

CUMULATE MODEL FOR KLB-128

	Major elements				Trace elements		
	KLB-128	MODEL	DIFF.		KLB-126	KLB-128	MODEL
SiO_2	50.28	50.37	.09	Rb	22	8.3	16
TiO_2	.78	.67	-.11	Ba	143	149	104
Al_2O_3	14.02	14.04	.02	Sr	198	170	177
Fe_2O_3*	11.65	11.65	.00	Zr	73	60	55
MnO	.19	.11	-.08	Nb	4.7	4.9	3.4
MgO	10.51	10.53	.02	Cr	335	497	452
CaO	10.03	10.02	.00	V	233	182	196
Na_2O	1.99	1.94	-.05	Sc	38	30	36
K_2O	.43	.57	.14	Ni	90	189	187
P_2O_5	.12	.10	-.02	Co	48	62	59
				Zn	82	83	79
				Cu	52	66	37
				Y	23	20	17
				La	7.6	7.5	5.4
				Ce	18	18	13
				Nd	9.1	10	6.6

SUM OF SQUARES OF MAJOR ELEMENT DIFFERENCES = 0.05

TABLE 6.1. A quantitative model to derive KLB-128 by phenocryst enrichment of a magma with a composition of KLB-126.

	MINERAL PHASES		
	Olivine	Plagioclase	Augite
Rb	.05	.05	.06
Ba	.0001	.3	.002
Sr	.07	1.6	.08
Zr	.04	.06	.6
Nb	.15	.1	.05
Cr	3	.02	5
V	.14	.01	1.8
Sc	.22	.01	3.2
Ni	6.414(**)	.05	2.8
Co	3.8	.02	1.2
Zn	1.8	.1	.5
Cu	.02	.05	.07
Y	.01	.1	.42
La	.0002	.07	.069
Ce	.0005	.1	.098
Nd	.001	.18	.18

TABLE 6.2. The trace element distribution coefficients used in the petrogenetic model (after Duncan *et al.*, 1989). The Ni distribution coefficient for olivine is calculated using the formula of Smith *et al.* (1980).

important accumulation process as it provides a mechanism for the segregation of early formed minerals towards the central axis of the conduit (Bhattacharji and Smith, 1964). Furthermore if flowage differentiation plays an important role in the accumulation process, the direction of phenocryst migration is unlikely to be dominated by vertical movement and the volume of the magma from which the cumulus crystals were derived and the volume of the cumulus enriched zone cannot be estimated by the relative thicknesses of the two zones as seen in a vertical section.

6.1.1.2 High-Na_2O LTZ basalts

The compositions of high-Na_2O LTZ basalts have been shown to resemble the whole rock compositions of the LTZ basalts for all major and trace elements, except for the elevated Na_2O concentrations and the associated depletion in CaO concentrations of the high-Na_2O LTZ basalts (see Fig. 2.3 and sections 2.3.2.2 and 4.1.1). In addition, within a single basalt flow unit the Na_2O concentration may vary such that different samples from the within the same flow can be classified as high-Na_2O LTZ basalts (*e.g.* KLB-187 and -055) and LTZ basalts (*e.g.* KLB-188 and -054).

In section 3.1.2.3 it was suggested that the albitization of plagioclase in the LTZ and high-Na_2O LTZ basalts occurred as result of alkali and alkali-earth cation exchange between plagioclase and saline hydrothermal solutions (Lagarche, 1984). However, in section 5.2.1.1 (see also Fig. 5.1) it was shown that the distribution of the high-Na_2O LTZ basalts could be interpreted in relation to their proximity to the salt plans and playa lakes associated with the ancient drainage patterns now preserved in the Kalahari Beds of Botswana. Furthermore, the composition of the water in the Karoo basalts is also known to be locally saline with the Ntane sandstone, the Karoo basalts and the Kalahari sands in hydraulic continuity (section 1.2.5). The high-Na_2O LTZ basalts may therefore possibly be related to the LTZ basalts either by alteration processes associated with percolating saline ground waters or by saline hydrothermal fluids.

6.1.1.3 Low-P_2O_5 LTZ basalts

The low-P_2O_5 LTZ basalts can be distinguished both petrographically and geochemically from the LTZ basalt type (see sections 3.1.1.1.2 and 4.1.1). The low-P_2O_5 LTZ basalts have a phenocryst assemblage which includes plagioclase, alkali feldspar (perthite), clinopyroxene and pseudomorphs after olivine, in contrast to the plagioclase-only phenocryst assemblage which typifies the LTZ basalts. The low-P_2O_5 LTZ basalts also have a higher modal proportion of oxide present than the LTZ basalts (see TABLE 3.1), where the oxide is concentrated in the mesostasis of the low-P_2O_5 LTZ basalts. The low-P_2O_5 LTZ basalts are characterised by their evolved whole rock geochemistry (MgO concentrations ranging from

6.17 to 4.72 wt%) and exhibit considerable scatter in their whole rock compositions (*e.g.* see Fig. 4.1A & B), where some of the scatter may reflect the extreme degree of alteration shown, in particular, by some of the low-P_2O_5 LTZ basalts collected from the borehole NG1. Although the compositions of the low-P_2O_5 LTZ basalts lie on the evolved end of the coherent trends defined by many of the inter-element ratios of the LTZ basalts, they can be clearly differentiated as a distinct geochemical type, *e.g.* see TiO_2/P_2O_5 ratios in Fig. 2.11. The low-P_2O_5 LTZ basalts tend to have lower SiO_2, Na_2O, P_2O_5, Ba and Nb contents and have elevated TiO_2, Fe_2O_3*, Ni, Co, V and Cu concentrations relative the more evolved LTZ basalt compositions. These slight differences are reflected in the higher Zr/Nb and Ti/Zr ratios of the low-P_2O_5 LTZ basalts with respect to the LTZ basalt types (see Fig. 6.1).

The low-P_2O_5 LTZ basalts are difficult to characterise as a compositional group because of the range in the whole rock compositions (including their chondrite-normalised REE patterns (see section 4.1.1.3)) and more detailed geochemical studies are required before their relationship with the LTZ basalt-type can be evaluated in detail. Any possible genetic relationship that may exist between the low-P_2O_5 LTZ basalts and the LTZ basalt type must account for the distinct phenocryst assemblage present in the low-P_2O_5 LTZ basalts (which includes the only recognised occurrence of alkali feldspar in a LTZ-type basalt of Botswana) and must also take into consideration the distribution of the low-P_2O_5 LTZ basalt type as they are found in both western Botswana and in the southeast of the Central Kalahari Sub-basin (see section 5.2.1.1). The low-P_2O_5 LTZ basalts and LTZ basalt type are unlikely to be related by any simple fractionation process as neither fractional crystallization nor partial melting provide a mechanism for the inclusion of alkali feldspar in the phenocryst assemblage of the low-P_2O_5 LTZ basalts and neither process can account for the differences that exist between the whole rock compositions of the two rock types. For example, the value of Zr/Nb and Ti/Zr ratios (see Fig. 6.1) are generally accepted to be relatively insensitive to continued fractional crystallization or to different degrees of partial melting (Pearce and Norry, 1979), and differences in the Zr/Nb and Ti/Zr ratios may therefore reflect heterogeneities in the source area of the LTZ basalt types. Although the compositionally diverse early formed magmas of the Central Karoo area have been interpreted to reflect source heterogeneities (Marsh and Eales, 1984), this seems an unlikely mechanism to explain the generation of the low-P_2O_5 LTZ basalts as it requires that the geographically separated low-P_2O_5 LTZ basalts must have a source composition which was distinctly different to that of the dominant LTZ basalt type. Furthermore, heterogeneities in the source are unlikely to account for the presence of alkali feldspar in the phenocryst assemblage of the low-P_2O_5 LTZ basalts. If alkali feldspar is present as a xenocryst phase in the low-P_2O_5 LTZ basalts, contamination of the low-P_2O_5 LTZ basalt liquid may have occurred, but without isotopic studies it is difficult to assess the role of contamination in the

petrogenesis of the low-P_2O_5 LTZ basalts. The high TiO_2, Fe_2O_3*, V and Ni concentrations of the low-P_2O_5 LTZ basalts with respect to the LTZ basalt compositions are inconsistent with the generation of the low-P_2O_5 LTZ basalt compositions by any AFC model involving the assimilation of typical upper crustal rock compositions into LTZ basalt composition (see Marsh, 1989). The petrogenesis of these low-P_2O_5 LTZ basalts is not clear at this time and the detailed studies which are required to elucidate their origin are beyond the scope of this thesis.

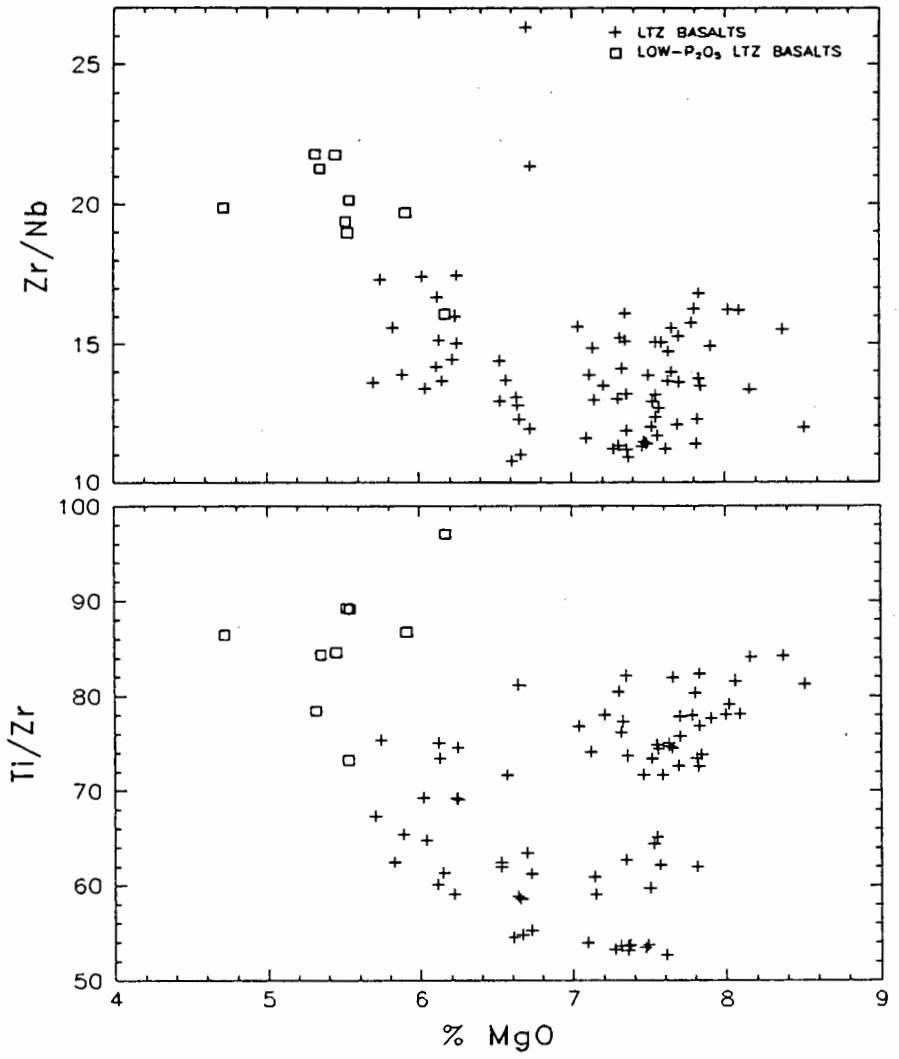

Fig. 6.1. (A) Zr/Nb and (B) Ti/Zr ratios of the low-P_2O_5 LTZ basalts and the LTZ basalts *vs.* MgO

6.1.1.4 LTZ basalt

The whole rock compositions of the LTZ basalts of Botswana have been shown to resemble very closely the compositions of the Lesotho Formation basalts of the Central Karoo area (see section 4.1.1.4) and the petrogenesis of the LTZ basalt type is therefore briefly discussed in relation to the models available in the literature for the generation of the Lesotho Formation basalts. The Lesotho Formation basalts of the Central Karoo area (and by inference the LTZ-type basalts of Botswana) are characterised by their monotonous

petrography and whole rock geochemistry. They have variable initial Sr-isotope ratios with most of the samples falling between 0.70458±5 - 0.70686±6 (Marsh and Eales, 1984). The recognition of the LTZ-type/Lesotho Formation basalts in Botswana therefore considerably expands the volume of this magma type.

The compositional variations shown by the Lesotho Formation basalts of the Central Karoo area are broadly consistent with low pressure gabbro fractionation involving 20-30% crystallization of an olivine-augite-plagioclase fractionating assemblage (Cox, 1980; Cox and Hornung, 1966; Pemberton, 1978). The Lesotho Formation basalts and the LTZ basalts, see for example data for P11 in Fig. 4.3, typically show an up-sequence differentiation and Pemberton (1978) showed that 25-30% fractionation of an assemblage consisting of 70% plagioclase, 15% augite and 15% olivine could account for the variation in composition displayed by the Lesotho Formation basalts of Naude's Nek Pass, although the high proportion of plagioclase is inconsistent with the approximately constant Al_2O_3 concentrations. Cox (1988b) suggests that replenishment, extrusion and fractionation can explain the disturbance between the expected correlation of basalt chemistry and stratigraphic height (see for example Fig. 4.3). Although all the fractional crystallization models proposed to explain the within-group variation of the Lesotho Formation basalts of the Central Karoo area require augite in the fractionating assemblage, augite is seldom seen as a phenocryst phase and Cox (1980) uses the absence of augite phenocrysts as evidence for the polybaric fractionation of the Lesotho Formation magma. He suggests that an initial period of olivine-augite-plagioclase fractionation occurred and this was followed by a change in pressure and subsequent crystallization until the liquids were in equilibrium with olivine and plagioclase only. Polybaric fractionation can cause a cross-trend scatter which may explain the poor correlation in the Al_2O_3 and CaO *vs.* MgO variation diagrams (see Fig. 4.1A). The polybaric fractionation of an olivine-augite-plagioclase phase assemblage is also proposed as an explanation for the uniformity of the Lesotho Formation basalt magma compositions as it offers a mechanism to buffer the compositional variation associated with fractionation from a picritic precursor (Cox, 1980). Marsh and Eales (1984), however, propose that the Lesotho Formation magma was generated by polybaric fractionation dominated by olivine from a picritic precursor melt with a composition of approximately 12-18% MgO. They suggest that it is plausible that melting, magma ascent and eruption approached a steady state and the compositionally restricted Lesotho Formation magmas, and therefore by inference the LTZ basalts of Botswana, could have undergone similar amounts of cooling and fractional crystallization.

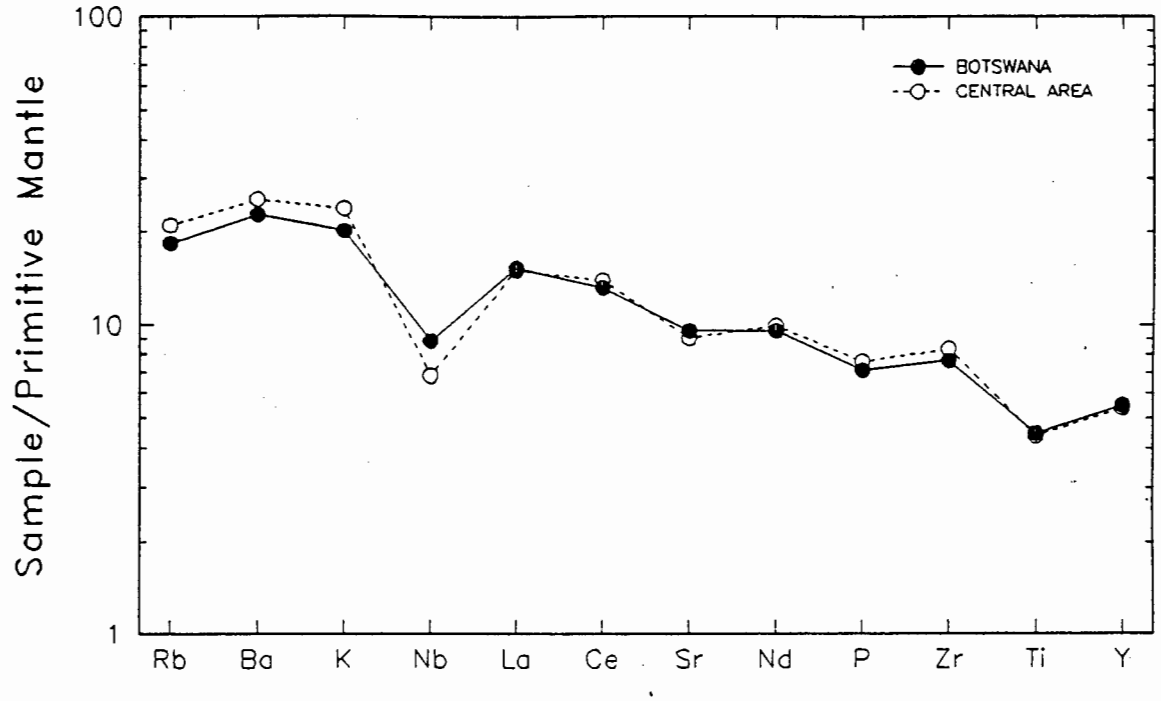

Fig. 6.2. Primitive normalised patterns of the average LTZ basalt of Botswana and the Lesotho Formation basalt of the Central Karoo area. Primitive mantle concentrations after Sun and McDonough (1989).

In Fig. 6.2 the average composition of the Lesotho Formation and LTZ-type basalts of Botswana are normalised to primitive mantle compositions (see Marsh and Eales, 1984; Marsh, 1987) where the basalt composition are enriched in Rb, Ba, K, REE, Nd and Nb and Sr, although Nb and Sr are relatively depleted in concentration with respect to the other incompatible elements. Duncan *et al.* (1984a) suggests that these negative anomalies shown by the Nb and Sr concentrations of the Lesotho Formation (and the LTZ-type) basalt compositions are inconsistent with either a fractional crystallization or partial melting origin and rather represent the compositional characteristics of the Central Karoo area (and Botswana) source area. The nature of this source for the LTZ basalt types of the Karoo Igneous Province, and of continental flood basalt provinces in general, is the subject of considerable debate in the literature. Arndt *et al.* (1992 & 1993) argue, using thermomechanical modelling, that continental flood basalts must have an asthenospheric/plume source where the LTZ-type basalts, in general, would be the product of a relatively high degree of partial melting of asthenospheric material which has ascended to a relatively shallow depth in areas where the lithosphere is relatively thin. They suggest that the characteristic relatively low Nb concentrations of continental flood basalts could result from processes which occur either in the passage of the magma through the lithosphere or in shallow level magma chambers. Sweeney *et al.* (1994) however, argue that the LTZ-type basalts of the Central Lebombo can be derived from a picritic precursor which represents a mixture of an asthenospheric (plume) source and a more depleted (with respect

to basaltic components, trace elements and isotopic ratios) source, which is correlated with a shallow level sub-continental lithosphere (after Sweeney *et al.* (1991). The location of the LTZ-type basalts of the Karoo Igneous Province peripheral to the Archaean cratons favours this shallow level of equilibrium (see Sweeney and Watkeys, 1990). Sweeney *et al.* (1994) propose that a process such as plume incubation (see Saunders *et al.*, 1992) offers a mechanism to provide the heat over a period of time sufficiently long to induce melting of, or at least equilibrium between, the lithospheric and asthenospheric components. In contrast, the distinct primitive mantle-normalised patterns defined by the LTZ-type basalts (*e.g.* see Fig. 6.2) and the characteristic low Ti/Y and Ti/Zr and high Rb/Ba compositions of the LTZ-type basalts of continental flood basalts provinces in general (Hawkesworth *et al.*, 1983; Hergt *et al.*, 1991) have been proposed to be in some way unique to an enriched sub-continental lithospheric source where the mantle plume is therefore required only to provide the heat required for the generation of the LTZ-type basalt (Hergt *et al.*, 1991). The possible processes involved in the source area enrichment are similarly the subject of considerable debate in the literature, with various authors proposing a hydrous alkali-rich fluid or small volume melt type enrichment process (Erlank *et al.*, 1980; Hawkesworth *et al.*, 1984; Duncan *et al.*, 1984a; Duncan, 1987) whereas other authors suggest that active subduction beneath southern Africa may be involved (Cox, 1978 & 1983; Hawkesworth *et al.*, 1983; Hergt *et al.*, 1989 & 1991). As the present study of the LTZ-type basalts of Botswana offers no new data for the above mentioned debates, any further discussion of the LTZ-type petrogenesis is beyond the scope of this thesis.

6.1.2 HTZ-TYPE BASALTS AND DOLERITES

The presence of "enriched" basalts and dolerites in the Karoo Igneous Province was first noted by Cox *et al.* (1967) (see section 2.3.1.1), although subsequently two chemically distinct enriched basalt types, *i.e.* the HTZ.LF or High Ti-Zr and the HTZ.HF or High-Fe sub-groups, have been recognised in the Central Lebombo and Tuli areas (Sweeney *et al.*, 1994; Duncan *et al.*, 1995). The petrogenesis of these two enriched basalt types from the Central Lebombo area is described in detail in Sweeney (1988) and Sweeney *et al.* (1994) and therefore the petrogenesis of the HTLZ/HTZ and HTZ (low Fe) basalt and dolerites of Botswana are described in relation to these enriched basalt types of the Central Lebombo area.

6.1.2.1 HTLZ/HTZ basalts and dolerites

The majority of the "enriched" samples from the low-K_2O lineage of Botswana are defined as having an HTLZ/HTZ-type geochemical signature in section 4.1.3. The HTLZ/HTZ basalts and dolerites of Botswana resemble, in many aspects, the HTZ.HF basalts of the

Central Lebombo area. In section 2.3.1.3.2 the HTLZ/HTZ basalts and dolerites were shown to have a similar whole rock geochemistry and REE composition to the HTZ.HF basalts (*e.g.* see Fig. 2.4 and Fig. 2.7 - 2.9), which implies that the HTLZ/HTZ and HTZ.HF magma compositions are produced by similar degrees of partial melting from a source which had broadly similar compositions, although these HTLZ/HTZ basalts and dolerites of Botswana do not have the characteristic low Zr/Nb ratio (12±2) of the HTZ.HF basalts (see Fig. 2.10C & D).

Sweeney (1988) and Sweeney *et al.* (1994) propose that the within-group compositional variation shown by the HTZ.HF basalts can be attributed to fractional crystallization, *i.e.* in a closed and/or RTF (replenished, tapped and fractionated) magma system, of a clinopyroxene and plagioclase fractionating assemblage which also includes minor amounts of olivine and titanomagnetite. The major element compositions, in particular the decreasing Al_2O_3 concentration with decreasing MgO concentrations (see section 4.1.3.1 and Fig. 6.3), of the HTLZ/HTZ basalts and dolerites suggest a similar type of gabbroic fractional crystallization can account for at least some of the variations in the major and trace element compositions shown by the HTLZ/HTZ basalts and dolerites. The HTLZ/HTZ basalts and dolerites initially show an increase in TiO_2 concentration with decreasing MgO concentrations, which excludes titanomagnetite/ilmenite from the fractionating assemblage. However at ±4-5% MgO the TiO_2, together with V and Sc, concentrations exhibit a change in slope direction *vs.* MgO which may reflect the later inclusion of titanomagnetite/ilmenite in the fractionating assemblage.

The HTLZ/HTZ basalts and dolerites are characterised by the considerable range in their petrography and mineralogy. The HTLZ/HTZ basalts and dolerites vary from aphyric to porphyritic, with variable modal proportions of phenocrysts present where plagioclase is commonly the dominant phenocryst phase, and in at least five basalt and dolerite samples, both a phenocryst and "megacryst" assemblage is recognised (see section 3.1.1.2). The mineral compositions of the HTLZ/HTZ basalts and dolerites reflect the complexity of the HTLZ/HTZ basalt and dolerite petrography. The "megacryst" and phenocryst plagioclase compositions are similar to the matrix plagioclase compositions (see section 3.1.2.3) and define similar Or *vs.* An trends with respect to the plagioclase compositions of the LTZ-type basalts (see Fig. 3.4). Furthermore, in a single example, an augite included in a "megacryst" aggregate in an HTZ basalt (KLB-096) shows a considerable range in Ti^{4+} concentrations from the core to the margin of this single grain. The Ti^{4+} concentration in the core of the augite "megacryst" resembles LTZ-type augite compositions, whereas the margin has typical HTLZ/HTZ basalt and dolerite augite Ti^{4+} concentrations, which suggests that the pyroxene "megacryst" has either re-equilibrated with a TiO_2-rich liquid or results from the continued

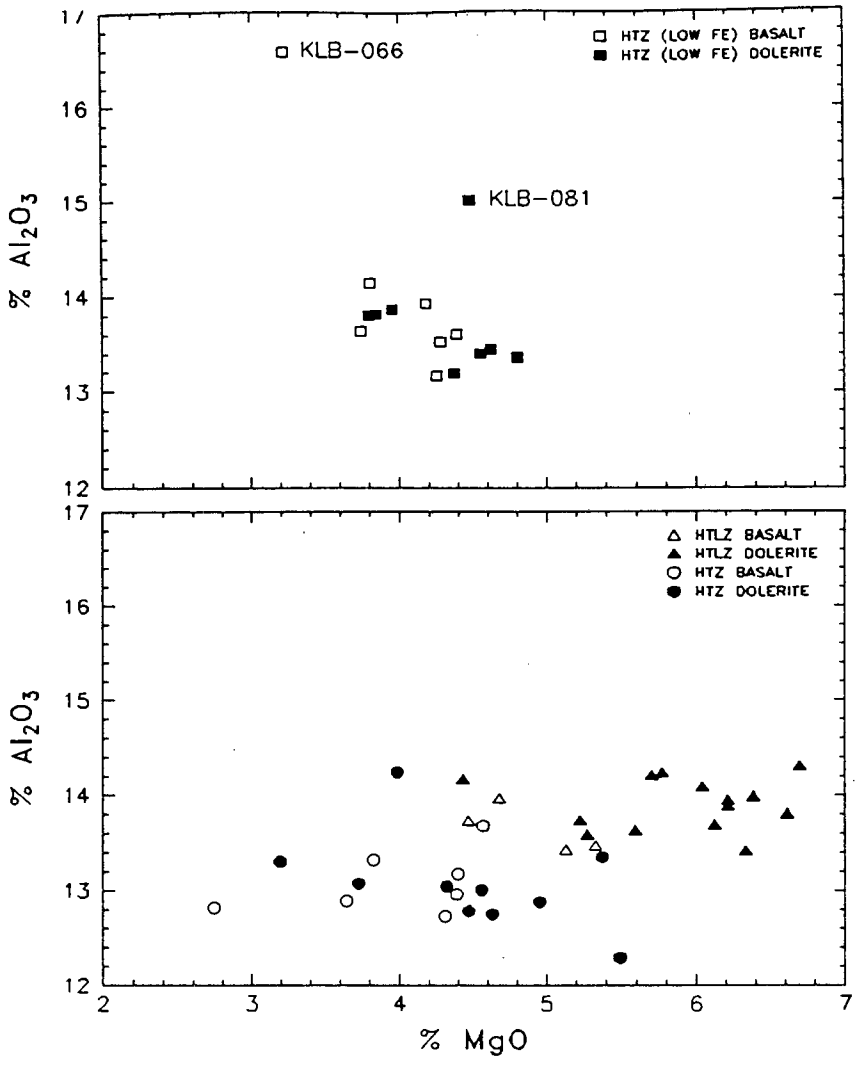

Fig. 6.3. Al_2O_3 *vs.* MgO for (A) the HTZ (low Fe) and (B) the HTLZ/HTZ basalts and dolerites.

fractional crystallization from a liquid enriched in TiO_2 (see Fig. 3.2). The range in Ti^{4+} concentrations, together with the resemblance in the plagioclase compositions of the LTZ basalts and the HTLZ/HTZ basalts and dolerites, may imply that the "megacrysts" are in fact xenocrysts and either mixing with, or contamination by, a LTZ-type magma or a LTZ-type source composition may be involved in the generation of the HTLZ/HTZ magma type. The observed compositional and petrographic variability of the HTLZ/HTZ basalts and dolerites and the geochemical and petrographic differences between the HTLZ/HTZ basalts and dolerites of Botswana and HTZ.HF basalts of the Central Lebombo may therefore be explained in terms of a mixing/contamination type process. The evolved nature of the HTLZ/HTZ magma composition limits any attempt to back-calculate the parent magma composition and hence the source composition can not be evaluated. More detailed studies, of radiogenic isotopes in particular, are therefore required in order to assess the relative importance of the asthenospheric (plume) and/or lithospheric components in the generation of the HTLZ/HTZ basalts and dolerites before the significance, if any, of contamination/mixing can be assessed.

The stratigraphic position of the HTLZ/HTZ basalts and dolerites in Botswana is obscured by poor outcrop, but in a single borehole, NG1, HTLZ/HTZ basalts lie above low-P_2O_5 LTZ basalts. The dyke swarm of Botswana which is associated with the failed rift arm of a triple junction rift centred in the Nuanetsi area (Burke and Dewey, 1973; Reeves, 1978) extends across a number of different lithospheric sources, reflecting differences in the Archaean/post-Archaean lithospheric structure of Botswana (Sweeney and Watkeys, 1990). It is, therefore, possible that either the thinning of the lithosphere associated with the failed rift arm in Botswana or the intrusion of the dyke swarm in this failed rift arm aided in the intrusion/extrusion of the HTLZ/HTZ magma type assuming that the igneous activity associated with the dyke swarm occurred after the eruption of the LTZ- and HTZ (low Fe) basalt types. The HTLZ/HTZ magma type would consequently be the youngest of the basalt types found in Botswana, *i.e.* in a similar stratigraphic position noted for the HTZ.HF basalt type in the Lebombo and Tuli areas (Sweeney *et al.*, 1994 and Duncan *et al.*, 1995). The dyke swarm could have acted as a magma conduit from deep crustal sills (as proposed by Cox, 1980) or may have facilitated the landward propagation of the HTLZ/HTZ magma in mid-crustal dykes from the Nuanetsi area, *i.e.* the area of maximum lithospheric thinning and the site of incipient continental break-up (Cox, 1992; White, 1992).

6.1.2.2 HTZ (low Fe) basalts and dolerites

In section 4.1.3 a sub-group within the Botswana "enriched" low-K_2O lineage was defined as the HTZ (low Fe) basalt and dolerite sub-group according to their Fe_2O_3* and TiO_2 concentrations (see Fig. 4.6A & B) and these HTZ (low Fe) basalts and dolerites are shown to closely resemble (both petrographically and geochemically) the HTZ.LF (or high Ti-Zr) basalts of the Central Lebombo area (see section 3.1.1.2 and 4.1.3.5), although the HTZ (low Fe) basalts and dolerites are characterised by their evolved geochemistry (with a range of 4.8 to 3.22% MgO). The plagioclase compositions of the HTZ (low Fe) basalts and dolerites define an enriched An *vs.* Or (Fig. 3.4) trend with respect to both the HTLZ/HTZ basalts and dolerites and the LTZ-type basalts. Similarly the augite compositions of the HTZ (low Fe) basalts and dolerites are enriched in Ti^{4+} *vs.* Mg^{2+} (Fig. 3.2) with respect to the augite compositions of the LTZ-type basalts of Botswana. The plagioclase and augite compositions of the HTZ.LF basalts of the Central Lebombo define similar enriched trends with respect to the LTZ basalt mineral compositions (see Sweeney *et al.*, 1994).

Sweeney *et al.* (1994) noted that the HTZ.LF basalts are compositionally similar to the Chikwedziwa Beds of the Nuanetsi Area. Cox and Bristow (1984) have modelled, using least square mixing models, the variation in the major element compositions of the Chikwedziwa Beds which can be produced by approximately 20% crystallization of an assemblage dominated by aluminous clinopyroxene, together with minor olivine and

titanomagnetite. The absence of plagioclase in the fractionating assemblage is reflected in an increase in the Al_2O_3 concentration with decreasing MgO concentrations (see Fig. 11 in Sweeney *et al.*, 1994). The absence of any correlation between MgO and Fe_2O_3* (see Fig. 4.6B) and the increase in the Al_2O_3 concentration with decreasing MgO concentrations (see section 4.1.3.1 and Fig. 6.3) suggests that crystal fractionation, dominated by clinopyroxene, can similarly account for at least some of the major and trace element concentration variations shown by the HTZ (low Fe) basalts and dolerites. The HTZ (low Fe) samples which clearly lie off trend in Fig. 6.3 (KLB-066 and KLB-081) are characterised by a high proportion of plagioclase phenocrysts (see section 3.1.1.2). The evolved nature of the HTZ (low Fe) basalts and dolerites would, therefore, reflect the continued fractionation of the magma in relatively deep crustal conditions where these high temperature/pressure conditions are compatible with the presence of aluminous pyroxene in the fractionation assemblage (Cox and Bristow, 1984).

Sweeney *et al.* (1994) propose that the HTZ.LF basalts are evolved low-MgO end-members of the Letaba Formation picritic basalts, which represent primary mantle melts (*e.g.* Ellam and Cox, 1989 & 1991; Sweeney, 1988; Sweeney *et al.*, 1991). The picritic compositions are believed to result from the mixing of two end-member mantle components, *i.e.* the low-K_2O asthenospheric component (a possible plume influence) and the high-K_2O lithospheric component enriched (metasomatically) in incompatible elements and Sweeney *et al.* (1994) propose that the low-K_2O plume component becomes more important with time, *i.e.* associated with a decrease in the depth of mantle source equilibration. More detailed analyses of radiogenic isotopes, in particular, are necessary before identification of the mantle source composition of the HTZ (low Fe) basalts and dolerites can be defined. The geochemical, petrographic and mineralogical resemblance between the HTZ (low Fe) basalts and dolerites and the HTZ.LF basalts of the Central Lebombo area does suggest that the source of the HTZ (low Fe) basalts and dolerites is compositionally similar to that of the HTZ.LF basalts of the Central Lebombo area.

The stratigraphic succession seen in northeast Botswana with the HTZ (low Fe) basalts overlying the LTZ-type basalts implies that the HTZ (low Fe) magma type is younger than the LTZ-type basalts in northeast Botswana and that continued deep plume-lithosphere interaction occurred (producing the HTZ (low Fe) primary magma type) either simultaneously with, or following, the generation at shallower depths of the primary LTZ-type magma. Although the magmatic activity associated with the dyke swarm appears to have occurred after the eruption of the LTZ- and HTZ (low Fe) basalts (see section 5.2.4) the lithospheric thinning associated with the failed rift arm may have facilitated the eruption of the HTZ (low Fe) magma type although no dykes with an HTZ (low Fe) chemistry are

recognised in Botswana outside the Tuli Syncline area. It is possible, however, that the HTZ (low Fe) magma originated to the north of Botswana as has been proposed (Ellis, 1978) for the basalts of northeast Botswana (see section 1.2.3.2.2).

6.2 HIGH-K_2O LINEAGE

6.2.1 WITHIN-GROUP VARIATION

6.2.1.1 High-K_2O picritic basalt

The Letaba Formation picritic basalts are extensively described in the literature (*e.g.* see Bristow, 1984b; Cox *et al.*, 1984; Ellam and Cox, 1989; 1991 and Sweeney *et.al.*, 1991) and the compositional variation shown by the Letaba Formation picritic basalts is reported to result from a combination of high pressure fractional crystallization of olivine and orthopyroxene followed by the low pressure fractionation of olivine ± clinopyroxene. A two end-member source composition is, however, required to explain the scatter in the incompatible element concentrations *vs.* MgO and the systematic variation in inter-element ratios within a narrow MgO window. Sweeney *et al.* (1991) used major element compositions to constrain the depth of segregation for these two end-member components, where the low-K_2O asthenospheric component (a possible plume influence) equilibrated at 10-22kbars and the high-K_2O lithospheric component equilibrated at >30kbars in a lithospheric mantle (*i.e.* the SiO_2-poor incompatible element poor end-member enriched in basaltic constituents and the high SiO_2 end-member enriched in incompatible elements but depleted in basaltic constituents of Ellam and Cox (1989; 1991) respectively). As the high-K_2O picritic basalts in Botswana are petrographically and geochemically identical to the Letaba Formation picritic basalts, they are not discussed in any more detail.

6.2.1.2 Shoshonites

The Botswana shoshonites exhibit little variation in their SiO_2 (49.57 - 50.33%) or MgO (4.69 - 4.99%) concentrations, but are characterised by greater ranges in concentration for some of the major and trace element concentrations (see Fig. 4.11A & B). The variation in concentrations of both major and trace elements defines no coherent trend *vs.* SiO_2 or MgO and three samples (KLB-058 to -060) which were collected from a single dyke have essentially identical SiO_2 concentrations although the range in concentrations shown by their major and trace elements is of the same order as the range in concentration displayed by that element for the complete shoshonite sample set. The recognition of the processes involved in the generation of this compositional variability (*e.g.* source heterogeneities, primary magma compositions, variable degrees of fractional crystallization and late-stage alteration) is limited by insufficient samples and the evolved nature of the shoshonites.

6.2.1.3 High-K_2O lineage

The shoshonite-type compositions of the Karoo Igneous Province have been reported (Bristow and Cox, 1984) to result from the low-pressure fractionation of olivine-clinopyroxene ± ilmenite ± apatite from high-K picritic basalt compositions. Cox and Bristow (1984) suggest that the range in compositions displayed by the Karoo shoshonites reflects the variability of the precursor picrite compositions although the range in TiO_2 and P_2O_5 concentrations can be accounted for by different degrees of ilmenite and apatite accumulation. The shoshonites of Botswana (and a single Tuli sample, TV-48) are enriched in Nb and have considerably lower Zr/Nb ratios (range of 1.76-2.67) with respect to the other Karoo shoshonites (*e.g.* TV-49: Zr/Nb=24.29) and the Letaba Formation picritic basalts (Zr/Nb: range = 10.3-39.2; mean = 21.22). Neither the high Zr/Nb ratio nor the range in whole rock compositions of the Botswana shoshonites can be explained in terms of fractional crystallization from Letaba Formation picritic precursor composition.

In section 4.2.2 the Nb concentrations and Zr/Nb ratios of the Botswana shoshonites were shown to resemble the Mashikiri Formation nephelinites (also see Fig. 4.12) which have average Zr/Nb ratios of 1.73 and 1.63 (Northern Lebombo and Sabi areas respectively). Bristow (1984a) argues that the Mashikiri Formation nephelinites and the Letaba Formation picritic basalts cannot be related by differing degrees of partial melting of a single source composition, even with significant (> 10%) residual garnet ($D_{Zr}=1.2$ and $D_{Nb}=0.01$) and the differences in the Zr/Nb ratios are attributed to source heterogeneities. Similar arguments can be applied to the high Nb concentrations and low Zr/Nb ratios of the Botswana (and Tuli) shoshonites, suggesting that the shoshonites and Letaba Formation picritic basalts cannot be related by different degrees of partial melting of a common mantle source. The similarities in Zr/Nb ratios of the shoshonites and the Mashikiri Formation nephelinites, as well as the similarities in their initial $^{87}Sr/^{86}Sr$ ratios (see section 4.2.2), suggests the nephelinites and shoshonites either had a similar mantle source composition or that their respective mantle source areas were influenced by similar enrichment processes. However as all of the Tuli Syncline shoshonites have similar whole rock compositions, apart from the Nb concentration (see Fig. 4.11A & B), the processes involved in the enrichment of the source area of the Botswana shoshonites appear to result predominantly in Nb fractionation.

Alkali basalts, in general, are characterised by low Zr/Nb ratios where the low Zr/Nb ratio has been attributed to fluid controlled source heterogeneities (Pearce and Norry, 1979). Evidence suggests that a local influx of metasomatic liquids rich in CO_2, H_2O and the lithophile elements (*i.e.* LREE, K_2O, Rb *etc.*) into the primary source in the mantle is required for the generation and relative enrichment of alkali magmas (BVSP, 1981; Bailey, 1980; Mysen and Boettcher, 1975a & b; McKenzie, 1989). Pearce and Norry (1979) suggest

that the correlation between alkalinity and the low Zr/Nb ratio may imply that the fluid which is responsible for the undersaturated nature of the magma may also transport the Nb. Furthermore, the increased concentration of volatiles associated with the metasomatic fluids may allow for the separation of very small partial melts and may also act as a trigger, or assist in, the eruption of alkali basalts (Fitton *et al.*, 1991; McKenzie, 1989; Bailey, 1982). The origin of this metasomatic fluid has essentially two very different possible sources, *i.e* either as an injection of very small degree carbonate-rich partial melts which have a deep mantle source (*e.g.* McKenzie, 1989) or as a result of fluid activity/lithospheric interaction (e.g. the introduction of subduction-related pelagic sediments where the metasomatic fluids inherit their trace element characteristics from these pelagic sediments (Fitton *et al.*, 1991)).

The shoshonites are therefore proposed to represent a small degree partial melt of a mantle source which has been enriched in incompatible elements, however as the shoshonites have evolved compositions any models involving partial melting of the mantle source cannot be well constrained and are therefore not discussed in any further detail. Furthermore, the identification of the possible processes involved in the enrichment of the source area of the shoshonites requires more detailed isotopic and trace element studies.

6.3 FELSITES

6.3.1 WITHIN GROUP VARIATION

As mentioned in section 4.3.1 no within-group variation can be modelled for the felsites as the two felsite samples available exhibit considerable variation in their whole rock geochemistry (major elements and Rb, Sr and Ba in particular), where the variations may reflect to some extent alteration and/or phenocryst proportions and compositions.

6.3.2 PETROGENESIS

As the two felsite samples which are available display considerable variation in their whole rock geochemistry no definitive modelling can be undertaken and the possible petrogenetic origins of the felsites are therefore discussed in context of existing models quoted in the literature for the formation of Karoo "felsic" magmas.

Cleverly *et al.* (1984) propose essentially four different possible petrogenetic hypotheses to account for the formation of acid rocks:

1) Fractional crystallization of a dacitic magma produced by:
   -fractional crystallization of a basaltic magma, or

-partial melting of a basaltic or an acidic source material

2) Varying degrees of partial melting of basic parent

3) Partial melting of ancient crustal materials (± subsequent fractional crystallization)

4) Direct derivation from mantle (however Cleverly *et al.* (1984) discount a direct mantle origin as it is highly unlikely that rhyolitic magmas would be in equilibrium with mantle compositions). In addition, Marsh and Eales (1984) discount the possibility of contamination of the tholeiitic basalt as possible petrogenetic process in the formation of the intermediate rocks of the Central Karoo area.

The absence of rocks with intermediate compositions in the continental flood basalts of southern Africa is commonly used to argue (*e.g.* Cleverly *et al.*, 1984; Marsh and Eales, 1984; Erlank *et al.*, 1984; Milner, 1988) that a continued fractional crystallization sequence is unlikely to be involved in the formation of "felsic" magmas. Furthermore, as the felsites of Botswana have similar Al_2O_3 but considerably lower CaO concentrations than both the LTZ- and HTLZ/HTZ-basalts, in any fractional crystallization model clinopyroxene, and not plagioclase, must be the dominant fractionating phase, which is considered highly unlikely.

Two remaining end-member petrogenetic hypotheses can therefore be used to model the formation of "felsic" magma compositions, *i.e.* partial melting of ancient crustal rocks and varying degrees of partial melting of a basic parent. In section 4.3.2 it was suggested that the felsites had a whole rock composition which was broadly comparable with the Lebombo and Nuanetsi rhyolites, which could imply that the Botswana felsites are the product of decompressive melting of underplated basaltic material (Cleverly *et al.*, 1984; Betton and Cox, 1979) where the age of the event associated with the underplating of mafic material at the base of the crust is open to debate. The single initial $^{87}Sr/^{86}Sr$ ratio of 0.70957 obtained for the Botswana felsites is higher than expected for a mafic source material, and together with the high Al_2O_3 concentration and normative corundum (see TABLE 4.11), suggest that some contamination of the felsite magma has occurred. The Nuanetsi rhyolites, which Cleverly *et al.* (1984) show to be lateral geochemical equivalents to the Jozini Formation, similarly have enriched initial $^{87}Sr/^{86}Sr$ compositions (0.7086 ± 6) and Betton *et al.* (1984) have shown, using Pb-isotopes, that the Nuanetsi rhyolites are contaminated by Limpopo Mobile Belt basement rocks.

The felsite samples of Botswana clearly require more detailed modelling and isotopic studies before a more specific petrogenesis can be proposed, but initial investigations suggest a probable lower crustal source (of either underplated Karoo basalt or mafic granulite), where the primary felsite magma composition appears to have undergone some contamination by crustal rocks.

7 CONCLUSIONS

This chapter summarises the conclusions reached during this study on the geochemistry of the Karoo igneous rocks of Botswana. A number of distinct geochemical sub-groups are recognised within the Botswana data set on the basis of whole rock geochemistry, normative mineralogy, petrography and outcrop character and the Karoo igneous rocks are assigned to one of three lineages, *i.e.* the low-K_2O, high-K_2O or felsite lineage. The low-K_2O lineage is subdivided into three broad sub-groups on the basis of the TiO_2 and Zr concentrations, *i.e.* into the LTZ-, HTLZ- and HTZ-type basalts and dolerites. The LTZ-type basalt and dolerite sub-group (with ≤2% TiO_2 and ≤250ppm Zr) is further subdivided into a number of sub-groups according to MgO concentrations, whole rock geochemistry and outcrop character, namely the low-MgO LTZ picritic basalt, the LTZ basalt, the high-Na_2O LTZ basalt, the low-P_2O_5 LTZ basalt, the TYPE I LTZ dolerite, the TYPE II LTZ dolerite and the high-MgO LTZ picrite sub-groups. The HTLZ-type (with ≥2% TiO_2 and ≤250ppm Zr) and HTZ-type (with ≥2% TiO_2 and ≥250ppm Zr) basalts and dolerites of Botswana define a continuous range in whole rock compositions and, in general, do not have the typical "enriched" signature of Karoo igneous rocks. Two sub-groups are recognised within the HTZ-type basalts and dolerites according to the TiO_2 and Fe_2O_3* concentrations, *i.e.* the HTLZ/HTZ and HTZ (low Fe) basalts and dolerites sub-groups. The high-K_2O lineage is sub-divided, using the MgO concentration, into the high-K_2O picritic basalts and the shoshonite sub-groups. The felsite lineage presently includes only two samples.

The characteristics of each of these geochemical sub-groups defined during this study are briefly summarised below. As this thesis is only a reconnaissance study, key subjects which require attention in the future have been mentioned.

(1) The LTZ basalts represent the bulk of the Botswana dataset, with the vast majority of these LTZ basalts being collected from borehole cores distributed throughout Botswana (*i.e.* the Central Kalahari Sub-basin and north to northeast Botswana) although no LTZ-type basalts were found in the Botswana portion of the Tuli Syncline. The LTZ basalts of Botswana are shown to closely resemble, petrographically and geochemically, the Lesotho-type basalts of the Central Karoo area. The LTZ basalts, like the Lesotho Formation basalts, are characterised by a relatively narrow range in concentration for many elements and relatively constant interelement ratios. The LTZ basalts have an ophitic to sub-ophitic texture and may be sparsely plagioclase-phyric.

(2) The low-MgO LTZ picritic basalts define a coherent compositional trend together with the LTZ basalts, although the whole rock compositions of the low-MgO LTZ picritic basalts (Al_2O_3, CaO, Ni, Co and Cr in particular) attest to the importance of olivine in the relationship between the low-MgO LTZ picritic basalts and the LTZ basalts. The high modal proportions of olivine, but otherwise analogous petrography of the low-MgO LTZ picritic basalt, reflects this comparable whole rock geochemistry. The low-MgO LTZ picritic basalts are successfully modelled as cumulus-enriched LTZ-type basalts.

(3) The high-Na_2O LTZ basalts are petrographically and geochemically identical to the LTZ basalts, except for the elevated Na_2O concentrations, and the associated CaO depletion, of the high-Na_2O LTZ basalts. The high-Na_2O LTZ basalts can be related to the LTZ-type basalt simply by the albitization of plagioclase, where the saline solutions involved in the albitization reaction are believed to originate from the adjacent salt pans and playa lakes preserved in the Kalahari Beds.

(4) Seven of the low-P_2O_5 LTZ basalt samples were collected from a ±15m thick interval from the borehole NG1 of western Botswana, while the other two samples were collected from two adjacent boreholes drilled in the southeast of the Central Kalahari Sub-basin. Although the low-P_2O_5 LTZ basalts, with their evolved whole rock compositions, have interelement ratios which are similar to those of the more evolved LTZ-type basalts, they can be identified as a separate geochemical group. The low-P_2O_5 LTZ basalts are, however, characterised by a unique phenocryst assemblage which includes plagioclase, alkali feldspar (perthite), clinopyroxene and pseudomorphs after olivine. The relationship between the low-P_2O_5 LTZ basalts and the LTZ basalts is uncertain, but initial investigations suggests that contamination of the LTZ-type basalt may be involved in the generation of the low-P_2O_5 LTZ basalts, although the contaminant in any AFC-type process does not have typical upper crustal compositions. Further research is therefore required to identify the processes involved in the generation of the low-P_2O_5 LTZ basalts.

(5) The TYPE I LTZ dolerites are petrographically and geochemically identical to the LTZ-type basalts and are the only recognised intrusive equivalents of the voluminous LTZ-type basalts of Botswana. The two TYPE I LTZ dolerites were sampled from two dolerite dykes located adjacent to the southern margin of the dyke swarm, however as the strike of the TYPE I LTZ dolerites is not known, the relationship, if any, between the TYPE I LTZ dolerites and the dyke swarm could not be established.

(6) The TYPE II LTZ dolerites are characterised by a low-grade greenschist metamorphic assemblage where the primary igneous texture has been extensively replaced by chlorite,

actinolite, epidote and albite and the TYPE II LTZ dolerites are therefore not Karoo aged. The TYPE II LTZ dolerites have been tentatively correlated, according to petrographic resemblances, with the Proterozoic suite of dolerites in Botswana, where at least some of these TYPE II LTZ dolerites may represent a westwards extension of the Plumtree Dyke swarm. A detailed geochemical investigation of these Proterozoic dolerites is required before a more conclusive comparison can be addressed.

(7) The high-MgO LTZ picrites, collected to the south of the Tuli Syncline, have a mesocumulus texture and are characterised by a relatively high modal proportion of biotite. The high-MgO LTZ picrites have been correlated with the Archaean Olivine-Norites, which are intruded into the basement gneisses of the Limpopo Mobile Belt in the Semolale-Tsetsebjwe area, as the high-MgO LTZ picrites closely resemble, petrographically, these Olivine-Norites.

(8) The HTLZ/HTZ basalts and dolerites, treated as a single group, are characterised by considerable range in their whole rock compositions and the HTZ basalts and dolerites, in particular, show a marked enrichment in incompatible element concentrations with decreasing MgO concentrations. The HTLZ/HTZ basalts and dolerites of Botswana are correlated with the HTZ.HF basalts of the Central Lebombo and Tuli areas as the whole rock compositions (including major, trace and rare earth elements) of the HTLZ/HTZ basalts and dolerites closely resembles those of the HTZ.HF basalts, although the HTLZ/HTZ basalts and dolerites of Botswana do not have a low Zr/Nb (12 ± 2) ratio which is considered characteristic of the HTZ.HF basalts of the Central Lebombo and Tuli areas. The HTLZ/HTZ basalts and dolerites exhibit a considerable range in their petrography and mineralogy and vary from aphyric, through sparsely plagioclase ($\pm$clinopyroxene) phyric to including a phenocryst and "megacryst" assemblage. The HTLZ/HTZ basalts show a widely scattered distribution in Botswana and are found in the Central Kalahari Sub-basin, in western Botswana and in the Tuli Syncline area where the HTLZ/HTZ basalts are found stratigraphically above the low-P_2O_5 LTZ basalts in the borehole NG1 of western Botswana. The majority, if not all, of the dolerite dykes associated with the dyke swarm have an HTLZ/HTZ geochemistry and the dyke swarm may have acted as a feeder system to the HTLZ/HTZ basalts of Botswana.

(9) The HTZ (low Fe) basalts and dolerites are recognised as a separate HTZ-type geochemical sub-group, although Fe_2O_3* *vs.* TiO_2 is the only interelement ratio which clearly discriminates between the two HTZ-type geochemical sub-groups. The HTZ (low Fe) basalts and dolerites are characterised by an enriched whole rock geochemistry (*e.g.* Ce/Y >2.1; high Ba and Zr concentrations) with respect to the HTLZ/HTZ- and LTZ-type

basalts and dolerites of Botswana, which has led to their correlation with the HTZ.LF basalts of the Central Lebombo and Tuli areas. The HTZ (low Fe) basalts and dolerites have a plagioclase-pyroxene (with minor oxide and pseudomorphs after olivine) phenocryst assemblage similar to that of the HTLZ/HTZ basalts and dolerites, although the HTZ (low Fe) basalts and dolerites have higher modal proportion of pyroxene in the phenocryst assemblage. Although petrographically and mineralogically similar to the HTLZ/HTZ basalts and dolerites, the HTZ (low Fe) basalts and dolerites tend to have a hyalopilitic texture and also have plagioclase compositions which are relatively enriched in orthoclase with respect to anorthite components. The petrogenesis of the HTZ (low Fe) basalts and dolerites is proposed to be equivalent to that described for the HTZ.LF basalts of the Lebombo (Sweeney *et al.*, 1994) and is not examined here in any additional detail. The HTZ (low Fe) basalts were sampled from the Tuli Syncline area and from northeast Botswana. In three separate borehole sections from northeast Botswana HTZ (low Fe) basalts lie stratigraphically above a considerable thickness of LTZ-type basalts. This stratigraphic sequence is consistent with the overall Karoo Igneous Province basalt stratigraphy as proposed by Marsh *et al.* (1995). HTZ (low Fe) dolerites have only been recognise in the Tuli Syncline area and it is not known if these dykes are associated with the dyke swarm or if they are part of a local feeder system to the adjacent HTZ (low Fe) basalts.

(10) The two high-K_2O picritic basalts were sampled from the southern margin of the Botswana portion of the Tuli Syncline in Botswana where the high-K_2O picritic basalts are lateral equivalents of the Letaba Formation picritic basalts. The high-K_2O picritic basalts can be correlated with the 1-P and 2-P types of the Letaba Formation picritic basalts, according to the individual phenocryst assemblage.

(11) The shoshonites were all collected in the Tuli Syncline, where four of the shoshonites were sampled from a single dyke in Zimbabwe. The shoshonites are sparsely phyric (<5 modal%), with a phenocryst assemblage of olivine, clinopyroxene and sometimes plagioclase and alkali feldspar and have a intergranular to hyalopilitic texture. The shoshonites sampled during this study (and TV-48 sampled by Vail *et al.*, 1969) have anomalously high Nb concentrations (120-160ppm), and therefore very low Zr/Nb ratios, with respect to the high-K_2O (Letaba Formation) picritic basalts. These shoshonites therefore cannot be related to the picritic basalts by either fractional crystallization or by different degrees of partial melting of a similar source as proposed by Cox and Bristow (1984) for the shoshonites of the Sabie River Basalt Formation. The shoshonite samples and the Mashikiri Formation nephelinites, however, have similar Nb concentrations and similar values for their Zr/Nb ratios, which suggests that their respective sources underwent a similar style of enrichment

by a CO_2-rich metasomatic fluid. Further research is required to identify the characteristics of the shoshonite source area and the possible processes involved in the enrichment of Nb in the shoshonite magma type.

(12) The felsite samples, collected from two dykes intruded near the southern margin of the Tuli Syncline, are the only known unequivocal examples of Karoo felsic magmatism in either Botswana or the Tuli Syncline. The term felsite is preferred although the samples, with >63% SiO_2 and >3% K_2O, could be classified as quartz latites. Although the two felsites have similar concentrations of many trace elements, they show considerable differences in their major element and Rb, Sr and Ba concentrations. The felsites are sparsely phyric (<7.5 modal%), with a phenocryst assemblage which includes feldspar (plagioclase and alkali feldspar), clinopyroxene, oxide, apatite and sometimes olivine pseudomorphs (KLB-080 only). The felsites have been tentatively interpreted as partial melts of underplated basaltic material, although the felsite magma appears to have been contaminated en route to the surface by upper crustal rocks. More detailed sampling and analytical work is required in order to characterise the composition of the source area and to assess the possible role of contamination in the generation of the felsite magma.

Cox *et al.* (1967) first noted the presence of basalts with "normal" and "enriched" chemistry in the Nuanetsi area of the Karoo Igneous Province. Subsequent studies suggested that a linear boundary separated the dominantly "enriched" basalts to the north from the exclusively "normal" basalts to the south, where this boundary could be extrapolated from the Central Lebombo across southern Africa through the Etendeka into the Paraná flood basalt province of South America (*e.g.* Erlank *et al.*, 1988). An initial investigation of the Botswana data, however, suggested that this boundary between geochemical types was poorly defined in Botswana and that it may not be continuous between the Lebombo and Etendeka areas (Erlank *et al.*, 1990). Sweeney and Watkeys (1990) also noted the tendency of "enriched" basalts to occur on Archaean crust stable since ±2500Ma or which has undergone "cold" reworking, where the crust is therefore underlain by a thick lithospheric keel which has undergone enrichment with respect to the incompatible elements since the Archaean. In contrast, the "normal" basalts overlie, or occur adjacent to, regions of post-Archaean crust which has a thinner more recently accreted lithospheric mantle.

A number of conclusions reached during this study concerning the distribution of basalt types in Botswana are inconsistent with the presence of an apparent linear boundary separating geochemical types extending across Botswana. The vast majority of the basalts sampled in Botswana (from both the Central Kalahari Sub-basin and northern Botswana) are characterised by a LTZ-/"normal" geochemical signature. The presence of LTZ-type

basalts in Botswana therefore considerably expands the known distribution of this rock type in the Karoo Igneous Province. Furthermore, the presence and distribution of the HTLZ/HTZ basalts in Botswana appears to be closely related to the intrusion of the dyke swarm, where the dyke swarm may have acted as a conduit from deep crustal sills (Cox, 1980) or facilitated in the landward propagation of the magma in mid-crustal sills from the site of maximum lithospheric thinning (Cox, 1992; White, 1992).

Burke and Dewey (1973) first noted that plume generated uplift caused rupture into triple junction rifts (intersecting at 120°) although the third arm was typically inactive and they interpreted the faulted areas of volcanic rocks extending west of Nuanetsi in the Limpopo Valley as the proposed failed arm of a triple junction centred at Nuanetsi. Reeves (1978) however proposed that the dyke swarm of Botswana represented the failed third arm of the rift-rift-rift triple junction as a projection of the dyke swarm along the dyke axis by approximately 300km to the east (from the Zimbabwe-Botswana border) results in a convergence of the dyke swarm axis with the Sabi and Lebombo axes which intersect at almost exactly 120° (Reeves, 1978). The width of the dyke swarm narrows away from the triple junction and the two sides converge somewhere to the north of the Etosha Pans in Namibia, which suggests that the slight opening along the axis of the dyke swarm propagated in a "westward" direction (Reeves, 1978), although crustal thinning was minimal as basement rocks have a continuous exposure across the dyke swarm. The dyke swarm was intruded into a basement high in northern Botswana known as the Makgadikgadi high. The Karoo sediments of the Central Kalahari Sub-basin thin up against this basement high and the Ntane sandstone oversteps the underlying younger sediments until it lies directly on the underlying basement (Smith, 1984), which suggests that uplift associated with the dyke swarm commenced during Karoo sedimentation. Daly *et al.* (1991) identify a central basement high (the Kiri high) in the Cuvette Centrale of Zaire with a WNW-ESE trend which is flanked by sedimentary basins and is associated with a late Permian - early Triassic unconformity in the adjacent sediments. They argue that the late Palaeozoic intercontinental deformational/compressional process associated with the formation of the Kiri high can be related directly to the collisional tectonics associated with the southern Gondwana margin (see Cox, 1978). A number of superficial similarities between the Makgadikgadi and Kiri highs suggests that the Makgadikgadi high may possibly represent further evidence of a compressional tectonic regime associated with subduction along the Pacific margin of Gondwanaland during the late Palaeozoic. Cox (1988a, 1989) speculates that the Central Kalahari Sub-basin owes its existence to the fact that it was unaffected by either Karoo or Paraná volcanism and was therefore free from the uplift due to associated mantle plume activity, which can cause 1-2km of uplift extending for more than 1000km from the plume centre (White and McKenzie, 1989). Cox (1989) suggests that the drainage

patterns of southern Africa reflect drainage away from the uplifted domes associated with the plumes of the Nuanetsi and Etendeka regions. The presence of both the Okavango delta and the former Lake Makgadikgadi, *i.e.* the topographically lowest parts of the Kalahari inland drainage basins (Reeves, 1978), along the axis of the dyke swarm, however, suggests that subsidence of the dyke swarm occurred. The subsidence of the dyke swarm would reflect the change in surface elevation which immediately follows rifting/crustal extension in order to maintain isostatic equilibrium (McKenzie, 1978).

The presence of both shoshonite and felsite rock types associated with the dyke swarm support the suggestion that the dyke swarm represents a failed Gondwana spreading axis and that the plume activity was centred around the Nuanetsi area (Cox, 1992). Duncan *et al.* (1984a) note that one of the most striking features of the geographic distribution of Karoo igneous rocks is the localization of acid volcanic rocks around the margins of the province (*i.e.* at sites of intercontinental warping and rifting) where the elevated temperatures at or near the base of the crust which are required for felsite generation are a direct result of asthenospheric upwelling below thinned crust. White (1992) argues that the presence of felsic melts close to rift margins is indicative of the bulk of magma generation occurring beneath areas of incipient continental break-up. Alkali olivine basalts (and therefore the shoshonites) are similarly characteristically found associated with continental rifts and paleorift environments, where the first melts associated with the plume activity in rift environments typically have a high-K_2O composition (McKenzie, 1989; Bailey, 1992). The alkali basalts recognised in the Rajpipla area of the Deccan Province (Krishnamurthy and Cox, 1980) have high and approximately equal concentrations of Na_2O and K_2O, and have compositions which are broadly comparable with the Botswana shoshonites. It is noteworthy that the Rajpipla alkali suite are found in close spatial association to other important examples of Deccan rocks with atypical compositions and is one of the few areas in the Deccan Province where rhyolites are also present; furthermore these alkali rocks are found adjacent to the tectonically active Narmada (interpreted as a failed rift arm of a Cretaceous triple junction) and West Coast (faults and flexures related to the splitting off of the Seychelles platform) zones (Devey *et al.*, 1992).

Cox (1992) argues that plume activity played an active role in the continental break-up of east Gondwana, particularly with respect to the formation of the Lebombo and Nuanetsi volcanic rocks, where a plume with a diameter of >2000km (after White and McKenzie, 1989), was centred to the east of Maputo and the distribution of magmatism and rifting within the area influenced by the plume, are controlled by local physical heterogeneities. Cox (1992) argues for a two stage model, where the first stage of break-up was associated with the bulk of plume-generated activity (*i.e.* rifting and magmatism). However as

Gondwana was under N-S compression at this time (Daly *et al.*, 1991), break-up essentially failed although lithosphere thinning sufficient for magma generation occurred. The second stage of break-up, involving the southwards movement of Madagascar and Antarctica (as a single plate) away from Africa, may have started as long ago as 170Ma (*e.g.* Martin and Hartnady; 1986). Cox (1992) suggests that it is tempting to relate the generation of the LTZ-type basalts to this second stage of break-up. The LTZ-type basalts of the Central Karoo are, however, postulated to be older than the basalts of the Nuanetsi and Lebombo areas (this study and Marsh *et al.*; 1995). The intrusion of the dyke swarm in Botswana is proposed to occur after the LTZ- and HTZ (low Fe) magmatic events and if the intrusion of the dyke swarm in Botswana is assumed to occur simultaneously with the bulk of the rifting and magmatic activity in the Nuanetsi area, rifting then post-dates the eruption of the voluminous LTZ-type basalts of Botswana. Considerable debate exists in the literature regarding the relationship between extension, continental break-up and the massive volumes of associated magmatism. Cox (1978) first noted the possible genetic connection between subduction along the southern margin of Gondwana and the broad band of continental flood basalt provinces parallel to the Gondwana margin. Many arguments concerning the break-up of Gondwana therefore support a model where the tensional environment associated with rifting and continental break-up is related to subduction beneath Gondwana (*e.g.* Cox, 1978; Storey *et al.*, 1992; Bott, 1992; Hergt *et al.*, 1991) rather than to an active plume-type model. The generation of the Gondwana continental flood basalts could therefore result from passive decompression of an upwelling mantle source, where the upwelling may occur in response to a convective roll type model, as proposed by Froidevaux and Nataf (1981), or could be related to a change in the boundary forces associated with subduction in Jurassic times which would result in a change from compression to extension of the Gondwana lithosphere (Storey *et al.*, 1992). The plume activity centred in the Nuanetsi area may therefore have controlled the ultimate position of rifting, but did not necessarily trigger the break-up of Gondwanaland. Any proposed model concerning the break-up of Gondwana in the Jurassic will need to account for the formation of the voluminous LTZ basalt type prior to the magmatism associated with rifting in the Nuanetsi and Lebombo areas.

REFERENCES

Aldiss, D.T., 1989. The geology of the Shashe area. *Bull. Geol. Surv. Botswana* **35**, 137pp.

Aldiss, D.T., 1983a. The geology of the Semolale area. *Bull. Geol. Surv. Botswana* **25**, 64pp.

Aldiss, D.T., 1983b. The geology of the Tsetsebjwe area. *Bull. Geol. Surv. Botswana* **24**, 86pp.

Aldiss, D.T., Benson, J.M. and Rundle, C.C., 1984. Jurassic pillow lavas and palynomorphs in the Karoo of eastern Botswana, *Nature* **310**, 302-304.

Arndt, N.T., Czamanske, G.K., Wooden, J.L. and Fedorenko, V.A., 1993. Mantle and crustal contributions to continental flood volcanism. *Tectonophysics* **223**, 39-52.

Arndt, N.T. and Christensen, U., 1992. The Role of Lithospheric Mantle in Continental Flood Volcanism: Thermal and Geochemical Constraints. *J. Geophys. Res.* **97 (B7)**, 10967-10981.

Bailey, D.K., 1992. Episodic alkaline activity across Africa: implications for the causes of continental break-up. In: Storey, B.C., Alabaster, T. and Pankhurst, R.J. (eds.), *Magmatism and the Causes of Continental Break-up. Geol. Soc. Lond. Spec. Publ.* **68**, 91-98.

Bailey, D.K., 1982. Mantle metasomatism - continuing chemical changes within the Earth. *Nature* **296**, 525-530.

Bailey, D.K., 1980. Volatile flux, geotherms, and the generation of the kimberlite-carbonatite-alkaline magma spectrum. *Miner. Mag.* 43, 695-699.

Betton, P.J., Armstrong, R.A. and Manton, W.I., 1984. Variations in the Lead Isotopic Compositions of Karoo Magmas. *Spec. Publ. Geol. Soc. S. Africa* **13**, 331-339.

Betton, P.J. and Cox, K.G., 1979. Production of rhyolites at continental margins: An example from the Lebombo monocline. *Extnd. Abstr., Geol. Soc. S. Afr., Geocongr. 79*, 29-31.

Bhattacharji, S. and Smith, C.H., 1964. Flowage differentiation. *Science* **145**, 150-153.

Bliss, N.W., 1971. The Deweras Group between the Umfoli and Umniati Rivers. *Trans. Geol. Soc. S. A.* **74**, 133-147.

Boocock, C and van Straten, O.J., 1962. Notes on the geology and hydrogeology of the Central Kalahari region, Bechuanaland Protectorate. *Trans. Geol. Soc. S. Africa* **65**, 125-171.

Bott, M.H.P., 1992. The stress regime associated with continental break-up. In: Storey, B.C., Alabaster, T. and Pankhurst, R.J. (eds.), *Magmatism and the Causes of Continental Break-up. Geol. Soc. Lond. Spec. Publ.* **68**, 125-136.

Bristow, J.W., 1984a. Nephelinites of the North Lebombo and South-East Zimbabwe. *Spec. Publ. Geol. Soc. S. Africa* **13**, 87-104.

Bristow, J.W., 1984b. Picritic Rocks of the Northern Lebombo and South-East Zimbabwe. *Spec. Publ. Geol. Soc. S. Africa* **13**, 105-123.

Bristow, J.W., 1980. The geochronology and geochemistry of Karoo volcanics in the Lebombo and adjacent areas. Ph.D. Thesis (unpubl.), University of Cape Town, 257pp.

Bristow, J.W and Cox, K.G., 1984. Volcanic rocks of the Lebombo-Nuanetsi-Sabi zone: classification and nomenclature, *Spec. Publ. Geol. Soc. S. Africa* **13**, 69-76.

Bristow, J.W., Allsopp, H.L., Erlank, A.J., Marsh, J.S. and Armstrong, R.A., 1984. Strontium Isotope Characterization of Karoo Volcanic Rocks. *Spec. Publ. Geol. Soc. S. Africa* **13**, 295-329.

Brooks, C.K., 1976. The Fe_2O_3/FeO ratio of basalt analyses: an appeal for a standardised procedure. *Bull. Geol. Soc. Denmark* **25**, 117-120.

Bryan, W.B., Finger, L.W. and Chayes, F., 1969. Estimating proportions in Petrogenetic Mixing Equations by Least-Squares Approximation. *Science* **163**, 926-927.

Burke, K and Dewey, J.F., 1973. Plume generated triple junctions: Key indicators in applying plate tectonics to old rocks. *J. Geol.* **81**, 406-433.

BVSP, 1981. Basalt Volcanism on the Terrestrial planets. Pergamom Press, Inc., New York, 1286pp

Cahen, L., Snelling, N.J., Delhal, J. and Vail, J.R., 1984. *The geochronology and evolution of Africa*, Oxford University Press, 512pp.

Cahen, L. and Lepersonne, J., 1952. Equivalence entra le Système du Kalahari du Congo Belge et les Kalahari Beds d'Afrique australe. *Mem. Soc. Belge. Geol., Paleontol., Hydrol.* **80**.

Clark, G.C. and Machacha, T.P., 1982. The geology of the Baines Drift area. *Bull. Geol. Surv. Botswana* **19**, 65pp.

Cleverly, R.W., Betton, P.J. and Bristow, J.W., 1984. Geochemistry and Petrogenesis of the Lebombo Rhyolites. *Spec. Publ. Geol. Soc. S. Africa* **13**, 171-194.

Coates, J.N.M., 1980. The Karoo Sequence in Botswana. *Geol. Surv. Botswana Unpubl. Rept.*

Coates, J.N.M., Davies, J., Gould, D., Hutchins, D.G., Jones, C.R., Key, R.M., Massey, N.W.D., Reeves, C.V., Stansfield, G. and Walker, I.R., 1979. The Kalatraverse one report. *Bull. Geol. Surv. Botswana* **21**, 408pp.

Compston, W. and McElhinny, M.W., 1975. The Rb-Sr age of the Mashonaland Dolerites of Rhodesia and Its Significance for Palaeomagnetic Correlations in Southern Africa. *Precambrian Research* **2**, 305-315.

Cox, K.G., 1992. Karoo igneous activity, and the early stages of the break-up of Gondwanaland. In: Storey, B.C., Alabaster, T. and Pankhurst, R.J. (eds.). *Magmatism and the Causes of Continental Break-up. Geol. Soc. Lond. Spec. Publ.* **68**, 137-148.

Cox, K.G., 1989. The role of mantle plumes in the development of continental drainage patterns. *Nature* **342**, 873-877.

Cox, K.G., 1988a. The Karoo Province. In: MacDougal, J.D. (ed.), *Continental Flood Basalts*, Kluwer Publishers, 239-271.

Cox, K.G., 1988b. Numerical modelling of a randomised RTF magma chamber: a comparison with continental flood basalt sequences. *J. Petrology* **29**, 681-697.

Cox, K.G., 1983. The Karoo Province of southern Africa: origin of trace element enrichment patterns. In: Hawkesworth C.J. and Norry, M.J. (eds.). *Continental Basalts and Mantle Xenoliths*, Shiva Publishing LTD, Cheshire, 139-157.

Cox, K.G., 1980. A Model for Flood Basalt Vulcanism. *J. Petrology* **21**, 629-650.

Cox, K.G., 1978. Flood basalts, subduction and the break-up of Gondwanaland. *Nature* **274**, 47-49.

Cox, K.G. and Bristow, J.W., 1984. The Sabie River Basalt Formation of the Lebombo Monocline and south-east Zimbabwe. *Spec. Publ. Geol. Soc. S. Africa* **13**, 125-144.

Cox, K.G., Duncan, A.R., Bristow, J.W., Taylor, S.R. and Erlank, A.J., 1984. Petrogenesis of the Basic Rocks of the Lebombo. *Spec. Publ. Geol. Soc. S. Africa* **13**, 149-169.

Cox, K.G., Bell. J.D. and Pankhurst, R.J., 1979. *The interpretation of Igneous Rocks*. George, Allen and Unwin (publishers) LTD, London, 450pp.

Cox, K.G., MacDonald, R. and Hornung, G., 1967. Geochemical and petrographic provinces in the Karoo basalts of Southern Africa. *Am. Miner.* **52**, 1451-1474.

Cox, K.G. and Hornung, G., 1966. The petrology of the Karoo basalts of Basutoland. *Am. Miner.* **51**, 1414-1432.

Cox, K.G., Johnson, R.L., Monkman, L.J., Stillman, C.J., Vail, J.R and Wood, D.N., 1965. The geology of the Nuanetsi Igneous Province. *Phil. Trans. R. Soc. Lond.* **A257**, 71-218.

Crocket, R.N., 1967. The geology of the Shashi area *Geol. Surv. Botswana Unpubl. Rept. (RNC/32a/67)*, 62pp.

Daly, M.C., Lawrence, S.R., Kimun'a, D. and Binga, M., 1991. Late Paleozoic deformation in central Africa: a result of distant collision? *Nature* **350**, 605-607.

Davis, J.C., 1986. *Statistics and data analysis in geology (2nd edition)*. John Wiley and Sons. Inc., New York, 646pp.

Deer, W.A., Howie, R.A. and Zussman, J., 1978. *Rock forming minerals: Single chain silicates, Vol. 2A*, Longmans, London, 668pp.

Deer, W.A., Howie, R.A. and Zussman, J., 1962. *Rock forming minerals: Ortho- and ring silicates, Vol. 1*, Longmans, Green and Co., LTD, London, 668pp.

Devey, C.W. and Stephens, W.E., 1992. Deccan-related magmatism west of the Seychelles-India rift. In: Storey, B.C., Alabaster, T. and Pankhurst, R.J. (eds.), *Magmatism and the Causes of Continental Break-up. Geol. Soc. Lond. Spec. Publ.* **68**, 271-292.

Duncan, A.R., 1987. The Karoo Igneous Province - A problem area for inferring tectonic setting from basalt geochemistry. *J. Volcan. & Geotherm. Res.* **32**, 13-34.

Duncan, A.R., Marsh, J.S., le Roex, A.P. and Richardson, S.H., 1995. Geochemical characterisation of Karoo volcanic rocks and associated dykes in the Tuli Syncline of Zimbabwe and Botswana. *Department of Geological Sciences, UCT, Centenary Conference, February 1995, Extended Abstracts.*

Duncan, A.R., Newton, S.R., van den Berg, C. and Reid, D.L., 1989. Geochemistry and petrology of dolerite sills in the Huab River Valley, Damaraland, north-western Namibia. *Communs Geol. Surv. Namibia* **5**, 5-17.

Duncan, A.R., Erlank, A.J. and Marsh, J.S., 1984a. Regional Geochemistry of the Karoo Igneous Province. *Spec. Publ. Geol. Soc. S. Africa* **13**, 355-388.

Duncan, A.R., Erlank, A.J. and Betton, P.J., 1984b. Appendix 1: analytical techniques and database descriptions. *Spec. Publ. Geol. Soc. S. Africa* **13**, 389-395.

Eales, H.V., Marsh, J.S. and Cox, K.G., 1984. The Karoo Igneous Province: An introduction. *Spec. Publ. Geol. Soc. S. Africa* **13**, 1-26.

Eales, H.V. and Marsh, J.S., 1979. High-Mg Tholeiitic Rocks and their Significance in the Karroo Central Province. *S. A. Journ. Sci.* **75**, 400-404.

Ellam, R.M. and Cox, K.G., 1991. An interpretation of Karoo continental flood basalts in terms of interaction between asthenospheric magmas and the mantle lithosphere. *Earth Planet Sci. Lett.* **105**, 230-242.

Ellam, R.M. and Cox, K.G., 1989. A Proterozoic source for Karoo magmatism: evidence from the Nuanetsi picrites. *Earth Planet. Sci. Lett.* **92**, 207-218.

Ellis, C.J.R., 1978. Exploration of Block 'P' Pandamatenga area. *Relinquishment Report (P.L. 3/76),* Shell Coal Botswana (Pty) LTD.

Erlank, A.J., Duncan, R.A., Marsh, J.S., Sweeney, R.J., Milner, S.C., Hawkesworth, C.J., McG. Miller, R. and Rogers, R.J., 1990. Distribution of mesozoic Karoo basalts from Southern Africa. *Geocongress 1990, Geol. Soc. S. Africa, Cape Town.*, Abstracts Volume, 754-757.

Erlank, A.J., Duncan, R.A., Marsh, J.S., Sweeney, R.J., Hawkesworth, C.J., Milner, S.C., McG. Miller, R. and Rogers, R.J., 1988. A laterally extensive geochemical discontinuity in the sub-continental Gondwana lithosphere. *Conf. Geochemical Evolution of Continental Lithosphere*, Abstracts Volume, 1-10.

Erlank, A.J., Marsh, J.S., Duncan, R.A., McG. Miller, R., Hawkesworth, C.J., Betton, P.J. and Rex, D.C., 1984. Geochemistry and petrogenesis of the Etendeka Volcanic Rocks from SWA/Namibia. *Spec. Publ. Geol. Soc. S. Africa* **13**, 195-246.

Erlank, A.J., Allsopp, H.L., Duncan, A.R. and Bristow, J.R., 1980. Mantle Heterogeneity beneath southern Africa: evidence from the volcanic record. *Phil. Trans. R. Soc. Lond.* **A297**, 295-307.

Fitch, F.J. and Miller, J.A., 1984. Dating Karoo Igneous Rocks By Conventional K-Ar and $^{40}Ar/^{39}Ar$ Age Spectrum Methods. *Spec. Publ. Geol. Soc. S. Africa* **13**, 247-266.

Fitton, J.G. and James, D., 1991. Basic magmatism associated with Late Cenozoic Extension in the Western United States: compositional variations in space and time. *J. Geophys. Res.* **96 (B8)**, 13693-13711.

Froidevaux, C. and Nataf, H.C., 1981. Continental Drift: What Driving Mechanism? *Geologische Rundschau* **70**, 166-176.

Gast, P.W., 1968. Trace element fractionation and the origin of tholeiitic and alkaline magma types. *Geochim. Cosmochim. Acta* **32**, 1057-1086.

Gerrard, I., 1965. Geology of West Tuli area (an explanation of QDS 2128D). *Records Geol. Surv. Bechuanaland Protectorate 1961-1962*, 5-23

Green, D., 1966. The Karoo System in Bechuanaland. *Bull. Geol. Surv. Bech.* **2**, 74pp.

Haggerty, S.E., 1991. Oxide Textures - A Mini-Atlas. In: Lindsley, D.H. (ed.), *Reviews in Mineralogy, Vol.25: Oxide Minerals, Petrogenetic and magnetic significance*, 129-137.

Haggerty, S.E., 1976. Opaque mineral oxides in terrestrial igneous rocks. In: Rumble, D. (ed.), *Reviews in Mineralogy, Vol.3: Oxide Minerals*, Hg101-300.

Hawkesworth, C.J., Marsh, J.S., Duncan, A.R., Erlank, A.J. and Norry, M.J., 1984. The role of Continental Lithosphere in the Generation of the Karoo Volcanic Rocks: Evidence from Combined Nd- and Sr-Isotope Studies. *Spec. Publ. Geol. Soc. S. Africa* **13**, 341-354.

Hawkesworth, C.J., Erlank, A.J., Marsh, J.S., Menzies, M.A. and van Calsteren, P., 1983. Evolution of the continental lithosphere: evidence from volcanics and xenoliths in southern Africa. In: Hawkesworth C.J. and Norry, M.J. (eds.). *Continental Basalts and Mantle Xenoliths*, Shiva Publishing LTD, Cheshire, 139-157.

Henoc, J., Heinrich, K.F.J. and Myklebust, R.L., 1973. A rigorous correction procedure for quantitative electron probe microanalysis (COR 2). U.S. Bureau of Standards, Technical Note 769. U.S. Govt. printing Office, Washington D.C.

Hergt, J.M, Peate, D.W. and Hawkesworth, C.J., 1991. The petrogenesis of Mesozoic Gondwana low-Ti flood basalts. *Earth Planet Sci. Lett.* **105**, 134-148.

Hergt, J.M., Chappell, B.W., McCulloch, M.T., McDougall, I. and Chivas, A.R., 1989. Geochemical and Isotopic Constraints on the Origin of Jurassic Dolerites of Tasmania. *J. Petrology* **30**, 841-883.

Jennings, C.M.H., 1965. The geology of the Serowe area. *Records Geol. Surv. Bechuanaland Protectorate 1961-1962*, 61-75.

Jones, M.T., 1968. Brief explanation of the Notwane and Limpopo River area (QDS 2326D and part of 2327C), *1:125 000 Map, Geol. Surv. Botswana.*

Joplin, G.A., 1964. *A Petrography of Australian Igneous Rocks*, Angus and Robertson LTD, 210pp.

Key, R.M., 1977. The geological history of the Limpopo Mobile Belt based on the field mapping of the Botswana Geological Survey. In: Ermanovics, I.F., Key, R.M. and McEwen, G. (eds.), *The Proceedings of a seminar pertaining to the Limpopo Mobile Belt, Bull. Geol. Surv. Botswana* **12**, 41-59.

Key, R.M., 1976. The geology of the area around Francistown and Pikwe, Northeast and Central Districts, Botswana. *District Memoir Geol. Surv. Botswana* **3**, 121pp.

Krishnamurthy, P and Cox, K.J., 1980. A Potassium-Rich Alkalic suite from the Deccan Traps, Rajpipla, India. *Contrib. Mineral. Petrol.* **73**, 179-189.

Kuno, H., 1968. High-alumina Basalt. *J. Petrology* **1**, 121-145.

Lagarche, M., 1984. The exchange equilibrium distribution of alkali and alkaline-earth elements between feldspars and hydrothermal solutions. In: Brown, W.L. (ed.), *Feldspars and Feldspathoids*, D. Reidel Publishing Company, Holland, 247-279.

le Roex, A.P., 1985. Geochemistry, Mineralogy and Magmatic Evolution of the Basaltic and Trachytic Lavas from Gough Island, South Atlantic. *J. Petrology* **26**, 149-186.

le Roex, A.P. and Reid, D.L., 1978. Geochemistry of Karoo dolerite sills in the Calvinia District, Western Cape Province, South Africa. *Contrib. Mineral. Petrol.* **66**, 351-360.

Lindsley, D.H., 1976. The crystal chemistry and structure of oxide minerals as exemplified by the Fe-Ti oxides. In: Rumble, D. (ed.), *Reviews in Mineralogy, Vol.3: Oxide Minerals*, L1-52.

Litherland, M., 1975. The geology of the area around Maitengawe, Sebina and Tshesebe, Northeast and Central Districts, Botswana. *District Memoir Geol. Surv. Botswana* **2**, 133pp.

MacDonald, R., Crossley, R. and Waterhouse, K.S., 1983. Karoo basalts of southern Malawi and their regional petrogenetic significance, *Min. Mag.* **47**, 281-289.

Mackenzie, D.E. and Chappell, B.W., 1972. Shoshonitic and calc-alkaline lavas from the highlands of Papua New Guinea. *Contrib. Mineral. Petrol.* **35**, 50-62.

Marsh, J.S., 1989. Geochemical constraints on coupled assimilation and fractional crystallization involving upper crustal compositions and continental tholeiitic magma. *Earth Planet. Sci. Lett.* **92**, 70-80.

Marsh, J.S., 1987. Basalt geochemistry and tectonic discrimination within continental flood basalt provinces. *J. Volcan. & Geotherm. Res.* **32**, 35-49.

Marsh, J.S., Hooper, P.R., Rehacek, J., Duncan, R.A. and Duncan A.R., 1995. The building of Lesotho - new geochemical, palaeomagnetic and age data from Karoo basalts in Lesotho and implications for correlations within the Karoo Igneous Province. *Department of Geological Sciences, UCT, Centenary Conference, February 1995, Extended Abstracts.*

Marsh, J.S. and Eales, H.V., 1984. The geochemistry and petrogenesis of Igneous Rocks of the Karoo Central Area, Southern Africa. *Spec. Publ. Geol. Soc. S. Africa* **13**, 27-68.

Martin, A.K. and Hartnady, C.J.H., 1986. Plate Tectonic Development of the Southwest Indian Ocean: a Revised Reconstruction of East Antarctica and Africa. *J. Geophys. Res.* **91 (B5)**, 4767-4786.

Mason, R., 1967. The geology of the country around Baines Drift, Eastern Botswana. M.Sc. Thesis (unpubl.), University of Newcastle upon Tyne, U.K.

Mazor, E., Verhagen, B.Th., Sellschop, J.P.F., Jones, M.T., Robins, N.E., Hutton, L.G. and Jennings, C.M.H., 1977. Northern Kalahari groundwaters: hydrologic, isotopic and chemical studies at Orapa, Botswana. *J. Hydrol.* **34**, 203-234.

McKenzie, D., 1989. Some remarks on the movement of small melt fractions in the mantle. *Earth Planet. Sci. Lett.* **95**, 53-72.

McKenzie, D., 1978. Some remarks on the development of sedimentary basins. *Earth Planet. Sci. Lett.* **40**, 25-32.

McKenzie, D. and Bickle, M.J., 1988. The volume and composition of melt generated by extension of the lithosphere. *J. Petrology* **29**, 625-679.

Meixner, H.M. and Peart, R.J., 1984. The Kalahari drilling Project. *Bull. Geol. Surv. Botswana* **27**, 224pp.

Milner, S.C., 1988. The geology and geochemistry of the Etendeka formation quartz-latites, Namibia. Ph.D. Thesis (unpubl.), University of Cape Town, 263pp.

Muir, I.D. and Tilley, C.E., 1964. Iron enrichment and pyroxene fractionation in tholeiites. *Geol. Journ.* **4**, 143-156.

Mysen, B.O. and Boettcher, A.L., 1975a. Melting of a hydrous mantle: I_o phase relations of a natural peridotite at high pressures and temperatures with controlled activities of water, carbon dioxide and hydrogen. *J. Petrology* **16**, 520-548.

Mysen, B.O. and Boettcher, A.L., 1975b. Melting of a hydrous mantle: II Geochemistry of crystals and liquids formed by anatexis of mantle peridotite at high pressures and high temperatures as a function of controlled activities of water, hydrogen and carbon dioxide. *J. Petrology* **16**, 549-593.

Norrish, K. and Hutton, J.T., 1969. An accurate X-ray spectrographic method for the analysis of a wide range of geological samples. *Geochim. Cosmochim. Acta* **33**, 431-453.

Parsons, I. and Brown, W.L., 1984. Feldspars and the thermal history of Igneous Rocks. In: Brown, W.L. (ed.), *Feldspars and Feldspathoids*, D. Reidel Publishing Company, Holland, 317-371.

Pearce, J.A. and Norry, M.J., 1979. Petrogenetic Implications of Ti, Zr, Y and Nb Variations in Volcanic Rocks. *Contrib. Mineral. Petrol.* **69**, 33-47.

Peate, D.W., 1989. Stratigraphy and Petrogenesis of the Paraná Continental Flood Basalts, Southern Brazil. Ph.D. Thesis (unpubl.), The Open University, 360pp.

Peccerillo, A. and Taylor, S.R., 1976. Geochemistry of Eocene calc-alkaline volcanic rocks from the Kastamonu area, northern Turkey. *Contrib. Mineral. Petrol.* **58**, 63-81.

Pemberton, J., 1978. The geochemistry and petrology of Karoo basalts of the Barkly East area, north-eastern Cape. M.Sc. Thesis (unpubl.), Rhodes University, 139pp.

Reeves, C.V., 1978. A failed Gondwana spreading axis in Southern Africa. *Nature* **273**, 222-223.

Ridgway, J. and Money, N.J., 1981. Karoo Basalts from western Zambia and Geochemical Provinces in Central and Southern Africa. *Geol. Rundsch.* **70**, 868-873.

Roeder, P.L. and Emslie, R.F., 1970. Olivine-Liquid Equilibrium. *Contrib. Mineral. Petrol.* **29**, 275-289.

Rundle, C.C., 1983. A K-Ar study of Karoo Basalts from Botswana. *Unpubl. Rept. (IGU 83/5 G), Geochemistry and Petrology Division, IGS, London.*

Saunders, A.D., Storey, M., Kent, R.W. and Norry, M.J., 1992. Consequence of plume-lithosphere interactions. In: Storey, B.C., Alabaster, T. and Pankhurst, R.J. (eds.). *Magmatism and the Causes of Continental Break-up. Geol. Soc. Lond. Spec. Publ.* **68**, 41-60.

Secco, L., Carbonin, S., Dal Negro, A., Mellini, M. and Piccirillo, E.M., 1988. Crystal Chemistry of Pyroxenes from Basalts and Rhyodacites of the Paraná Basin (Brazil). In: Piccirillo, E.M. and Melfi, A.J. (eds.). *The Mesozoic Flood Volcanism of the Paraná Basin: petrogenetic and geophysical aspects.* Instituto Astronômico e Geofísico Publishers, 93-106.

Smith, D. and Lindsley, D.H., 1971. Stable and metastable augite crystallization trends in a single basalt flow. *Am. Miner.* **56**, 225-233.

Smith, H.S., Erlank, A.J. and Duncan, A.R., 1980. Geochemistry of some ultramafic komatiite flows from the Barbeton Mountain Land, South Africa. *Precambrian Research* **11**, 399-415.

Smith, R.A., 1984. The lithostratigraphy of the Karoo Supergroup in Botswana. *Bull. Geol. Surv. Botswana* **26**, 239pp.

Smith, R.A. and Phofuetsile, P., 1985. The geology of the Foley area. *Bull. Geol. Surv. Botswana* **31**, 107pp.

Stansfield, G. The geology of the area around Dukwe and Tlalamabele, Central District, Botswana. *District Memoir Geol. Surv. Botswana* **1**, 133pp.

Storey, B.C., Alabaster, T., Hole, M.J., Pankhurst, R.J. and Wever, H.E., 1992. Role of subduction-plate boundary forces during the initial stages of Gondwana break-up: evidence from the proto-Pacific margin of Antarctica. In: Storey, B.C., Alabaster, T. and Pankhurst, R.J. (eds.), *Magmatism and the Causes of Continental Break-up. Geol. Soc. Lond. Spec. Publ.* **68**, 125-136.

Sun, S.-s. and McDonough, W.F., 1989. Chemical and isotopic systematics of oceanic basalts: implications for mantle composition and processes. In: Saunders, A.D. and Norry, M.J. (eds.). *Magmatism in the Ocean Basins. Geol. Soc. Spec. Publ.* **42**, 313-345.

Sweeney, R.J., 1988. Geochemistry of the Sabie River Basalt Formation in the Central Lebombo, Karoo Igneous Province. Ph.D. Thesis (unpubl.), University of Cape Town, 309pp.

Sweeney, R.J., Duncan, R.A. and Erlank, A.J., 1994. Geochemistry and Petrogenesis of Central Lebombo Basalts of the Karoo Igneous Province. *J. Petrology* **35**, 95-125.

Sweeney, R.J., Falloon, T.J., Green, D.H. and Tatsumi, Y., 1991. The mantle origins of Karoo Picrites. *Earth Planet. Sci. Lett.* **107**, 256-271.

Sweeney, R.S. and Watkeys, M.K., 1990. A possible link between Mesozoic lithospheric architecture and Gondwana flood basalts. *J. African Earth Sci.* **10**, 707-716.

Swift, W.H., 1961. An outline of the Geology of Southern Rhodesia. *Bull. S. Rhodesia Geol. Surv.* **50**, 73pp.

Tankard, A.J., Jackson, M.P.A., Eriks'son, K.A., Hobday, D.K., Hunter, D.R. and Minter, W.E.L., 1982. *Crystal evolution of Southern Africa, 3.8 Billion years of Earth History*, Springer-Verlag, New York, 523pp.

Tennick, F.P. and Phaup, A.E., 1976. The Geology of the Country around Magondi, Lomagundi, Hartley and Gatooma Districts. *Bull. Geol. Surv. Rhodesia* **65**, 314pp.

Thomas, C.M., 1969. A short description of the geology of south Ngamiland. *Unpubl. Rept. Geol. Surv. Botswana.*

Vail, J.R., Hornung, G. and Cox, K.G., 1969. Karoo basalts of the Tuli Syncline, Rhodesia. *Bull. Volc.* **33**, 398-418.

Walker, F. and Poldervaart, A., 1949. Karoo dolerites of the Union of South Africa. *Bull. Geol. Soc. Amer.* **60**, 591-706.

White, R.S., 1992. Magmatism during and after continental break-up. In: *Magmatism and the Causes of Continental Breakup. Geol. Soc. Lond. Spec. Publ.* **68**, 1-16.

White, R. and McKenzie, D., 1989. Magmatism at Rift Zones: The generation of Volcanic Continental Margins and Flood Basalts. *J. Geophys. Res.* **94 (B6)**, 7685-7729.

Williams, H., Turner, F.J. and Gilbert, C.M., 1954. *Petrography - An introduction to the study of rocks in thin sections.* W.H. Freeman and Company, 406pp.

Wilson, J.F., Jones, D.L. and Kramer, J.D., 1987. Mafic Dyke Swarms in Zimbabwe. In: Halls, H.C. and Fahrig, W.F. (eds.), *Mafic Dyke Swarms*, Geol. Assoc. Canada Spec. Paper 34, 433-444.

Winkler, H.G.F., 1979. *Petrogenesis of Metamorphic Rocks.* Springer-Verlag, New York, 348pp.

Yoder, H.S. and Tilley, C.E., 1962. Origin of basalt magmas: An experimental study of natural and synthetic rock systems. *J. Petrology* 3, 342-532.

CONTENTS

APPENDIX A
BOTSWANA BASALT AND DOLERITE SAMPLE SET

A.1 THE UCT BOTSWANA SAMPLE COLLECTION

KLB-001 Locality: 26°38'E 22°22'S
A dolerite dyke intruded into basalt.

KLB-002 Locality: Serwe Pan (17.6km N of Serowe)
Basalt from borehole core S326'

KLB-003 Locality: Serwe Pan
Possible intrusive dolerite from borehole core S171'

KLB-004 Locality: Mashoro (72km N of Serowe)
Basalt from borehole core M121'

KLB-005 Locality: Mashoro
Basalt from borehole core M202'

KLB-006 Locality: Kolokome (46.4km N of Serowe)
Basalt from borehole core K21'

KLB-007 Locality: Kolokome
Basalt from borehole core K355'

KLB-014 Locality: borehole NG1 (21°18'E 20°39'S)
Very altered and veined basalt from depth: 83.0-83.2m

KLB-015 Locality: NG1
Very altered and veined basalt from depth: 93.0-93.2m

KLB-016 Locality: NG1
Very altered and veined basalt from depth: 103.0-103.25m

KLB-017 Locality: borehole CKP6 (23°04'E 22°17'S)
Very altered and veined basalt from depth: 102.44-102.65m

KLB-018 Locality: CKP6
Very altered and veined basalt from depth: 103.0-103.45m

KLB-019 Locality: borehole CKP11 (25°06'E 18°36'S)
Very altered basalt from depth: 82.5-82.9m

KLB-020 Locality: CKP11
Very altered basalt from depth: 86.7-87.0m

KLB-021 Locality: borehole C2 (26°14'E 22°15'S)
Altered basalt from depth: 139.40m

KLB-022 Locality: borehole C6 (26°19'E 22°15'S)
Altered basalt from depth: 65.5m

KLB-023 Locality: borehole K2 (25°45'E 23°19'S)
Altered basalt from depth: 33.6-34.0m

KLB-024 Locality: borehole K3 (25°51'E 23°21'S)
Altered basalt from depth: 70.2-70.5m

KLB-025 Locality: borehole E7 (26°14'E 23°42'7"S)
Altered basalt from depth: 90.75-91.0m

KLB-026 Locality: borehole N13 (26°46'E 22°25'S)
Basalt from depth: 33.8-34.2m

KLB-027 Locality: borehole N13
Basalt from depth: 61.8m

COLLECTED BY A.E. MOORE (MAY 1989)
KLB-028 to KLB-037 were taken over ±300m from three different dykes intruded into acid metavolcanics downstream from the major bend in the Tati River (27°33'E, 21°12'S).

KLB-028 NE chill margin (±50cm wide) of a 10m wide dolerite dyke.

KLB-029 Coarse-grained centre of the dolerite dyke.

KLB-030 A ±30cm wide dyke (with no chill margins) intruded into NE chill margin of the above dyke.

KLB-031 A float block in the river bed adjacent to the SW margin of the above dyke.

KLB-032 SW chill margin of the above dolerite dyke.

KLB-033 Centre of a 2m wide dolerite dyke found 12m to the NE, and parallel to, the above dolerite dyke.

KLB-034 The chill margin of a 25m wide dolerite dyke.

KLB-035 Coarse-grained centre of the above dyke.

KLB-036 A narrow (30cm wide) dyke which is parallel to, and to the NE of, the above dyke.
KLB-037 Coarse-grained centre of an 8m wide dyke, which is found 100m SW of the reservoir.
KLB-038 Locality: The Golden Eagle mine (27°34'E, ±21°15'S), with permission of Phelps Dodge.
A core sample of a fine-grained dolerite dyke.
KLB-039 A second core sample of a fine-grained dolerite dyke.

The samples KLB-040 to 043 were taken along a small N-S track running just E of the Sikukwe River (27°39'30"E, 21°19'30"S) and appear to be roughly parallel with a ±E-W strike.

KLB-040 Coarse-grained centre of a narrow dolerite dyke.
KLB-041 Chilled margin of a narrow dyke.
KLB-042 Coarse-grained centre of the above dolerite dyke.
KLB-043 A narrow dolerite dyke located between the dolerite dykes sampled by KLB-040, 041 and -042.

COLLECTED BY GEOFF GUSHEÉ (JUNE 1989)

KLB-044 Locality: Nora Mine, ±3km SSW of the Tati River area in which KLB-028 to -037 were sampled.
A basalt core sample.

COLLECTED BY JOHN BRISTOW (AUGUST 1989)

Core samples KLB-045 to -048 are from the borehole LGT2, which was drilled within 100m of the edge of the Letlhakane kimberlite pipe (at 25°41'23"E, 21°31'10"S).

KLB-045 Depth 44.2-44.3 metres.
KLB-046 Depth 58.1-58.3 metres.
KLB-047 Depth 84.1-84.2 metres.
KLB-048 Depth 95.2-95.3 metres.

COLLECTED BY A.E. MOORE (NOVEMBER 1989)

KLB-049 A dolerite dyke from the southern margin of Sua Pan.
KLB-050 A second dolerite dyke from the southern margin of Sua Pan.

COLLECTED BY A.E. MOORE (DECEMBER 1989)

KLB-051 Locality: 41km N of Palapye on the Gaberone - Francistown road.
Strike: 320°. The ±30m wide dolerite dyke consists of rounded boulders which are presumably essentially in situ, although none represents unequivocal outcrop. This finer-grained sample (relative to KLB-052) is from the centre of the dyke.
KLB-052 A coarser grained dolerite from the "south margin" of the above dolerite dyke.
KLB-053 Locality: 3km N of Palapye on the Gaberone - Francistown road.
Sampled from an isolated pile of dolerite boulders (up to 500m in diameter).

COLLECTED BY A.E. MOORE (NOVEMBER 1990)

KLB-054 Locality: 22km from the turn-off to Orapa just outside Serowe (*i.e.* 22km NW of Serowe).
A basalt outcrop in the road cuttings.
KLB-055 A second basalt sample from the above outcrop.
KLB-056 Locality: 3km from the turn-off to Orapa just outside Serowe (*i.e.* 3km NW of Serowe).
A dolerite sill exposed in road cuttings.

COLLECTED BY A.E. MOORE (MARCH 1991)

KLB-057 Locality: 29°20.7'E, 22°0.6'S
Strike: ±E-W. A dolerite dyke with an estimated width of 10-30m.
KLB-058 A second sample from the above site.
KLB-059 Locality: 29°18.5'E, 22°0.5'S
Sampled 3km to the west from the same dyke as above (KLB-057 and -058).
KLB-060 A second sample from the above site.

Samples KLB-061 to KLB-066 are all collected from the same general area (at ±29°18.15'E, 21°59.2'S).

KLB-061 A narrow dyke to the south of the general area.
KLB-062A A narrow dyke to the north of the general area.
KLB-062B A second sample from the above dyke.
KLB-063 A basalt with rare plagioclase phenocrysts.
KLB-066 A basalt with a high proportion of plagioclase phenocrysts.
KLB-067 Locality: 1km N of the area sampled in KLB-061 to -066 (±29°18.3'E, 21°58.7'S).
A narrow dolerite dyke.
KLB-068 Second sample from the above dyke.
KLB-070 A basalt sample collected from the same general area sampled by KLB-069.

A.2 A SUMMARY OF THE SAMPLES COLLECTED IN EASTERN BOTSWANA (JUNE 1991)

KLB-071 Locality: 3.3km along Mabalei Estate - Kees cut line[1]
Strike: 85°. A coarse-grained dolerite dyke with a width of ≥5m and extensive strike length.

KLB-072 Locality: 4.4km past the river on the Mabalei Estate- Kees cut line.
Strike: 300±5°. A coarse-grained dolerite dyke with a width ≥19m. The relative position of the sample within the dyke is obscured by poor outcrop.

KLB-073 Locality: 1.2km from Zanzibar turn-off on the road to Baines Drift.
Strike: 135±15°. A dolerite dyke with a width ≥10m and extensive strike length.

KLB-077 Locality: 23.4km from Baines Drift
Strike: Apparently NNW - SSE. A coarse-grained gabbro/mafic pod with poor outcrop exposure and alteration products that are more red than usual.

KLB-078 Locality: 24.3km from Baines Drift
Strike: ±175 - 180°. A coarse-grained dolerite dyke with a width ≥35m and well defined chill margins, where the dolerite is in contact with the country rock (gneiss).

KLB-079 Locality: 30.9km from Baines Drift.
Strike: 110°. Sampled from a set of at least four narrow, fine grained, plagioclase-phyric dolerite dykes which range in thickness from ±1m to 2½m (including chill margins).

KLB-080 Locality: Approximately parallel to the Matloutse River where the Baines Drift-Pont Drift road crosses the river bed.
Strike: ±65°. A ±10m wide, grey coloured, very fine-grained, felsite dyke with small aggregates of plagioclase, pyroxene and oxide phenocrysts. The dyke defines a positive topographic feature with a minimum strike length of ±2km in the aerial photograph MOT 29 (333)[2].

KLB-081 Locality: ±500m NW of KLB-080
Strike: A local strike of 290° measured. A ±80m wide plagioclase-phyric sinuous dolerite dyke with chill margins present where contact with the country rock is exposed. A minimum strike length of ±8km is observed in the aerial photograph MOT 29 (333).

KLB-082 Locality: ±1.5km SW of KLB-080.
Strike: ±N-S. A fine-grained grey coloured felsite dyke with rare altered phenocrysts of plagioclase, pyroxene and oxide. This felsite dyke defines a positive topographic feature and has a minimum strike length of ±3.5km in the aerial photograph MOT 29 (333).

KLB-083 Locality: On the border between the farms Uithuis and Merryhill adjacent to the Limpopo River.
A basal picritic basalt filling a basin/trough (which extends ±NNE - SSW (35°) towards the paleolimpopo river) defined by the underlying aeolian sandstone.

KLB-084 Locality: 5km from the Merryhill farm house on route to Jwala (the Pont Drift road).
A picritic basalt.

KLB-085 Locality: 9.8km from Pont Drift
Strike: ±E - W. A fine-grained plagioclase-pyroxene-phyric dolerite dyke which is intruded into basalt (altered flow tops seen in contact with the dyke margins).

KLB-087 Locality: 10.7km along Pont Drift road
Strike: 295°. A ≥10n wide fine-grained plagioclase-pyroxene-oxide-phyric dolerite dyke.

KLB-088 Locality: 11.9km from Pont Drift.
Sample taken from within a plagioclase-pyroxene-oxide-phyric basalt flow with altered material from the flow top (including amygdale "agates") present in the scree slope.

KLB-089 Locality: Success Hide ±9km N of the Jwala Game Reserve Lodge.
Strike: 100°. A dolerite dyke with a width of ±5m and a minimum strike length of ±10km as observed in the aerial photograph MOT 26 (006).

KLB-090 Locality: ±3km SSW of Success Hide.
A dolerite found as float in a dry river bed, probably from a dolerite dyke north of Success Hide.

KLB-091 Locality: 4.4km from Jwala lodge on route to Semolale.
Strike: A local strike of 190° measured. A fine-grained plagioclase-pyroxene-phyric dolerite collected from a set of roughly parallel dolerite dykes which intrude both basalt and dolerite.

KLB-092 Locality: 8km from the cordon fence
Strike: ±WNW. A plagioclase-pyroxene-phyric (≤6mm) dolerite dyke which defines a 15-20km

---

[1] The Mabalei-Kees cutline is on the Palapye map, sheet no. 24, Botswana 1:250 000.

[2] Aerial photographs from Botswana photography 1/88 (Motlouse Block)

long topographic feature on the aerial photographs MOT 26 (004-008).

KLB-093 Locality: ±9km from the cordon fence
A fine-grained plagioclase-pyroxene-phyric (≤2.5mm) dolerite dyke.

KLB-094 Locality: The river bed of the Mjali River.
A fine-grained basalt with amygdales which ranged in size from ≥4cm to ≤15cm.

KLB-095 Locality: 8.5km from the cordon fence gate on the Semolale road
Strike: 310°. A fine-grained dolerite dyke with a width of ±1m.

KLB-096 Locality: 13.8km from the cordon fence gate
A plagioclase-phyric (≤1.5cm) basalt.

KLB-097 Locality: 18.2km from the cordon fence gate
A fine-grained amygdaloidal basalt (with a high proportion of tiny amygdales).

KLB-098 Locality: 18.8km from the cordon fence gate
Strike: ±E - W. Sampled from one of apparently two plagioclase-pyroxene-phyric dolerite dykes intruded into basalt, but poor outcrop exposure obscures distinction between basalt and dolerite.

KLB-099 Locality: 20.4km from the cordon fence gate
Strike: ±280°. A medium-grained plagioclase-pyroxene-phyric dolerite dyke.

KLB-100 Locality: 27km from the cordon fence gate
Collected from a basalt (with rare tiny amygdales) flow which defines a horse-shoe shaped ridge.

KLB-101 Locality: The Semolale Police Station.
A basalt flow which may overly granite and/or sandstone as both are seen in the scree slope.

KLB-102 Locality: 11km from Tshesebe.
Strike: ±80°. A ±40m wide dolerite dyke, intruded into a granite, with well defined fine-grained chill margins. Sample was collected from a bulldozer pile on the side of the road.

KLB-103 Locality: 10km from Tshesebe.
Strike: 120°. The outcrop of this fine-grained dolerite dyke was poor, but it was estimated to be >10m wide. The samples were collected from a bulldozer pile.

KLB-104 Locality: See KLB-103
A possible chill phase of the dolerite dyke of KLB-103, but the sample collected from a mixed jumble of scree in a bulldozer pile.

KLB-105 Locality: 4km S of Tshesebe.
A ±50m wide dolerite dyke with the sample collected from near the centre of the dyke. Patches of pegmatitic schlieren were evident in many of the boulders of dolerite in the bulldozer rubble.

KLB-106 Locality: 2.5km S of Tshesebe.
Strike: 250°. A fine-grained dolerite collected from the bulldozer rubble associated with the dyke.

KLB-107 Locality: ±500m S of Tshesebe.
A dolerite dyke seen predominantly as scree adjacent to the road.

KLB-108 Locality: ±4km N of Tshesebe.
A plagioclase-phyric (≤2cm) dolerite dyke with a "salt & pepper" appearance in hand specimen.

KLB-109 Locality: ±8.5km S of Ramokgwebane.
The sample collected from the chill margin of a dolerite dyke, one in a set of prominent dykes which have a different strike direction (predominantly NNE) to the dyke swarm.

KLB-110 The coarse-grained centre of the above dolerite dyke.

KLB-111 Locality: 1.3km N of Ramokgwebane
The second dolerite dyke of the set mentioned in KLB-109.

KLB-112 Locality: ±3.5km E of Habangana.
Strike: 25°. The third and poorly exposed dolerite dyke of the above mentioned set.

KLB-113 Locality: Exact locality unknown as the roads have changed considerably since they were last mapped, but possibly on the NE corner of a dolerite dyke in the Sebina-Tshesebe map (*i.e.* quarter degree sheet no. 2027C with parts of 2027D and 2027B (M. Litherland).
Strike: 70°. A dolerite dyke with rare altered phenocrysts.

A.3 A SUMMARY OF THE SAMPLES COLLECTED IN THE CORE SHED OF THE GEOLOGICAL SURVEY OF BOTSWANA, LOBATSE.

P11

Locality: 25°45'E, 19°15'S
129.6-156.10m: A fine-grained dark grey basalt with well defined and altered flow margins.
KLB-114: 139.5-139.8m
156.10-179.15m: A medium-grained grey-green basalt with well defined and altered flow margins.

KLB-115: 165.85-166.13m
KLB-116: 169.95-170.20m
179.15-186.10: A medium-grained basalt with well defined and altered flow margins.
KLB-117: 185.20-185.45m
186.10-188.70m: A fine-grained and amygdaloidal basalt.
188.70-197.2m: A medium-grained grey-green basalt with well defined and altered flow margins.
KLB-118: 195.47-195.75m
197.20-205.35m: A medium-grained basalt with well defined flow margins.
KLB-119: 197.35-197.60m
KLB-120: 204.05-204.35m
205.35-205.45m: An interval of highly altered, tuffaceous basalt.
205.45-217.6m: A medium-grained grey-green basalt flow with well defined and altered flow margins.
KLB-121: 209.00-209.24mn
KLB-122: 213.20-
217.60-233.65m: A basalt with well defined and altered flow margins.
KLB-123: 230.25-230.55m
233.65-254.60m: A medium-grained basalt with well defined and altered flow margins.
KLB-124: 242.57-242.85m
KLB-125: 245.70-245.97m
254.60-307.80m: A coarse-grained basalt with an altered and amygdaloidal flow top.
KLB-126: 265.43-265.62m
KLB-127: 269.75-269.90m
KLB-128: 289.00-289.30m
307.80-319.00m: A very amygdaloidal and altered interval probably reflecting adjacent flow margins.
KLB-129: 311.50-311.73m
319.00-325.40m: An altered basalt with poorly defined flow margins.
325.40-356.05m: A medium-grained basalt with an altered and amygdaloidal flow top.
KLB-130: 332.80-333.00m
356.05m-367.15m: An altered medium-grained basalt with an altered and amygdaloidal flow top.
367.15-372m: An altered basalt with an altered and amygdaloidal flow top.
372-404m: An interval of shattered and unlabelled core.
KLB-131: 373.2-373.5m
419.05-491.60m: A medium-grained basalt with an altered and amygdaloidal flow top.
KLB-133: 472.12-472.38m
491.60-499.55m: An altered basalt with very altered and amygdaloidal flow margins.
The Shell Coal logs identify ±40cm of green tuff in the interval 498.8 to 491.60m.
KLB-134: 496.48-496.76m
499.55m: SANDSTONE

P 12

Location: 25°38'E, 18°46'S

41.50-64.10m
An interval of very altered and amygdaloidal basalt with poor core recovery.
64.10-72.50m: An altered, medium-grained basalt with altered and amygdaloidal flow margins.
KLB-135: 69.50-69.75m
72.50-77.22m: A basalt with an altered and amygdaloidal flow top.
KLB-136: 75.70-75.97m
77.22-79.73m: A basalt with an altered and amygdaloidal flow top.
79.73-105.82m: A thick basalt with an altered and amygdaloidal flow top and the base of the flow is very veined. **KLB-137:** 95.15-95.37m
105.82-109.80m: A fine-grained basalt with an altered and amygdaloidal flow top.
KLB-138: 109.00-109.22m
109.80-123.20m: A basalt with well defined flow margins.
KLB-139: 119.35-119.62m
123.20-124.55m: A basalt with well defined flow margins.
124.55-149.10m: A basalt with an altered and amygdaloidal flow top with amygdales concentrated in layers within the basalt.
KLB-140: 133.90-134.15m
149.10-165.80m: A basalt with poorly defined flow margins.
KLB-141: 150.20-150.47
165.80 -183.20m: A basalt with well defined flow margins.
183.20-185.10m: A thin, altered and amygdaloidal basalt.

185.10-191.50m: A fine-grained, altered basalt with an altered and amygdaloidal flow top.
KLB-142: 189.60-189.97
191.50-199.10m: An altered basalt with well defined flow margins.
199.10-215.90m: A basalt with an altered and amygdaloidal flow top.
KLB-143: 208.20-208.43m
215.90-231.25m: A basalt with well defined flow margins.
KLB-144: 228.20-228.43m
231.25-254.10m: A medium-grained basalt with well defined flow margins.
KLB-145: 253.25-253.50m
254.10-287.00m: A medium-grained basalt with well defined flow margins.
KLB-146: 279.00-279.25m
287.00-301.85m: A basalt with well defined flow margins.
KLB-147: 297.70-297.96m
301.85-315.20m: A medium grained basalt with an altered and amygdaloidal flow top.
KLB-148: 311.65-311.90m
315.20-334.55m: A basalt flow with well defined flow margins.
KLB 149: 331.50-331.74m
234.35-359.05m: A basalt flow with well defined flow margins.
KLB-150: 339.95-340.20
359.05m: SANDSTONE

P8

Location: 26°02'E, 19°24'S
155.70-187.88m: A fine-grained dark grey basalt with a very altered and amygdaloidal flow top.
KLB-152: 166.26-165.81m
187.88-191.60m: Two basalt flows, each ±2m thick, with well defined flow margins are present in this interval.
191.60-192.31m: Red-brown siltstone.
192.31-196.33m: A shattered interval of core with a poor recovery. The basalt is altered and amygdaloidal. The Shell Coal logs identify a thin (30cm) fine-grained interbedded sandstone at ±193.90m.
196.33-196.80m: Grey siltstone.
196.80-204.04m: A basalt with an altered and amygdaloidal flow top.
A ±20cm thick sandstone lens appears to be included into the basalt at ±201.30m as the appearance of the basalt is similar on either side of the sandstone.
KLB-155: 201.60-202.04m
204.04-205.98m: A narrow amygdaloidal basalt.
205.98-206.12m: Red-brown siltstone.
206.12-216.25m: A basalt with well defined flow margins.
KLB-156: 211.70-211.94m
216.2-225.10m: A fine-grained basalt with an amygdaloidal flow top.
KLB-157: 216.3-216.5m
KLB-158: 222.26-222.60m
225.10-229.70m: A basalt with well defined flow margins.
KLB-159: 228.54-228.84m
229.70-234.66m: A basalt with well defined flow margins.
KLB-160: 232.71-233.00m
234.66-244.6m: A basalt with well defined flow margins.
KLB-161: 244.13-244.45m
244.60-254.60m: A basalt with an altered and amygdaloidal flow top with amygdales concentrated in layers in the basalt.
KLB-162: 251.90-252.20m
254.35-259.82m: A narrow flow with well defined flow margins.
KLB-163: 258.00-258.32m
259.82-264.97m: A basalt with well defined flow margins.
264.97-269.10m: An amygdaloidal basalt.
269.10-272.50m: A fine-grained basalt.
KLB-164: 270.58-270.90m
272.50-280.13m: A fine-grained basalt with an amygdaloidal flow top.
KLB-165: 278.62-278.92m
280.13-284.54m: A very altered and amygdaloidal basalt.
284.54-321.33m: A basalt with well defined flow margins.
KLB-166: 299.42-299.75m
KLB-167: 319.07-319.35m

321.33-332.85m: A basalt with well defined flow margins.
KLB-168: 331.15-331.40m
332.85-335.05m: A fine-grained amygdaloidal basalt.
335.05-341.10m: A fine-grained basalt with an amygdaloidal flow top.
KLB-169: 340.25-340.48m
341.10-348.83m: A fine-grained basalt with well defined flow margins.
KLB-170: 346.70-346.95m
348.83-361.52m: A veined, amygdaloidal and altered basalt with well defined flow margins.
KLB-171: 359.90-360.14m
361.52-370.96m: A fine-grained basalt with well defined flow margins and a high degree of veining.
KLB-172: 368.25-368.60m
370.96-376.53m: A fine-grained basalt with well defined flow margins and a high degree of veining.
KLB-173A: 375.39-375.57m
376.53-383.50m: A fine-grained basalt with well defined flow margins.
383.50-385.18m: An altered, veined and amygdaloidal basalt.
KLB-173B: 384.00-384.29m
385.18-387.22m: An altered and amygdaloidal basalt with well defined flow margins.
387.22-407.69m: A fine-grained basalt with well defined flow margins and a high degree of veining.
KLB-174: 406.81-407.11m
407.69-420.85m: A fine-grained basalt with an altered and amygdaloidal flow top and a high degree of veining.
KLB-175: 413.10-413.33m
420.85-425.47m: A fine-grained basalt with an altered and amygdaloidal flow top and a high degree of veining.
425.47-433.87m: A very altered and amygdaloidal basalt. The core was shattered and recovery was poor.
433.87m: SANDSTONE

NG1

Locality: 21°18'E, 20°39'S
67.6-87.05m: There was a poor recovery of the core in this interval as the basalt is highly altered and fractured.
KLB-177: 74.48-74.70m
KLB-178: 80.90-81.07m
87.05-88.25m: Red-brown sandstone interbedded with the altered and fractured basalt. (BGR Kalahari Project (GS-17-G)-Drill log notes the presence of a red sandstone layer interbedded with the basalts at 87.5-88.8m)
88.25-90.85m: A narrow basalt flow with amygdaloidal and very altered flow margins. (BGR Kalahari Project (GS-17-G)-Drill log notes the presence of a second red sandstone layer interbedded with the basalts at 89.43-89.77m) and in the sample KLB-179 a contact between a sandstone (quartzite) and the basalt is preserved.
KLB-179: 89.55-89.87m
90.85-103.25m: A new basalt interval with a very altered and fractured "flow top" and the remaining basalt is essentially similar in appearance, colour, alteration style and veining.
KLB-180: 92.2-92.41m
KLB-181: 95.5-95.65m
KLB-182: 98.5-98.7m
KLB-184: 101.0-101.15m

CKP6

Locality: 23°04'E, 22°17'S
72.50-77.00m: A basalt flow with well defined flow margins and a very altered and veined flow top.
KLB-185: 75.32-75.54m
77.00-93.29m: A coarse-grained basalt with a well defined flow margins.
KLB-186: 81.54-81.83m
93.29-122.63m: A coarse-grained basalt with well defined flow margins and a veined and amygdaloidal flow top.
KLB-187: 100.89-101.14m
KLB-188: 118.28-118.50m
122.63-133.72m: A basalt with a veined and amygdaloidal flow top.
KLB-189: 132.49-132.72m
133.72-178.66m: Five different basalt flows with well defined flow margins are recognised in this interval.
178.66m: SANDSTONE

GWETA

Locality: 25°13'25"E, 20°16'19"S
160.25-180.23m:
Appears to be a single flow with an extensively veined and slightly amygdaloidal flow top. The grain size increases into the flow while the concentration of amygdales and veins decrease. The base of the flow is recognised by an increase in the concentration of amygdales, veining and the increased degree of alteration. At 173.6m ±5cm of highly fractured basalt is associated with calcite development.
KLB-195: 169.3-169.6m (The basalt contained a high concentration of tiny amygdales and was sorted prior to sample preperation)

C1

Locality: 23°46'E, 21°24'S
104.10-112.08m: A basalt with a very altered, veined and amygdaloidal flow top.
KLB-196: 110.79-111.08m
112.08-164.39m: A very altered, veined and amygdaloidal interval with three different basalt flows with well defined flow margins identified.
164.39-167.93m: A basalt flow with well defined flow margins.
KLB-197: 165.68-165.92m
167.93-187.11m: The first 4-4½m of this interval are highly vesicular, but grades rapidly into a typical basalt. ±1m of altered basalt is included at ±180m. The base of the basalt interval is altered and amygdaloidal.
KLB-198: 171.5-171.81m
187.11-264.40m: A basalt with well defined and altered flow margins. The increased concentration of amygdales towards the end of the borehole interval suggests that the base of this flow is at ±264.5m.
KLB-199: 211.88-
KLB-200: 248.40-248.73.

CKP11

Locality: 25°06'E, 18°36'S
31.0-37.5m: Very altered and veined basalt
37.5-48.6m: A basalt with an amygdaloidal flow top and amygdales concentrated in layers within the basalt.
48.6-50.4m: An interval of very altered basalt.
50.4-63.2m: A basalt with poorly defined flow margins.
KLB-201: 52.57-52.77m
KLB-202: 58.13-58.32m
63.2-67.37m: A basalt with well defined flow margins.
67.37-72.92m: A basalt with well defined and altered flow margins.
KLB-203: 71.67-72.00m
72.92-87.00m: A basalt with well defined and altered flow margins.
KLB-204: 85.70-85.90m
87.00-100.78m: A basalt with an altered and amygdaloidal flow top. An increase in the concentration of amygdales towards the end of the borehole interval suggests that the base of the flow is at ±101m.
KLB-205: 98.15-97.95m

C7

Locality: 23°57'E, 21°06'S
64.0-81.0m: An altered and veined basalt.
81.0-89.20m: A basalt with well defined flow margins and a very veined and amygdaloidal flow top.
KLB-206: 87.75-88.0m
89.2-93.3m: A basalt with a well defined flow top.
93.3-94.57m: A basalt with a very vesicular to amygdaloidal flow top.
94.57 and 99.0m. A basalt with a very altered and vesicular to amygdaloidal flow top.
KLB-207: 96.6-96.87m
99-120.0m: A basalt with well defined flow margins.
KLB-208: 118.8-119.05m
120.0-141.0m: A basalt with well defined and veined flow margins.
141-160.3m: A basalt with well defined flow margins.
KLB-209: 155.8-156.09m
160.3m: SANDSTONE

T529

Locality: 26°38'E, 22°12'S

11-270.5m: This borehole was not logged as the cores were neither sorted nor well labelled. Samples were taken where approximate depths within the basalt interval were available. At approximately 100m a ±6m thick mudstone layer is interbedded with the basalt.

KLB-210: ±203.4m
KLB-211: ±213.2m
KLB-212: ±32.6m
KLB-213: ±75.1m
KLB-214: ±136m

A.4 DRILL CHIPS COLLECTED AT DE BEERS PROSPECTING, BOTSWANA.

NXAI PAN (or borehole 8X004)

Locality: 24°46'E, 19°31'36"S

Chips were collected over every metre during drilling and the samples were taken from these drill chips. Geophysical analyses were run concurrently with drilling and the total gamma (measured using a neutron tool) showed a sharp decrease at ±275m from ±100 to ≤20 API.

±241-±264m: A plagioclase-phyric basalt with an amygdaloidal and altered (predominantly green coloured) flow top.

DB-14: 260-261m

±264-±272m: A plagioclase-phyric basalt with an amygdaloidal and altered (predominantly green coloured) flow top.

DB-16: 269-270m

±287-±301m: A basalt with an amygdaloidal and altered (predominantly red-brown coloured) flow top.

DB-19: 298-299m

±302±312m: A basalt with an amygdaloidal and altered (predominantly red-brown coloured) flow top.

DB-20: 308-309m

TABLE A.1 SUMMARY OF THE SAMPLE LOCALITIES (LATITUDE AND LONGITUDE) FOR THE GEOCHEMICAL SUB-GROUPS DEFINED IN THIS STUDY

SAMPLE NUMBER	LATITUDE	LONGITUDE
LOW-K_2O LINEAGE		
Low-MgO LTZ picritic basalts		
KLB-128	19°15'	24°45'
KLB-172	19°24'	26°02'
KLB-009	-	-
LTZ basalts		
KLB-004	21°56'	26°24'
KLB-005	21°56'	26°24'
KLB-006	22°04'	26°38'
KLB-007	22°04'	26°38'
KLB-010	-	-
KLB-012	-	-
KLB-013	-	-
KLB-019	18°36'	25°06'
KLB-020	18°36'	25°06'
KLB-021	22°15'	26°14'
KLB-022	22°15'	26°19'
KLB-025	23°42'7"	26°14'
KLB-026	22°25'	26°46'
KLB-027	22°25'	26°46'
KLB-045	21°31'10"	25°41'23"
KLB-046	21°31'10"	25°41'23"
KLB-047	21°31'10"	25°41'23"
KLB-054	22°13'	26°43'
KLB-115	19°15'	25°45'
KLB-116	19°15'	25°45'
KLB-118	19°15'	25°45'
KLB-119	19°15'	25°45'
KLB-120	19°15'	25°45'
KLB-121	19°15'	25°45'
KLB-122	19°15'	25°45'
KLB-123	19°15'	25°45'
KLB-124	19°15'	25°45'
KLB-125	19°15'	25°45'
KLB-126	19°15'	25°45'
KLB-127	19°15'	25°45'
KLB-129	19°15'	25°45'
KLB-130	19°15'	25°45'
KLB-131	19°15'	25°45'
KLB-133	19°15'	25°45'
KLB-134	19°15'	25°45'
KLB-135	18°46'	25°38'
KLB-137	18°46'	25°38'
KLB-138	18°46'	25°38'
KLB-139	18°46'	25°38'
KLB-140	18°46'	25°38'
KLB-141	18°46'	25°38'
KLB-142	18°46'	25°38'
KLB-143	18°46'	25°38'
KLB-144	18°46'	25°38'
KLB-145	18°46'	25°38'
LTZ basalts (continued)		
KLB-146	18°46'	25°38'
KLB-147	18°46'	25°38'
KLB-148	18°46'	25°38'
KLB-149	18°46'	25°38'
KLB-150	18°46'	25°38'
KLB-155	19°24'	26°02'
KLB-156	19°24'	26°02'
KLB-157	19°24'	26°02'
KLB-158	19°24'	26°02'
KLB-160	19°24'	26°02'
KLB-161	19°24'	26°02'
KLB-162	19°24'	26°02'
KLB-163	19°24'	26°02'
KLB-164	19°24'	26°02'
KLB-166	19°24'	26°02'
KLB-167	19°24'	26°02'
KLB-168	19°24'	26°02'
KLB-188	22°17'	23°04'
KLB-189	22°17'	23°04'
KLB-196	21°24'	23°46'
KLB-200	21°24'	23°46'
KLB-201	18°36'	25°06'
KLB-202	18°36'	25°06'
KLB-203	18°36'	25°06'
KLB-204	18°36'	25°06'
KLB-205	18°36'	25°06'
KLB-210	22°12'	26°38'
KLB-211	22°12'	26°38
KLB-212	22°12'	26°38'
KLB-213	22°12'	26°38'
KLB-214	22°12'	26°38'
DB-19	19°31'36"	24°46'
DB-20	19°31'36"	24°46'
High-Na_2O LTZ basalts		
KLB-011	-	-
KLB-017	22°17'	23°04'
KLB-018	22°17'	23°04'
KLB-048	21°31'10"	25°41'23"
KLB-055	22°13'	26°43'
KLB-117	19°15'	25°45'
KLB-165	19°24'	26°02'
KLB-170	19°24'	26°02'
KLB-171	19°24'	26°02'
KLB-173A	19°24'	26°02'
KLB-173B	19°24'	26°02'
KLB-174	19°24'	26°02'
KLB-175	19°24'	26°02'
KLB-185	22°17'	23°04'
KLB-186	22°17'	23°04'
KLB-187	22°17'	23°04'
High-Na_2O LTZ basalts (continued)		
KLB-195	20°16'19"	25°13'25"
KLB-197	21°24'	23°46'
KLB-198	21°24'	23°46'
KLB-199	21°24'	23°46'
KLB-206	21°06'	23°57'
KLB-207	21°06'	23°57'
KLB-208	21°06'	23°57'
KLB-209	21°06'	23°57'
Low-P_2O_5 LTZ basalts		
KLB-015	20°39'	21°18'
KLB-016	20°39'	21°18'
KLB-023	23°19'	25°45'
KLB-024	23°21'	25°51'
KLB-179	20°39'	21°18'
KLB-180	20°39'	21°18'
KLB-181	20°39'	21°18'
KLB-182	20°39'	21°18'
KLB-184	20°39'	21°18'
Type I LTZ dolerites		
KLB-049	21°14'	26°04'
KLB-050	21°14'	26°04'
HTLZ basalts		
KLB-100	21°58'	28°54'
KLB-177	20°39'	21°18'
KLB-178	20°39'	21°18'
HTLZ dolerites		
KLB-028	21°12'	27°33'
KLB-029	21°12'	27°33'
KLB-032	21°12'	27°33'
KLB-033	21°12'	27°33'
KLB-034	21°12'	27°33'
KLB-035	21°12'	27°33'
KLB-036	21°12'	27°33'
KLB-037	21°12'	27°33'
KLB-038	±21°15'	27°34'
KLB-039	±21°15'	27°34'
KLB-041	21°19'30"	27°39'30"
KLB-042	21°19'30"	27°39'30"
KLB-044	21°13'	27°34'
KLB-068	±21°58.7'	±29°18.3'
KLB-095	22°05'	28°58'
KLB-030	21°12'	27°33'
HTZ basalts		
KLB-002	22°14'	26°44'
KLB-014	20°39'	21°18'
KLB-063	±21°59.2'	±29°18.15'
KLB-070	±21°59.2'	±29°18.15'
KLB-096	22°03'	28°56'
KLB-097	22°02'	28°55'
KLB-101	21°55'	28°53'

SAMPLE NUMBER	LATITUDE	LONGITUDE
HTZ dolerites		
KLB-001	22°22'	26°38'
KLB-003	22°14'	26°44'
KLB-031	21°12'	27°33'
KLB-040	21°19'30"	27°39'30"
KLB-056	22°18'	26°44'
KLB-067	±21°58.7'	±29°18.3'
KLB-089	22°00'	29°02'
KLB-092	22°01'	28°59.5'
KLB-093	22°03'	28°59.4'
KLB-098	22°00'	28°54'
HTZ (low Fe) basalts		
KLB-066	±21°59.2'	±29°18.15'
KLB-088	22°07'	29°08'
KLB-094	22°04'	28°59.2'
KLB-114	19°15'	25°45'
KLB-152	19°24'	26°02'
DB-14	19°31'36"	24°46'
DB-16	19°31'36"	24°46'
HTZ (low Fe) dolerites		
KLB-061	±21°59.2'	±29°18.15'
KLB-062A	±21°59.2'	±29°18.15'
KLB-062B	±21°59.2'	±29°18.15'

SAMPLE NUMBER	LATITUDE	LONGITUDE
HTZ (low Fe) dolerites (continued)		
KLB-079	22°19'	28°54'
KLB-081	22°13'	29°00'
KLB-085	22°11'	29°08'
KLB-087	22°09'	29°08'
KLB-091	22°03'	29°01'
HIGH-K_2O LINEAGE		
High-K_2O picritic basalts		
KLB-083	22°17'	29°07'
KLB-084	22°12'	29°08'
Shoshonites		
KLB-057	22°0.6'	29°20.7'
KLB-058	22°0.6'	29°20.7'
KLB-059	22°0.5'	29°18.5'
KLB-060	22°0.5'	29°18.5'
KLB-090	22°02'	29°03'
KLB-099	21°59'	28°53'
FELSITES		
KLB-080	22°14'	29°02'
KLB-082	22°15'	29°00'
TYPE II LTZ DOLERITES		
KLB-043	21°19'30"	27°39'30"
KLB-051	22°07'	27°15'

SAMPLE NUMBER	LATITUDE	LONGITUDE
TYPE II LTZ DOLERITES (continued)		
KLB-052	22°07'	27°15'
KLB-053	22°29'	27°11'
KLB-071	22°35'	28°13'
KLB-073	22°32'	28°25'
KLB-102	20°52'	27°38'
KLB-103	20°51'	27°38'
KLB-104	20°51'	27°38'
KLB-105	20°48'	27°38'
KLB-106	20°47'	27°37'
KLB-107	20°45'	27°37'
KLB-108	20°41'	27°38'
KLB-109	20°39'	27°40'
KLB-110	20°39'	27°40'
KLB-111	20°34'	27°41'
KLB-112	20°30'	27°34'
KLB-113	20°29'	27°32'
HIGH-MGO LTZ DOLERITES		
KLB-072	22°34'	28°12'
KLB-077	22°21'	28°50'
KLB-078	22°21'	28°52'

APPENDIX B
THE CALCULATION AND TABULATION OF THE CANONICAL SCORES

The scores for the first two canonical variables for each observation (sample) in the appropriate datasets, *i.e.* for the LTZ- and HTZ-type basalts and dolerites, are plotted in Fig. 2.13 and 2.16 to summarise the results of the discriminant function analysis. These scores are listed in the output of **PROC DISCRIM** and are tabulated in Tables B.1.2 and B.2.2. The scores are calculated using the equation:

$$Canonical\ variable\ score = \sum \frac{X_i - \overline{X_i}}{S_i} \times C_i$$

where $\overline{X_i}$ = mean
X_i = variable concentration for each sample
S_i = standard deviation
C_i = canonical coefficient (*i.e.* either CAN1 or CAN2 in B.1)

The output from the SAS procedure **PROC DISCRIM** includes a number of canonical discriminant analyses, each using different calculation procedures. The canonical scores are calculated using the coefficients of the canonical discriminant analysis referred to in the output as the "*TOTAL-SAMPLE STANDARDISED CANONICAL COEFFICIENTS*" and are referred to as CAN1 COEFFICIENT and CAN2 COEFFICIENT in the subsequent tables (B.1.1 and B.2.1). The datasets used (*i.e.* the LTZ- and HTZ-type basalts and dolerites) for the discriminant function analysis and for the calculation of the means and standard deviation are re-calculated to 100% on a volatile-free basis and the whole rock compositions for the LTZ- and HTZ-type basalts and dolerites are included in APPENDIX E. In the recalculation of the canonical scores, using the data tabulated below and the compositions listed in APPENDIX E, an accumulated error is introduced due to the rounding off of the decimal places, which result in a slight variation in the value, usually in the order of 10^{-2}, of the canonical scores.

B.1 CANONICAL SCORES FOR THE LTZ DATASET (INCLUDING HIGH-Na_2O LTZ BASALTS) WHICH EXCLUDES THE LOW-P_2O_5 BASALTS

The dataset used in the discriminant function analysis excluded the low-P_2O_5 LTZ basalts, but included all the LTZ-type basalts and dolerites which contained ≤9wt% MgO. The samples KLB-004, -005, -007, -010,- 011, -012 and -013 were dropped from the statistical analysis due to missing data for the variables Ba or Nb (*i.e.* N = 116).

TABLE B.1.1 DATA REQUIRED FOR THE CALCULATION OF THE CANONICAL SCORES

VARIABLE	MEAN	STANDARD DEVIATION	CAN1 COEFFICIENT	CAN2 COEFFICIENT
Rb	15.7672	13.4208	1.909523713	3.028477060
K_2O	0.6663	0.2628	-1.248163595	-1.318123279
TiO_2	0.9933	0.1881	1.349609935	-0.829450123
Y	24.4682	3.8457	-1.264381500	-0.369800263
Ba	175.7463	56.5242	0.919781549	-0.242608681

SiO_2	52.1648	1.0167	-0.971441344	0.047616722
Al_2O_3	15.4827	0.5722	-0.785107959	0.011254878
Zr	86.9449	18.1872	1.401731093	-2.005015696
Nb	6.0584	1.5158	-0.471453295	0.948029213
P_2O_5	0.1496	0.0285	-0.907789123	1.946106701
FeO	10.2920	0.8768	-1.004481146	1.001775213
MnO	0.1749	0.0191	0.281118412	-0.346607100

TABLE B.1.2. SCORES FOR THE FIRST TWO CANONICAL VARIABLES

	CAN1	CAN2		CAN1	CAN2		CAN1	CAN2
KLB-131	-2.43	1.04	KLB-173A	-1.37	-0.05	KLB-207	-0.72	-0.19
KLB-124	-2.36	-0.05	KLB-123	-1.32	-0.19	KLB-170	-0.72	-0.48
KLB-173B	-2.30	0.38	KLB-168	-1.31	0.33	KLB-118	-0.69	1.02
KLB-135	-2.30	-0.04	KLB-203	-1.30	-0.30	KLB-210	-0.58	-0.67
KLB-185	-2.24	-1.03	KLB-120	-1.29	0.88	DB-20	-0.55	-0.28
KLB-143	-2.17	1.16	KLB-174	-1.26	0.31	KLB-026	-0.53	-0.27
KLB-209	-2.14	-0.85	KLB-160	-1.26	-0.51	KLB-155	-0.44	-0.67
KLB-055	-2.14	-2.21	KLB-163	-1.26	0.08	KLB-165	-0.42	-1.22
KLB-127	-2.12	2.03	KLB-141	-1.25	0.86	KLB-157	-0.37	-0.84
KLB-149	-2.09	0.50	KLB-045	-1.21	-0.79	KLB-213	-0.32	-0.77
KLB-130	-2.08	0.18	KLB-019	-1.20	0.32	KLB-025	-0.19	-0.02
KLB-048	-2.08	0.04	KLB-138	-1.16	0.12	KLB-116	-0.09	-0.82
KLB-119	-1.98	0.62	KLB-214	-1.15	-0.23	KLB-144	0.03	1.21
KLB-195	-1.92	2.68	KLB-208	-1.14	-0.59	KLB-115	0.08	1.06
KLB-148	-1.88	0.78	KLB-198	-1.12	0.61	KLB-117	0.14	-0.03
KLB-137	-1.88	-0.43	KLB-161	-1.11	-0.09	DB-19	0.62	0.77
KLB-022	-1.85	0.16	KLB-206	-1.10	-0.85	KLB-199	1.83	-0.47
KLB-146	-1.78	1.06	KLB-171	-1.08	-0.44	KLB-049	0.18	-0.01
KLB-212	-1.78	1.33	KLB-125	-1.08	0.27	KLB-050	2.04	-0.20
KLB-054	-1.76	-0.25	KLB-017	-1.07	-0.79	KLB-043	3.90	-2.39
KLB-134	-1.72	0.68	KLB-200	-1.06	0.19	KLB-108	4.45	-0.61
KLB-175	-1.69	0.83	KLB-126	-1.03	1.51	KLB-051	4.53	-1.04
KLB-121	-1.69	2.22	KLB-166	-0.99	-1.30	KLB-052	4.88	0.64
KLB-187	-1.66	-0.78	KLB-201	-0.96	0.24	KLB-103	5.05	-0.02
KLB-142	-1.64	0.34	KLB-167	-0.96	-0.68	KLB-106	5.08	-0.79
KLB-186	-1.62	0.41	KLB-133	-0.95	0.00	KLB-110	5.20	0.04
KLB-147	-1.61	0.31	KLB-027	-0.94	-0.76	KLB-071	5.45	0.23
KLB-020	-1.57	-0.14	KLB-202	-0.94	-0.02	KLB-073	5.64	0.44
KLB-145	-1.56	1.02	KLB-021	-0.93	-1.69	KLB-102	5.88	-0.16
KLB-046	-1.56	-1.02	KLB-188	-0.93	-0.32	KLB-053	5.98	3.60
KLB-189	-1.55	-0.86	KLB-018	-0.91	0.33	KLB-109	6.06	0.80
KLB-196	-1.52	-0.25	KLB-139	-0.91	-0.32	KLB-107	6.34	-2.10
KLB-150	-1.51	0.52	KLB-122	-0.89	-0.53	KLB-030	6.81	-0.51
KLB-047	-1.50	0.17	KLB-162	-0.89	-0.12	KLB-112	7.12	-1.16
KLB-140	-1.49	0.49	KLB-158	-0.88	-0.28	KLB-111	7.17	0.55
KLB-129	-1.42	0.81	KLB-205	-0.78	1.21	KLB-113	7.24	-0.74
KLB-156	-1.41	-0.01	KLB-211	-0.76	-1.00	KLB-104	7.87	0.05
KLB-197	-1.38	-0.03	KLB-006	-0.76	-3.16	KLB-105	8.05	3.35

KLB-204	-1.38	0.07	KLB-164	-0.73	-1.46			

B.2 CANONICAL SCORES FOR THE HTZ DATASET

The dataset used in the discriminant function analysis included all the HTZ-type basalt and dolerite samples, *i.e.* all the samples from the low-K_2O lineage with ≥2% TiO_2 and ≥250ppm Zr. The samples KLB-004, -005, -007, -010,- 011, -012 and -Samples DB-14 and -16 were dropped from the HTZ dataset for the statistical analysis (*i.e.* N=30).

TABLE B.1.1 DATA REQUIRED FOR THE CALCULATION OF THE CANONICAL SCORES

VARIABLE	MEAN	STANDARD DEVIATION	CAN1 COEFFICIENT	CAN2 COEFFICIENT
MgO	4.2236	0.6005	0.334093639	1.135781056
TiO_2	3.5619	0.4350	1.253122445	-0.560976544
Co	43.8782	8.5952	-0.928236874	0.438164016
Nb	25.3909	7.6653	-1.955724956	1.290420327
P_2O_5	0.6163	0.1918	4.912152544	-0.095459073
Zr	417.937	129.483	-2.758654778	-0.349709787
K_2O	1.5803	0.5199	-1.091660409	-0.263659116
Cu	178.354	65.7516	-2.250109954	0.429035241

TABLE B.2.2. SCORES FOR THE FIRST TWO CANONICAL VARIABLES

	CAN1	CAN2		CAN1	CAN2		CAN1	CAN2
KLB-002	-3.65	1.49	KLB-070	0.13	-0.90	KLB-031	0.76	2.67
KLB-066	-3.16	-1.10	KLB-101	1.15	-0.40	KLB-061	0.88	-0.25
KLB-152	-2.95	-1.36	KLB-040	0.00	-1.04	KLB-079	1.04	-1.22
KLB-114	-2.32	0.33	KLB-093	0.09	-0.16	KLB-091	1.12	-1.50
KLB-097	-1.88	0.19	KLB092	0.44	0.07	KLB-001	1.41	1.47
KLB-088	-1.36	0.10	KLB-087	0.48	-0.42	KLB-062A	1.44	-0.68
KLB-014	-1.10	0.21	KLB-085	0.61	-0.59	KLB-067	1.45	0.13
KLB-063	-1.03	1.47	KLB-098	0.66	0.38	KLB-062B	1.62	-0.59
KLB-094	-0.83	-0.81	KLB-081	0.68	1.24	KLB-003	1.73	-0.26
KLB-096	-0.12	0.78	KLB-089	0.72	-0.16	KLB-056	1.98	0.89

APPENDIX C
MINERAL CHEMISTRY

The mineral compositions of olivine, pyroxene, plagioclase and oxide were analyzed using the Cameca-Camebax electron microprobe on carbon-coated polished thin-sections. The operating conditions of the electron microprobe include a beam current of ±40nA and an accelerating voltage of 15kV, where the beam was tightly focused (2-4μm excited area) for the analysis of olivine, pyroxene and oxide and was defocused (8-12μm excited area) for the analysis of plagioclase. The analyzing crystal used were TLAP for the elements Na, Mg, Si and Al, LiF (200) for the elements Fe, Mg and Ni and PET for the elements Ca, K, Ti, Cr and P. Standardization was undertaken prior to each analytical run. Counting times of 10 seconds for the peak and 5 seconds for the background peaks on either side of the analyte peak were used. The raw counts were corrected for dead time losses and background and the nominal concentrations were calibrated using the routine standards (see, for example, Sweeney, 1988). The nominal concentrations were corrected for inter-element matrix effects using the ZAF procedure (modified after Henoc *et. al.*, 1973).

Due to the relatively large number of mineral analyses undertaken, only selected mineral compositions (*i.e.* excluding those listed in the appropriate TABLES in chapter 3) are tabulated below as the probe data were not critical in discriminating between rock types and were not used in any petrogenetic modelling. A full listing of mineral analyses is available from the author on request.

C.1 LOW-K_2O LINEAGE

	1	2	3	4	5	6	7
SiO_2	33.15	33.35	33.33	35.29	33.89	33.83	34.55
FeO	48.80	47.01	46.14	37.50	43.92	45.35	40.37
MnO	.81	.79	.74	.58	.65	.57	.49
MgO	16.63	17.59	18.39	25.37	20.84	19.36	23.76
CaO	.47	.48	.44	.30	.25	.17	.19
TOTAL	99.86	99.22	99.04	99.04	99.55	99.28	99.36
OXYGEN	4	4	4	4	4	4	4
SI	.999	1.001	.998	1.005	.996	1.003	.997
FE	1.229	1.181	1.156	.893	1.079	1.124	.974
MN	.021	.020	.019	.014	.016	.014	.012
MG	.746	.787	.821	1.077	.913	.855	1.022
CA	.015	.016	.014	.009	.008	.005	.006
SUM	3.010	3.005	3.008	2.998	3.012	3.001	3.011
FO	37.390	39.600	41.140	54.280	45.450	42.900	50.890
FA	62.610	60.400	58.860	45.720	54.550	57.100	49.110

LTZ-type basalts
1: Coarse anhedral olivine (KLB-199)
2: Anhedral olivine (KLB-199)
3: Anhedral olivine (KLB-199)
4: Olivine inclusion in a pyroxene (KLB-199)
5: Olivine inclusion in a pyroxene (KLB-199)
6: Anhedral olivine (KLB-200)
7: Olivine inclusion in a pyroxene (KLB-200)

	1A	1B	2A	2B	3A	3B	4A	4B	5	6	7
SiO_2	49.61	49.88	51.09	50.54	51.84	49.94	50.94	50.86	50.59	51.25	49.87
TiO_2	1.40	1.23	.99	.92	.77	1.34	1.28	1.11	1.27	.90	1.39
Al_2O_3	3.60	2.66	3.44	3.24	2.41	3.20	2.83	2.06	3.07	1.18	3.13
Cr_2O_3	.24		.62	.32	.21	.14	.58	.13	.39		.13
FeO	10.41	11.82	8.76	12.57	11.96	11.90	9.84	12.69	10.06	14.87	13.60
MnO	.20	.20		.30	.20	.39	.14	.28	.20	.33	.21
MgO	14.87	14.95	16.82	15.80	18.22	14.93	16.44	15.46	15.54	15.68	13.38
CaO	19.30	18.80	18.50	17.01	14.81	18.39	18.37	17.65	19.36	15.78	19.01
Na_2O	.25	.22	.30	.29	.20	.26	.35	.30	.27	.18	.26
K_2O											
TOTAL	99.88	99.76	100.52	100.99	100.62	100.49	100.77	100.54	100.75	100.17	100.98
OXYGEN	6	6	6	6	6	6	6	6	6	6	6
SI	1.861	1.883	1.885	1.879	1.911	1.870	1.882	1.904	1.877	1.933	1.875
TI	.039	.035	.028	.026	.021	.038	.035	.031	.035	.025	.039
AL	.159	.118	.150	.142	.105	.141	.123	.091	.134	.052	.139
CR	.007		.018	.009	.006	.004	.017	.004	.011		.004
FE	.327	.373	.270	.391	.369	.373	.304	.397	.312	.469	.427
MN	.006	.006		.010	.006	.012	.004	.009	.006	.011	.007
MG	.831	.842	.925	.876	1.001	.833	.905	.863	.859	.882	.749
CA	.776	.761	.731	.678	.585	.738	.727	.708	.770	.638	.766
NA	.018	.016	.022	.021	.014	.019	.025	.022	.019	.013	.019
K											
SUM	4.024	4.034	4.029	4.032	4.018	4.028	4.022	4.029	4.023	4.023	4.025
WO	39.990	38.380	37.960	34.690	29.830	37.720	37.470	35.810	39.520	31.900	39.280
EN	42.850	42.470	48.010	44.820	51.050	42.600	46.630	43.650	44.130	44.100	38.450
FS	17.160	19.150	14.030	20.490	19.120	19.680	15.900	20.540	16.350	24.000	22.270

	8A	8B	8C	9A	9B	10A	10B	11A	11B	12A	12B
SiO_2	51.17	51.51	50.98	50.85	50.34	51.04	50.78	51.77	51.65	52.59	51.97
TiO_2	1.10	.94	.76	.96	.93	1.04	1.10	.84	.86	.42	.36
Al_2O_3	2.51	1.59	1.06	1.58	1.52	2.52	2.36	2.16	1.96	2.05	2.64
Cr_2O_3	.46					.21	.10	.16	.08	.25	.65
FeO	9.25	14.97	20.32	13.96	14.17	11.19	12.01	13.23	15.22	8.80	8.08
MnO	.20	.26	.42	.27	.26	.21	.32	.28	.28	.22	.25
MgO	16.90	14.03	11.31	15.52	14.39	15.99	15.92	16.37	15.48	17.33	17.62
CaO	18.28	17.14	16.13	16.52	17.86	17.94	17.59	15.46	14.36	18.87	18.91
Na_2O	.27	.42	.20	.22	.22	.30	.30	.20	.16	.21	.23
K_2O									.05		
TOTAL	100.14	100.86	101.18	99.88	99.69	100.43	100.48	100.47	100.10	100.74	100.71
OXYGEN	6	6	6	6	6	6	6	6	6	6	6
SI	1.896	1.937	1.953	1.921	1.916	1.900	1.896	1.927	1.940	1.929	1.905
TI	.031	.027	.022	.027	.027	.029	.031	.023	.024	.012	.010
AL	.110	.070	.048	.070	.068	.111	.104	.095	.087	.089	.114
CR	.013					.006	.003	.005	.002	.007	.014
FE	.287	.471	.651	.441	.451	.348	.375	.412	.478	.270	.248
MN	.006	.008	.014	.008	.008	.006	.010	.009	.009	.007	.008
MG	.934	.786	.646	.874	.816	.887	.886	.908	.866	.948	.963
CA	.726	.691	.662	.668	.729	.715	.704	.617	.578	.742	.743
NA	.019	.031	.015	.016	.016	.021	.022	.015	.012	.015	.017
K									.002		
SUM	4.022	4.021	4.011	4.025	4.031	4.023	4.031	4.011	3.998	4.019	4.027
WO	37.170	35.300	33.570	33.560	36.350	36.540	35.630	31.690	29.920	37.720	37.870
EN	47.820	40.200	32.740	43.870	40.730	45.330	44.860	46.690	44.870	48.190	49.090
FS	15.010	24.500	33.700	22.570	22.920	18.130	19.500	21.620	25.220	14.090	13.030

HTLZ/HTZ basalts and dolerites

1: A) Core and B) margin of a sub-ophitic pyroxene (KLB-095)
2: A) Core and B) margin of a sub-ophitic pyroxene (KLB-032)
3: A) Core and B) margin of a sub-ophitic pyroxene (KLB-044)
4: A) Core and B) margin of an interstitial pyroxene (KLB-178)
5: Interstitial pyroxene (KLB-014)
6: Interstitial pyroxene (KLB-067)
7: Interstitial pyroxene (KLB-096)
8: A) Core, B) between core and margin and C) core of a pyroxene phenocryst (KLB-178)
9: A) Core and B) margin of a pyroxene phenocryst (KLB-067)
10: A) Core and B) margin of a pyroxene phenocryst (KLB-067)
11: A) Core and B) margin of a pyroxene phenocryst (KLB-096)
12: A) Core and B) margin of a pyroxene in a megacryst assemblage (KLB-096)

	13	14	15A	15B	16A	16B	17A	17B	18A	18B	19A
SiO_2	50.53	51.07	50.65	50.70	50.56	50.85	51.12	50.96	50.71	50.74	50.35
TiO_2	1.00	1.31	1.57	1.59	1.14	.81	.66	1.04	1.27	.89	1.42
Al_2O_3	1.66	1.97	2.91	2.83	2.65	1.34	1.57	1.80	2.42	1.62	2.32
Cr_2O_3			.09	.14	.10				.19		
FeO	14.87	12.23	10.07	11.15	10.37	15.99	13.86	13.62	10.94	15.74	13.92
MnO		.20	.23	.26	.22	.50	.52			.32	.28
MgO	14.07	14.78	16.31	15.39	15.81	14.15	13.70	14.43	15.34	13.67	13.82
CaO	17.50	18.58	18.27	19.16	18.49	16.31	18.72	18.17	18.55	17.49	17.71
Na_2O	.28	.27	.30	.31	.36	.23	.22	.23	.24	.24	.25
K_2O			.12								
TOTAL	99.91	100.41	100.52	101.53	99.70	100.18	100.37	100.25	99.66	100.71	100.07
OXYGEN	6	6	6	6	6	6	6	6	6	6	6
SI	1.926	1.914	1.878	1.874	1.893	1.934	1.934	1.927	1.904	1.921	1.906
TI	.029	.037	.044	.044	.032	.023	.019	.030	.036	.025	.040
AL	.074	.087	.127	.123	.117	.060	.070	.080	.107	.072	.103
CR			.003	.004	.003				.006		
FE	.474	.383	.312	.345	.325	.509	.439	.431	.344	.498	.441
MN		.006	.007	.008	.007	.016	.017			.010	.009
MG	.799	.826	.901	.848	.882	.802	.773	.813	.859	.772	.780
CA	.715	.746	.726	.759	.742	.665	.759	.736	.746	.710	.718
NA	.021	.020	.021	.022	.026	.017	.016	.017	.017	.018	.018
K			.006								
SUM	4.038	4.019	4.025	4.027	4.027	4.026	4.027	4.034	4.019	4.026	4.015
WO	35.960	38.030	37.290	38.720	37.920	33.370	38.200	37.180	38.310	35.660	36.880
EN	40.210	42.090	46.300	43.260	45.110	40.280	38.890	41.070	44.070	38.780	40.030
FS	23.840	19.870	16.410	18.020	16.970	26.340	22.910	21.750	17.630	25.570	23.090

	19B	20A	20B	21A	21B	22A	22B	23A	23B	24A	24B
SiO_2	50.58	50.63	51.27	54.06	53.28	52.98	51.15	52.47	52.69	52.27	52.37
TiO_2	1.13	1.17	1.26	.29	.37	.28	.35	.70	.34	.45	.54
Al_2O_3	1.82	2.32	2.41	.72	.72	1.86	2.34	1.58	2.11	1.89	1.27
Cr_2O_3			.09			.81	1.02		.71	.21	
FeO	13.61	10.25	10.60	16.59	19.37	6.41	5.89	10.79	6.91	7.66	11.36
MnO	.23	.20	.22	.41	.41	.21		.22	.21	.20	.30
MgO	14.09	16.89	16.37	24.30	22.26	17.97	17.61	16.50	17.29	17.15	16.56
CaO	18.14	18.08	18.29	4.26	4.16	19.52	20.68	18.04	19.50	19.38	17.93
Na_2O	.25	.25	.27		.09	.17	.19	.18	.18	.16	.18
K_2O											
TOTAL	99.85	99.79	100.78	100.63	100.66	100.21	99.23	100.48	99.94	99.37	100.51
OXYGEN	6	6	6	6	6	6	6	6	6	6	6
SI	1.917	1.892	1.898	1.971	1.965	1.938	1.902	1.944	1.937	1.937	1.945
TI	.032	.033	.035	.008	.010	.008	.010	.019	.009	.013	.015
AL	.081	.102	.105	.031	.031	.080	.102	.069	.091	.083	.055
CR			.002			.024	.030		.021	.006	
FE	.431	.320	.328	.506	.598	.196	.183	.334	.212	.238	.353
MN	.007	.006	.007	.013	.013	.006		.007	.006	.006	.010
MG	.796	.941	.903	1.320	1.224	.980	.976	.911	.947	.947	.916
CA	.737	.724	.726	.166	.164	.765	.824	.716	.768	.770	.713
NA	.019	.018	.020		.007	.012	.014	.013	.013	.012	.013
K											
SUM	4.020	4.036	4.024	4.015	4.012	4.008	4.041	4.013	4.004	4.012	4.020
WO	37.370	36.350	36.950	8.300	8.230	39.290	41.550	36.380	39.710	39.250	35.810
EN	40.380	47.250	45.990	65.850	61.230	50.320	49.210	46.290	48.970	48.320	46.000
FS	22.250	16.400	17.060	25.850	30.540	10.400	9.240	17.330	11.320	12.430	18.190

HTZ (low Fe) basalts and dolerites
13: Interstitial pyroxene (KLB-114)
14: Interstitial pyroxene (KLB-152)
15: A) Core and B) margin of an interstitial pyroxene (KLB-062A)
16: A) Core and B) margin of a pyroxene phenocryst (KLB-114)
17: A) Core and B) margin of a pyroxene phenocryst (KLB-114)
18: A) Core and B) margin of a pyroxene phenocryst (KLB-114)
19: A) Core and B) margin of a pyroxene phenocryst (KLB-152)
20: A) Core and B) margin of a pyroxene phenocryst (KLB-062A)

Low-MgO LTZ picritic basalts
21: A) Core and B) margin of an interstitial pyroxene (KLB-128)
22: A) Core and B) margin of a sub-ophitic pyroxene (KLB-128)
23: A) Core and B) margin of a sub-ophitic pyroxene (KLB-128)
24: A) Core and B) margin of a ophitic pyroxene (KLB-172)

	25A	25B	26A	26B	27A	27B	28A	28B	29A	29B	30A
SiO_2	51.91	51.22	53.14	51.86	52.46	52.98	52.04	53.71	52.86	52.03	52.96
TiO_2	.44	.62	.33	.40	.54	.37	.53	.22	.25	.46	.30
Al_2O_3	2.46	1.62	1.28	2.02	1.84	1.04	1.21	.59	1.42	2.07	1.14
Cr_2O_3	.62		.33	.47					.51	.31	.16
FeO	8.56	12.86	9.74	8.73	10.30	12.03	18.32	17.69	7.96	8.21	10.29
MnO	.20	.30	.34	.24	.25	.36	.41	.39	.19	.17	.32
MgO	16.56	14.97	17.88	16.52	17.06	18.45	19.30	22.79	18.21	16.58	19.46
CaO	19.05	17.63	16.99	19.22	17.73	14.65	7.73	4.83	17.96	19.32	15.16
Na_2O	.19	.16	.17	.18	.15	.13	.09	.06	.19	.13	.11
K_2O											
TOTAL	99.99	99.38	100.20	99.64	100.33	100.01	99.63	100.28	99.55	99.28	99.90
OXYGEN	6	6	6	6	6	6	6	6	6	6	6
SI	1.921	1.938	1.957	1.929	1.940	1.962	1.955	1.975	1.951	1.935	1.952
TI	.012	.018	.009	.011	.015	.010	.015	.006	.007	.013	.008
AL	.107	.072	.055	.089	.080	.045	.053	.026	.062	.091	.049
CR	.018		.010	.014					.015	.009	.005
FE	.265	.407	.300	.272	.318	.373	.575	.544	.246	.255	.317
MN	.006	.010	.011	.008	.008	.011	.013	.012	.006	.005	.010
MG	.913	.844	.982	.916	.940	1.019	1.081	1.249	1.002	.919	1.069
CA	.755	.715	.671	.766	.703	.581	.311	.190	.710	.770	.599
NA	.014	.012	.012	.013	.011	.010	.007	.004	.013	.010	.008
K											
SUM	4.011	4.016	4.007	4.018	4.015	4.011	4.010	4.006	4.012	4.007	4.017
WO	38.940	36.190	34.160	39.050	35.680	29.310	15.720	9.540	36.160	39.490	30.020
EN	47.080	42.740	50.020	46.710	47.750	51.350	54.570	62.590	51.010	47.140	53.580
FS	13.980	21.080	15.820	14.240	16.570	19.350	29.710	27.860	12.830	13.370	16.390

	30B	31A	31B	32A	32B	33A	33B	34A	34B	35A	35B
SiO_2	51.22	53.01	51.92	53.02	51.67	51.47	51.35	51.21	51.91	51.37	51.78
TiO_2	.63	.28	.39	.29	.50	.56	.61	.58	.49	.63	.62
Al_2O_3	1.90	.80	.77	1.42	1.84	2.31	1.40	3.24	2.26	1.38	1.40
Cr_2O_3				.29	.10	.46		.27	.25		
FeO	12.02	18.28	21.52	7.97	9.04	8.74	15.02	9.08	9.24	11.40	13.53
MnO	.26	.46	.43	.19	.24	.20	.36	.25	.18	.24	.33
MgO	15.92	22.05	20.07	17.88	16.60	15.83	14.62	16.86	16.56	15.68	15.64
CaO	17.49	4.25	4.35	18.36	18.94	19.56	16.54	18.32	19.46	18.57	16.41
Na_2O	.16	.09	.10	.18	.17	.21	.19	.29	.22	.20	.19
K_2O											
TOTAL	99.60	99.22	99.55	99.60	99.10	99.34	100.09	100.10	100.57	99.47	99.90
OXYGEN	6	6	6	6	6	6	6	6	6	6	6
SI	1.925	1.975	1.962	1.956	1.932	1.922	1.942	1.894	1.917	1.935	1.946
TI	.018	.008	.011	.008	.014	.016	.017	.016	.014	.018	.018
AL	.084	.035	.034	.062	.081	.102	.062	.141	.098	.061	.062
CR				.009	.003	.013		.008	.007		
FE	.378	.570	.680	.246	.283	.273	.475	.281	.285	.359	.425
MN	.008	.014	.014	.006	.007	.006	.012	.008	.006	.008	.011
MG	.892	1.224	1.130	.983	.925	.881	.825	.930	.911	.880	.876
CA	.704	.170	.176	.726	.759	.783	.670	.726	.770	.750	.661
NA	.011	.006	.007	.013	.013	.015	.014	.021	.016	.015	.014
K											
SUM	4.020	4.002	4.014	4.009	4.017	4.011	4.017	4.025	4.024	4.026	4.013
WO	35.530	8.580	8.810	37.020	38.440	40.290	33.830	37.350	39.030	37.550	33.510
EN	44.990	61.890	56.510	50.130	46.850	45.340	41.610	47.810	46.210	44.080	44.400
FS	19.480	29.530	34.680	12.850	14.700	14.370	24.560	14.840	14.760	18.370	22.090

LTZ-type basalts

25: A) Core and B) margin of a sub-ophitic pyroxene (KLB-115)
26: A) Core and B) margin of an interstitial pyroxene (KLB-115)
27: A) Core and B) margin of a sub-ophitic pyroxene (KLB-134)
28: A) Core and B) margin of an interstitial pyroxene (KLB-134)
29: A) Core and B) margin of a sub-ophitic pyroxene (KLB-155)
30: A) Core and B) margin of a sub-ophitic pyroxene (KLB-171)
31: A) Core and B) margin of an interstitial pyroxene (KLB-199)
32: A) Core and B) margin of a sub-ophitic pyroxene (KLB-046)
33: A) Core and B) margin of a sub-ophitic pyroxene (DB-19)

Low-P_2O_5 LTZ basalts

34: A) Core and B) margin of a pyroxene phenocryst (KLB-015)
35: A) Core and B) margin of an interstitial pyroxene (KLB-015)

	1A	1B	2	3	4	5	6	7	8	9A	9B
SiO_2	52.07	55.14	53.76	58.78	56.86	55.15	56.28	55.07	56.53	48.70	53.79
Al_2O_3	29.88	26.60	28.50	22.99	26.13	28.01	26.87	28.03	27.19	31.68	27.98
FeO	.71	1.03	1.17	2.02	1.30	.73	.82	.87	.70	.85	.77
MgO	.21	.14	.23	.50	.08	.08		.07	.07	.40	.13
CaO	14.10	11.07	12.96	8.58	10.56	11.62	10.54	11.26	10.16	16.30	12.72
Na_2O	3.29	4.96	3.87	5.59	5.62	4.80	5.46	4.88	5.48	2.09	3.97
K_2O	.15	.35	.25	.63	.42	.29	.41	.41	.57	.11	.20
TOTAL	100.41	99.29	100.74	99.09	100.97	100.68	100.38	100.59	100.70	100.13	99.56
OXYGEN	8	8	8	8	8	8	8	8	8	8	8
SI	2.363	2.517	2.430	2.677	2.553	2.481	2.536	2.480	2.535	2.235	2.452
AL	1.598	1.431	1.518	1.234	1.383	1.485	1.427	1.488	1.437	1.714	1.503
FE	.027	.039	.044	.077	.049	.027	.031	.033	.026	.033	.029
MG	.014	.009	.016	.034	.005	.005		.005	.005	.027	.009
CA	.686	.541	.627	.419	.508	.560	.509	.543	.488	.801	.621
NA	.289	.439	.339	.494	.490	.419	.477	.427	.477	.186	.351
K	.008	.021	.014	.036	.024	.017	.024	.023	.033	.006	.012
SUM	4.985	4.997	4.988	4.971	5.012	4.994	5.004	4.999	5.001	5.002	4.977
AB	29.420	43.840	34.560	52.010	47.930	42.060	47.230	42.940	47.770	18.740	35.680
OR	.860	2.060	1.470	3.840	2.340	1.680	2.340	2.360	3.290	.650	1.180
AN	69.720	54.100	63.970	44.140	49.730	56.260	50.420	54.690	48.930	80.600	63.150

	9C	10A	10B	11A	11B	12A	12B	13A	13B	14A	14B
SiO_2	50.92	51.49	55.30	54.98	57.30	53.30	54.38	55.68	55.90	53.69	55.06
Al_2O_3	30.40	30.36	27.14	27.91	26.57	29.18	28.50	27.96	27.25	29.24	27.79
FeO	.69	.56	1.04	.61	.66	.55	.79	.45	.83	.76	.75
MgO	.23	.13	.14	.07		.12	.09		.08	.15	.11
CaO	14.70	15.06	11.61	11.89	10.02	13.35	12.42	11.55	11.17	12.73	11.23
Na_2O	3.01	2.89	4.96	4.79	5.84	4.05	4.59	4.90	5.13	3.96	4.78
K_2O	.15	.10	.37	.30	.46	.11	.24	.33	.38	.30	.40
TOTAL	100.10	100.59	100.56	100.55	100.85	100.66	101.01	100.87	100.74	100.83	100.12
OXYGEN	8	8	8	8	8	8	8	8	8	8	8
SI	2.324	2.336	2.497	2.478	2.565	2.407	2.446	2.497	2.512	2.418	2.489
AL	1.635	1.623	1.445	1.482	1.401	1.553	1.511	1.478	1.444	1.552	1.480
FE	.026	.021	.039	.023	.025	.021	.030	.017	.031	.029	.028
MG	.015	.009	.010	.005		.008	.006		.005	.010	.008
CA	.719	.732	.562	.574	.480	.646	.599	.555	.538	.615	.544
NA	.266	.254	.434	.419	.507	.355	.400	.426	.447	.346	.419
K	.009	.006	.021	.017	.027	.007	.014	.019	.022	.017	.023
SUM	4.994	4.981	5.008	4.998	5.005	4.997	5.006	4.992	4.999	4.987	4.991
AB	26.770	25.580	42.700	41.460	49.990	35.240	39.500	42.630	44.430	35.390	42.480
OR	.880	.610	2.080	1.730	2.620	.650	1.390	1.880	2.160	1.740	2.370
AN	72.350	73.810	55.230	56.810	47.390	64.110	59.110	55.490	53.410	62.880	55.160

HTLZ/HTZ basalts and dolerites

1: A) Core and B) margin of a sub-ophitically enclosed plagioclase (KLB-095)
2: Plagioclase lath in mesostasis (KLB-095)
3: Plagioclase lath in mesostasis (KLB-095)
4: Plagioclase lath (KLB-032)
5: Plagioclase lath (KLB-178)
6: Plagioclase lath (KLB-178)
7: Plagioclase lath (KLB-067)
8: Plagioclase lath (KLB-067)
9: A) Core, B) between core and margin and C) core of a plagioclase phenocryst (KLB-095)
10: A) Core and B) margin of a plagioclase phenocryst in a glomeroporphyritic aggregate (KLB-032)
11: A) Core and B) margin of a plagioclase phenocryst (KLB-178)
12: A) Core and B) margin of a plagioclase phenocryst (KLB-178)
13: A) Core and B) margin of a plagioclase phenocryst (KLB-014)
14: A) Core and B) between core and margin of a plagioclase phenocryst (KLB-067)

	14C	15A	15B	16	17	18	19A	19B	20	21A	21B
SiO_2	57.25	51.74	54.75	56.70	65.46	65.57	56.17	57.18	54.21	54.18	54.60
Al_2O_3	26.69	30.31	28.30	26.49	18.37	19.21	26.93	24.73	27.86	28.65	28.56
FeO	.62	.55	.65	.69	.42	.55	.72	1.19	1.26	.57	.62
MgO	.07	.14	.09		.06			.31	.06	.07	
CaO	9.57	14.77	12.23	9.86	1.65	1.66	10.98	10.04	11.44	12.58	12.00
Na_2O	5.76	3.21	4.58	5.53	4.90	5.01	5.03	5.20	4.43	4.13	4.40
K_2O	.60	.10	.31	.73	8.59	8.20	.66	1.43	.56	.46	.51
TOTAL	100.56	100.82	100.91	100.00	99.45	100.20	100.49	100.08	99.82	100.64	100.69
OXYGEN	8	8	8	8	8	8	8	8	8	8	8
SI	2.565	2.342	2.461	2.561	2.978	2.958	2.532	2.595	2.468	2.444	2.460
AL	1.409	1.617	1.499	1.410	.985	1.021	1.430	1.323	1.495	1.523	1.517
FE	.023	.021	.024	.026	.016	.021	.027	.045	.048	.022	.023
MG	.005	.010	.006		.004			.021	.004	.005	
CA	.459	.716	.589	.477	.080	.080	.530	.488	.558	.608	.579
NA	.500	.281	.399	.484	.432	.438	.440	.458	.391	.361	.384
K	.034	.006	.018	.042	.499	.472	.038	.083	.032	.026	.029
SUM	4.995	4.993	4.996	5.000	4.994	4.990	4.997	5.013	4.996	4.989	4.992
AB	50.320	28.050	39.680	48.220	42.730	44.250	43.650	44.490	39.820	36.270	38.700
OR	3.440	.550	1.760	4.210	49.310	47.660	3.760	8.060	3.290	2.640	2.940
AN	46.230	71.400	58.560	47.570	7.960	8.090	52.590	47.450	56.890	61.090	58.360

	21C	22A	22B	23A	23B	24A	24B	25	26A	26B	26C
SiO_2	54.20	55.77	56.33	55.26	54.74	51.63	52.84	50.54	52.20	53.00	59.09
Al_2O_3	27.84	27.61	27.19	27.52	28.28	30.15	29.05	30.93	29.82	28.89	25.47
FeO	.65	.72	.66	.58	.73	.79	.94	.76	.63	.62	.80
MgO		.07		.12		.08	.08	.10	.17	.15	
CaO	11.56	11.28	10.63	10.94	11.81	13.92	12.70	14.91	13.80	12.95	8.54
Na_2O	4.69	4.70	5.04	4.85	4.46	2.93	3.40	2.44	3.02	3.51	5.51
K_2O	.38	.60	.73	.63	.53	.16	.22	.13	.10	.18	.52
TOTAL	99.32	100.75	100.58	99.90	100.55	99.66	99.23	99.81	99.74	99.30	99.93
OXYGEN	8	8	8	8	8	8	8	8	8	8	8
SI	2.474	2.505	2.533	2.503	2.469	2.357	2.416	2.311	2.377	2.420	2.646
AL	1.498	1.462	1.441	1.469	1.503	1.623	1.565	1.667	1.600	1.555	1.344
FE	.025	.027	.025	.022	.027	.030	.036	.029	.024	.024	.030
MG		.005		.008		.006	.005	.007	.011	.010	
CA	.566	.543	.512	.531	.571	.681	.622	.731	.673	.634	.410
NA	.415	.409	.440	.426	.390	.260	.301	.216	.266	.311	.478
K	.022	.034	.042	.037	.031	.009	.013	.007	.006	.010	.030
SUM	5.000	4.985	4.993	4.996	4.991	4.966	4.958	4.968	4.957	4.964	4.938
AB	41.370	41.480	44.260	42.860	39.350	27.340	32.180	22.630	28.160	32.560	52.110
OR	2.210	3.490	4.210	3.690	3.100	.970	1.400	.770	.630	1.070	3.220
AN	56.420	55.030	51.540	53.450	57.550	71.700	66.420	76.600	71.200	66.360	44.670

HTLZ/HTZ basalts and dolerites (continued)
14: C) Margin of a plagioclase phenocryst (KLB-067)
15: A) Core and B) margin of a plagioclase in a megacryst aggregate (KLB-096)

HTZ (low Fe) basalts and dolerites
16: Plagioclase lath (KLB-114)
17: Plagioclase microlite in mesostasis (KLB-152)
18: Plagioclase lath in mesostasis (KLB-152)
19: A) Core and B) margin of a plagioclase lath (KLB-152)
20: Plagioclase lath (KLB-062A)
21: A) Core, B) between core and margin and C) core of a plagioclase phenocryst in glomeroporphyritic aggregate (KLB-114)
22: A) Core and B) margin of a plagioclase phenocryst (KLB-062A)
23: A) Core and B) margin of a plagioclase phenocryst in a glomeroporphyritic aggregate (KLB-062A)

Low-MgO LTZ picritic basalts
24: A) Core and B) margin of a sub-ophitically enclosed plagioclase (KLB-128)
25: Plagioclase lath (KLB-128)
26: A) Core, B) between core and margin and C) margin of a sub-ophitically enclosed plagioclase (KLB-172)

	27	28	29	30	31A	31B	32A	32B	33A	33B	33C
SiO_2	67.50	59.23	57.40	55.27	51.00	53.25	51.13	52.95	52.67	56.31	59.06
Al_2O_3	20.34	24.97	26.46	27.38	30.54	28.94	30.43	29.48	27.34	27.28	25.86
FeO	.19	.72	.81	.89	.54	.82	.54	.66	2.41	.70	.81
MgO			.07	.12	.21	.16	.24	.22	1.79	.12	.08
CaO	1.31	8.25	10.37	11.24	14.35	12.65	14.48	13.39	11.69	10.74	9.11
Na_2O	9.66	5.98	4.35	4.29	2.87	3.72	2.80	3.45	3.50	4.64	5.53
K_2O	.13	.48	.38	.30	.12	.20	.08	.13	.13	.29	.45
TOTAL	99.13	99.63	99.84	99.49	99.63	99.74	99.70	100.28	99.53	100.08	100.90
OXYGEN	8	8	8	8	8	8	8	8	8	8	8
SI	2.967	2.661	2.581	2.508	2.331	2.422	2.335	2.398	2.416	2.533	2.624
AL	1.054	1.322	1.402	1.464	1.646	1.551	1.638	1.573	1.478	1.447	1.354
FE	.007	.027	.031	.034	.021	.031	.020	.025	.092	.026	.030
MG			.004	.008	.014	.011	.016	.015	.123	.008	.005
CA	.062	.397	.499	.546	.703	.616	.708	.650	.575	.518	.434
NA	.824	.521	.380	.377	.254	.328	.248	.303	.311	.405	.476
K	.007	.027	.022	.017	.007	.012	.005	.008	.008	.016	.025
SUM	4.921	4.955	4.919	4.954	4.976	4.971	4.970	4.972	5.003	4.953	4.948
AB	92.260	55.100	42.150	40.110	26.360	34.280	25.820	31.520	34.830	43.110	50.900
OR	.820	2.900	2.390	1.830	.710	1.240	.500	.810	.870	1.750	2.720
AN	6.930	42.010	55.460	58.060	72.920	64.470	73.680	67.680	64.300	55.140	46.370

	34	35A	35B	36	37	38	39	40	41	42	43
SiO_2	64.30	52.42	51.07	54.76	53.93	58.62	68.06	56.56	64.34	52.55	52.31
Al_2O_3	21.37	29.25	29.78	27.87	27.81	24.72	19.66	25.88	21.02	28.86	28.71
FeO	.34	.73	.70	.87	.72	.84	.18	.75	.26	.57	.58
MgO		.10	.11		.10	.11		.10		.12	.12
CaO	2.84	13.42	14.23	11.40	11.79	7.72	.98	9.76	2.87	13.01	12.91
Na_2O	8.33	3.67	3.25	4.82	4.54	6.84	10.10	4.78	8.27	3.84	3.91
K_2O	1.95	.21	.16	.24	.22	.51	.05	.38	2.08	.17	.13
TOTAL	99.13	99.80	99.30	99.96	99.11	99.36	99.03	98.21	98.84	99.12	98.67
OXYGEN	8	8	8	8	8	8	8	8	8	8	8
SI	2.873	2.391	2.348	2.483	2.466	2.649	2.993	2.586	2.884	2.409	2.409
AL	1.125	1.572	1.613	1.489	1.499	1.317	1.019	1.395	1.110	1.559	1.558
FE	.013	.028	.027	.033	.028	.032	.007	.029	.010	.022	.022
MG		.007	.008		.007	.007		.007		.008	.008
CA	.136	.656	.701	.554	.578	.374	.046	.478	.138	.639	.637
NA	.721	.324	.290	.424	.402	.599	.861	.424	.719	.341	.349
K	.111	.012	.009	.014	.013	.029	.003	.022	.119	.010	.008
SUM	4.979	4.990	4.996	4.997	4.993	5.007	4.929	4.941	4.980	4.988	4.991
AB	74.470	32.690	28.970	42.760	40.540	59.800	94.580	45.880	73.690	34.450	35.130
OR	11.480	1.220	.940	1.380	1.280	2.920	.330	2.420	12.180	.990	.760
AN	14.040	66.090	70.100	55.860	58.180	37.200	5.090	51.700	14.120	64.560	64.110

LTZ-type basalts
27: Margin of a plagioclase lath (KLB-115)
28: Margin of a plagioclase lath (KLB-115)
29: Plagioclase lath (KLB-115)
30: Plagioclase lath (KLB-117)
31: A) Core and B) margin of a plagioclase lath (KLB-134)
32: A) Core and B) margin of a sub-ophitically enclosed plagioclase (KLB-171)
33: A) Core, B) between core and margin and C) margin of a plagioclase lath (KLB-171)
34: Plagioclase lath (KLB-199)
35: A) Core and B) margin of a plagioclase lath (KLB-046)
36: Plagioclase lath (DB-19)
37: Plagioclase lath (DB-19)
38: Plagioclase lath in mesostasis (DB-19)
39: Plagioclase phenocryst (KLB-117)
40: Margin of a plagioclase phenocryst in a glomeroporphyritic aggregate (KLB-155)
41: Plagioclase phenocryst in a glomeroporphyritic aggregate (KLB-199)
42: Plagioclase phenocryst in a glomeroporphyritic aggregate (DB-19)
43: Plagioclase phenocryst in a glomeroporphyritic aggregate (DB-19)

	44A	44B	44C	45	46A	46B	47A	47B	48A	48B	48C
SiO_2	52.82	58.66	60.97	59.29	54.83	57.25	64.68	68.82	53.64	53.86	59.43
Al_2O_3	29.21	25.85	24.42	25.10	28.19	27.00	18.57	19.78	29.05	28.59	24.83
FeO	.65	.54	.56	.70	.76	.81		.28	.55	.59	.57
MgO	.15	.05			.10	.07			.10	.14	
CaO	12.64	8.28	6.65	7.47	11.30	9.69		.29	12.44	12.20	7.40
Na_2O	3.86	6.07	6.69	6.59	4.42	5.08	.14	11.99	3.59	4.11	6.35
K_2O	.17	.54	.78	.60	.29	.40	16.78	.06	.17	.21	.61
TOTAL	99.50	99.99	100.07	99.75	99.89	100.30	100.17	101.22	99.54	99.70	99.19
OXYGEN	8	8	8	8	8	8	8	8	8	8	8
SI	2.408	2.627	2.715	2.661	2.480	2.564	2.991	2.979	2.436	2.446	2.676
AL	1.570	1.364	1.282	1.328	1.503	1.425	1.012	1.009	1.555	1.530	1.318
FE	.025	.020	.021	.026	.029	.030		.010	.021	.022	.021
MG	.010	.003			.007	.005			.006	.010	
CA	.618	.397	.317	.359	.548	.465		.013	.605	.594	.357
NA	.342	.527	.577	.573	.388	.441	.012	1.006	.316	.362	.555
K	.010	.031	.044	.034	.017	.023	.990	.003	.010	.012	.035
SUM	4.983	4.969	4.956	4.981	4.972	4.953	5.005	5.020	4.949	4.976	4.962
AB	35.240	55.180	61.470	59.270	40.720	47.490	1.230	98.390	33.910	37.420	58.600
OR	1.040	3.220	4.730	3.570	1.760	2.470	98.770	.300	1.060	1.260	3.690
AN	63.720	41.600	33.800	37.170	57.510	50.040	.000	1.310	65.030	61.320	37.710

	1	2	3	4	5	6	7	8	9	10	11
SiO_2	.12	.25	.13	.11	.24		.11		.11	.09	
TiO_2	48.66	23.78	58.62	19.61	19.65	51.76	26.53	49.61	51.85	39.25	46.70
Al_2O_3	.24	2.24	.30	1.85	1.71	.24	1.41	.32	.31	.22	.25
Cr_2O_3				.19	.17						
FeO	40.04	52.21	32.95	46.98	47.11	42.76	52.40	40.70	42.78	52.15	36.57
Fe_2O_3	9.47	19.42		24.68	25.38	2.68	12.67	7.00	2.32		9.29
MnO	.51	.66	.53	.91	.99	.55	1.38	.36	1.05	.22	.36
MgO	1.52	.24	.22			1.34		1.84	1.50	1.66	2.48
CaO	.33	.13	.16	.07			.07		.12	.07	.07
TOTAL	100.88	98.94	92.91	94.39	95.24	99.32	94.57	99.82	100.04	93.66	94.79
OXYGEN	3	4	3	4	4	3	4	3	3	4	3
SI	.003	.010	.003	.005	.010		.005		.003	.003	
TI	.935	.719	1.126	.642	.639	.988	.823	.953	.979	1.116	.940
AL	.007	.106	.009	.095	.087	.007	.069	.010	.009	.010	.008
CR				.007	.006						
FE	1.038	2.343	.704	2.518	2.531	.959	2.200	1.004	.942	1.648	1.005
MN	.011	.023	.012	.034	.036	.012	.048	.008	.022	.007	.008
MG	.058	.014	.008			.051		.070	.056	.093	.099
CA	.009	.006	.004	.003			.003		.003	.003	.002
SUM	2.061	3.220	1.866	3.304	3.309	2.017	3.148	2.045	2.014	2.880	2.062

Low-P_2O_5 LTZ basalts
44: A) Core, B) between core and margin and C) margin of a plagioclase lath (KLB-016)
45: Plagioclase lath projecting into mesostasis (KLB-016)
46: A) Core and B) margin of a plagioclase lath (KLB-016)
47: A) Core and B) margin of a feldspar (perthite) phenocryst (KLB-015)
48: A) Core, B) adjacent to margin and C) margin of a plagioclase phenocryst (KLB-016)

HTLZ/HTZ basalts and dolerites
1: Anhedral interstitial ilmenite (KLB-032)
2: Anhedral interstitial titanomaghemite (KLB-044)
3: Anhedral interstitial ilmenite (KLB-178)
4: Anhedral interstitial titanomaghemite (KLB-067)
5: Anhedral interstitial titanomaghemite (KLB-067)
6: Anhedral interstitial ilmenite (KLB-067)
7: Anhedral interstitial titanomaghemite (KLB-067)

HTZ (low Fe) basalts and dolerites
8: Skeletal interstitial ilmenite (KLB-114)
9: Anhedral interstitial ilmenite (KLB-152)
Low-MgO LTZ picritic basalts
10: Skeletal interstitial titanomaghemite (KLB-128)
11: Anhedral interstitial ilmenite (KLB-128)

	12	13	14	15	16	17	18	19
SiO_2	.28	.21	.27	.11		.44	.10	.36
TiO_2	21.94	26.10	20.99	24.63	26.93	27.19	27.63	25.73
Al_2O_3	1.34	1.60	1.83	.99	1.33	1.70	.81	1.49
Cr_2O_3								
FeO	48.55	52.74	47.28	51.78	52.42	53.13	53.57	50.47
Fe_2O_3	21.33	14.16	22.55	19.02	15.07	10.00	9.94	10.71
MnO	1.11	.71	.99	.59	.54	1.84	.29	1.70
MgO	.11	.44	.35	.56	1.27	.09	.45	.11
CaO	.26	.10	.24			.11	.12	.11
TOTAL	94.91	96.06	94.49	97.67	97.55	94.51	92.90	90.67
OXYGEN	4	4	4	4	4	4	4	4
SI	.012	.009	.012	.004		.018	.004	.015
TI	.704	.797	.677	.757	.809	.831	.861	.824
AL	.067	.077	.093	.048	.062	.081	.040	.075
CR								
FE	2.415	2.225	2.423	2.355	2.205	2.111	2.168	2.141
MN	.040	.024	.036	.021	.018	.063	.010	.061
MG	.007	.027	.022	.034	.075	.006	.028	.007
CA	.012	.004	.011			.005	.005	.005
SUM	3.257	3.162	3.273	3.219	3.169	3.115	3.116	3.128

C.2 HIGH-K_2O LINEAGE

	1A	1B	2A	2B	3	4A	4B	5	6	1A	1B
SiO_2	37.56	37.39	37.13	36.94	36.68	39.12	38.56	37.60	38.01	48.41	48.75
TiO_2										1.89	2.16
Al_2O_3										5.18	4.61
Cr_2O_3										.45	
FeO	28.46	28.22	30.43	30.95	32.16	15.25	20.29	24.19	21.72	7.70	8.98
MnO	.40	.41	.49	.54	.58	.16	.19	.29	.34		.16
MgO	34.33	34.20	32.89	32.06	31.05	44.21	40.59	37.25	38.96	13.63	13.37
CaO	.38	.43	.39	.40	.40	.27	.27	.22	.25	22.49	22.16
Na_2O										.47	.47
NIO		.20				.43	.35	.27	.25		
TOTAL	101.13	100.85	101.33	100.89	100.87	99.44	100.25	99.82	99.53	100.22	100.66
OXYGEN	4	4	4	4	4	4	4	4	4	6	6
SI	1.000	.996	.994	.998	.998	.994	.994	.994	.995	1.812	1.822
TI										.053	.061
AL										.228	.203
CR										.01	
FE	.634	.629	.682	.700	.731	.324	.438	.535	.475	.241	.281
MN	.009	.009	.011	.012	.013	.003	.004	.007	.007		.005
MG	1.362	1.357	1.313	1.292	1.259	1.674	1.560	1.467	1.520	.761	.744
CA	.011	.012	.011	.012	.012	.007	.007	.006	.007	.902	.887
NA										.034	.034
NI		.004				.009	.007	.008	.005		
SUM	3.016	3.007	3.011	3.014	3.013	3.011	3.010	3.015	3.009	4.044	4.037
WO										47.380	46.270
EN										39.960	38.830
FS										12.660	14.900
FO	67.940	67.890	65.450	64.470	62.830	83.280	77.650	72.840	75.680		
FA	32.060	32.110	34.550	35.530	37.170	16.720	22.350	27.160	24.320		

LOW-K_2O LINEAGE
Low-MgO LTZ picritic basalts (continued)
12: Skeletal titanomaghemite in mesostasis (KLB-172)
LTZ-type basalts
13: Skeletal titanomaghemite in mesostasis (KLB-115)
14: Anhedral interstitial titanomaghemite (KLB-115)
15: Anhedral interstitial titanomaghemite (KLB-199)
16: Anhedral interstitial titanomaghemite (KLB-199)
17: Skeletal interstitial titanomaghemite (DB-19)

Low-P_2O_5 LTZ basalts
18: Anhedral interstitial titanomaghemite (KLB-015)
19: Skeletal interstitial titanomaghemite (KLB-015)

HIGH-K_2O LINEAGE
Olivine
1: A) Core and B) margin of an anhedral interstitial olivine (KLB-099)
2: A) Core and B) margin of an anhedral olivine phenocryst (KLB-099)
3: Anhedral interstitial olivine (KLB-099)
4: A) Core and B) margin of a subhedral olivine phenocryst (KLB-083)
5: Anhedral interstitial olivine (KLB-083)
6: Anhedral interstitial olivine (KLB-083)
Pyroxene
1: A) Core and B) between core and margin of pyroxene phenocryst (KLB-099)

	1C	2	3A	3B	4A	4B	5A	5B	6A	6B	1
SiO_2	48.23	47.38	48.10	50.07	51.31	49.02	49.90	50.05	51.18	51.31	62.55
TiO_2	2.48	2.78	1.94	1.63	1.32	2.04	2.11	1.91	1.33	1.20	
Al_2O_3	4.30	3.65	5.11	3.05	2.01	3.79	3.08	2.88	1.94	1.81	23.30
Cr_2O_3					.79		.33	.26	.81	.75	
FeO	9.61	13.86	8.26	9.07	6.10	7.89	6.88	6.28	6.19	6.26	.34
MnO	.18	.29	.16	.16	.15	.22	.13	.16	.16		
MgO	12.47	8.75	13.21	13.99	17.01	15.37	15.79	15.84	16.83	17.06	.04
CaO	21.97	21.91	22.61	22.08	20.87	20.95	21.18	21.70	20.84	20.74	4.84
Na_2O	.49	.87	.49	.41	.26	.28	.28	.25	.29	.30	7.32
K_2O											2.23
TOTAL	99.73	99.49	99.88	100.46	99.82	99.56	99.68	99.33	99.57	99.43	100.62
OXYGEN	6	6	6	6	6	6	6	6	6	6	8
SI	1.826	1.840	1.810	1.872	1.897	1.838	1.858	1.867	1.899	1.908	2.775
TI	.070	.081	.055	.046	.037	.057	.059	.054	.037	.033	
AL	.192	.167	.227	.135	.088	.168	.135	.127	.085	.079	1.218
CR					.002		.01	.008	.002	.002	
FE	.304	.450	.260	.283	.189	.247	.214	.196	.192	.195	.013
MN	.006	.010	.005	.005	.005	.007	.004	.005	.005		
MG	.703	.507	.741	.779	.938	.859	.876	.880	.930	.945	.003
CA	.891	.912	.912	.885	.827	.842	.845	.867	.828	.826	.230
NA	.036	.066	.035	.030	.019	.020	.020	.018	.021	.022	.629
K											.126
SUM	4.028	4.033	4.045	4.035	4.023	4.038	4.021	4.022	4.021	4.030	4.994
AB											63.840
OR											12.820
AN											23.340
WO	46.790	48.540	47.540	45.300	42.240	43.060	43.570	44.500	42.350	42.020	
EN	36.930	26.970	38.640	39.920	47.900	43.940	45.180	45.190	47.580	48.070	
FS	16.280	24.480	13.820	14.780	9.870	13.000	11.250	10.310	10.070	9.900	

	2	3	4	5	6	7	8A	8B	1	2	3
SiO_2	55.82	59.21	58.66	66.24	65.69	58.30	57.44	56.92	.12	.11	
TiO_2									24.43	28.30	49.32
Al_2O_3	27.70	25.15	25.63	19.42	19.57	25.03	25.57	25.50	.86	1.53	.33
FeO	.53	.32	.39	.18	.15	.57	.80	.92	68.15	63.74	43.61
MnO									.95	1.02	.40
MgO	.07	.05	.04		.04	.08	.28	.54	.19	.41	4.11
CaO	9.69	7.01	7.10	1.09	1.58	7.61	8.39	8.77	.06	.06	.06
Na_2O	5.58	6.53	6.84	4.97	5.20	5.89	5.59	5.32			
K_2O	.35	1.04	.91	8.81	8.43	1.72	1.35	1.26			
TOTAL	99.74	99.31	99.57	100.71	100.66	99.20	99.42	99.23	94.76	95.17	97.83
OXYGEN	8	8	8	8	8	8	8	8	4	4	3
SI	2.520	2.665	2.639	2.968	2.948	2.644	2.604	2.589	.005	.004	
TI									.760	.849	.947
AL	1.474	1.334	1.359	1.026	1.035	1.338	1.366	1.367	.042	.072	.010
FE	.020	.012	.014	.007	.006	.022	.030	.035	2.359	2.126	.931
MN									.033	.034	.009
MG	.005	.004	.003		.003	.005	.019	.037	.012	.024	.156
CA	.469	.338	.342	.052	.076	.370	.408	.427	.002	.003	.002
NA	.488	.570	.596	.432	.452	.518	.491	.469			
K	.020	.060	.052	.503	.482	.099	.078	.073			
SUM	4.996	4.983	5.005	4.988	5.002	4.996	4.996	4.997	3.213	3.112	2.055
AB	49.970	58.910	60.180	43.710	44.760	52.480	50.270	48.390			
OR	2.040	6.160	5.270	50.990	47.740	10.060	8.000	7.530			
AN	47.990	34.930	34.550	5.290	7.510	37.460	41.730	44.070			

Pyroxene (continued)
1: C) Margin of a pyroxene phenocryst (KLB-099)
2: Interstitial pyroxene lath (KLB-099)
3: A) Core and B) margin of a pyroxene phenocryst (KLB-099)
4: A) Core and B) margin of an interstitial pyroxene (KLB-083)
5: A) Core and B) margin of an interstitial pyroxene (KLB-083)
6: A) Core and B) margin of an interstitial pyroxene (KLB-083)
7: A) Core and B) margin of an interstitial pyroxene (KLB-083)

Plagioclase
1: Plagioclase lath in glomeroporphyritic aggregate (KLB-099)
2: Plagioclase lath in glomeroporphyritic aggregate (KLB-099)

Plagioclase (continued)
3: Plagioclase lath in glomeroporphyritic aggregate (KLB-099)
4: Plagioclase lath in glomeroporphyritic aggregate (KLB-099)
5: Alkali feldspar lath in glomeroporphyritic aggregate (KLB-099)
6: Alkali feldspar lath in glomeroporphyritic aggregate (KLB-099)
7: Plagioclase lath (KLB-083)
8: Stubby plagioclase lath (KLB-083)
9: Stubby plagioclase lath (KLB-083)

Oxide
1: Anhedral interstitial titanomaghemite (KLB-099)
2: Anhedral interstitial titanomaghemite (KLB-099)
3: Acicular ilmenite (KLB-099)

C.3 FELSITE

	1	2A	2B	3A	3B	4	5	6	7	8
SiO_2	50.90	50.18	50.97	50.69	50.36	52.70	61.90	70.44	65.70	69.68
TiO_2	1.18	.87	.53	1.25	1.13	.74				
Al_2O_3	2.44	2.79	1.58	2.78	2.79	1.94	24.32	17.30	18.83	19.64
Cr_2O_3	.16			.16	.15	.51				
FeO	9.99	13.03	14.21	9.26	10.17	8.03	.37	.43	.24	
MnO	.17	.26	.35	.19	.17	.19				
MgO	15.84	14.14	13.43	15.34	15.23	17.08	.05			
CaO	18.78	17.79	18.05	20.08	18.94	19.24	4.92	.06	.40	.13
Na_2O	.27	.37	.21	.27	.27	.35	6.83	4.97	2.74	11.23
K_2O							1.44	7.80	12.20	.08
TOTAL	99.73	99.43	99.33	100.02	99.21	100.78	99.83	101.00	100.11	100.76
OXYGEN	6	6	6	6	6	6	8	8	8	8
SI	1.902	1.904	1.946	1.891	1.895	1.930	2.751	3.103	2.991	3.016
TI	.033	.025	.015	.035	.032	.020				
AL	.107	.125	.071	.122	.124	.084	1.274	.898	1.010	1.002
CR	.037			.005	.004	.015				
FE	.312	.413	.454	.289	.320	.246	.014	.016	.009	
MN	.005	.008	.011	.006	.006	.006				
MG	.882	.800	.764	.853	.854	.932	.003			
CA	.752	.723	.739	.802	.764	.755	.234	.003	.020	.006
NA	.020	.027	.016	.020	.020	.025	.588	.424	.242	.943
K							.081	.438	.709	.004
SUM	4.018	4.025	4.016	4.023	4.019	4.013	4.945	4.882	4.981	4.971
AB							65.070	49.010	24.920	98.900
OR							9.010	50.660	73.060	.450
AN							25.920	.330	2.020	.650
WO	38.530	37.190	37.530	41.140	39.290	38.930				
EN	45.210	41.130	38.840	43.740	43.960	48.080				
FS	16.270	21.680	23.630	15.120	16.750	12.990				

(Felsite - KLB-080)
1: Anhedral pyroxene phenocryst
2: A) Core and B) margin of an anhedral pyroxene phenocryst
3: A) Core and B) margin of an subhedral pyroxene phenocryst
4: Subhedral pyroxene phenocryst
5: Plagioclase phenocryst
6: Plagioclase phenocryst
7: Margin of a plagioclase phenocryst
8: Coarse plagioclase phenocryst

APPENDIX D
WHOLE ROCK CHEMISTRY

D.1 SAMPLE PREPARATION AND ANALYTICAL TECHNIQUES

All samples were prepared for X-ray fluorescence (XRF) analysis by manually splitting with a hydraulic splitter followed by crushing in a jaw-crusher with Mn-steel jaws. The jaw-crushed samples, where necessary, were hand-picked to remove amygdaloidal material. The final grinding to a -300# powder was done in a carbon-steel grinding vessel using the Siebtechnik swing mill.

Whole rock samples were analyzed for major and trace elements using the Siemens SRS303AS and Phillips PW1400 XRF spectrometers according to the routine techniques presently utilised in the Department of Geological Sciences at UCT (see Duncan *et. al.*, 1984b and le Roex, 1985). The major elements (except Na) were analyzed using the procedure of Norrish and Hutton (1969) where the sample is fused with a lithium tetraborate flux. Volatile constituents (H_2O^- and loss-on-ignition) were determined by drying the sample at 110°C (H_2O^-) and then roasting the sample at 950°C in a furnace for 12 hours (LOI). The trace elements and Na were analyzed using pressed powder briquettes.

D.2 WHOLE ROCK DATA

The whole rock data tabulated below includes all available data for the Karoo-aged basalts and dolerites of Botswana and includes the data published (graphically) by Erlank *et. al.* (1988; 1990) and the major and trace element concentrations for 128 new samples which were obtained during this study. The un-normalised data in the subsequent tables has all Fe as Fe_2O_3. The data is listed numerically within the geochemical sub-groups defined in chapter 2.

LOW-K_2O LINEAGE

	Low-MgO LTZ picritic basalts			LTZ basalts														
KLB	-009	-128	-172	-004	-005	-006	-007	-010	-012	-013	-019	-020	-021	-022	-025	-026	-027	-045
SiO_2	50.06	48.66	48.26	48.98	49.41	50.28	49.99	51.68	52.55	52.72	49.45	50.80	48.00	49.53	48.89	49.78	49.97	49.66
TiO_2	.82	.76	.83	.92	.79	.90	.86	1.00	.96	1.29	.88	.79	.83	.80	.87	.89	.86	.91
Al_2O_3	14.30	13.57	14.73	15.18	15.20	15.55	14.88	15.09	15.75	14.20	15.11	15.37	14.93	15.11	14.90	14.63	14.90	15.26
Fe_2O_3*	11.78	11.27	11.04	11.04	10.47	11.08	10.45	11.21	10.60	12.72	10.47	9.96	9.80	10.14	10.82	10.92	10.37	10.24
MnO	.12	.18	.17	.20	.15	.16	.16	.14	.14	.16	.16	.14	.21	.13	.17	.18	.22	.17
MgO	10.14	10.17	8.85	7.57	7.82	6.52	7.79	6.73	7.35	5.83	7.66	7.57	7.57	8.03	7.24	6.93	7.49	7.38
CaO	9.99	9.70	9.55	10.30	10.57	9.85	10.36	10.60	8.21	8.09	10.43	11.04	10.05	9.68	9.94	10.45	10.22	10.56
Na_2O	2.04	1.93	2.87	2.02	2.07	2.20	2.27	2.55	2.96	3.25	2.24	2.19	1.77	1.90	2.68	2.43	1.74	2.29
K_2O	.59	.41	.42	.59	.41	.66	.47	.82	1.30	1.50	.46	.43	.27	.50	.35	.62	.42	.66
P_2O_5	.16	.12	.13	.16	.12	.14	.13	.19	.18	.25	.14	.12	.13	.12	.14	.16	.14	.15
H_2O-		1.55	1.76	2.00	1.57	1.05	1.97				1.54	1.22	3.45	2.37	2.37	1.59	2.60	.45
LOI		1.44	1.63	2.06	1.85	2.14	1.55				.97	1.00	1.46	1.46	1.65	.40	1.03	2.52
Total	100.00	99.77	100.24	101.02	100.43	100.53	100.88	100.00	100.00	100.00	99.52	100.64	98.47	99.76	100.03	98.99	99.96	100.25
Rb	15	8.0	6.7	6.8	6.1	9.2	8.4	18	18	36	8.9	7.3	3.3	8.3	8.4	12	7.0	11
Ba		144	109	178	127	198	157				131	114	85	134	131	169	128	151
Sr	177	165	163	178	175	185	187	221	228	264	186	185	217	193	162	185	218	199
Th																		
U																		
Zr	84	58	62	89	58	85	66	98	92	124	68	61	64	57	80	88	66	76
Nb	4.7	4.7	5.3			3.2		4.6	6.1	7.9	4.6	4.0	3.9	3.7	5.3	5.9	4.2	5.0
Cr	345	481	357	351	347	181	328	279	309	131	367	349	339	341	323	303	325	281
V	202	176	211	237	233	239	218	267	237	267	219	196	214	210	207	216	210	199
Sc		29	30								34	33	33	35	31	34	33	30
Ni	189	183	135	91	88	70	92	92	87	54	98	106	92	94	112	81	90	89
Co	61	60	57	58	56	59	59	47	44	46	47	48	46	48	47	47	48	46
Pb		4.3	3.8															
Zn	85	81	77	75	69	78	68	87	86	101	71	72	68	78	80	72	64	77
Cu	63	64	72	97	61	107	61	92	89	155	72	105	80	82	76	47	78	55
Y	23	20	21	23	18	23	20	27	27	33	23	21	21	20	23	24	22	24
La		7.3	8.3								8.9	6.5	8.0	9.7	9.4	9.8	8.6	12
Ce		17	17								16	12	15	14	20	16	17	46
Nd		9.9	8.8								12	7.0	8.4	7.8	13	14	11	15

LOW-K_2O LINEAGE

	LTZ basalts																	
KLB	-046	-047	-054	-115	-116	-118	-119	-120	-121	-122	-123	-124	-125	-126	-127	-129	-130	-131
SiO_2	50.47	49.26	51.46	50.82	51.21	48.99	52.00	48.91	47.86	50.81	49.07	51.31	49.99	50.47	50.36	48.70	49.60	50.67
TiO_2	1.05	.98	.95	1.15	1.15	1.31	1.20	1.33	1.07	.99	.82	.76	.83	.90	.93	.86	.81	.87
Al_2O_3	14.84	15.68	15.07	13.12	13.59	14.14	13.96	14.39	14.31	14.50	15.10	14.97	15.28	14.45	14.12	14.69	14.92	14.88
Fe_2O_3*	10.88	10.50	11.19	13.20	13.15	13.08	12.34	13.15	12.01	11.67	10.62	10.26	10.83	10.52	10.65	10.51	10.10	10.44
MnO	.17	.16	.16	.18	.19	.20	.19	.19	.18	.19	.16	.14	.16	.16	.16	.17	.16	.16
MgO	7.44	7.59	6.12	6.03	5.88	5.71	5.53	5.87	6.31	6.42	7.19	6.45	6.56	6.77	6.24	7.16	6.99	7.06
CaO	9.50	9.34	10.23	7.76	8.97	10.22	8.08	9.97	9.68	8.12	10.60	10.11	11.08	9.71	9.07	9.67	9.88	9.58
Na_2O	2.22	2.42	2.29	3.05	2.63	2.29	2.70	2.39	2.74	2.91	2.11	2.08	2.00	2.29	2.55	2.65	2.25	2.47
K_2O	.67	.76	.81	1.26	.75	.73	.81	.69	.50	.89	.52	.56	.63	.77	.74	.33	.53	.50
P_2O_5	.16	.16	.16	.16	.16	.21	.19	.22	.18	.17	.14	.13	.14	.14	.16	.14	.13	.14
H_2O-	.65	.79	1.30	1.04	1.14	1.58	.46	1.28	.51	.38	1.64	1.53	1.20	.86	.69	1.89	1.24	.87
LOI	1.93	2.41	.68	1.73	1.17	1.20	2.06	1.62	4.10	3.05	1.46	1.37	1.38	2.82	3.50	2.88	3.07	2.39
Total	99.99	100.04	100.43	99.51	99.98	99.67	99.52	100.01	99.46	100.10	99.43	99.68	100.07	99.86	99.16	99.67	99.68	100.04
Rb	9.1	16	16	34	17	16	16	11	14	17	7.8	9.2	14	22	20	5.3	9.6	9.2
Ba	163	177	186	239	200	194	254	216	90	261	155	165	163	137	164	135	135	124
Sr	198	221	180	341	215	181	234	197	101	253	202	196	193	191	203	226	179	220
Th			2.9	3.1	2.6	3.7			3.4				2.8					
U										1.9					1.8			1.8
Zr	84	80	97	100	99	120	107	123	110	101	92	83	90	70	78	69	63	65
Nb	5.7	5.9	6.7	6.2	5.7	8.6	7.9	9.2	9.0	7.7	8.0	7.6	7.5	4.5	5.7	5.3	4.4	5.0
Cr	293	300	184	155	156	143	146	140	204	207	212	205	206	322	275	342	277	322
V	205	225	225	263	263	265	259	265	260	229	193	192	186	224	225	217	205	218
Sc	32	34	35	37	35	37	38	36	39	34	28	31	30	36	37	34	36	34
Ni	97	84	65	66	65	57	54	56	78	78	97	93	92	87	74	103	101	99
Co	46	46	45	49	49	46	45	46	50	48	47	46	46	47	45	48	49	48
Pb		2.7	4.1	5.3	5.0	4.9	5.2	4.2	6.7	4.1	4.6	5.3	4.0	5.3	5.5	4.3	3.9	4.1
Zn	86	70	84	106	93	89	93	94	111	85	84	82	78	79	85	84	78	80
Cu	95	79	93	115	139	144	143	96	100	91	64	71	73	50	92	60	61	84
Y	25	25	26	30	28	33	29	33	28	26	23	21	23	23	25	22	21	22
La	11	17	13	11	9.5	12	12	11	13	11	11	11	9.6	7.3	8.0	5.8	5.5	6.7
Ce	57	59	26	25	20	32	29	29	29	28	23	21	24	17	19	19	15	15
Nd	34	22	15	14	14	17	16	17	16	16	12	12	13	8.7	11	9.7	8.9	9.0

LOW-K_2O LINEAGE

	LTZ basalts																	
KLB	-133	-134	-135	-137	-138	-139	-140	-141	-142	-143	-144	-145	-146	-147	-148	-149	-150	-155
SiO_2	49.92	49.19	50.17	49.74	49.03	50.00	49.94	50.91	49.87	48.80	49.80	48.38	50.15	50.06	49.05	48.67	49.32	50.31
TiO_2	.91	.85	1.17	.84	.82	.91	.86	.95	.85	1.01	.85	.79	.89	.92	.92	.89	.93	.94
Al_2O_3	14.88	15.20	14.15	15.23	15.21	14.71	14.67	15.10	14.96	15.00	14.25	15.27	15.35	14.97	14.84	15.07	15.08	15.01
Fe_2O_3*	10.54	10.19	13.11	10.69	10.65	11.05	10.53	11.01	10.43	10.71	10.72	10.11	10.50	10.75	10.61	10.55	10.66	11.47
MnO	.18	.16	.20	.18	.17	.18	.17	.17	.16	.17	.17	.16	.15	.17	.16	.15	.17	.17
MgO	7.29	7.41	5.99	6.87	7.03	6.95	7.02	7.13	7.60	6.31	7.85	8.13	7.39	7.34	7.49	7.47	7.20	6.38
CaO	10.29	10.98	10.40	10.77	10.46	10.68	9.59	10.85	10.64	10.26	10.18	10.30	10.64	10.39	10.11	10.08	10.19	9.43
Na_2O	2.19	2.02	1.95	1.82	1.90	1.99	2.39	2.13	1.87	1.87	1.82	1.84	2.06	2.00	2.00	2.02	2.22	3.10
K_2O	.51	.13	.38	.47	.65	.58	.64	.50	.51	.54	.45	.41	.54	.50	.51	.50	.60	.71
P_2O_5	.14	.13	.17	.15	.14	.15	.13	.15	.14	.15	.12	.12	.14	.14	.14	.14	.14	.15
H_2O-	1.60	2.09	1.54	2.15	1.90	1.35	.67	.83	1.65	.93	1.80	2.33	1.25	1.64	2.12	2.64	1.95	1.49
LOI	1.09	1.45	1.16	1.56	1.64	1.42	3.44	.72	1.64	3.29	1.30	1.93	1.11	1.39	1.64	1.47	1.28	1.30
Total	99.55	99.78	100.39	100.45	99.60	99.98	100.03	100.46	100.31	99.03	99.31	99.76	100.18	100.26	99.59	99.64	99.75	100.45
Rb	9.4	1.7	4.6	6.2	13	11	15	9.9	9.2	11	12	8.3	9.7	8.8	9.3	8.3	11	12
Ba	148	60	115	155	170	150	136	145	117	132	120	102	146	139	134	136	160	248
Sr	200	208	196	210	202	193	173	188	177	190	177	182	198	194	195	199	197	214
Th							2.5			2.4								
U									1.8							1.8		2.1
Zr	75	70	96	93	92	93	67	73	66	74	61	58	72	73	75	73	78	91
Nb	6.2	5.8	6.3	8.0	8.1	7.2	4.4	5.4	4.8	5.8	4.6	4.8	6.2	5.9	6.6	6.0	6.9	7.0
Cr	304	341	123	221	230	288	318	290	287	296	338	362	324	305	305	316	321	211
V	217	217	274	193	202	212	206	211	201	232	217	210	190	211	215	210	223	239
Sc	29	32	34	29	32	32	33	32	32	37	31	34	31	31	30	30	33	34
Ni	98	104	61	100	100	85	99	100	108	58	113	107	106	99	100	100	94	63
Co	46	49	47	48	48	47	49	49	49	44	49	53	48	48	48	50	47	48
Pb	6.0	4.8	6.3	4.4	4.0	4.6	6.2		4.9	4.6	4.8	4.2	3.5	4.5	3.5	4.1	4.2	3.7
Zn	76	77	89	72	82	70	81	73	79	83	77	76	82	78	80	70	82	88
Cu	80	72	158	86	80	71	62	68	70	55	62	81	62	63	77	72	69	85
Y	23	22	30	24	24	25	22	24	22	24	20	20	23	24	24	24	24	24
La	9.7	7.7	9.1	12	11	9.6	7.2	9.4	6.6	6.9	6.7	7.9	7.6	8.5	9.7	9.3	8.1	10.0
Ce	22	20	27	24	23	25	13	22	17	19	21	15	20	21	21	18	23	28
Nd	10	10	15	14	12	13	8.3	13	11	11	11	8.2	11	12	11	9.6	12	15

LOW-K_2O LINEAGE

	LTZ basalts																	
KLB	-156	-157	-158	-160	-161	-162	-163	-164	-166	-167	-168	-188	-189	-196	-200	-201	-202	-203
SiO_2	48.35	48.95	49.85	48.15	48.51	49.26	49.58	49.27	48.79	49.87	49.68	49.80	48.88	49.94	50.84	50.94	50.70	49.33
TiO_2	.81	.84	.83	.82	.82	.80	.81	.94	.88	.89	.85	.89	.90	.95	.93	.95	.95	.94
Al_2O_3	14.77	15.23	15.11	15.93	15.66	15.41	15.49	15.14	14.95	15.02	15.08	15.31	15.07	15.46	15.42	14.60	14.98	15.32
Fe_2O_3*	10.68	10.84	10.68	10.39	10.71	10.56	10.24	11.36	10.88	10.98	10.62	10.20	10.46	10.12	10.92	10.92	10.84	10.90
MnO	.14	.21	.18	.17	.18	.17	.16	.18	.18	.17	.17	.14	.16	.14	.17	.16	.15	.17
MgO	7.24	7.11	7.06	7.21	7.11	7.11	6.41	7.36	7.31	7.37	7.51	7.39	7.31	7.12	7.05	7.87	7.66	7.45
CaO	10.05	10.55	10.26	10.53	10.43	10.08	10.98	10.44	10.18	10.22	10.33	10.10	10.27	9.63	10.76	10.28	10.28	10.89
Na_2O	2.41	2.37	2.40	2.43	2.29	2.51	2.49	2.74	2.74	2.69	2.70	2.36	1.93	2.58	2.15	1.84	1.97	1.84
K_2O	.54	.49	.59	.44	.58	.60	.69	.59	.53	.50	.46	.55	.51	.63	.53	.50	.55	.44
P_2O_5	.14	.15	.14	.14	.14	.14	.14	.16	.14	.14	.14	.13	.13	.15	.14	.15	.14	.14
H_2O-	2.64	1.89	1.86	2.47	1.87	1.75	1.40	1.19	1.78	1.55	1.54	1.81	2.05	1.75	.35	.90	1.03	1.66
LOI	1.40	1.42	1.26	1.70	1.43	1.40	1.62	1.03	1.10	.87	1.26	1.18	1.53	1.45	.32	.99	1.16	1.47
Total	99.17	100.04	100.23	100.37	99.73	99.79	100.01	100.41	99.48	100.27	100.34	99.85	99.19	99.89	99.57	100.11	100.42	100.53
Rb	8.5	6.9	9.7	5.9	10	12	14	7.1	6.4	7.5	7.5	9.5	7.9	10	11	9.6	10	6.1
Ba	157	167	165	137	163	162	172	177	150	147	116	143	133	160	155	148	150	121
Sr	193	198	196	199	194	184	193	196	177	178	174	198	191	222	197	173	184	183
Th							2.5											
U			2.8				2.2				2.2							
Zr	92	95	93	91	91	89	90	95	85	83	67	72	72	77	75	72	71	69
Nb	8.2	8.5	8.3	8.0	8.4	7.5	8.3	6.8	6.7	6.5	4.9	5.3	5.2	5.8	5.4	4.4	4.3	4.4
Cr	235	239	215	227	219	222	236	298	329	318	286	321	292	311	289	417	391	354
V	205	205	201	201	200	200	200	235	220	217	221	224	223	219	219	214	220	227
Sc	31	31	30	30	31	30	32	36	32	34	32	32	32	32	32	32	34	33
Ni	103	104	100	107	96	97	99	89	106	104	103	85	82	88	92	122	104	100
Co	49	49	47	52	50	47	47	51	52	48	49	47	48	49	47	52	51	49
Pb	4.6	4.0	4.7	3.0	4.0	3.6	5.1	3.7	5.1	5.2	5.2					3.0		2.6
Zn	80	79	74	76	73	73	79	85	81	85	76	78	77	105	100	85	84	86
Cu	66	74	74	81	73	51	73	96	72	93	58	66	72	79	83	52	70	74
Y	23	24	22	23	23	22	23	27	24	24	22	21	23	22	24	24	23	23
La	12	11	12	11	11	11	12	12	13	10	7.2	11	10	11	12	8.5	8.2	11
Ce	24	26	27	27	27	28	22	25	25	24	17	17	13	17	19	19	19	17
Nd	12	13	14	13	14	14	11	15	13	15	11	9.7	11	10	11	11	11	11

LOW-K_2O LINEAGE

	LTZ basalts									High-Na_2O LTZ basalts								
KLB	-204	-205	-210	-211	-212	-213	-214	DB-19	DB-20	-011	-017	-018	-048	-055	-117	-165	-170	-171
SiO_2	49.56	50.15	51.31	51.53	51.06	50.22	50.39	51.09	51.16	50.06	51.30	49.44	49.16	51.27	49.88	48.62	49.67	49.49
TiO_2	.90	.90	1.03	1.02	1.24	1.21	1.04	1.36	1.08	.98	.92	.82	.83	.93	1.32	.88	.86	.82
Al_2O_3	15.01	14.82	15.57	15.61	14.20	13.61	14.82	14.27	15.59	15.57	14.98	14.44	14.44	15.12	14.13	15.17	15.35	15.05
Fe_2O_3*	10.44	10.67	11.15	10.85	12.93	13.03	11.70	13.56	11.34	11.12	10.45	10.16	10.14	10.92	12.96	10.73	10.48	10.46
MnO	.15	.17	.18	.17	.20	.18	.17	.20	.17	.13	.16	.15	.16	.17	.20	.19	.17	.17
MgO	7.53	7.11	6.08	6.05	5.99	6.04	6.37	5.71	6.24	6.49	7.02	6.84	7.26	6.23	5.61	7.77	8.02	7.98
CaO	10.20	10.01	10.82	10.85	9.30	9.78	10.81	9.69	10.21	9.34	8.13	8.46	6.91	8.90	7.59	10.05	10.28	10.09
Na_2O	1.76	2.27	2.00	2.04	2.08	1.80	1.81	2.81	3.12	5.22	4.94	4.39	3.18	3.69	3.56	2.85	2.95	2.67
K_2O	.41	.47	.65	.63	.70	.63	.32	.71	.71	.88	.66	.87	.83	.83	.84	.49	.38	.35
P_2O_5	.13	.14	.16	.16	.18	.16	.16	.19	.17	.22	.15	.13	.13	.16	.22	.14	.13	.12
H_2O-	2.08	1.05	.72	.66	1.52	1.48	1.60	.90	1.01		.82	.60	2.70	.91	.40	2.18	1.34	1.40
LOI	1.74	2.16	1.09	.92	1.30	1.31	1.17	.45	.62		2.15	2.31	3.97	1.48	3.17	1.36	1.19	1.31
Total	99.91	99.92	100.77	100.50	100.69	99.45	100.37	100.96	101.43	100.00	101.68	98.60	99.71	100.61	99.89	100.43	100.81	99.93
Rb	7.6	14	15	13	21	14	4.9	20	14	15	9.9	18	18	11	16	6.2	5.1	5.2
Ba	118	117	187	192	141	178	145	185	193		170	165	218	194	360	139	108	98
Sr	182	230	181	185	163	148	178	177	190	184	196	211	304	182	282	172	171	169
Th		2.2	2.5	2.8	2.3									3.0	2.5			
U								1.7			1.8		1.9		3.2			
Zr	65	66	101	102	99	97	100	108	93	89	76	70	67	94	122	84	67	65
Nb	3.9	4.1	7.4	7.2	5.9	5.6	6.9	6.3	6.2	7.9	5.6	5.2	4.8	6.5	8.6	6.6	5.0	4.8
Cr	322	337	193	190	129	170	228	123	208	227	287	319	274	175	150	322	323	326
V	209	223	232	225	285	270	247	286	240	329	230	219	208	217	272	221	219	223
Sc	32	32	34	34	38	35	36	35	33		30	30	31	34	39	32	33	33
Ni	95	92	63	67	62	67	79	58	64	76	79	84	80	62	60	109	101	99
Co	48	48	45	46	49	50	49	47	45	49	44	45	41	45	48	50	48	50
Pb			4.5	2.9	2.8				3.2		3.3	3.0		3.3	4.4	4.4		3.7
Zn	64	73	100	93	96	112	99	94	85	87	77	76	69	83	102	78	80	74
Cu	63	80	42	73	84	114	100	104	99	92	78	71	62	91	147	85	60	75
Y	22	22	26	26	32	30	27	31	26	27	23	22	23	25	33	24	22	22
La	7.5	8.4	14	12	14	14	14	13	13		12	9.2	10	11	13	11	6.9	6.2
Ce	13	15	23	21	22	23	24	25	24		13	18	47	28	29	22	21	21
Nd	8.0	7.5	14	10	14	15	16	15	12		9.0	9.9	33	15	18	13	11	9.8

LOW-K_2O LINEAGE

	High-Na_2O LTZ basalts															Low-P_2O_5 LTZ basalts		
KLB	-173A	-173B	-174	-175	-185	-186	-187	-195	-197	-198	-199	-206	-207	-208	-209	-015	-016	-023
SiO_2	49.33	48.52	49.78	49.42	48.01	48.31	48.84	48.82	49.89	49.43	51.09	49.22	49.41	49.43	51.38	49.39	49.92	47.06
TiO_2	.87	.85	.81	.93	.87	.87	.90	1.08	.91	.92	.88	.90	.93	.87	.86	1.41	1.87	1.54
Al_2O_3	14.99	15.22	15.53	14.48	13.89	14.18	14.89	14.63	15.00	15.11	15.23	14.91	15.14	15.22	15.14	14.48	14.15	13.33
Fe_2O_3*	10.64	10.40	10.21	10.97	9.82	9.81	10.28	10.38	10.55	10.57	10.18	10.59	10.55	10.25	10.48	13.89	13.40	14.51
MnO	.17	.17	.17	.17	.13	.15	.14	.15	.15	.16	.16	.14	.13	.15	.14	.19	.18	.21
MgO	7.56	7.08	7.74	6.95	7.23	7.07	7.46	6.80	7.08	7.21	7.06	7.35	7.12	7.28	7.31	5.18	5.35	5.02
CaO	8.06	8.03	9.72	7.83	7.70	7.68	8.14	9.40	7.96	8.09	10.89	8.19	9.56	9.37	9.28	9.14	8.36	10.15
Na_2O	4.31	4.39	3.05	3.85	3.94	4.68	3.74	3.73	3.94	3.94	4.00	4.24	3.36	3.78	3.44	2.19	2.00	1.99
K_2O	.58	.41	.59	.93	.73	.62	.60	1.73	.68	.58	.49	.62	.64	.55	.68	.86	1.22	.28
P_2O_5	.14	.14	.13	.15	.14	.16	.15	.20	.14	.14	.12	.14	.14	.14	.13	.15	.22	.19
H_2O-	1.01	.91	1.45	.45	1.07	1.24	1.41	1.60	1.30	1.59	.10	1.49	1.90	1.70	1.09	1.98	1.39	1.05
LOI	2.82	4.02	1.30	3.19	2.87	3.22	1.89	2.47	2.54	2.52	1.01	1.82	1.42	1.39	1.02	1.62	2.00	4.53
Total	100.48	100.15	100.47	99.32	96.39	97.98	98.46	100.99	100.14	100.25	101.22	99.61	100.30	100.13	100.94	100.48	100.05	99.85
Rb	7.7	5.2	9.5	17	8.2	8.8	7.7	35	14	13	10	7.9	11	7.7	9.7	33	86	8.8
Ba	155	107	149	215	166	161	156	154	154	145	148	190	170	144	139	181	194	86
Sr	145	137	189	365	265	260	197	169	174	172	210	192	200	205	178	231	299	129
Th								2.2	3.8						2.6			
U								1.6					1.6			2.0	3.0	1.9
Zr	64	63	58	70	70	67	76	78	72	72	64	75	75	69	66	100	153	117
Nb	4.6	4.6	4.8	5.6	4.9	4.4	5.2	5.4	4.8	5.4	4.6	5.9	5.1	4.8	4.5	4.7	8.1	5.4
Cr	338	330	366	308	381	354	301	298	284	271	311	315	312	290	272	107	90	65
V	209	215	222	226	251	234	219	229	217	221	228	235	240	214	220	297	311	318
Sc	31	32	36	34	34	32	31	31	32	32	31	33	33	30	32	41	39	31
Ni	111	106	98	90	92	94	84	78	86	87	78	88	87	91	85	81	72	57
Co	49	49	49	49	44	44	47	45	47	49	44	50	46	47	49	51	51	50
Pb	3.3	2.7	3.0	4.3					2.8	3.2	2.8						3.4	4.4
Zn	81	81	78	88	78	78	81	82	112	158	76	86	84	80	80	104	101	112
Cu	73	76	64	83	67	66	75	36	63	68	87	78	48	79	71	154	158	168
Y	21	21	20	23	22	22	23	23	22	23	19	23	23	22	22	28	26	32
La	8.3	6.6	5.4	7.5	8.4	9.8	8.2	10	7.4	9.9	11	10	10	9.3	7.9	11	15	12
Ce	16	18	15	18	16	13	21	21	16	17	17	21	21	19	17	18	32	28
Nd	7.4	10	8.4	10	10	9.3	12	12	11	9.2	7.7	14	13	10	12	14	24	18

LOW-K_2O LINEAGE

	Low-P_2O_5 LTZ basalts						TYPE I LTZ dolerites		HTLZ basalts				HTLZ dolerites					
KLB	-024	-179	-180	-181	-182	-184	-049	-050	-044	-100	-177	-178	-028	-029	-032	-033	-034	-035
SiO_2	50.76	47.95	48.37	49.59	48.31	48.12	51.53	49.87	50.17	51.31	50.03	50.62	50.34	50.38	50.32	50.06	50.06	50.61
TiO_2	1.46	1.55	1.48	1.54	1.52	1.41	1.06	1.02	2.66	2.81	2.17	2.88	2.41	2.30	2.45	2.23	2.39	2.30
Al_2O_3	13.51	13.37	14.45	14.10	14.10	14.60	14.60	14.11	13.35	13.42	13.85	13.70	13.71	13.83	13.37	13.83	13.95	13.95
Fe_2O_3*	14.36	15.27	14.05	14.04	13.97	14.06	12.11	11.56	14.41	14.24	15.33	14.90	13.34	13.27	13.41	13.04	13.02	12.80
MnO	.15	.12	.14	.17	.16	.21	.20	.19	.20	.19	.23	.19	.18	.19	.19	.18	.17	.17
MgO	5.30	4.35	5.32	5.38	5.68	5.98	6.20	5.98	5.28	5.13	4.64	4.46	6.13	6.62	6.30	6.15	5.99	6.36
CaO	9.18	5.55	9.10	9.53	9.41	9.82	10.46	10.16	9.50	9.09	9.12	8.84	10.27	10.04	9.89	9.90	10.21	9.84
Na_2O	1.90	2.73	2.18	2.23	2.17	2.02	3.01	2.92	2.36	2.50	2.47	2.59	2.75	2.55	2.66	2.79	2.43	2.63
K_2O	.43	1.07	.70	.76	.61	.61	.84	.86	.89	.94	1.06	1.21	.73	.71	.72	.68	.58	.79
P_2O_5	.16	.16	.15	.16	.16	.14	.18	.17	.32	.34	.24	.33	.28	.28	.29	.25	.28	.29
H_2O-	2.84	3.48	2.01	1.85	2.20	2.13	.08	.84	.73	.54	.86	.77	.31	.47	.32	.55	.89	.54
LOI	.99	3.72	2.84	1.91	1.90	1.79	1.05	3.59	.29	.24	.93	.69	.00	.35	-.11	.76	.31	.60
Total	101.04	99.32	100.78	101.26	100.20	100.89	101.31	101.25	100.17	100.75	100.93	101.18	100.45	100.97	99.81	100.41	100.29	100.89
Rb	10	22	22	22	20	20	17	19	16	19	31	36	14	14	13	13	9.8	16
Ba	94	113	124	144	141	159	218	321	252	298	294	328	222	211	216	284	212	321
Sr	164	245	227	224	217	220	190	196	403	446	271	395	376	384	369	352	380	387
Th									3.8	3.4		2.5				2.9		3.0
U		3.6	1.8		2.4							2.0						
Zr	103	107	99	103	105	87	101	101	219	228	157	222	185	180	189	167	184	187
Nb	4.7	5.4	4.9	5.3	5.3	5.4	7.2	7.7	12	14	8.2	12	11	11	12	10	12	11
Cr	70	142	126	121	114	114	204	199	87	91	89	113	146	157	142	137	124	141
V	279	273	317	313	322	324	233	231	360	335	363	356	341	334	352	321	335	310
Sc	33	50	45	43	42	41	31	32	31	31	38	34	33	31	33	31	31	31
Ni	71	84	77	71	78	73	56	56	95	73	67	80	96	105	99	85	97	100
Co	47	42	44	47	51	55	44	44	47	48	56	50	45	46	47	45	48	45
Pb	3.0		3.3				2.9	2.6	4.5	7.0			4.0	2.9	3.7		2.8	3.2
Zn	109	104	106	99	107	97	87	88	116	117	111	117	103	97	111	87	104	95
Cu	162	157	127	113	110	146	99	97	219	127	145	149	189	192	198	211	192	208
Y	32	23	27	27	28	24	27	27	39	40	36	37	34	34	35	33	34	33
La	9.0	11	12	9.3	11	11	13	17		23	17	23						
Ce	20	22	24	26	21	21	58	48		58	37	51						
Nd	15	14	16	15	14	15	11	30		37	24	34						

LOW-K_2O LINEAGE

	HTLZ dolerites									HTZ basalts							HTZ dolerites	
KLB	-036	-037	-038	-039	-041	-042	-068	-095	-030	-002	-014	-063	-070	-096	-097	-101	-001	-003
SiO_2	50.10	50.07	50.36	50.02	49.06	47.57	50.20	51.01	49.27	53.07	49.90	50.18	49.41	49.89	51.68	51.08	50.51	48.04
TiO_2	2.33	2.53	2.59	2.63	2.72	2.80	2.89	2.02	1.82	2.89	3.24	4.34	3.54	3.02	2.95	3.51	3.31	3.04
Al_2O_3	14.08	13.49	13.73	13.53	13.85	13.82	13.93	14.31	14.84	12.46	13.59	12.83	13.06	12.84	12.92	12.68	13.42	12.50
Fe_2O_3*	13.39	13.92	14.37	14.42	13.87	13.77	14.14	12.38	12.12	13.92	14.71	15.43	15.34	14.99	14.95	14.57	14.41	15.01
MnO	.18	.19	.19	.20	.20	.19	.16	.17	.17	.16	.19	.19	.17	.19	.19	.17	.18	.18
MgO	5.65	5.53	5.22	5.25	6.19	5.60	4.36	6.69	7.63	2.66	4.54	4.34	3.74	4.29	4.38	3.58	5.40	3.00
CaO	10.32	9.31	9.73	9.66	10.03	9.96	8.16	10.59	10.02	6.91	8.54	8.47	8.23	8.67	8.19	7.50	9.68	7.86
Na_2O	2.40	2.88	2.73	2.73	2.51	2.06	2.64	2.21	2.33	3.18	2.65	2.75	2.29	2.55	2.63	2.84	2.36	2.07
K_2O	.35	.77	.72	.79	.94	.94	1.53	.35	.58	.94	1.59	1.65	1.66	.64	1.35	1.61	.83	1.26
P_2O_5	.27	.29	.30	.31	.33	.32	.32	.24	.22	1.00	.39	.59	.60	.40	.42	.85	.39	1.04
H_2O-	.68	.59	.64	.75	.52	.46	1.21	.33	.57	.17	<.18	.30	.80	.75	.44	.63	.23	2.40
LOI	.58	.42	.07	.17	.04	2.60	1.14	.68	1.09	2.36	1.73	.08	1.66	1.35	.42	1.27	.46	3.19
Total	100.33	99.98	100.65	100.45	100.27	100.08	100.68	100.98	100.66	99.72	100.87	101.13	100.51	99.59	100.53	100.30	101.18	99.59
Rb	21	16	15	14	21	20	32	17	8.1	27	39	36	23	15	30	33	20	16
Ba	169	241	229	226	236	291	418	235	170	857	388	516	985	361	395	713	358	794
Sr	360	353	354	353	386	416	420	340	408	815	458	547	645	464	401	862	570	868
Th			2.7		2.8	2.5	2.4				3.6	4.2	4.2		3.9	6.5		
U	1.8		2.7				1.8	1.7			4.1	1.9	1.8		2.2	3.0		
Zr	176	190	197	197	210	208	217	167	104	681	262	394	389	284	318	555	272	715
Nb	11	11	12	11	13	13	14	13	6.3	34	15	35	22	17	18	32	11	34
Cr	168	143	97	95	94	53	57	163	193	7.1	129	56	44	47	56	11	100	5.9
V	340	336	367	370	368	386	356	279	188	143	371	340	286	306	312	229	306	188
Sc	32	30	29	29	36	29	33	31	22		34	26	27	28	29	19		
Ni	122	94	84	85	77	56	63	110	237	19	93	47	76	75	72	47	99	22
Co	49	47	43	45	52	42	40	48	55	80	47	44	47	46	43	40	54	35
Pb	3.1		3.8		3.7	2.7	4.2	5.1			5.1	7.5	6.8	8.6	7.4	16		
Zn	106	102	108	109	114	97	105	89	77	150	126	136	150	118	129	133	111	162
Cu	196	231	244	246	210	224	174	147	154	266	204	268	193	197	173	203	183	286
Y	34	37	39	40	36	35	35	27	20	61	39	47	60	47	49	62	35	65
La							24	21			25	46	45	27	31	57		
Ce							57	51			64	107	97	74	72	143		
Nd							36	28			43	63	72	46	50	91		

LOW-K_2O LINEAGE

	HTZ dolerites								HTZ (low Fe) basalts							HTZ (low Fe) dolerites		
KLB	-031	-040	-056	-067	-089	-092	-093	-098	-066	-088	-094	-114	-152	DB-14	DB-16	-061	-062A	-062B
SiO_2	49.92	51.37	50.61	50.04	49.96	50.84	50.46	50.84	51.09	52.47	52.30	52.22	51.02	49.76	50.63	51.79	51.57	51.37
TiO_2	3.22	3.64	3.44	3.50	3.38	3.23	3.22	3.51	3.43	3.01	3.99	2.82	3.68	4.20	3.82	4.21	4.37	4.38
Al_2O_3	12.27	13.03	12.94	12.85	14.05	12.76	12.63	13.02	16.70	13.35	13.09	13.52	13.26	13.89	13.37	13.36	13.44	13.48
Fe_2O_3*	15.52	14.55	14.99	15.04	14.03	15.51	15.32	15.24	11.98	12.15	12.73	11.81	12.55	13.15	13.39	13.09	13.16	13.39
MnO	.21	.17	.20	.18	.18	.19	.19	.18	.14	.15	.17	.15	.16	.14	.14	.13	.15	.16
MgO	5.48	3.70	4.98	4.25	3.92	4.63	4.42	4.56	3.25	4.31	4.22	4.06	3.64	3.73	4.24	4.80	4.56	4.63
CaO	8.94	7.86	9.48	8.41	8.32	8.67	8.45	8.18	9.01	7.13	7.64	7.18	6.73	7.43	7.32	7.50	8.15	8.13
Na_2O	2.85	2.75	2.71	2.63	2.96	2.69	2.54	2.54	3.24	2.54	2.70	2.63	2.72	2.79	3.29	2.58	2.41	2.39
K_2O	1.02	1.92	.76	1.08	1.34	1.16	1.19	1.51	1.50	2.33	2.01	2.05	2.75	2.24	1.92	1.93	1.85	1.73
P_2O_5	.38	.64	.41	.58	.48	.41	.42	.58	.44	.70	.62	.70	.80	.85	.79	.62	.64	.63
H_2O-	.54	.38	.38	.79	.45	.59	.81	.67	.33	.39	.37	.99	1.12	1.19	1.00	.40	.31	.46
LOI	.44	.55	.19	.61	1.02	.03	.12	-.09	.23	.82	.32	1.20	1.30	.88	.61	-.16	-.23	
Total	100.78	100.55	101.08	99.96	100.08	100.72	99.76	100.84	101.34	99.34	100.17	99.32	99.71	100.25	100.53	100.40	100.61	100.76
Rb	21	40	17	23	26	25	25	31	34	52	38	33	56	24	28	35	33	34
Ba	335	634	375	486	472	371	362	505	445	851	677	954	942	856	1016	684	712	691
Sr	368	617	587	649	543	397	400	581	764	916	847	1078	957	960	1000	859	998	983
Th	3.0	5.5	3.7	4.0	4.0	3.6	6.0	4.2	3.7	5.0	4.2	4.6	5.8	7.2	6.8	5.7	3.7	4.3
U				1.9	1.8	1.8	1.8	1.8	1.7	3.3		2.4	2.4	1.8	1.8	1.8	1.8	1.9
Zr	249	423	279	383	290	278	292	386	323	436	453	461	590	552	485	451	455	451
Nb	16	25	15	21	22	15	16	22	29	29	27	32	35	31	33	26	26	26
Cr	55	34	69	43	26	53	53	41	29	78	68	144	23	31	34	73	47	47
V	414	278	349	308	269	331	336	319	253	230	254	189	202	229	244	261	275	275
Sc	33	24	30	25	26	29	31	24	20	21	22	17	17	19	18	21	22	22
Ni	58	49	74	70	30	73	70	66	31	46	92	45	60	63	58	93	83	84
Co	43	39	44	46	36	45	46	47	34	39	45	37	37	38	41	44	45	45
Pb	3.0	7.0	5.1	7.1	3.6	6.2	5.3	4.3	3.8	12	12	11	10	9.1	9.1	9.8	5.6	7.1
Zn	110	132	122	130	111	125	131	143	103	119	125	114	123	140	137	134	133	136
Cu	277	262	197	185	268	157	146	180	213	54	124	50	108	158	127	133	148	129
Y	44	56	42	50	42	47	47	50	39	44	47	46	56	55	51	47	47	45
La			24	39	36	30	30	39	37	60	45	64	66	61	66	47	49	47
Ce			72	96	90	67	67	97	83	127	110	141	163	147	159	120	123	116
Nd			47	62	55	44	47	62	53	78	70	85	99	91	96	73	76	72

	LOW-K_2O LINEAGE					HIGH-K_2O LINEAGE								FELSITE				
	HTZ (low Fe) basalts					High-K_2O picritic basalts		Shoshonites								TYPE II LTZ dolerites		
KLB	-079	-081	-085	-087	-091	-083	-084	-057	-058	-059	-060	-090	-099	-080	-082	-043	-051	-052
SiO_2	50.37	50.34	52.45	52.21	52.72	46.96	48.88	48.78	49.28	49.65	49.37	49.64	49.64	64.59	65.58	48.23	52.72	53.71
TiO_2	3.96	3.79	3.61	3.44	4.20	2.39	2.42	1.75	1.78	1.99	2.27	2.51	2.22	.85	.93	1.76	.52	.61
Al_2O_3	13.46	15.09	13.65	13.52	13.22	7.22	8.33	17.18	16.05	15.83	15.41	15.29	15.56	14.59	14.47	14.64	15.55	15.45
Fe_2O_3*	12.53	13.15	12.34	12.21	12.45	12.63	11.24	10.11	10.01	10.47	11.16	11.61	11.03	5.32	5.54	14.67	9.04	9.95
MnO	.14	.16	.15	.14	.16	.15	.14	.15	.15	.15	.16	.16	.16	.06	.08	.22	.16	.18
MgO	3.83	4.51	3.79	3.72	4.38	19.27	15.61	4.72	4.89	4.87	4.85	4.66	4.86	1.24	1.98	5.82	7.13	5.87
CaO	7.83	9.58	7.49	7.30	7.79	6.28	6.44	7.59	7.95	7.88	7.59	7.77	8.02	1.66	2.21	10.05	11.59	10.11
Na_2O	1.93	2.33	2.59	2.78	2.70	1.40	1.22	3.80	2.97	3.13	2.85	3.59	3.27	3.11	2.91	2.04	1.78	1.83
K_2O	2.32	1.10	1.94	1.88	1.97	1.46	1.79	3.58	4.06	3.93	3.70	3.46	3.72	5.50	3.61	.48	.95	1.14
P_2O_5	.76	.51	.80	.82	.62	.40	.41	.75	.76	.75	.74	.74	.76	.22	.24	.21	.06	.08
H_2O-	.54	.46	.58	.43	.74	.24	.38	.44	.30	.31	.50	.28	.29	.84	.41	.20	.17	.20
LOI	1.81	.14	.93	.91	-.03	.99	2.20	1.35	1.28	1.19	1.42	1.13	1.27	1.30	2.22	1.49	.86	1.36
Total	99.50	101.17	100.31	99.38	100.96	99.39	99.06	100.20	99.48	100.15	100.02	100.85	100.81	99.27	100.17	99.82	100.52	100.48
Rb	41	20	49	53	39	23	36	88	137	123	116	107	113	104	78	14	38	51
Ba	801	432	990	1028	693	754	643	1985	1959	1829	1637	1588	1737	2211	1507	157	228	277
Sr	676	578	1136	1194	836	870	720	1346	1386	1329	1093	980	1109	510	404	143	136	136
Th	6.0	2.3	6.6	6.1	6.9	4.0		20	20	21	18	15	18	17	16	3.3	4.9	5.5
U	1.8	1.8	2.1	1.8	1.8	3.2	2.9	3.3	3.6	3.2	3.8	2.6	1.8	2.8	4.0			
Zr	483	329	519	527	447	297	322	275	275	289	309	319	300	822	811	148	62	81
Nb	31	28	35	35	25	26	13	156	156	146	132	120	132	23	23	8.1	3.0	4.0
Cr	32	89	45	37	68	1022	856	200	208	207	184	157	183	34	42	118	249	119
V	243	286	206	198	258	189	179	155	158	169	192	191	178	42	48	341	175	184
Sc	19	25	19	18	21	19	21	11	12	14	17	15	14	6.5	7.9	30	33	32
Ni	57	68	50	44	88	1084	844	94	96	96	92	78	88	18	21	94	136	101
Co	39	40	35	36	43	90	72	29	32	32	34	31	32	12	11	52	68	52
Pb	8.9		9.0	7.3	7.1	14	13	13	14	13	11	9.9	11	20	21		8.1	6.5
Zn	142	102	133	132	124	114	107	84	88	91	99	93	88	75	76	116	55	76
Cu	129	228	119	111	103	82	83	157	156	172	188	201	182	21	25	217	63	68
Y	47	40	48	49	46	24	25	25	25	27	30	32	29	54	56	36	16	18
La	60	33	66	68	47	41	35	122	118	113	104	100	108	103	101		13	16
Ce	143	82	159	162	110	91	79	222	220	210	203	195	201	227	223		23	36
Nd	85	53	96	96	69	56	51	82	79	83	80	79	83	111	111		10	15